Nucleases and histone acetyltransferases in DNA repair and immune diversity

Submitted by Emily Charlotte Sheppard to the University of Exeter
as a thesis for the degree of
Doctor of Philosophy in Biological Sciences
September 2018

I certify that all material in this thesis which is not my own work has been identified and that any material that has previously been submitted and approved for the award of a degree by this or any other University has been acknowledged.

Signature ……..

Thesis abstract

DNA repair mechanisms are essential for genome maintenance and adaptive immunity. A careful balance must be achieved whereby highly accurate and efficient canonical repair protects the genome from accumulating mutations that lead to aging and cancer, and yet mutation and error-prone non-canonical repair is required for generating immune diversity.

Immune diversity is achieved within a tightly regulated environment in which mutator proteins are directed to the antibody locus to introduce a swathe of DNA damage. This produces high affinity antibodies that recognise an infinite number of invading pathogens. This process of secondary antibody diversification is dependent on both active transcription and DNA repair.

Downstream of histone signalling, DNA repair nucleases are recruited to remove the damaged bases. The structure of damaged regions in the DNA can have very different conformations depending on whether the source of the damage is endogenous or exogenous. Specific DNA nucleases recognise particular DNA substrates and generate DNA intermediates that are repaired in conjunction with polymerases and ligases.

Despite their multitude and importance to DNA repair, very few nucleases have been characterised, while the activities of some studied nucleases remain controversial. Conventional techniques for studying DNA nucleases have several disadvantages; they are hazardous, laborious, time-consuming, and capture nuclease activity in a discontinuous manner. Recognising a need for a safer, faster alternative, a fluorescence-based method has been developed for the study of DNA nucleases, nickases and polymerases.

Key histone modifications that are known to orchestrate canonical DNA repair have since been discovered to regulate non-canonical repair at the antibody locus. The Kat5 histone lysine acetyltransferase functions highly upstream of DNA repair and promotes active transcription, yet a role for Kat5 in secondary antibody diversification has not yet been established. Using chemical inhibitors to prevent the catalytic activities of Kat5, and the genetic method of an inducible degron system for rapid and reversible downregulation of Kat5, a role for Kat5 in

secondary antibody diversification is recognised, and the research contributes to our current understanding of the DNA repair signal transduction pathway.

Acknowledgements

First and foremost, I would like to extend my gratitude to my supervisor, Dr Richard Chahwan, for his eternal support and advice. Richard has always made the time to help me cultivate my projects in an open and discursive environment. I am also grateful to Dr Nic Harmer; as my secondary supervisor, he has imparted a wealth of advice that affected my attitude towards research and gave me a healthy, productive approach.

I am thankful to the BBSRC DTP for funding my research. In addition to financial support, they have also provided me with several opportunities to represent the Exeter student cohort and arrange training and networking events for all South West DTP students. As such, I have enjoyed working as a DTP student and influencing the programme for future intakes.

I am very grateful for all members of my lab group who have made it such a pleasant, kind and entertaining working environment. Laurence Higgins, Rikke Morrish, Laura Reffo, Kevin Yim, Sally Rogers and Michael Dillon have made these four years a wonderful experience. Without your friendship and guidance, my thesis would be in a very different state. I am particularly grateful to Sally who provided the first constructive criticisms of my thesis.

To both lab technicians Agnieszka Kaczmar and Chris Baxter, thank you for maintaining such an organised and structured workplace, and for all the time you have given to placing and chasing our orders.

Dr Ivana Gudelj and Dr Francesca Fiegna both deserve a special thank you. Ivana recommended the PhD project to me after I worked in her lab for my research project in the final year of my undergraduate degree. During this time, I worked closely with Francesca, and it was her influence that drove me to consider working towards a PhD. Without their encouragement, I am not sure that I would have had the confidence to apply for postgraduate positions.

Contents

List of figures

4 Validation of a fluorescence-based toolkit for measuring structure-specific nuclease activity and their substrates

5 Chemical inhibition of Kat5 impacts efficiency of class switch recombination

6 Design of mouse and human Kat5 degron knockout constructs

7 Discussion and future work

List of tables

List of abbreviations

- AID, activation-induced deaminase;
- ATM, ataxia telangiectasia mutated
- ATR, ataxia telangiectasia and Rad3-related
- APE, apurinic/apyrimidinic endonuclease;
- BER, base excision repair;
- bp, base pair;
- CSR, class switch recombination;
- D, diversity gene segment;
- DDR, DNA damage repair;
- DNA-PKcs, DNA-dependent protein kinase, catalytic subunit,
- DSB, double-stranded break;
- Exo1, exonuclease 1;
- ExoIII, exonuclease III;
- GC, germinal centre
- Ig, immunoglobulin;
- J, joining gene segment;
- PG, PicoGreen;
- pol, polymerase;
- MMR, mismatch repair;
- NER, nucleotide excision repair;
- NHEJ, non-homologous end joining;
- Nt, nucleotide
- SHM, somatic hypermutation;
- ssDNA, single-stranded DNA
- T7 Exo, T7 exonuclease;
- UNG, uracil DNA glycosylase;
- V, variable gene segment.

1 General Introduction

1.1 DNA repair, immunity and cancer

DNA repair is a tightly regulated process that is integral for maintenance of genomic integrity and adaptive immunity. In this regard, there is a conflict whereby, on one hand, highly efficient repair is essential for genome maintenance and protection from aging and cancer and, on the other hand, we need mutation and the subsequent repair pathways to generate the diversity we need for an effective innate and adaptive immune response (1,2). As will be discussed in detail, mutation and subsequent recombination of the DNA at the immunoglobulin locus enables the immune system to produce a vast repertoire of antibodies from a relatively small segment of the genome (3). This intentional DNA damage takes place at two developmental stages of B cells and is very acutely controlled (3,4). Loss of these constraints can lead to the uncontrolled accumulation of genomic mutations and tumourigenesis, or immunodeficiencies may develop that increase susceptibility to pathogenic invasion. A careful balance must therefore be achieved to minimise and/or localise mutagenesis (5).

1.2 Histone modifiers and DNA nucleases drive DNA repair at polar ends of the DNA damage signalling pathway

This thesis examines proteins functioning upstream and downstream of DNA damage during the process of DNA repair signalling (Fig. 1). Once damage has been inflicted on the genome, proteins that scan the integrity of the DNA and recognise deformation in the duplex structure alert histone modifiers to induce local changes in the chromatin and recruit enzymes that directly repair the damage. DNA damage can exist in several different forms, such as breaks, chemical adducts or pyrimidine dimerization, and in all stages of the cell cycle, each of which determine the most appropriate form of repair (6–8).

The DNA damage response is a complex network of interacting pathways that determine the cellular response to damage; this involves halting cell cycle progression, inducing apoptosis when the damage is too extensive, altering the transcription profile of the cell and increasing expression of repair proteins in order to carry out the

necessary repair programmes (9) (Fig. 1). In the first instance following DNA damage, sensory proteins that scan the genome recognise sites of damage (9–11), and signal to ‘transducer’ proteins (9). These include histone proteins that undergo grand scale remodelling at the break site, altering chromatin structure, and ataxia telangiectasia mutated (ATM) kinase, which activates a series of ‘effector’ repair proteins to resect along the damaged region, ligate broken DNA ends, and replicate across the break (9,12).

Kat5 is a histone acetyltransferase with known roles supporting both DNA repair and transcription. DNA repair and transcription are mutually important for the secondary antibody diversification processes of somatic hypermutation (SHM) and class switch recombination (CSR), which produce high affinity antibodies during the adaptive immune response. A role for Kat5 in the context of SHM and CSR has yet to be established. With the use of chemical and genetic methods, the role of Kat5 in CSR is explored. A more detailed description of Kat5 is provided below and in Chapter 5.

FIGURE 1

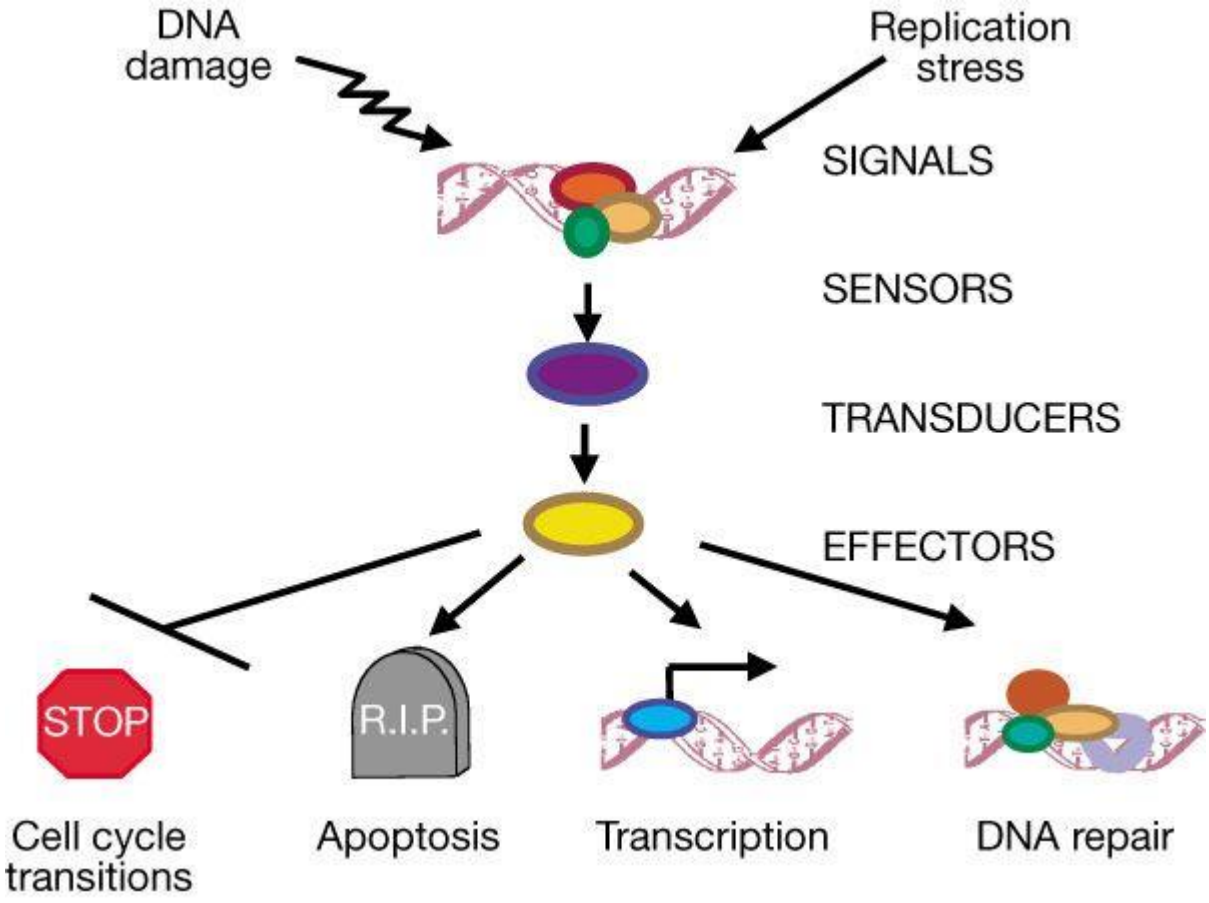

Figure 1 | General outline of the DNA repair signal transduction pathway

Illustration of the DNA repair signalling pathway and outcomes broadly summarises the sequential process of 1) accumulating damage, 2) signalling and sensing the damage by 'sensory' proteins that scan the DNA helix for breaks and distortions, 3) alerting 'transducers' that co-ordinate and activate 'effectors' that directly repair the damage. Arrowheads represent activation events and perpendicular ends represent inhibitory events. (Source: Zhou NB and Elledge, SJ, 2000, p433) (9).

Many DNA nucleases involved in these processes have yet to be characterised, and the activities of known nucleases have yet to be fully elucidated. Several techniques have been developed to study nuclease activity and their binding partners, yet they are either too time-consuming and hazardous to health, such as using radiolabelled DNA nucleotides (13), or the technology is not universally accessible (14,15). As such, there is a need for a simple, fast, inexpensive and safe alternative to support the study of nucleases, and this has been achieved using the commercially available DNA dye, PicoGreen.

1.3 DNA damage signalling upstream of the DNA break site

1.3.1 Kat5 promotes transcription and DNA repair

Kat5 is a member of the MYST family of histone acetyltransferases, based on their founding members ((MOZ, Ybf2/Sas3, SAS2, Tip60/Kat5). These play diverse roles in gene regulation, DNA damage repair, chromatin remodelling, and tumourigenesis (16,17). Recombinant Kat5 acetylates core histones H2AK5, H3K4, H4K5, H4K8, H4K12 and H4K16 *in vitro* (16,17). Kat5 predominantly functions as part of transient multiprotein complexes with the appropriate binding partners. The majority of Kat5 exists within the NuA4-Kat5 complex which performs most of its transcriptional and DNA repair functions (18). Members of this complex include p400 (an ATPase with chromatin remodelling activity) (19,20), RuvBL1/2 (ATP-dependent chromatin remodelling complexes) (21) and Brd8 (recognises acetyl-lysines in cellular proteins and histones to regulate gene transcription) (22,23).

Kat5 is proposed to function upstream of both error-free homologous recombination (HR) and error-prone nonhomologous end-joining (NHEJ). During HR-mediated DSB repair, repressive chromatin complexes are rapidly recruited to the DSB, including the Suv39h1/kap-1/HP1 H3K9 methyltransferase complex (24). This complex briefly tethers itself to H3K9me2/3 through the HP1 chromodomain (25), and radiates rapidly either side of the DSB to form compact nucleosomal arrays (24,26).

Transitioning to an open chromatin state first requires recruitment of the Kat5 complex to DSBs. The shift from the repressive to an open chromatin state requires a mechanism dependent on its key subunits, H2A.Z exchange by p400, coupled with rapid acetylation of histones H2A/H2AX and H4 by Kat5 (20,27–29).

Histone H2A.Z possesses an extended acidic domain that binds to the H4 tail, holding the chromatin in a compact state (30,31). Removal of H2A.Z by NuA4-Kat5 provides an opportunity for Kat5 to rapidly acetylate the liberated H4 tail on lysine 16 (32). Acetylation at this site prohibits further interaction with acidic patches on replacement histones, and loosens the chromatin structure (30,31). It also promotes HR by disrupting the formation of a salt bridge between the positively charged H4K16 and

negatively charged Glu1551 in the NHEJ-promoting 53BP1 Tudor domain (33). H4K16ac also prevents 53BP1 binding to the adjacent H4K20me1/2, which is also present at sites of DNA damage (33). Loss of 53BP1 encourages binding of BRCA1, and thus favours repair by HR. At sites of active transcription, with elevated local acetylation already in place, BRCA1 accrues at the site while 53BP1 is specifically obstructed (33).

BRCA1 activates 5'–3' end resection of DSBs by MRN and CtIP to generate tracts of single-stranded DNA (ssDNA) (34–38). This resection intermediate is coated in Rad51 recombinase and, together, invade the sister chromatid to seek a complementary region to functions as a template for repair (39).

Kat5 may also function upstream of NHEJ through activation of ATM kinase (40,41). ATM phosphorylates a number of targets involved in DNA repair, including HP1 to release it from the chromatin and unveil H3K9me3 for Kat5 binding (24,28). Kat5 binds H3K9me3 directly through its chromodomain following phosphorylation by c-Abl kinase on Tyr44. Concordantly, treatment with Kat5 preparations from IR-treated cells with λ-phosphatase reduces binding affinity of Kat5 to this motif (42). Interestingly, the phosphorylation status of Kat5 bears no effect on its acetylation of H4, yet interaction between Kat5 and H3K9me3 is necessary to stimulate Kat5-mediated acetylation of ATM at Lys-3016 (42). Therefore, H3K9me3 binding functions as an allosteric regulator by increasing Kat5 catalytic activity (28,43). Mutations within the chromodomain that prohibit this interaction also attenuate Kat5 acetylation of ATM. Correspondingly, mutation of the ATM acetylation site inhibits activation of ATM's kinase activity, indicating Kat5 is required for its activation (43).

Along with HP1, ATM also phosphorylates H2AX (γH2AX) (44), which is a marker for DNA repair, and functions as a binding site for several downstream DNA repair proteins. Indeed, phosphorylation of H2AX mediates recruitment of E3 ubiquitin ligases, RNF8/RNF168 through MDC1 (45,46). These generate polyubiquitin binding sites, H2AK14/15ub, for 53BP1. 53BP1 recognises moieties H2AK14/15ub and H4K20me2, and γH2AX is itself a platform for 53BP1 binding (46,47). As such Kat5 is implicit highly upstream of both homologous and

nonhomologous DSB repair, and factors such as cell cycle stage may influence the pathway of repair (26).

FIGURE 2

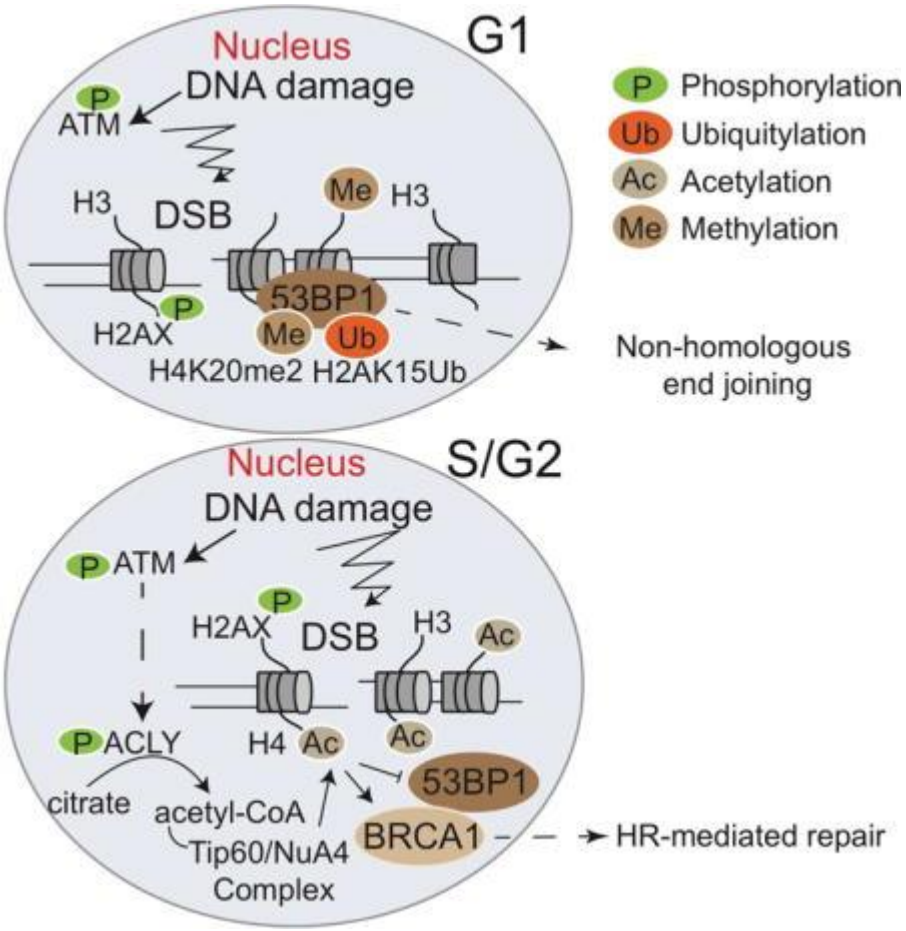

Figure 2 | Overview of Kat5-mediated repair in NHEJ and HR

Illustration of the Kat5 DNA repair pathways that ultimate in recruitment and binding of 53BP1 for NHEJ, or binding and activation of BRCA1 and specific obstruction of 53BP1 for HR (Source: Sivanand S, Mol Cell, 2017, p453) (48).

In addition to its role in DNA repair, Kat5 is also a transcriptional regulator (18). For example, Kat5 can directly acetylate and stabilise the Myc family of transcription factors; these directly influence G1/S progression by regulating genes required for growth, DNA replication and apoptosis (49). Kat5 can also be recruited to Myc-dependent transcription promoters and enhance Myc transactivation activity (50). Whilst Kat5 is generally involved in transcription activation via recruitment of other complexes, it can also co-repress transcription

factors, such as CREB binding protein (51). Intriguingly, dynamic H2A.Z exchange observed at DSBs has also been reported at transcription start sites of many poised genes, and its ejection may allow progression by RNA polymerase II. Whether the Kat5 complex is involved is not yet known (26,52,53).

1.4 Transcription and DNA repair are integral for SHM and CSR

1.4.1 AID relies on active transcription to induce DNA mutations requisite for somatic hypermutation and class switch recombination

Both somatic hypermutation (SHM) and class switch recombination (CSR) are initiated by the mutator protein AID. AID is a small protein of 198–210 amino acids, and is encoded by the *Aicda* gene in humans and mice (54). It is a member of the RNA-editing APOBEC family of cytidine deaminases and converts cytidine residues to uracil exclusively in single-stranded DNA, resulting in a C:G to T:A transition. Processing of uracil by base excision repair (BER) and mismatch repair (MMR) pathways leads to the broader spectrum of point mutations characterising SHM, and to DNA double-stranded breaks (DSBs) which are necessary intermediates of CSR (55,56).

AID activity, and therefore CSR and SHM, is dependent on the ssDNA revealed during transcription. AID interacts with RNA polymerase II and its subunits *in vivo* (57), enabling it to access ssDNA in the wake of the transcription complex. Mutations directed to the human Vλ promoter resulted in abrogation of gene rearrangement and limited production of high-affinity antibodies (58), indicating AID's reliance on transcription. With regards to CSR, placing a non-functional IgH transgene under the transcriptional control of its natural RNA polymerase II-dependent promoter, an RNA polymerase I promoter, or no promoter entirely, saw the mutation frequency in cells lacking a promoter to be greatly diminished in comparison (59).

It is appropriate that AID is linked to transcription considering its affinity for mutating ssDNA rather than RNA or dsDNA. R loops are RNA:DNA structures that occur naturally as a by-product of transcription, and contribute towards transcriptional pausing (60,61). R loops are generally quite rare yet are prevalent during CSR. R loop formation requires high G content on the non-transcribed strand, DNA supercoiling and DNA cleavage, all of which are abundant in S regions (62).

The precise mechanism by which AID deaminates cytidines is unclear. While APOBEC family members may have similar structures, their binding mechanisms and functions differ (63). Indeed, AID binds to DNA structures in a specific manner that is not shared by other APOBECs (64). Evidence suggests that AID acts on cytidines that have been flipped out of alignment. Other deaminases, such as tRNA adenosine deaminase (tadA) and adenosine deaminase acting on dsDNA (ADAR) both act on pre-flipped bases (65,66). Base flipping is employed by other DNA-modifying enzymes such as methyltransferases and uracil glycosylases (67–69). APOBEC3G requires the target cytidine to be flipped out into its catalytic pocket (70), which is likely to be replicated by AID as it deaminates R loop structures that are likely to force DNA bases out of alignment caused by torsional constraints (71). UNG actively flips its target uracil from duplex DNA through a 'pinch-push-pull' mechanism (72), but as AID acts on ssDNA, it is unlikely to entail such a complicated mechanism.

1.4.2 Error-prone DNA repair of AID-induced mutations introduces further sequence mutations

In both mice and humans, SHM mutates the recombined V(D)J region to an accelerated rate of 10^{-5}–10^{-3} mutations per base pair per generation, far exceeding the basal rate of mutation in other cells of ~10^{-9} mutations per base pair per generation (73).

AID recognises 'hotspot' motifs within the V region, selectively mutating WGCW (74). Upon deamination of the target cytosine, a combination of the BER and MMR pathways co-ordinate to repair the break via error-prone mechanisms. In BER, uracil DNA glycosylase (UNG) recognises and cleaves the damaged base, triggering APE1-mediated excision of the abasic site, and re-synthesis of the damaged region by error-prone polymerases (75).

MMR, however, is the major repair pathway in SHM (76). MutSα (Msh2/Msh6) recognises the U:G mismatch and recruits the MutL complex (MLH/PMS2) and proliferating cell nuclear antigen (PCNA). PMS2 exhibits endonuclease activity and introduces nicks spanning the damaged site. Exo1 is a 5'–3' nuclease which resects from this nick and through the damaged region (77).

PCNA helps accumulate mutations at Ig variable regions by recruiting error-prone translesion polymerases, such as θ, η and ζ (78). This is dependent on its mono-ubiquitylation and, correspondingly, B cells of $PCNA^{K164R}$ mice display reduced mutations at A:T sites. In wild-type B cells, mutations at A and T bases are caused by polymerase η, which is particularly error-prone when copying A and T (79,80). It is the accumulation of A:T mutations visualised in SHM and not CSR that indicates that MMR is the dominant pathway in SHM. UNG-deficiency has no impact on A:T mutations at V regions, whereas deficiency in any of the MMR proteins results in cells lacking 80-90% of all A:T mutations (76).

1.4.3 B cells are reliant on DNA repair factors to induce CSR to distinct antibody isotypes

Prior to activation, B cells express solely IgM or IgD antibodies, which have identical, low affinity variable regions. CSR allows for the expression of the IgM and IgD constant region genes (Cμ and Cδ) to be replaced by downstream Cγ, Cε or Cα elements to express IgG, IgE or IgA (81,82) (Figure 1). In doing so, antibody class, or isotype, switching alters the effector function of the antibody (81,82).

Antibody isotype confers the localisation of the antibody within the body, and its functions in response to antigen. IgM is exposed on B cells prior to secondary diversification, and so binds with very low affinity. This is compensated by its ability to form pentamers, endowing high overall avidity. IgM also most efficiently activates the complement system, which involves the sequential proteolytic cleavage of inactive components to cleave and activate enzymes that coat the pathogen surface (83). IgE is found in the mucus and saliva, and antigen-binding triggers mast cells to release potent chemical mediators to induce coughing, sneezing, vomiting and diarrhoea (84). IgA and IgG both neutralise toxins, viruses and bacteria to prevent their adhesion to host cells and inhibit pathogenesis. IgG antibodies typically exhibit higher affinity, and opsonises viruses and bacteria for phagocytosis (85).

Each antibody isotype is associated with a unique upstream G-rich switch (S) region, which is preceded by an intervening (I) exon. The importance of S regions in CSR was observed following deletion of most of Sμ, which dramatically reduced CSR to

downstream C_H regions (86,87). Furthermore, deletion of Sγ1 prevents isotype switching to IgG1 (88,89), without affecting CSR to other isotopes (90).

The cytokines secreted by T cells directs CSR to specific isotypes. For example, IL-4 induces germline transcription from upstream of the S regions of the un-rearranged Cγ1 and Cε genes to induce CSR to IgG1 and IgE (91,92). IL-4 concomitantly downregulates germline transcription of the Cγ2b gene to inhibit CSR to IgG2b (93). In contrast, TGF-β and LPS-stimulated B cells induce CSR to IgA, while impeding IgM and IgG secretion (94,95). The mouse CH12F3-2A cell line is a model of CSR, and specific switches from IgM to IgA-presenting cells in the presence of anti-CD40, IL-4 and TGF-β (96).

The germline transcripts direct AID to the specific S region where AID deaminates cytosine to uracil, prompting uracil excision by UNG (uracil DNA glycosylase). The frequency of AID-induced mutations and subsequent base-excision generates double-stranded breaks, and ultimately results in a recombination event described above.

FIGURE 3

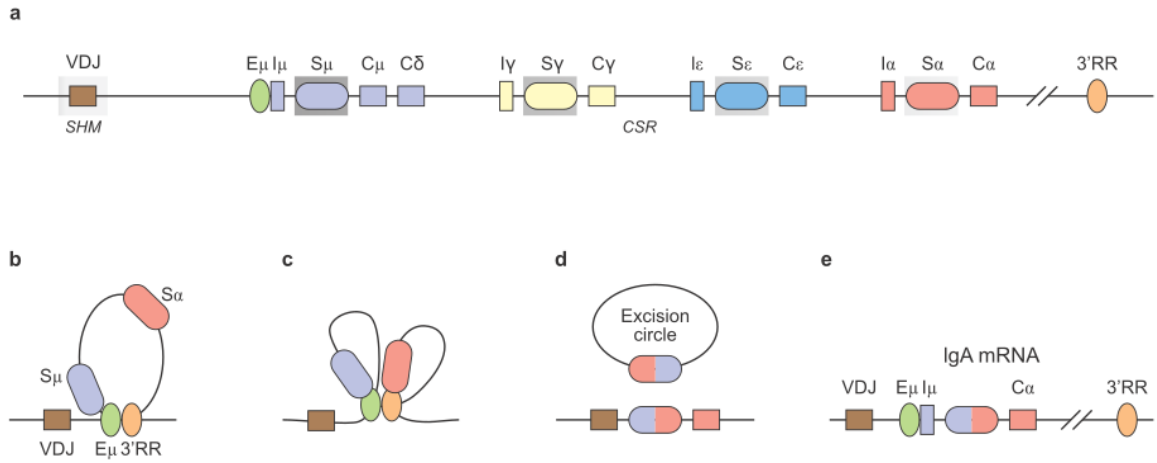

Figure 3 | Illustration of the CSR process

a, Represents the IgH locus which has already undergone V(D)J recombination in the V regions by this point. The C_H region is composed of each isotypic element. Each isotype is associated with an upstream (S)witch region, which is itself associated with an (I)ntervening exon; **b,** Class switching proceeds when Eμ binds to 3'Eα; **c,** This brings the Sμ and Sα regions close together as a consequence; **d,** CSR machinery targets this loop for recombination, removing Cμ; **e,** this allows for expression Cα, which corresponds to IgA.

Numerous components of DNA repair pathways have been implicated in efficient CSR. Processing of the AID-induced DSBs requires ATM (97–103), γH2AX (104–107), MDC1 (45,108–110), 53BP1 (111–115), MSH2 (116–118), MSH6 (119–121), MLH1 (116,117,122), PMS2 (117,123), Exo1 (116,124), and is debatable for MRN (125–132), Ku70/80 (133–136), DNA-PKcs (137–141), XRCC4-DNA ligase IV complex (142,143). These proteins are representative of classical-NHEJ, alternative-NHEJ, HR and mismatch repair. Alternative DNA repair proteins, such as DDX1 helicase has been found to have a role in CSR (144), whereas PARP1 and PARP2, have been shown not to be required (145). Essentially, CSR is highly dependent on the activities of a number of DNA repair factors from diverse repair pathways; HR, classical-NHEJ, alternative-NHEJ, MMR. The extent of their individual contributions in CSR will be discussed in the following review.

1.4.4 Several histone modifiers have been implicated in SHM and CSR

The published review followed at the end of the introduction discusses all known histone modifications and related histone writers and readers that orchestrate SHM and CSR. The sheer number of histone marks that specifically promote an open chromatin state, or recruit AID or DNA repair factors, suggests that Kat5 may also make a valuable contribution to SHM and CSR.

1.5 DNA damage signalling downstream of the DNA break site

1.5.1 Nuclease primary sequences are too poorly conserved to accurately predict function and substrate specificity

DNA nucleases maintain genome integrity. DNA is subjected to exogenous stresses, including reactive oxygen species, radiation, UV light and carcinogens, which all modify the DNA. Endogenous factors can also harm the DNA or form unusual structures, and are generated during replication, recombination, or as the result of mutagenic proteins. It is essential that these errors are corrected to avoid changing the genomic sequence or entangling the DNA, and the vast range of DNA repair mechanisms that have evolved, including base excision repair, nucleotide excision repair, mismatch repair and DSB repair, gives some indication of the range of insults that can be inflicted on the genome (6,146).

TABLE 1

DNA repair pathways	Pathway effectors	Target lesions/functions	Human disease associated with DNA repair defects
NER	XPA, XPB, XPC-RAD23B, XPD, XPE, XPF, XPG, RPA, TFIIH, ERCC1	Bulky and helix-distorting lesions	Xeroderma pigmentosum, Cockayne syndrome, trichothiodystrophy
BER	APE1, MUTYH, UNG, OGG1, NEIL1, NEIL2, NEIL3, NTHL1, MPG, TDG, SMUG1, POLβ, XRCC1, APTX, TDP1, PNKP, LIG1, LIG3, FEN1, PCNA	Base modifications	Cancer predisposition, neurodegenerative disorders, immunodeficiency
MMR	MSH2, MSH3, MSH6, MLH1, PMS2, EXO1	Sequence mismatches	Lynch syndrome (hereditary nonpolyposis colorectal cancer), Lynch syndrome variants, sporadic colon cancer, noncolonic tumors
HRR	BRCA1, BRCA2, RAD50, RAD51, MRN, XRCC2, XRCC3	DSBs- S–G_2 phase acting	Hereditary breast ovarian cancer syndrome
NHEJ	KU70, KU80, XRCC4, DNA-PKc, DNA ligase IV	DSBs- G_1–S phase acting	Syndromes with brain development defects and immunologic abnormalities
Fanconi anemia pathway	FANCA, FANCC, FANCD1/BRCA2, FANCD2,	Interstrand DNA cross links	Fanconi anemia

Table 1 | DNA repair pathways, target lesions and diseases associated with repair defects
(Source: repurposed from Saccà HS, *et al*, 2012) (6).

The primary sequences of nucleases are poorly conserved, except for motifs related to their catalytic sites (147,148). Active sites typically contain acidic and basic residues that coordinate catalytically essential divalent cations, such as magnesium, calcium, manganese or zinc as a cofactor to stabilise reaction intermediates. Cleavage reactions take place either at the terminal end or within the DNA, categorising nucleases as either exonucleases or endonucleases, respectively. Exonucleases can then be classified further as 5' or 3' processing due to their polarity of consecutive cleavage (147).

Tertiary structures of nucleases offer more resolute properties, and fold into more conserved features that facilitate classification into enzyme families (147,148). Despite these preserved features, the specific activity and substrate preferences remains wildly divergent. Furthermore, crystalizing nucleases has often proven tricky to perform. Either because the nuclease under study is 1) too toxic when overexpressed

(149,150), 2) insoluble without its proper substrate (150–152), 3) not pure enough because it co-precipitates with non-specific binders (150), or 4) the substrate is unknown hence the lack of adequate enzyme:substrate structure which is more informative than enzyme structure alone (153). The DNase I-like fold is observed in DNase I (154), ExoIII (155), Ape1 (156,157) and some phosphatases (147). While similarities are present in the active sites, the topology surrounding the active sites are different. As such, while both DNase I and ExoIII digest ssDNA and dsDNA, ExoIII exhibits 3'–5' polarity, resecting just one strand of duplex DNA. Likewise, FEN1 and Exo1 share a resolvase-like domain, and both cleave 5' overhangs, such as is required in Okazaki fragment processing during replication (158), only Exo1 exhibits a powerful 5'–3' exonuclease function that is important for repair of mismatched nucleotides, replication and meiotic recombination (159,160). Therefore, quick and high throughput biochemical analyses are essential to be combined with structural analysis to fully decipher the specific roles of nucleases. Understanding their structural preferences and directionality will ultimately determine how they are implicated in repair.

1.5.2 DNA repair nucleases are generally structure-specific and not sequence-specific

As illustrated by the above examples of FEN1, Exo1 and DNase I, DNA repair nucleases recognise specific structures rather than nucleotide sequence to trigger cleavage. This is typical of most DNA repair nucleases involved in replication, repair and recombination (148). Most DNA polymerases possess proofreading 3'–5' exonuclease activities to minimise incorporation of non-complementary nucleotides. DNA polymerases recognise the geometry of correct base pairing, slow catalysis and transfer the mismatch into the exonuclease active site (161); this quality control process is thought to enhance replication fidelity 100 to 1000-fold (162–164). *Pold1* or *Pole1* exonuclease-deficient mice exhibit 10-fold more mutagenesis and exhibit cancerous phenotypes and reduced survival (165–167). Furthermore, sequence changes have been identified in *POLD1* in human colon cancer cell lines and patient tumour samples (168). While most of these changes bore no functional effect, an R689W mutation caused lethality when modelled as a homozygous mutant in the catalytic subunit of POLδ in *S. cerevisiae* (169).

In some cases, nucleases do exhibit some sequence preference. The *E. coli* Exonuclease III recognises short 3' overhangs, yet it has been suggested that it preferentially cleaves bases C>A~T>G (170). DNase I has also shown a general proclivity for AT base pairs as opposed to GC base pairs (171).

1.5.3 DNA nucleases rarely act autonomously

DNA nucleases tend to function as part of larger complexes for improved efficiency. Nbs1 is critical for triggering Mre11 endonuclease activity in the MRN complex for optimal DSB repair (15). The MRN complex also functions as a processivity factor to maintain Exo1 on DNA and promote extensive resection (15). Human SOSS1, a protein that shares structural homology to *E. coli* single-stranded binding protein (SSB), also promotes long-range resection by Exo1 (14), whereas BLM helicase increases Exo1 affinity for DNA ends (172). Artemis is an end-processing nuclease in the error-prone DSB repair mechanism of nonhomologous end-joining. Independently it possesses 5'-3' exonuclease activity, and interaction with DNA-PKcs permits its endonucleolytic processing of hairpin loops (173). This ability to open hairpin loops is particularly important for V(D)J recombination. It represents the primary stage of antibody diversification which involves the rearrangement of antigen-binding variable (V), diversity (D) and joining (J) regions. Here, hairpin-capped DSBs are generated by the RAG1/2 recombinase. Terminal deoxynucleotidyl transferase (TdT) incorporates nontemplated nucleotides to the ends before the break is sealed, introducing more diversity into the coding sequence (173). Defects in either Artemis or DNA-PKcs are associated with the immune disorder severe combined immunodeficiency (SCID) (174,175).

To date, only 8 autonomously-acting 3'–5' DNA nucleases have been identified (176,177). These may support polymerases that lack intrinsic 3'–5' exonuclease activities; of the 14 human DNA polymerases, only 3 display proofreading capabilities (178), and these autonomous nucleases may provide this, such as is suspected for Trex1 and Trex2 (179,180).

1.6 Current methods for characterisation of DNA nucleases

Conventional nuclease assays predominantly involve the use of radioactive labelling to visualise DNA substrates on an agarose gel (181–183). The use of radioactive

isotopes delivers highly specific, sensitive assays that are free from interference. However, these assays are often inefficient, time-consuming, qualitative, and potentially hazardous (184,185). Additionally, the assays are discontinuous, and must be stopped at discrete, often arbitrary, time points before measuring readouts (13). Whilst this can provide an indication of reaction rate, it does not allow for real-time visualisation of the catalytic resection activity.

Radiolabelled oligonucleotides are gradually being replaced with fluorescent nucleic acid stains such as DAPI (186) and other commercially-available dyes including, but not limited to, Midori Green, SYBR Green I and Acridine Orange (187). PicoGreen (PG) is a commercially available dye that emits a fluorescent signal upon intercalation with double-stranded DNA (dsDNA), emitting a fluorescent signal 1,000-fold stronger compared to when it is free in solution. The superior sensitivity can quantify picogram or nanogram levels of dsDNA, respectively, unlike other fluorescent dyes, including Hoechst (188), ethidium bromide (188), EvaGreen (189), SYBR Green (189) and YOYO-1 (189).

One particularly impressive technique is the recently published design of DNA curtains for single-molecule imaging (14,15). DNA is tethered to one end of a fluid lipid bilayer and targeted by nucleases stained with fluorescently-tagged antibodies. Reaction progression is captured through a total internal reflection fluorescence microscope (TIRFM) (14,15). This technique aims to obtain statistically relevant information on these biochemical reactions. Although effective and highly sensitive, this technology may not be accessible to researchers worldwide.

Several other sophisticated fluorescent techniques have been devised, building upon the use of FRET, whereby fluorescence is either quenched or dequenched following nuclease activity (190). A recently published DNA curtain method involving graphene oxide surfaces (191), electrochemical redox reactions (192–194), complexing of DNA with a polycationic polymer (195), or immobilising nucleotides on magnetic beads (196) have also been developed. While highly sensitive, these methods have been designed purely for the detection of a very limited number of DNA and RNA nucleases rather than for general characterisation (197).

A very different technique studies the kinetics of proteins following DNA damage to measure their stepwise recruitment *in vivo* (198). Using transgenic cell lines that stably express eGFP-tagged DNA repair proteins, under the control of their own regulatory sequences, ensures the expression of these proteins at close to physiological levels (198). Again, this offers a new perspective on repair and provides a global view of how dysregulation of one repair factor affects the entirety of DNA repair kinetics (198).

1.6.1 Development of an alternative nuclease resection assay

Despite the myriad techniques available to study DNA nucleases, there exists a need for a rapid, cost-effective and safe protocol that monitors reaction progression in real-time and is accessible to all lab groups. With these parameters, a highly versatile fluorescence-based nuclease resection assay has been developed to study nuclease activity on a selection of DNA substrates with the sensitivity to calculate reaction kinetics.

1.7 Research objectives

DNA nucleases function downstream of Kat5 signalling to remove damaged bases in the genome and to generate DNA substrate intermediates that are subsequently replicated and ligated by DNA polymerases and ligases (6,146,199). Many of the DNA nucleases directly involved in DNA repair have yet to be fully characterised, while many have yet to studied at all. Conventional techniques for studying nuclease activities are hazardous, laborious, time-consuming, and capture activity in a discontinuous manner (13,184,185). As such, there is a need for a safer alternative method that can visualise reaction progress in real-time. Using the commercially available dsDNA dye, PicoGreen, it is hoped that the methods described in Chapters 3 and 4 represent that safer alternative.

Chapters 3 shall describe:

1) The stabilisation of PicoGreen;
2) DNA substrate optimisation to generate a highly fluorescent substrate that is less-sensitive to photobleaching;
3) The development and validation of a real-time nuclease assay using well-characterised nucleases.

Chapter 4 shall describe:

1) The further improvement of the assay to study the kinetics of both single- and double-stranded DNA nucleases and nickases;
2) The development of the assay to study DNA polymerisation;
3) The expansion of the DNA substrate library to include physiologically relevant DNA modifications.

Evidence suggests that Kat5 functions upstream of both canonical homologous and non-homologous repair pathways (26,200,201). Kat5 also promotes transcription by acetylating histone proteins at promoter regions (202–204). Yet, although CSR is dependent on both transcription and DNA repair, no known role for Kat5 in secondary antibody diversification has been described. This may be due to the fact that, as Kat5 is essential for viability (205), it is a challenging protein to manipulate intracellularly. It is hoped that the studies described in Chapters 5 and 6 shall contribute towards elucidating the mechanistic pathway leading from the histone code and culminating in DSB repair in both DNA canonical repair and in CSR (18).

Chapters 5 shall describe:

1) The optimisation of Kat5-specific chemical inhibitors; imatinib (206), iChromo and TH1834 (207), which differentially target Kat5 activities
2) The comparison of the phenotypes that result from chemical inhibition should enable separation of function analyses of Kat5 during DNA repair;
3) The use of a CH12F3 mouse cell line that models CSR (96) to quantify class switching efficiency in the presence of these inhibitors; this will establish a role for Kat5 as an essential component of class switching.

Chapter 6 shall describe:

1) The design of mouse and human inducible Kat5 degron constructs to avoid the lethality of Kat5 knockout cell lines (208).

2 Review: Epigenomic modifications mediating antibody maturation

This review was published in Frontiers in Immunology on 26th February 2018 and has been resubmitted as part of this thesis.
https://doi.org/10.3389/fimmu.2018.00355

Epigenetic modifications, such as histone modifications, DNA methylation status, and non-coding RNAs (ncRNA), all contribute to antibody maturation during somatic hypermutation (SHM) and class-switch recombination (CSR). Histone modifications alter the chromatin landscape and, together with DNA primary and tertiary structures, they help recruit Activation-Induced Cytidine Deaminase (AID) to the immunoglobulin (Ig) locus. AID is a potent DNA mutator, which catalyzes cytosine-to-uracil deamination on single-stranded DNA to create U:G mismatches. It has been shown that alternate chromatin modifications, in concert with ncRNAs and potentially DNA methylation, regulate AID recruitment and stabilize DNA repair factors. We, hereby, assess the combination of these distinct modifications and discuss how they contribute to initiating differential DNA repair pathways at the Ig locus, which ultimately leads to enhanced antibody–antigen binding affinity (SHM) or antibody isotype switching (CSR). We will also highlight how misregulation of epigenomic regulation during DNA repair can compromise antibody development and lead to a number of immunological syndromes and cancer.

2.1 Chromatin landscape modulates DNA repair and antibody diversification

B cells experience dramatic fluctuations in their epigenomic landscape throughout haematopoiesis. During B cell development, the genetic rearrangement of germline variable (V), diversity (D) and joining (J) gene segments in the Immunoglobulin heavy chain locus (Igh) and V and J gene segments in the Immunoglobulin light chain locus (Igk) creates a diverse B-cell receptor (BCR) repertoire, which mediates a primary antibody response upon antigen encounter. To ensure an effective and long-lasting antibody response, upon binding of antigen to the BCR, in a T-cell dependent response, B-cells are triggered to enter the germinal centre (GC) microenvironment. Here, the affinity of the BCR is increased via a process called somatic hypermutation (SHM) and the class of the constant region is switched to increase the effector function

in a process called class switch recombination (CSR). Subsequently, class switched B-cells expressing a high affinity BCR will be positively selected in the light zone of the germinal centre and will differentiate into long lived plasma cells and memory B-cells. It has become increasingly apparent that epigenetic modifications are indispensable for the antibody maturation processes during SHM and CSR at antibody producing genes. Both SHM and CSR are initiated by the mutator protein, Activation-Induced Cytidine Deaminase (AID), which catalyses cytosine-to-uracil deaminations on single-stranded DNA (ssDNA) at immunoglobulin genes, to create U:G mismatches, which ultimately leads to immune diversity (209). It is the divergent downstream processing of this regulated DNA damage, by DNA repair mechanisms, which forms the highly mutated antibody-binding variable (V) regions in SHM. This ultimately gives rise to B-cell receptors (BCR) of differing affinities. Furthermore, the double-stranded breaks at the Switch (S) regions integral for CSR, give rise to a range of BCR constant regions which results in secretion of antibodies with varying effector functions (210,211).

Precursory circulating IgD^+ naïve B cells that have yet to undergo antibody diversification have hypermethylated immunoglobulin (Ig) loci and minimal histone acetylation signatures, rendering the underlying DNA inaccessible to transcriptional machinery and AID catalysis. This is in stark contrast to activated GC B cells, which accumulate open chromatin marks at the Ig loci that correlate with the induction of SHM and CSR, and the onset of transcription-coupled AID-dependent mutations (212–214). Specific histone modifications are responsible for relaxing local chromatin structure (such as H3K4me3 H3K14ac), whereas others directly propagate DNA repair pathways (such as H2AK119ub and H4K20me2; discussed below). More recently, both histone marks and RNA-based structures have been implicated in targeting AID to the Ig locus (Figure 3) (214,215).

FIGURE 1

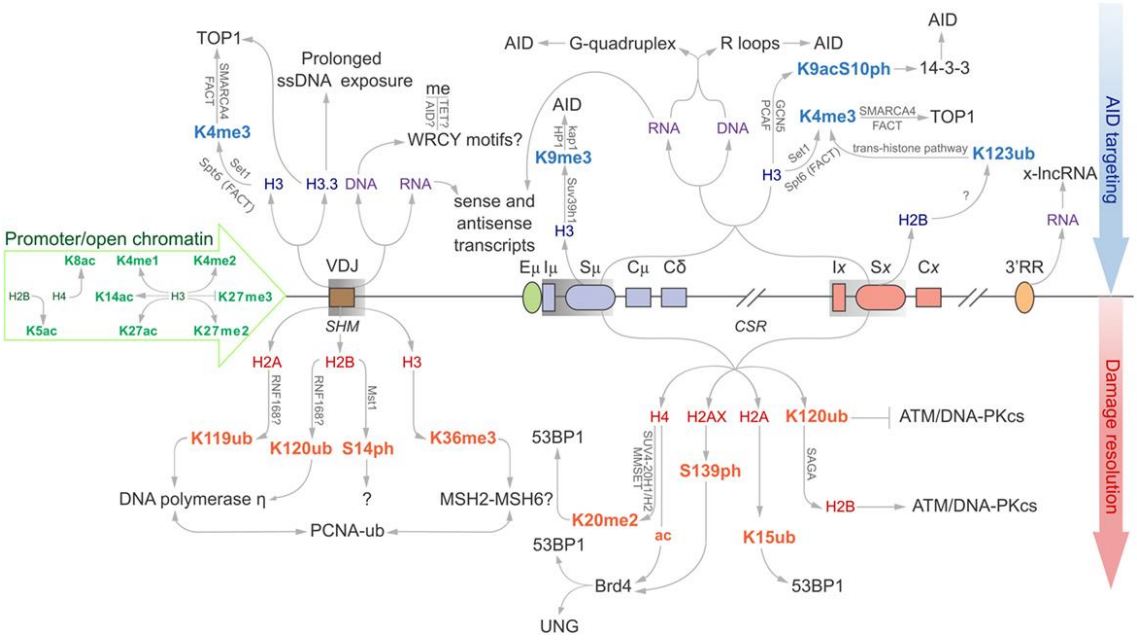

Figure 1 | Epigenomic modifications directing antibody-diversification processes somatic hypermutation (SHM) and class switch recombination (CSR).

Green core histones and associated modifications are involved in chromatin de-compaction and enable transcription through the immunoglobulin (Ig) locus. All factors above the locus are important for the generation of DSBs while everything below encourages mutagenic repair at the V region, and DSB repair at donor and acceptor S regions (Sμ and Sx, respectively). Blue histones and affiliated modifications help recruit or tether AID and other factors that facilitate production of DSBs. Purple DNA and RNA are linked with sequences and structures that facilitate AID recruitment or targeting. Red core histones and accessory modifications recruit DNA repair proteins to ensure excision of intervening C_H region for successful class switching as well as error-prone polymerases to the V region.

The physiological activity of AID is critical to maintain immune diversity, while high-fidelity DNA repair factors are important to maintain genome integrity. Misregulation of, or mutations in, these DNA repair processes can have serious consequences, spanning cancerous transformation (216), developmental defects (217), autoimmunity (218) and immunodeficiency syndromes (219). In this review, we aim to provide a cohesive understanding of higher-order epigenomic processes critical for the regulation of B cell maturation, manipulation of DNA repair mechanisms, and insights into the development of debilitating cancer- and immune-based diseases.

2.2 Epigenomic factors target AID to V Regions for SHM

SHM enhances antibody affinity through the accumulation of point mutations at the antigen-binding V region (220). Histone marks help target AID to key sites of the Ig locus. AID preferentially deaminates cytosines in WRC motifs. These AID 'hotspots' are present in Ig genes undergoing SHM (Igh, Igk) and CSR (Igh) which are mutated in high abundance. However, these hotspots are also prevalent at non-Ig genes, but carry significantly less mutational load (221), indicating that the presence of these hotspots alone is insufficient to recruit AID. Rather, higher order mechanisms must be in place to regulate AID activity and targeting. RNA structures, specifically coding messenger RNAs (mRNA), non-coding RNAs (ncRNAs), and defined histone signatures, represent additional mechanisms for AID targeting.

2.3 Role of mRNA and ncRNA in SHM

Sense mRNA transcripts have been detected at Cμ regions, which seem refractory for AID-induced mutations, while both sense and antisense transcripts have been observed at the neighbouring V and S regions (215). Interestingly, V and S regions are susceptible to AID deamination, but not C regions. Whether that is due to efficient error-free repair or lack of AID targeting remains to be addressed (222–224). The sense and antisense transcripts are thought to be free to bind to complementary regions on both stands of the transcription bubble during SHM and CSR. This forms an R-loop, a three-stranded DNA:RNA hybrid and the associated non-template ssDNA that can provide a ready target for AID the biochemistry (54). This should be reflected in the mutation profile observed at the V region, which should be equally prolific along the V region. Instead, most mutations take place within the first few hundred base pairs, before tapering off as distance from the TSS increases. Antisense transcripts originating from downstream of the recombined VDJ region should compensate for this, and AID should be equally able to access this downstream DNA. As there is no clearly defined antisense TSS, it is possible that there is reduced antisense transcription relative to sense. It is also possible that anti-sense transcripts suffer shorter half-lives (225). Regardless, this offers further proof that RNA transcripts support SHM and CSR, despite the imbalance in mutation frequency along the V region.

2.4 V region histone modifications stabilize AID substrates and recruit DNA repair proteins to support SHM

Various histone modifications have been implicated in SHM. Many of these are generally associated with open chromatin and active transcription, while others appear to have more defined roles in actively supporting antibody maturation (Figure 3) (226). A significant histone mark enriched at sites of SHM and CSR is H3K4me3. Transcription elongation factor Spt5 helps to introduce H3K4 tri-methylation through the trans-histone modification pathway (227), alongside the Facilitates Chromatin Transcription (FACT) complex, to support transcription elongation. Spt5 has an additional role as an adapter protein to link AID and RNA polymerase II (228).

H3K4me3, SMARCA4 and FACT complex components are equally important for recruitment of Topoisomerase I (Top1) (229). Top1 typically acts to correct transcription-induced negative supercoiling caused by RNA polymerase II by nicking one strand of the DNA helix, passing the other strand through the break, and re-ligating the nicked end. Reduction of Top1 increases SHM mutagenesis, whereas overexpression of Top1 downregulates SHM. Interestingly, treatment with the Top1 catalytic inhibitor, camptothecin, suppresses SHM. These results indicate that the cleavage activity of Top1 is required for SHM, and not its ligation activity (230).

The H3.3 histone variant is another feature associated with SHM and is enriched at the VDJ region in chicken DT40 cells (228). H3.3 appears to be responsible for stabilising the ssDNA substrate for AID activity. R-loops are often cited as a predominant AID substrate in C regions, although treatment with RNase H to remove these R-loops from the V region of wild type and H3.3-null DT40 cells identified that loss of these structures does not impede accumulation of AID-induced point mutations. H3.3 may instead be responsible for mediating RNA polymerase II pausing, prolonging exposure of the transcription bubble, and promoting AID targeting (231,232). Other structures have been proposed to facilitate ssDNA exposure, such as the formation of negative supercoils upon activation of RNA polymerase II transcription. It appears that topoisomerase is unable to repair this topological strain at the same rate that RNA polymerase II progresses (233), and this creates localised denaturation bubbles that are ideal substrates for AID (234). Unfortunately, the mechanism by which H3.3 stabilises ssDNA substrates remains elusive.

Ubiquitination of proteins is an essential modification to propagate repair of mutated regions in SHM; histones and Proliferating Cell Nuclear antigen (PCNA) are well-known targets. Ubiquitinated (Ub) H2AK119 and H2BK120 are specifically associated with V regions, but not with constant region exons (C_H) (Figure 3). These histones co-localise with translesion DNA polymerase η, which possesses a ubiquitin-binding domain that binds to mono-ubiquitinated PCNA at lysine 164. DNA polymerase η introduces all the A:T mutations in SHM, but limited mutations in CSR, indicating polymerase η of mismatch repair (MMR) is the dominant repair polymerase only in SHM (235,236). It is not known whether PCNA is ubiquitinated before or after being recruited to V regions (237). Surprisingly, the E3 ubiquitin-ligase RNF8 is known to ubiquitinate PCNA, yet has only been shown to support CSR (238–240). It is therefore possible that although mono-ubiquitinated PCNA enhances the mutation profile for SHM, its downstream repair effects in CSR are selected against, as large regions of DNA containing these mutations are disposed of following recombination at S regions.

Resolution of mismatched bases is heavily dependent on “corrupted” repair mechanisms. However, there are conflicting reports over the relative involvement of MMR and BER components. DNA uracil glycosylase recognises and cleaves uracil bases from the genome in BER, while MutSα recognises mismatched bases and recruits several downstream effectors during antibody diversification, e.g. exonuclease I (Exo1) in MMR (241). MSH6 likely promotes SHM and CSR following recruitment by mono-, di- and tri-methylated H3K36 through its PWWP motif. Many other proteins involved in DNA damage responses and histone modifications also carry this PWWP motif to promote chromatin interactions (242), including PCNA. Indeed, MMR has been implicated as the principle repair pathway in SHM, following observations that the absence of UNG of the BER pathway has very little impact on the accumulation of A:T mutations, and loss of MSH2, MSH6 and Exo1 lose 80-90% of A:T mutations independently (243). Interestingly, PCNA also interacts with MSH6, which may account for its targeting to appropriate regions during antibody maturation (237,244). However, it is worth noting that these latter chromatin modifications are not specific to antibody genes and could happen genome-wide. Though it is possible that they acquire added importance by being combined with antibody gene-specific chromatin valencies (245).

One histone modification without a clear role in SHM is H2BS14ph (246). While it serves as a marker for SHM in B1-8 GC B cells, the implications of losing this modification are unknown. H2BS14ph is not present at VJλ1, V_H or Sμ in naïve B cells, or B cells 14 days post-activation, but was reproducibly detected at day 10. Consistent with these observations, the only known H2B kinase, Mst1, is present at these sites only at day 10 (246). It is possible that this histone mark is linked to a distinct DSB repair response at V regions around day 10, whereas γH2AX is associated with DSB repair at S regions (104,246). The strict temporal restriction of the occurrence of this histone mark at day 10 may signify that AID-dependent lesions occur at earlier stages of the GC response, or it may only be required at earlier stages, perhaps for recruitment of downstream proteins (246).

2.5 DNA and RNA structures target AID to S regions for CSR

CSR is achieved through the generation of DNA DSBs and subsequent ligation of two distal S regions (220). Transcription alone cannot determine deamination targets for AID, as many genes transcribed in activated B cells are not targeted by AID (247). Instead, S regions encode unusually high densities of the overlapping AID hotspot WGCW sequences that place two WRC motifs in on opposite strands of the dsDNA helix. AID preferentially deaminates the underlined cytosines and, in the event of parallel deaminations, the resulting nicks on each strand (following UNG and APE1 activity) would inevitably produce a DSB. CGC is yet another hotspot, although it rarely appears within S regions. Indeed, WGCW density correlates strongly with CSR efficiency, much better than when WRC alone was considered to predict S region quality (74).

2.5.1 DNA secondary structures affect mutation targeting preference

Recent work has shown how AID preferentially binds guanine-rich DNA quadruplex structures compared to linear DNA of the same sequence (64). Through dissection of the core quadruplex unit, it was determined that AID binds to the adjacent ssDNA strands at a stoichiometry of AID_2/DNA (64). It requires a binding site of at least 5 nucleotides (64). By studying the distance of the deoxycytidine (dC) in hotspot (AGCT) and cold spot (TTCT) motifs from the quadruplex, it became clear that peak deamination occurs when dC is at third position, and is independent of the sequence,

suggesting that the quadruplex structure overrides sequence motif preferences (64). However, as the dC is shifted further from the quadruplex, this preference for AGCT is approximately double that of the TTCT, recapitulating hotspot preference seen in a multitude of *in vitro* and *in vivo* assays (248,249). Interestingly, in S regions, a dC is often present at precisely the third position from the G-repeat (64). This binding preference is also observed in RNA quadruplexes (64). Accordingly, AID has two DNA-binding faces: the substrate binding channel and the 'assistant patch' (64). In such a model, the assistant patch enhances AID affinity for the substrate, and increases its deamination activity. This bifurcate binding structure is unique to AID, and is not seen in AID homologues, explaining why this bifurcate binding phenomenon and cooperativity is not observed in APOBEC3A or APOBEC3G (64).

This preferential binding to quadruplex DNA has previously been observed, whereby AID targets proto-oncogenes to introduce translocations at c-MYC and BCL6, among others (247). Lymphomas in which these proto-oncogenes are unstable derive from germinal centre B cells. For example, a hallmark of Burkitt's lymphoma is c-MYC recombination with S regions, promoting deregulated expression of this crucial gene (250). In addition, c-MYC, PAX5 and BCL6 translocations are associated with progression from follicular lymphoma to the more aggressive diffuse large B cell lymphoma (251), and PAX5/IgH translocations have been identified in a subset of non-Hodgkin's lymphomas (252). This genomic instability does not correlate with WRC sequence, but instead correlates with G-rich regions (247). Furthermore, this G-richness does not characterise translocation breakpoints in AID-null B and T cell malignancies (247). Most translocations associated with leukaemias in AID-null cells results from a mechanism that is independent of G-rich content, yet the data suggest that in germinal centre B cells in which AID is highly expressed, AID preferentially targets transcribed G-rich regions, and therefore its stringent targeting to the Ig region is essential to maintain genomic stability.

2.5.2 RNA secondary structures also contribute to mutation targeting

Transcription through S regions has been associated with AID targeting to the IgH locus through the formation of R-loops and the interaction between AID and RNA polymerase II (232). While germline transcripts through I_H-S_H-C_H regions have been implicated in antibody diversification, their mechanistic function has only recently been

demonstrated. AID binds directly to sense germline transcripts as well as to telomere RNA (253). These transcripts are also G-rich and form G-quadruplex structures. Ablating the G-quadruplex structure through G-to-C mutations, or inhibiting the splicing machinery that supports formation of these secondary structures, disrupts AID interaction with the transcripts and concomitantly reduces CSR (253). Amino acids 130–138 in AID show homology to the RNA-binding domain of RHAU, a known binder of G-quadruplex RNAs. Mutations in this binding region also perturb AID:RNA binding capacity, consistent with hyper-IgM patients possessing a G133V mutation (253). Whether this mutation impedes AID:DNA binding is unknown, though it may be involved in the transfer of AID from its RNA guide to the DNA substrate. This is also suggests that some RNA splicing proteins such as PTBP2 and CTNNBL1 may also play an indirect role in CSR by shaping the ncRNA architecture (253–255).

Although this provides a detailed explanation of the mechanism behind AID targeting to S regions for CSR, it fails to explain AID targeting to V regions. More research is needed to determine if this RNA binding capability is indeed distinct for CSR, as it may be responsible for deviance in processes downstream of AID-induced mutation in SHM and CSR. As previous reports have shown that the C-terminal amino acids 189-198 are vital only for CSR (256,257), it is unlikely that the RNA-binding region explains this whole process.

Studies suggest that the RNA exosome complex is recruited to S regions in an AID-dependent manner, and makes the transcribed strand accessible to AID deaminations by degrading the complementary-bound nascent RNA strand (258). Knockdown of the RNA exosome reduces CSR by 30–50% compared to controls. The RNA exosome also promotes quality control on the antisense transcription of ncRNA from TSSs, which have the ability to both recruit AID and generate ssDNA substrates for its catalytic activity (259). By degrading superfluous antisense RNAs, which increases the formation of RNA:DNA hybrid structures and heighten risk of premature transcription termination and genomic instability, the RNA exosome protects genomic integrity (259). In addition, the RNA exosome appears to control a long ncRNA (lncRNA) expressed from a divergent enhancer element, which directly regulates the 3’RR of the IgH locus by enhancing the looping activity known to promote CSR activity(260,261) (Figure 3). Unexpectedly, although histone acetylation and

deposition of H3K4me3 coincides with B cell development stages along the *Igh* locus, major epigenetic alternations have not been detected at the 3'RR upon splenic B cell activation (262,263).

2.5.3 miRNA Control of Antibody Production by Regulation of SHM and CSR

It has been well-documented that miRNAs can regulate SHM and CSR in B cells, chiefly through modulating AID and Blimp-1 expression (261,264–267). miRNAs such as miR-155, miR-181b and miR-361 can silence AID expression (264,266,268,269), whereas miR-30a and miR-125b can silence Blimp-1 expression (270–272) which is required for plasma cell differentiation and antibody production. These miRNAs bind to evolutionary conserved target sites in the 3'UTR of *Aicda* and *Prdm1* mRNAs. More recently, histone deacetylase inhibitors have been reported to repress the expression of AID and Blimp-1 by upregulation of these miRNAs (273).

In particular the more prominent role of miR-155 in regulating activated B-cells and the GC response is becoming more established. MiR-155 is directly repressed by BCL-6, the master regulator of GC formation, which is upregulated in the dark zone, repressing genes involved in cell cycle arrest, DNA damage response and plasma cell differentiation and thus allowing SHM to take place. miR-155 deficiency in B-cells has been shown to decrease the number of IgG1+ plasma cells and memory B cells and abolish the production of high affinity IgG1+ antibodies indicating that miR-155 plays a key role in affinity maturation and CSR. More recently, miR-155 has been reported to be involved in the survival of positively selected GC B-cells (274–278).

What is now beginning to emerge however, is the notion that miRNA can be transferred from one immune cell to another through an understudied "epigenetic shuttle" called exosomes that can transport RNA and protein factors (279). Exosome 'shuttling' of miRNAs and antigen between B and T cells occurs following construction of the immune synapse (280–282). This may indirectly support CSR by potentiating a feedback loop between T helper cells and activated B cells. B cells persistently stimulate T helper cells to secrete cytokines that promote CSR, such as TGFβ1, IL-2, and IL-4 (283). 12% of B cell-internalised antigen is spared destruction and is instead secreted on exosomes that are received by the bound T helper cells to encourage cytokine production (284). A specific role for miRNAs in directing this targeted

approach towards antibody maturation has yet to be elucidated and further research in the regulatory potential of this process is required.

2.6 Histone modifications decorate the donor and recipient S regions to recruit AID in CSR

Specific cytokine stimuli act on activated B cells to drive recombination between donor and desired recipient S regions to select for a particular Ig isotype. The Sμ region is always primed for class switching as histone modifications that are generally associated with an open chromatin state (including H2BK5ac, H3K9ac, H3K14ac, H3K27ac, H4K8ac, H3K4me3 and H3K36me3) are enriched at this site prior to antigen-engagement. As such, Iμ-Sμ-Cμ transcripts are also constitutively expressed (213,285–291). The remainder of the chromatin modifications could be broadly categorized into two general pools, targeting modifications upstream of AID recruitment and downstream modifications mostly associated with the general DNA damage response (Figure 3). Indeed, acetylated H3 and H4 fall broadly within these two categories as H3ac correlates with germline transcription in unstimulated splenic B cells, while H4 acetylation is observed following B cell activation, likely in response to AID-induced DSBs (285). This is observed in the 1. B4.B6 B cell line. These B cells undergo CSR to γ3 upon treatment with LPS+CD40, and CSR to γ1 and ε1 following treatment with LPS+CD40+IL-4. Following LPS+CD40 treatment, γ3 GLTs are induced, while γ1 and ε1 GLTs are repressed. Correspondingly, H4ac levels at Sμ, Iγ3 and Sγ3 are increased, whereas S regions and promoters for γ1 and ε1 loci are marginally affected. The reciprocal is observed upon LPS+CD40+IL-4 treatment for GLT expression and H4ac. This suggests that regions of chromatin are specifically remodelled to identify the S region for AID mutation (285).

Permissive transcriptional histone marks are abundant in S regions, including H3K4me1/2/3. NHEJ-compliant protein PTIP typically facilitates distribution of these marks through its interaction with MLL3/MLL4 to support DNA repair and transcription. Unexpectedly, the interaction between PTIP and MLL3/MLL4 is dispensable for *Igh* germline transcription and is mostly responsible for H3K4me1/2 production. Recently, a sub-complex made up of PTIP-PA1 appears to promote H3K4me3 formation through other unidentified histone methyltransferases. The function of this complex facilitates the transcription preceding AID deaminations, promoting CSR to IgG isotypes, and

appears to have very little influence on DNA repair(35,292). Nevertheless, MLL4 is important for maintaining effective CSR; it is frequently mutated in diffuse large B cell lymphoma and follicular lymphoma (293), and hypogammaglobulinaemia is common in the heritable Kabuki syndrome, often attributed to MLL4 mutations (294).

Specific chromatin modifications have been implicated as markers for the donor and recipient, and thus as possible recruiters of AID and/or other components of the CSR machinery. Tri-methylation of H3K4 is facilitated by the FACT complex. Knockdown of FACT components SSRP1 and SPT16 in the CH12 B cell lines results in a significant decrease in IgA switching (290), and corresponds with an overall decrease in H3 methylation in the Sμ region, and a specific reduction of H3K4me3 in the Sα region. The components acting downstream of the H3K4me3 marker that lead to CSR remain elusive, although DNA cleavage assays have shown that breaks in the Sμ and Sα regions are significantly reduced in SSRP1 and SPT16 knockdown cells (290,295).

H3K4me3, SMARCA4 and FACT help mediate CSR through recruitment of Top1, as they do for SHM (229,290). Reduced levels of Top1 renders it unable to keep pace with RNA polymerase II, accumulating negative DNA supercoiling at the rear. Repeat sequences and palindrome-rich regions are prone to this non-B DNA structure, and are prevalent in S regions (296). In addition, there is an interesting relationship between AID expression and Top1 levels. AID overexpression coincides with abated Top1 mRNA translation, the mechanisms of which have not been thoroughly explored (296).

AID has recently been shown to interact with Suv4-20H H4K20me methyltransferases, though whether this is a direct interaction, or mediated through other proteins or RNA structures, is not known (297). Without AID, Suv4-20H is not recruited to S regions, and the level of H4K20me3 is reduced at these sites(297). Concordantly, *Suv4-20h* double-null mice are defective in CSR (298). It has been proposed that H4K16ac and Suv4-20H-mediated H4K20me3 play antagonistic roles in RNA pol II pausing. H4K16ac promotes release from pausing, while H4K20me3 prolongs RNA pol II pausing (299). AID-induced mutations are long-understood to be reliant on RNA pol II pausing, so it is possible that AID reinforces this pausing step through Suv4-H20 recruitment (232). However, this has not been confirmed.

Histones H3K9me3 and H3K9ac decorate S regions that undergo recombination (213,289). These modifications are dependent on cytokine stimulation but are independent of AID expression. It has therefore been suggested that the two histone marks precede AID-induced mutations and recombination, and perhaps even function in the recruitment of AID to the appropriate sites (289). H3K9me3 has been shown to be essential for general DSB repair through its direct interaction with the lysine acetyltransferase Kat5 and loss of H3K9me3 results in defective DSB repair (300,301). The link between DSB recognition and H3K9 methylation is currently unknown, however it is understood that it participates in NHEJ, indicative of a role in CSR, but not SHM or the preceding V(D)J recombination. H3K9 is methylated by its methyltransferase, Suv39h1, which exists in a complex with kap-1 and HP1. HP1 possesses a chromodomain, which binds to the newly tri-methylated histone and retains the complex at the S region site.

There is specific evidence supporting a role for H3K9me in CSR. The kap-1 and HP1 complex functions as the structure that tethers AID to Sμ (214). Similar to the G-rich quadruplexes mentioned previously, the binding of AID to kap-1 is not reliant on its C-terminal domain and, as such, it is unlikely that this association explains the requisite of the C-terminus for CSR (214).

H3K9ac phosphorylated at serine 10 (S10ph) is another histone modification that has been implicated as a marker of donor and recipient S regions. This mark has been found to be enriched at the donor Sμ region and, after B cell activation, in the cytokine-selected recipient S region (302). 14-3-3 adapters interact directly with H3S10ph and the affinity of this interaction is increased with the addition of an acetyl group on lysine 9 of the same histone (303,304). ChIP assays have shown that, upon lipopolysaccharide stimulation, 14-3-3 is recruited specifically to the S regions enriched in H3K9acS10ph (302). Upregulation of the 14-3-3 complex coincides with CSR. The complex directly binds AID and associates specifically with 5’-AGCT-3’ motifs that occur frequently in S regions and are particularly common within the V region. Reduced 14-3-3 activity correlates with a decrease in AID at active S regions (305). This implies that 14-3-3 is an important factor for recruiting AID and associated

proteins to recombination sites for CSR. It seems H3K9acS10ph recruits and/or stabilises 14-3-3, which in turn recruits AID to the appropriate S region.

2.7 Chromatin modifications recruit DSB repair proteins in CSR

Chromatin markers participate in the recruitment of the required repair proteins. 53BP1 is one protein confirmed to hold an essential role in DSB repair, and promotes NHEJ for CSR by bridging the broken ends (306–312). Recruitment of 53BP1 to DSBs is dependent on various chromatin modification pathways (Figure 4). It is a bivalent chromatin reader and interacts directly with the histone marker H4K20me2 through its tudor domain, which recognises methylated histones (313,314). Independent of its role in S region DSB repair, 53BP1 exerts a secondary influence on CSR by enforcing the temporal separation of Sμ and Sγ breaks and ensures that subsequent ligation of the broken ends results in a deletion event (315). It does this by orchestrating the preferential breaking of the upstream switch region Sμ. *53bp1*$^{-/-}$ B cells lose the ability to ensure Sμ breaks first, which introduces inversional rearrangements that negatively impact CSR efficiency (315). 53BP1 recognises H4K20me1 *in vitro*, but it is its specific recognition of di- and tri-methylated H4K20 made accessible to 53BP1 during the DNA damage response that may regulate break order in CSR (313).

FIGURE 2

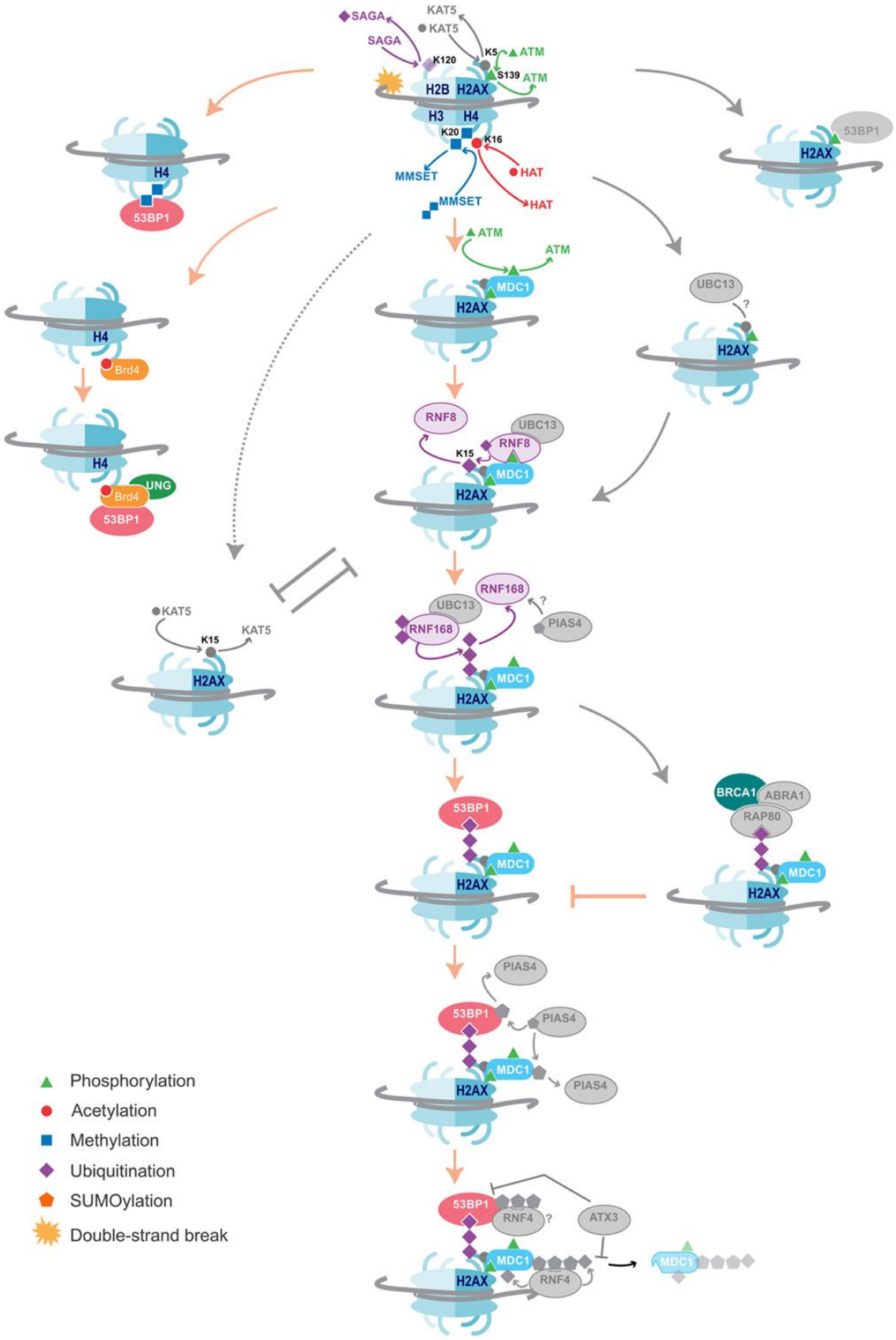
SAGA
KAT5
SAGA
KAT5
K120
K5
ATM
S139
ATM
H2B
H2AX
H3
H4
K20
K16
MMSET
HAT
MMSET
HAT
ATM
ATM
MDC1
H2AX
H4
53BP1
53BP1
H2AX
UBC13
H2AX
H4
Brd4
H4
Brd4
UNG
53BP1
RNF8
UBC13
RNF8
K15
MDC1
H2AX
KAT5
K15
KAT5
H2AX
RNF168
UBC13
RNF168
PIAS4
MDC1
H2AX
53BP1
MDC1
H2AX
BRCA1
ABRA1
RAP80
MDC1
H2AX
PIAS4
53BP1
PIAS4
MDC1
PIAS4
H2AX
53BP1
RNF4
ATX3
MDC1
MDC1
RNF4
H2AX
Phosphorylation
Acetylation
Methylation
Ubiquitination
SUMOylation
Double-strand break

Figure 2 | DNA damage repair pathways dictate class-switch recombination (CSR) efficiency. An overview of the histone modifications, and the writers and readers associated with them that are essential for CSR, as well as suggestions of additional likely factors. Color = confirmed in NHEJ and CSR, Gray = DNA damage repair factors not yet shown to affect CSR. The key proteins and histone modifications that have been shown to be essential for resolving the DNA double-strand breaks in CSR are summarized. A common theme is the recruitment of 53BP1, which is essential for efficient repair and isotype switching. Importantly, these repair pathways also function in NHEJ. Additional DNA damage repair proteins and histone modifications that have not yet been shown to play a role in CSR are indicated in gray. Some proteins and histone marks involved in other repair pathways, such as homologous recombination (HR), are also indicated in the figure. As these pathways inhibit the NHEJ pathways, they may provide negative control of CSR. Indeed, knockdown of BRCA1 has been shown to increase isotype switching efficiency.

Depleting cells of SUV4-20H1/H2, the predominant methyltransferases producing H4K20me2, slows the rate of 53BP1 accumulation at break sites and reduces CSR efficiency by 50%, however, the absence of the H4K20me2 mark has no impact on S region break order (316). This may be due to the activity of another H4K20me1 methyltransferase called MMSET that had not been considered by Rocha et al. Indeed, loss of MMSET hampers H4K20me2 enrichment, significantly reduces 53BP1 binding, and leads to inefficient CSR (317). MMSET specifically methylates H4K20me1 and H4K20me1/2/3 are all locally increased at DSBs (Figure 4) (318). This may explain why the loss of SUV4-20H1/H2 only slows 53BP1 recruitment and does not completely abolish it. Additionally, MMSET, and not SUV4-20H1/H2, is uniquely overexpressed in GC B cells, possibly ascribing MMSET as the dominant methyltransferase in antibody diversification (319). MMSET is activated and recruited after ATM-mediated phosphorylation during typical DNA repair, allowing it to complex with MDC1. MDC1 binds γH2AX, a mark only introduced once DNA repair signalling has been initiated (318). MDC1 is important for enlisting ubiquitin ligases RNF8 and RNF168, which lay a polyubiquitin motif also recognised by 53BP1 (239) (Figure 4).

Unfortunately, it is impossible to study the impact of H4K20me1 knockdown on CSR efficiency as it is a global histone mark implicit in proliferation and cellular viability (320), however, introducing a single point mutation in the 53BP1 Tudor domain, preventing it from recognising H4K20me1/2, disrupts S region break order. Taken together with the aforementioned findings that the absence of H4K20me1 has no

impact on S break order, these suggest that the dimethyl mark is dispensable, and that it is the H4K20me1 mark that determines break order (315).

Ubiquitin ligases are proving to be pervasive in DNA repair, including CSR. RNF168 monoubiquitinates H2A on 13 and 15 lysine residues (321,322). Knockdown of either RNF8 or RNF168 results in a decrease in 53BP1 accumulation at AID-induced DNA breaks, and a corresponding reduction in CSR is observed (239). Furthermore, expression of a ubiquitin-H2AX fusion protein can rescue 53BP1 recruitment to DSBs in RNF8- or RNF168-deficient cells (323). In the absence of DNA damage, Polycomb group protein L3MBTL1 and demethylase JMJD2A mask H4K20me2. RNF8 and RNF168 are responsible for ubiquitinating these proteins, removing them from the damage site to expose H4K20me2 (324,325). This secondary role of the ubiquitinases has not been explored in the context of CSR. The bivalent binding by 53BP1 to H4K20me2 and ubiquitin marks could serve to correctly orientate 53BP1 for it to bridge across a DSB. Delayed accumulation of these histone marks might prevent 53BP1 from orientating correctly, which would thus lead to increased CSR inversion events. Methyl and ubiquitin modifications appear to have different influences on 53BP1. H4K20me2 more likely serves as a signal to recruit 53BP1 to the DSB, while ubiquitination H2A/H2AX serves as an anchor to 53BP1, maintaining it at the site of the DSB, such that 53BP1 can bridge the gap between donor and recipient S regions for isotype switching.

Upstream in the signalling cascade, a deubiquitination event also promotes DNA repair and CSR. Ubiquitination of H2BK120 is associated with an open chromatin and interferes with chromatin compaction. DSB repair cannot occur until histone H2BK120ub is deubiquitinated to allow access to NHEJ factors (326). A genome-wide loss-of-function RNAi screen identified several components of the SAGA deubiquitinase module required for CSR and DSB repair, including Usp22, Eny2, and Atxn7. Knockdown of any of these components using shRNAs or CRISPR/Cas9 reduces CSR (327). Knockdown did not impair AID function indicating that the defect lies somewhere downstream. Interestingly, Eny2 knockdown also interferes with ATM and/or DNAPK activity, and thus indirectly limits γH2AX formation, which further reduces CSR (327,328).

BET family member Brd4 interacts with acetylated histones *via* its two bromodomains (329). Studies have shown that, upon induction of AID, occupancy of Brd4 at Sμ and Sα regions increases. ChIP and immunoprecipitation assays have confirmed an interaction between Brd4, the modified histones H4 and γH2AX, as well as between Brd4, 53BP1 and UNG (330). Treatment with the Brd4 inhibitor JQ1 or siBrd4 knockdown significantly reduces CSR frequency. The levels of both 53BP1 and UNG are reduced, without affecting the levels of H4ac. Brd4 is therefore thought to function as a chromatin-bound platform that recruits 53BP1 and UNG to DSBs (330) (Figure 4). Finally, the chromatin remodelling complex INO80 has also been implicated as a regulator of CSR (331). Knockdown of INO80 in various mammalian cell lines has been shown to inhibit 53BP1 accumulation at DSBs (332). More recently, MEFs from *mino80* knockout mice contradict this observation. Rather, INO80 is suggested to participate early on during DSB repair, where it first binds γH2AX, and then exposes H4K20me2 for 53BP1 recruitment. Paradoxically, INO80 is involved in 5'–3' DNA end resection to support repair by homologous recombination (333). How it then functions to support NHEJ in CSR is yet another mystery.

2.8 Potential role for other repair proteins in CSR

The histone modifications and DNA damage repair proteins important for CSR (Figure 4) have parallel roles in NHEJ. This is particularly interesting because a multitude of proteins, modifiers, and readers involved in NHEJ have not yet been implicated in CSR. These include the E2 ubiquitin-conjugating enzyme Ubc13, which functions in complex with RNF8 and RNF168. Ubc13, and its γH2AX independent recruitment through the Kat5 complex (27,334–336) are potential important factors in CSR. Indeed, H2AX-deficient mice experience reduced CSR (104), while a link with SHM fails to be seen (246). A SUMOylation pathway, initiated by PIAS4 (337,338) and further expanded by STUbL RNF4 (339), provides a potential role of SUMO-ubiquitin cross-talk in CSR. The importance of this pathway in general DNA damage repair is exemplified by Ataxin-3, which counteracts the RNF4-mediated ubiquitination. As a result, Ataxin-3 promotes prolonged retention of MDC1, resulting in reduced recruitment of 53BP1 and BRCA1 (316).

The possible impact of NHEJ regulatory factors specifically should be considered on antibody diversification. The recently discovered tudor interacting repair regulator

(TIRR) stabilises 53BP1 in the nuclear fraction, but blocks NHEJ-directed repair by binding the tudor domain and guarding against H4K20me2 binding upon DNA damage (340). As such, it may act to hinder CSR when either over- or under-expressed, and would determine whether the turnover rate or instability of 5BP1 will compensate for more favourable H4K20me2 binding. Equally, the contribution of RIF1 in suppressing DNA resection for NHEJ and separating the 53BP1-TIRR complex may similarly serve to deregulate CSR at differential expression levels (341). The HR pathway also represents a potential research avenue as it may provide inhibitory effects on CSR efficiency. Knockdown of BRCA1, a key HR factor, has been shown to increase isotype switching (342). Similar effects are observed from downregulation of other inhibitory modifications, such as the H2AXK15ac by the Kat5 complex, which inhibits the RNF8 mediated ubiquitination of H2AXK15 (343).

2.9 Influence of AID and TET activity on the DNA methylome during B Cell Development

2.9.1 Role of AID in DNA Demethylation via Deamination

Aside from its mutagenic activity, AID has been associated with coordinating DNA demethylation during zebrafish development (344), stem cell reprogramming (345), and primordial germ cell formation (346). The combined results of these studies support the notion that AID could function as a genome-wide epigenetic regulator by deaminating 5-methylcytosine (5mC) to 5-methyluracil (5mU); thereby replacing a 5mC base with an unmethylated C or a thymine (T) via base excision repair (BER). GC B cells have more heterogeneous DNA methylation patterns than naïve B cells (212), and this has established a potential role for AID during this maturation step.

Several studies have debated whether AID is responsible for DNA demethylation or activated gene expression in B cells (347). The methylation status of CpG motifs at VDλ1 is unchanged between naïve and day 14 GC B cells (246), AID does not induce demethylation at either Sμ or Cμ (297), and 5mC is a poor substrate for AID, although it does not prevent its activity on neighboring cytosines (348,349). In contrast, fewer studies have found that DNA demethylation events can be attributed to AID. CpGs have been observed to have increased methylation pattern variation in wild type

tissues, compared to AID-null tissues. Interestingly, 90% of the methylome alterations seen in naïve to GC transition were lost in AID-null mice (350). SHM targets are also suggested to be enriched with AID-dependent hypomethylation, and the significant reduction of both demethylation and SHM *ex vivo* (such as in the contribution by Fritz et al) is due to these two events being coupled *in vivo* (350). Furthermore, a recent study suggested that cytosine demethylation is over-represented in WRCG/CGYW motifs in follicular lymphomas, which overlays the WRC AID hotspot motif and the methylated CpG dinucleotide. This contrasts SHM of immunoglobulin genes whereby cytosine demethylation is under-represented at WRCG/CGYW motifs. Thus, this mutational process appears distinct from conventional SHM, and is solely applied to the CpG methylation/demethylation process (351).

2.9.2 Role of TET Protein in DNA Demethylation via Hydroxylation

As the involvement of AID in DNA demethylation remains to be fully established, the regulation of DNA methylation by another family of proteins is now being explored. Ten-eleven translocases (TET1, TET2, and TET3) oxidize 5mC to 5-hydroxymethylcytosine (5hmC), and further oxidises 5hmC to 5-formylcytosine (5fC) and 5-carboxycytosine (5caC) (352,353). TET proteins predominantly support demethylation via dilution through successive rounds of replication(352). Nevertheless, it is possible that TET enzymes support active (replication-independent) demethylation. TET enzymes often accompany transcription-associated H3K36me3 histone modifications, and possibly RNA polymerase II, depositing 5hmC and generating a more accessible DNA substrate for subsequent cycles of transcription (354). TET enzymes are involved in iterative rounds of 5mC oxidation to 5fC and 5caC (355). Demethylation could then be achieved either ii) indirectly via thymidine DNA glycosylase (TDG) which recognises and excises 5fC an 5caC (356); or ii) directly by yet unidentified decarboxylases (357), (358).

TET proteins appear to be important for programming B cell methylation throughout development. 5hmC is enriched in lineage-specific transcription factors, such as *Bcl6*, *EBF1* and *IRF4*, which are important for germinal centre transition (359,360). The methylation status of follicular B cells from conditional *Tet2*$^{-}$/*Tet3*$^{-}$ double knockout mice were partially hyper-methylated when compared to wild type cohorts. Single knockout mice failed to show such noticeable effects on methylation levels (359). Of

the sequences that are specifically demethylated in wild type B cells during differentiation into germinal centre B cells, 95% are prevented in *Tet2*$^{-}$/*Tet3*$^{-}$ mice, providing some evidence that TET proteins may be responsible for most DNA demethylation that occurs at this stage (359). In addition, the Igκ locus is known to undergo DNA demethylation during antibody diversification, and this demethylation step is not observed in *Tet2*$^{-}$/*Tet3*$^{-}$ knockout mice (359).

2.9.3 Cooperation between AID and TET Proteins during Epigenomic Regulation

In addition to regulating B cell development, TET proteins are essential tumour suppressors in B cells. Of all patients diagnosed with diffuse large B cell lymphoma, 5.7% carry a Tet2 deletion or loss-of-function mutation (361). In mouse genetic studies, Tet1-deficient B cell progenitors developed B cells lymphomas (362); in analogous human studies, the Tet1 promoter was found to be hypermethylated with concomitant reduction in Tet1 expression in patients with non-Hodgkin lymphoma (362). In additional studies, mice with a combined Tet2- and Tet3- deficiency in developing B cells developed B cell lymphoma and succumbed to disease within 5–6 months of age, much earlier than the 15–20 months observed in Tet1/Tet2-deficient mice (363,364).

It has been proposed that the product of TET protein-dependent 5mC oxidation may be a target for AID. Few studies have addressed the cooperative activities of TET proteins and AID. Some have concluded that it is unlikely that AID deaminates 5mC or 5hmC: 5mC is deaminated only at 10% the rate of cytosine due to the steric hindrance of the methyl group (349). 5hmC is an even poorer substrate for AID (365). Deamination of 5hmC *in vitro* has not been observed, and *in vivo* studies overexpressing AID have also failed to generate 5hmU (349). As 5hmU is not yet detected in genomic DNA, AID targeting 5hmC as a target for deamination was claimed unlikely, and further supports a role for TET enzymes in B cell developmental demethylation (349). On the contrary, a study in 2011 found that AID quite significantly promotes 5hmC demethylation in HEK293 cells and in mouse brain. While overexpression of AID had little effect on the demethylation of a strand of 5mC-GFP DNA, it led to a significant decrease of 5hmC levels induced by TET1 and significant increase of 5hmU (366). This is significant because there no detectable endogenous 5hmU in HEK293 cells. Additionally, the pattern of 5hmC demethylation events were

broadly distributed along the 5mC-GFP DNA, 5hmC was also selectively demethylated at WCR ‘hotspot’ motifs, and demethylation showed strand bias in the same manner as AID deamination (366). Taken together, this could indicate that AID and TET may act in tandem to promote DNA demethylation. Whether this is replicated in the context of antibody diversification is yet to be seen.

2.9.4 Epigenomic Role of Immune Diversification in Disease Development

AID defects are associated with hyper-IgM syndrome, causing severe immunodeficiency (367). The epigenetic effect of AID on health however, particularly lymphomas, is poorly understood. DNA methylation’s role in gene silencing makes it essential in regulating normal development, with epigenetic mutations allowing cells to grow and reproduce uncontrollably, leading to tumorigenesis. DNA methylation can have malignant effects through two main alterations: hypermethylation of tumour suppressor genes and hypomethylation of oncogenes. It has come to light in recent years that such mutations are a common cause of B cell lymphomas, with hypomethylation in GCB-derived lymphomas correlating with AID expression (368). Off target effects of AID are also seen in non-B cell cancers, for example, T cell malignancy (369), and also in non-lymphatic cancers, such as stomach cancer (370), lung cancer (371), breast cancer (372), and liver cancer (373).

From this observation it could be hypothesised that ectopic AID expression plays a critical role in lymphomagenesis. Increased epigenetic heterogeneity in lymphomas reflects diverse tumour cell populations, which increases risk of resistance to cytotoxic drugs (368). Understanding AID, and its role in lymphomas, could provide guidance in the development of new epigenetic drugs. Currently the main epigenetic cancer therapy drugs are azacytidine and decitabine which function as DNA methyltransferase inhibitors, combating DNA hypermethylation. These drugs have shown substantial potency in reactivating epigenetically silenced tumour suppressor genes *in vitro* (374). Reducing levels of AID could be used in a similar way against hypomethylation or the resistance caused by epigenetic heterogeneity in lymphomas. The protein HSP90 is important in the protection of AID from proteasomal degradation, with inhibition by the drug 17-AAG, leading to polyubiquitination and degradation of AID (375). 17-AAG is currently in clinical trials for the treatment of other cancer types, due to its role in inhibiting the degradation of

proteins involved in tumour cell proliferation and survival (376). The above observations suggest a possibility of using 17-AAG in the treatment of hypomethylated lymphomas (Figure 3). In a recent study 17-DMAG, a derivative of 17-AAG, has been found to reduce CSR and SHM in mice, while B-cell survival and proliferation remain unaffected (377).

2.10 Concluding Remarks

The epigenome is made up of several critical components that must work together to promote antibody maturation and diversification in B cells. This is an intricate process; each component simultaneously functions both independently and dependently on the others, and disruption at any step can have catastrophic downstream affects. For example, histone modifications relax the chromatin, allowing for AID transcription. Simultaneously, multiple different ncRNAs regulate transcription and target AID to mutate Ig region genes. Next, different histone modifications recruit DNA repair proteins which then multiple different ncRNAs target. The entire process is further complicated depending on *which* histone modifications are used and *which* ncRNAs are present whether a B cell is returned to the *status quo*, undergoes CSR, or undergoes SHM. It is a tremendously complicated process and abrogation at any step can result in various forms of cancer and/or immunodeficiencies. Despite advancements of our knowledge of this field, several important questions remain unanswered. These include the mechanisms controlling AID transcription and the mechanisms that direct AID to target neutral, CSR, or SHM region genes. Furthermore, we have yet to determine how ssDNA is stabilized for AID activity.

2.11 Author Contributions

RC conceived the theme/direction. ECS, RBM, MJD, RL, and RC researched and wrote the manuscript. ECS and RBM designed the figures.

2.12 Conflict of Interest Statement

The authors declare that the research was conducted in the absence of any commercial or financial relationships that could be construed as a potential conflict of interest.

2.13 Acknowledgments

The authors wish to apologize to all colleagues whose work they could not cite due to space constraints. The authors wish to thank Matthew Scharff, Shanzhi Wang, Sergio Roa, and Emma Knight for their insight, and funding for RC from the Biotechnology and Biological Research Council [BB/N017773/1], Royal Society [IE150290], and Academy of Medical Sciences Springboard Award. ECS and RBM are funded by Ph.D. studentships from the Biotechnology and Biological Research Council-funded South West Doctoral Training Partnership [BB/J014400/1] and the Engineering and Physical Sciences Research Council-funded Doctoral Training Partnership [EP/M506527/1], respectively.

Keywords: epigenetic modifications, epigenomics and epigenetics, antibody diversity, cytosine deamination, somatic hypermutation, class-switch recombination, B cell maturation

Citation: Sheppard EC, Morrish RB, Dillon MJ, Leyland R and Chahwan R (2018) Epigenomic Modifications Mediating Antibody Maturation. *Front. Immunol.* 9:355. doi: 10.3389/fimmu.2018.00355

Received: 27 November 2017; **Accepted:** 08 February 2018; **Published:** 26 February 2018

Edited by:
Deborah K. Dunn-Walters, University of Surrey, United Kingdom

Reviewed by:
David Jonathan Fear, King's College London, United Kingdom
Anne Corcoran, Babraham Institute (BBSRC), United Kingdom

***Correspondence:** Richard Chahwan, **r.chahwan@ex.ac.uk**

†These authors have contributed equally to this work.

3 Development and optimisation of a fluorescence-based toolkit for real-time quantification of DNA resection activity

3.1 Summary

DNA nucleases are integral for maintaining genomic stability. Nucleases recognise particular structural features that arise following endogenous or exogenous sources of damage, and characterising their preferences is invaluable to understanding their specific roles in DNA repair. Understanding how nuclease activity is influenced by catalytic or structural mutations, binding partners, and different DNA structures, may illustrate how nucleases are implicated in cancer and age-related diseases. Contemporary methods used to study nucleases require radiolabelled substrates to visualise nuclease-dependent DNA digestion. While this is a robust approach, there are several flaws associated with this method; it is time-intensive, captures nuclease activity in a discontinuous manner, and it is inherently dangerous to work with radioactive substances. As such, an alternative method for capturing nuclease activity in a continuous fashion using the fluorescent double-stranded DNA (dsDNA) dye, PicoGreen, has been developed herein. Indeed, PicoGreen has proven to be a stable dye that is permissive to nuclease processivity. Furthermore, the dsDNA substrates have been optimised to emit a strong fluorescent signal upon PicoGreen binding.

3.2 Nucleases in DNA repair

Nucleases are a hallmark of the DNA damage response. They help dictate many DNA repair pathway choices by controlling the DNA damage substrates created downstream during the signalling cascade. The complex roles nucleases play in DNA repair pathways underpin several premature ageing-related syndromes, and cancerous transformation can result from structural or catalytic mutations in nuclease genes (reviewed in (378)). Nucleases hydrolyse the phosphodiester bonds between sugar residues in DNA, RNA, or both. DNA repair is critical for proof-reading genomic DNA during replication, halting the replication fork, Okazaki fragment processing and correcting many forms of genomic insults that require mismatch repair, base excision repair, nucleotide excision repair or double-strand break repair (DSB) (147). The defining characteristics of nucleases are their substrate specificity, directionality, and processivity.

3.3 Current approaches for studying nuclease activity and their limitations

A significant limitation of nuclease studies has been the adequate identification of their catalytic functions and/or their relative activities against different DNA intermediates. Indeed, the activities of numerous DNA nucleases are debated (e.g. human Mre11, CtIP etc (379,380)), and yet there remain many more uncharacterised proteins with strong predictions for nuclease domains in mammalian genomes (381,382).Conventional nuclease assays predominantly involve the use of radioactive labelled ^{32}P-dATP to visualise DNA substrates on an agarose gel (181,182). The use of radioactive isotopes delivers highly specific, sensitive assays that are free from interference. However, these assays are often inefficient, time-consuming, qualitative, and potentially hazardous (184,185). Additionally, the assays are discontinuous, and must be stopped at discreet time points before measuring readouts (13). Whilst this can provide an indication of reaction rate, it does not allow for real-time visualisation of the catalytic reaction.

3.4 PicoGreen is a highly sensitive dsDNA dye used in discontinuous enzyme assays

Radiolabelled DNA oligonucleotides are gradually being replaced with fluorescent nucleic acid stains such as DAPI (186) and other commercially-available dyes including, but not limited to, Midori Green, SYBR Green I and Acridine Orange (187). PicoGreen (PG) is a commercially available dye that emits a fluorescent signal upon intercalation with double-stranded DNA (dsDNA), emitting a fluorescent signal 1,000-fold stronger compared to when free in solution. Its superior sensitivity can quantify picogram levels of dsDNA, unlike other fluorescent dyes, including Hoechst (188), ethidium bromide (188), EvaGreen (189), SYBR Green (189) and YOYO-1 (189).

A method using PG to stain the DNA and monitor nuclease activity in real-time is faster, cheaper, and safer than conventional DNA resection assays using radioisotopes. It works cross-species and is platform agnostic. Furthermore, this protocol has the sensitivity for enzyme reaction kinetic calculations and can distinguish the structural preferences exhibited by an enzyme for its substrate. Similar to other nucleic acid dyes, PG has proven to be a versatile DNA stain in different experimental conditions. It has been used to visualise dsDNA in agarose electrophoresis as a quality control marker to identify fragmented and nicked DNA (383). It has also been

implemented in flow cytometry analysis of cell-free DNA which can increase in certain pathologies, such as cancer and autoimmune syndromes (384). PG exhibits readily detectable, albeit reduced, fluorescence readings at temperatures of 37°C, despite manufacturer recommendations to work at room temperature (385), allowing for assays to run at physiologically-appropriate temperatures. As PG very preferentially binds dsDNA compared to ssDNA and RNA structures (386), it has been an important feature of discontinuous enzyme-mediated DNA-modifying studies, such as nucleases (387), helicases (388), polymerases (389,390), polymerase inhibitors (391), telomerases (392), and primases (393). However, the full potential of PG in real-time visualisation of reaction progression in a continuous assay remains limited (394). The discontinuous PG assay described herein will be advanced to create a continuous PG assay.

3.5 Materials and Methods

3.5.1 Plasmid and oligonucleotide substrates

DNA substrates were prepared by diluting pNIC28-BSA4 or CTIP in HyClone water™ (GE healthcare), and unmodified HPLC-purified oligonucleotide substrates (Eurofins) in 1X annealing buffer (Sigma-Aldrich). Oligonucleotides were designed and optimised against secondary structure formation using the 'Predict a Secondary Structure Web Server' (https://rna.urmc.rochester.edu/RNAstructureWeb/Servers/Predict1/Predict1.html) (114) and annealed at a 1:1 molar ratio. Table 1 shows all the oligonucleotides and their respective illustrations.

Table 1

Oligo code	Sequence (5–'3')
RCOL381	GATACGGCATACGTCTATGGCTACTTGGAGCGAGTATCCTTCGAGCTTGCTCGAGCTTGCCTACTTGGAGGATACGGCAT
RCOL468	ATGCCGTATCCTCCAAGTAGGCAAGCTCGAGCAAGCTCGAAGGATACTCGCTCCAAGTAGCCATAGACGTATGCCGTATC
RCOL396	GGGTCTTAAAGTTAAACCTTAAGGTTCTCCTATAGTGAGTCGTATTAAGTATCAATGTTCCGGACAAATTACCCTAATTA
RCOL400	TAATTAGGGTAATTTGTCCGGAACATTGATACTTAATACGACTCACTATAGGAGAACCTTAAGGTTTAACTTTAAGACCC
RCOL556	GATGGTTTGTTGGTCTATTACTACTTGGAGCTTGTATGATTCGAAACCTTGGAGTACTTGCCTACTTGGAGTGAACTTAG
RCOL557	CTAAGTTCACTCCAAGTAGGCAAGTACTCCAAGGTTTCGAATCATACAAGCTCCAAGTAGTAATAGACCAACAAACCATC

3.5.2 Nucleases and buffers

The nucleases used were RQ1 RNase-Free DNase I (Promega), T7 exonuclease (New England Biolabs), Exonuclease III (New England Biolabs). In preparation for each assay, nucleases used were diluted on ice in their appropriate storage buffers, omitting glycerol. All storage buffers and reaction buffers were made according to the recipes available on their respective NEB and Thermo Fisher web pages. DNase I storage buffer (10mM HEPES (pH 7.5), 10mM $CaCl_2$ and 10mM $MgCl_2$) and reaction

buffer (400mM Tris-HCl (pH 8.0), 100mM $MgSO_4$ and 10mM $CaCl_2$), T7 exonuclease storage buffer (10 mM Tris-HCl, 5 mM DTT, 0.1 mM EDTA, (Ph 8 at 25ºC)) and reaction buffer (50 mM potassium acetate, 20 mM Tris-Acetate, 10 mM magnesium acetate, 1 mM DTT), and Exonuclease III storage buffer (5 mM KPO_4, 200 mM KCl, 5 mM β-ME, 0.05 mM EDTA, 200 µg/mL BSA, (pH 6.5 at 25ºC)) and reaction buffer (10 mM Bis-Tris-Propane-HCl, 10 mM $MgCl_2$, 1 mM DTT (pH 7 at 25ºC)) were all filtered prior to use, and autoclaved where possible.

3.5.3 Preparation of PicoGreen

The PG reagent from the Quant-iT™ PicoGreen™ dsDNA Assay Kit (Invitrogen) was prepared immediately before use by making a 1:200 dilution of the PG in TE buffer (10 mM Tris-HCl, 1 mM EDTA, pH 7.5) and 40% (v/v) glycerol.

3.5.4 Discontinuous assay experimental procedure

Each DNA substrate reaction mixture contained 50 nM DNA substrate, 1X reaction buffer (specific for each enzyme), 0.02 mg/mL streptavidin (cat. 21125, Thermo Fisher Scientific) if required, 0.25 mM dNTPs if required, 5 µL enzyme or relevant storage buffer. For the DNA nucleases, Milli-Q water was added to bring the total reaction volume to 50 µL. Reaction mixtures were prepared on ice and samples were tested in a 96-well, black flat bottom plate (cat. M9685, Sigma-Aldrich). The final components added were the storage buffers, then the enzyme mixtures to start the reaction. DNase I reactions were stopped with 5 mM EDTA, after which 50 µL PG solution was added and incubated on ice for 15 minutes.

An i-control Infinite 200Pro (Tecan) was pre-heated to 37°C. Samples were read every 40–50 s for 30–60 mins. Excitation and emission wavelengths used were 483-15 nm and 530-30 nm, with a shake before each read.

3.5.5 Continuous assay experimental procedure

Each DNA substrate reaction mixture contained 50 nM DNA substrate, 1X reaction buffer (specific for each enzyme), 50 µL PG solution, 0.02 mg/mL streptavidin (cat. 21125, Thermo Fisher Scientific) if required, 0.25 mM dNTPs if required, 5 µL enzyme or relevant storage buffer. For the DNA nucleases, Milli-Q water was added to bring the total reaction volume to 100 µL. Reaction mixtures were prepared on ice and

samples were tested in a 96-well, black flat bottom plate (cat. M9685, Sigma-Aldrich). The final components added were the storage buffers, then the enzyme mixtures to start the reaction.

Either a i-control Infinite 200Pro (Tecan) or a CLARIOstar microplate reader (BMG labtech) was pre-heated to 37°C. Samples were read every 40–50 s for 30–60 mins. Excitation and emission wavelengths used were 483-15 nm and 530-30 nm, with a focal height of 10.2, 20 flashes per well, with a shake before each read.

3.5.6 Data analysis

For statistical analysis of the data, one-way ANOVA with the Tukey's post-hoc tests were used. This was implemented using GraphPad Prism v7.03. An example of the workflow is available in the appendix.

3.6 Results

Here, PG is shown to be a highly sensitive dye to measure DNA nuclease activity in a continuous manner, developing upon the current discontinuous approaches published. Its specificity for DNA limits its utility to studying only DNA nucleases, as opposed to RNA nucleases (386). The methods to stabilise PG for real-time experiments and optimise its fluorescence are described within, alongside the approach taken to maximise the fluorescent signal emitted from the DNA substrates upon PG binding.

3.7 Optimisation and development of the assay from a discontinuous to continuous methodology

Several factors were considered before progressing to a continuous study of nuclease activity. First, it was integral to determine that the fluorescence signal could be measurably different between a substrate following nuclease-dependent degradation and a substrate not treated with a nuclease. Second, the stability of PG had to be ensured for it to be used to monitor enzyme activity over the period of the reaction. Third, it was necessary to determine whether PG would permit nuclease processivity and whether the products of the reaction (free nucleotides) would contribute towards the fluorescent signal. Fourth, the oligonucleotide substrates had to be optimised to produce a strong fluorescent signal to capture nuclease activity with precision.

To address the first issue concerning the sensitivity of PG on DNase I-treated and untreated substrates, the activities of a range of DNase I concentrations on plasmid DNA were compared (Fig. 1a). It was only after the reaction was stopped that PG was added to the reaction mixtures. Higher concentrations of DNase I (200 nM) digested more of the substrate than lower concentrations (25 nM), which is to be expected. The results indicate that PG can be used to compare differential enzyme activity. In addition, the results also demonstrate the range of concentrations of DNase I that would cause an observable decrease in fluorescence over the course of the reaction.

Secondly, the stability of PG was confirmed. Rapid photobleaching would be disadvantageous as it would create a very short window within which the reaction could be monitored, so a stable reaction mixture is essential. Unexpectedly, it was found that the fluorescent signal from PG was almost entirely lost after 5 minutes at

37°C (Fig. 1b). This indicates that PG is very unstable and is rapidly photobleached under these conditions. Furthermore, DNase I activity failed to be captured, suggesting that PG is generally unreliable. Fortunately, PG fluorescence has already been characterised, and was found to be stabilised upon addition of glycerol (395). In keeping with these results, 20% glycerol in the final reaction mixture was sufficient to prevent rapid photobleaching (Fig. 1c).

To capture activity in real-time, PG was added before addition of DNase I. Free nucleotides (dNTPs) were added to the reaction mixture where the fluorescent signal was negligible, confirming that the reaction products do not contribute towards fluorescence signal to distort the results. This assay also established that the PG:dsDNA complex does not inhibit DNase I as it processes the DNA (Fig. 1d).

FIGURE 1

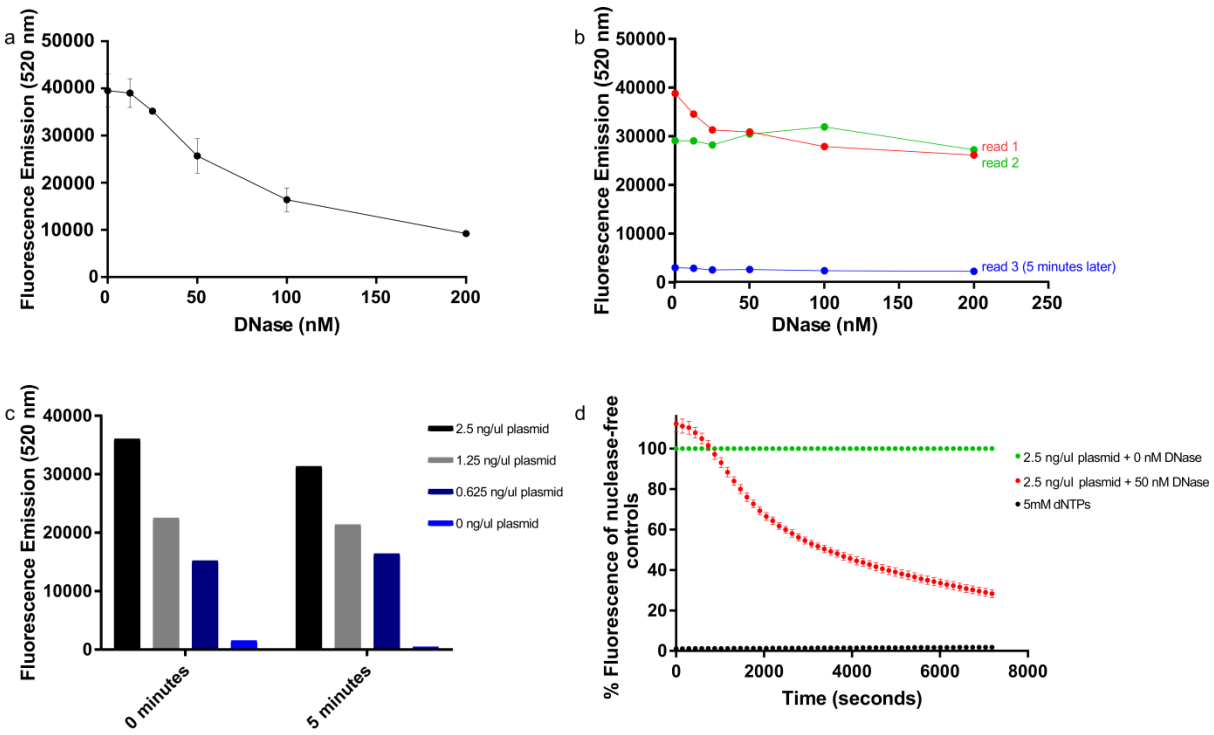

Figure 1 | Assay progression from a discontinuous to a continuous methodology

a, Discontinuous assay performed with a DNase I titration on 2 ng/µL 7284 bp plasmid. A dilution series was carried out to provide a range of DNase I concentrations: 0, 12.5, 25, 50, 100 and 200 nM. Reaction was run at 37°C for 15 minutes. PG was subsequently added, and the fluorescence was read after 10 minutes incubation to allow for PG saturation of the dsDNA. Error bars represent standard deviation, n=2. **b**, PG was added to the reaction mixture containing 2 ng/µL plasmid for 15 minutes prior to addition of different concentrations of DNase I. Two reads were taken in quick succession at 37°C, followed by a third read 5 minutes later to determine the extent of photobleaching. **c,** 20% glycerol was added to the reaction mixture and the fluorescent signal was observed after 5 minutes. **d,** Continuous assay run with 50 nM DNase I at 37°C and 5 mM dNTPs as a control. Error bars represent SD; n=2.

3.8 Oligonucleotide sequence optimisation for highly fluorescent substrates

Oligonucleotides are far more suitable than large plasmids to study nucleolytic activity on a range of different substrate termini. Oligonucleotides are far more versatile substrates than plasmids as they can be designed to have different terminal structures, such as 5’ or 3’ overhangs, Y-structures, Holliday junctions or strand invasions, amongst many more physiologically relevant structures (13,396). The much shorter length of the oligonucleotides ensures that each enzyme is exposed to a higher proportion of these alternative structures and, for these reasons, only oligonucleotides were used for furthering the development of the assay. The oligonucleotides used in this assay were designed to be 80 base pairs (bp) in length to emit a suitably high

fluorescent signal with the addition of PG (Fig. 2), and were sequence-optimised so as to reduce the likelihood of secondary structure formation (114) and thus increase the fluorescent read-out (Fig. 3 and 4). 80-bp was deemed an appropriate length due to limitations in synthesis. According to Integrated DNA Technologies and Eurofins, 90–100-bp is typically the maximum length for HPLC-purified oligonucleotides, respectively. In addition, reducing the length of one strand to create overhangs would affect the fluorescent signal emitting from dsDNA, and would require synthesis of more control, 'ladder' sequences, rather than simply extending the length of one strand when required.

FIGURE 2

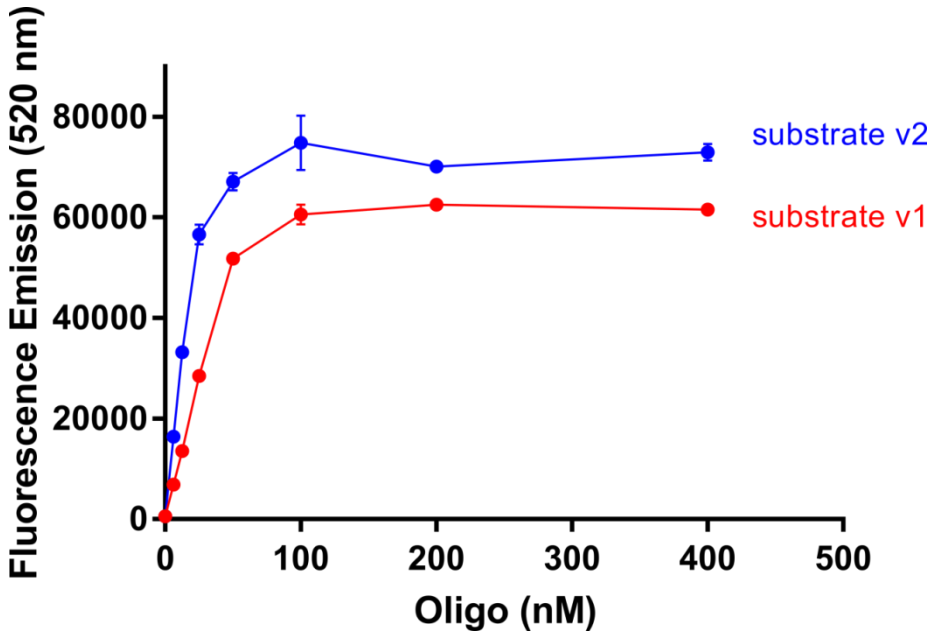

Figure 2 | Calibration curve of substrates equal in length emit different fluorescent signals. Two 80-bp substrates composed of different nucleotide sequences and incubated with PG emit different fluorescent signals. Error bars represent standard deviation; n=3.

Two 80-bp oligonucleotides (substrates v1 and v2) were treated with PG, and their fluorescence was compared (Fig. 2). Each substrate has a GC content of 53% and 35%, respectively. As PG fails to show any base preference (395), it is probable that this disparity in fluorescence can be attributed to the likelihood of secondary structure formation. Secondary structures are the formation of intramolecular structures, such as stem loops (397). Secondary structure prediction software (https://rna.urmc.rochester.edu/RNAstructureWeb/Servers/Predict1/Predict1.html) was used to calculate the likelihood of secondary structure formation for each oligonucleotide at 37°C (114). This was to cater for the fact that all enzyme assays are to be run at this temperature. The software uses thermodynamics, prediction of base pair probabilities, bimolecular structure prediction and other algorithms to calculate the probability of secondary structure formation in an RNA or DNA sequence. It attributes each oligonucleotide with a ΔG value, which is a measurement of a sequence's thermodynamic stability. It is recommended to have a ΔG value that is more positive than -9 kcal/mole. Using the software as a guide, the sequences were edited to reduce the probability of secondary structure formation.

Substrate v1 was made up of two 80-mer oligonucleotides called 381 and 468. Secondary structure prediction software found a high probability of secondary structure formation in these sequences (ΔG is -16.9 kcal/mole and -15.6 kcal/mole for 381, and -12.9 kcal/mole and -11.7 kcal/mole for 468; Fig 3). Substrate v2 is formed from two 80-mer oligonucleotides called 396 and 400 and have more positive (or less negative) predicted ΔG values (-4.1 kcal/mole and -3.9 kcal/mole for 396, and -6.9 kcal/mole and -6.2 kcal/mole for 400; Fig. 7). Substrate v1 exhibits the lowest fluorescent signal compared to substrate v2, and their ΔG values corresponded with their divergent fluorescence signatures. Substrate v1 was composed of two 80-mer oligonucleotides called 381 and 468. Their predicted secondary structures have very low ΔG values

FIGURE 3

Substrate v1: 381/468

381 secondary structure prediction

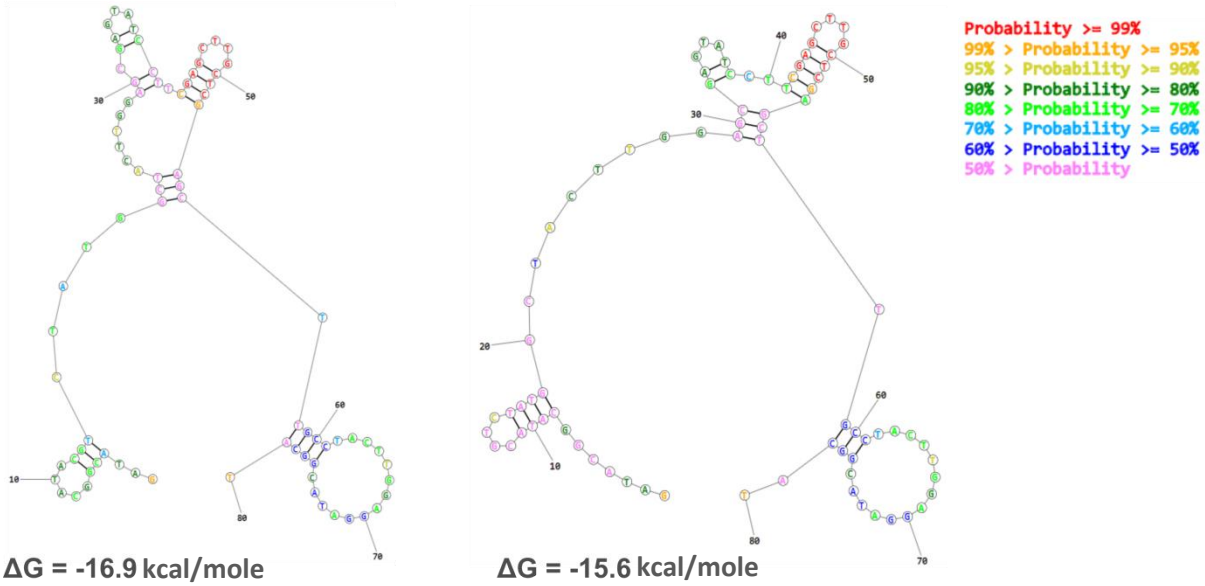

468 secondary structure prediction

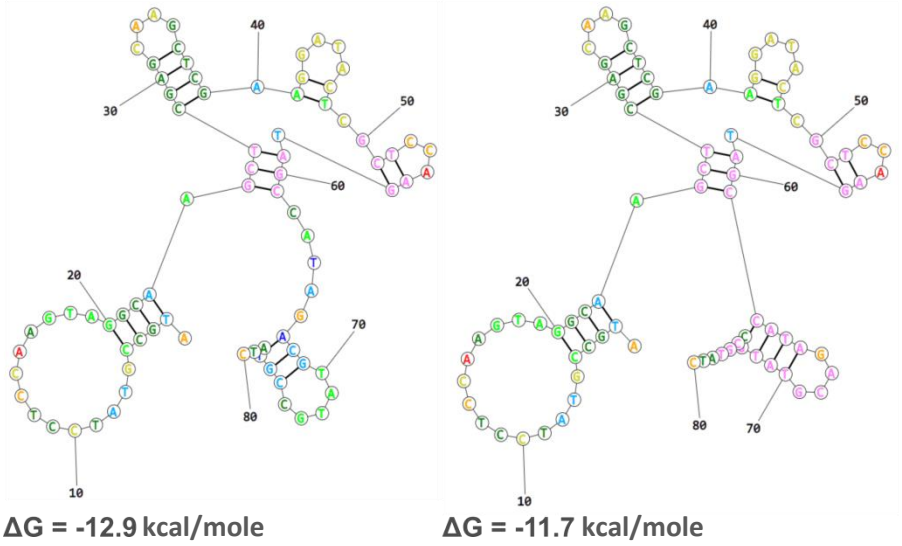

Figure 3 | Predicted secondary structures for the less fluorescent substrate v1 have ΔG values below the minimum recommended -9 kcal/mole

Substrate v1 is composed of two oligonucleotides, 381 and 468. The predicted ΔG values for their secondary structures are -16.9 kcal/mole and -15.6 kcal/mole for 381, and -12.9 kcal/mole and -11.7 kcal/mole for 468.

FIGURE 4

Substrate v2:396/400

396 secondary structure prediction

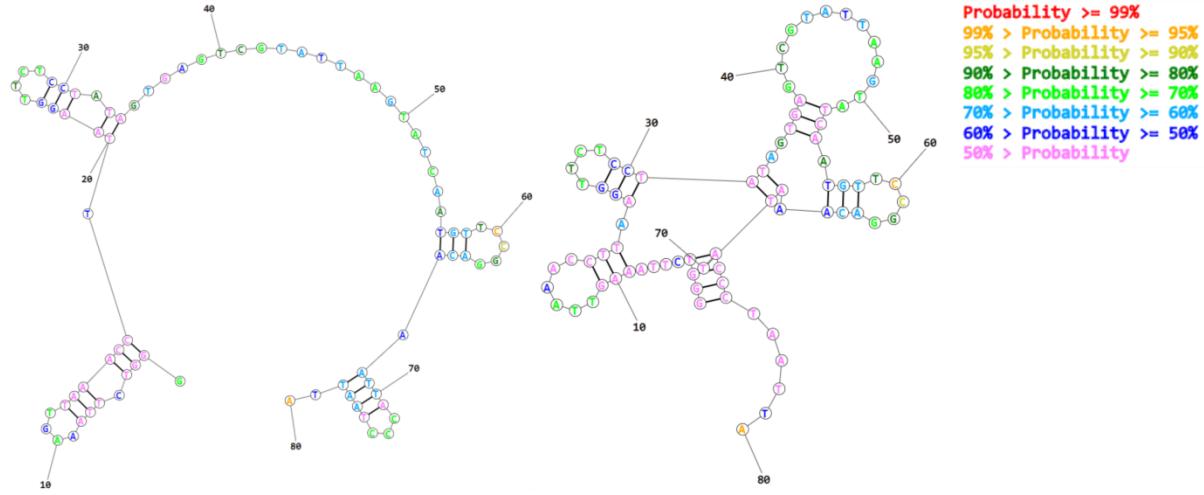

ΔG = -4.1 kcal/mole ΔG = -3.9 kcal/mole

400 secondary structure prediction

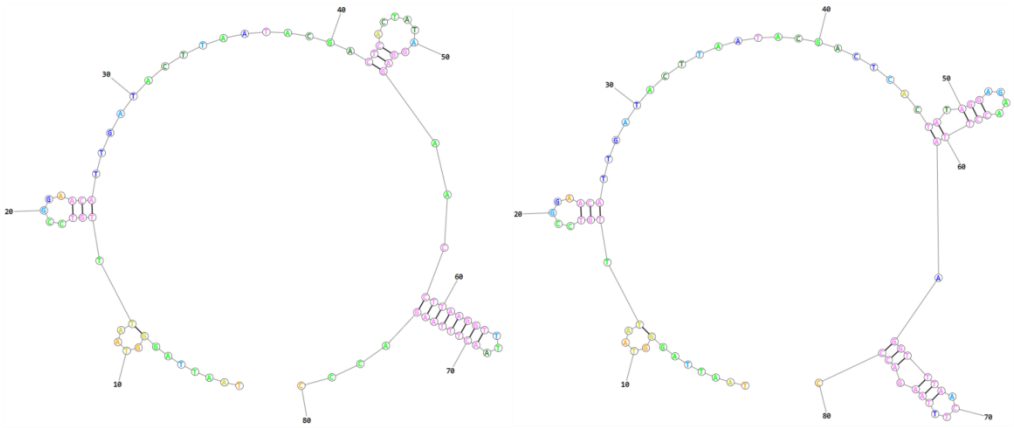

ΔG = -6.9 kcal/mole ΔG = -6.2 kcal/mole

Figure 4 | Predicted secondary structures for the less fluorescent substrate v1 have higher ΔG values than the minimum recommended -9 kcal/mole

Substrate v2 is composed of two oligonucleotides; 396 and 400. The predicted ΔG values of their secondary structures are -4.1 kcal/mole or -3.9 kcal/mole for 396, and -6.9 kcal/mole or -6.2 kcal/mole for 400.

To confirm whether the secondary structures are responsible for the strength of the fluorescent signal, the less fluorescent substrate (substrate v1; 381/468) was edited to try and obtain a fluorescent signature that was equal to, or greater than, the signal produced from the more fluorescent substrate (substrate v2; 396/400). Using the secondary structure prediction software as a guide to edit the relevant bases,

oligonucleotides 556 and 557 (enhanced substrate v1) were successfully designed with more positive ΔG values (-2.8 kcal/mole for both predictions of 556, and -3.5 kcal/mole for both predictions of 557; Fig. 5).

FIGURE 5

Enhanced substrate v1: 556/557

556 secondary structure prediction

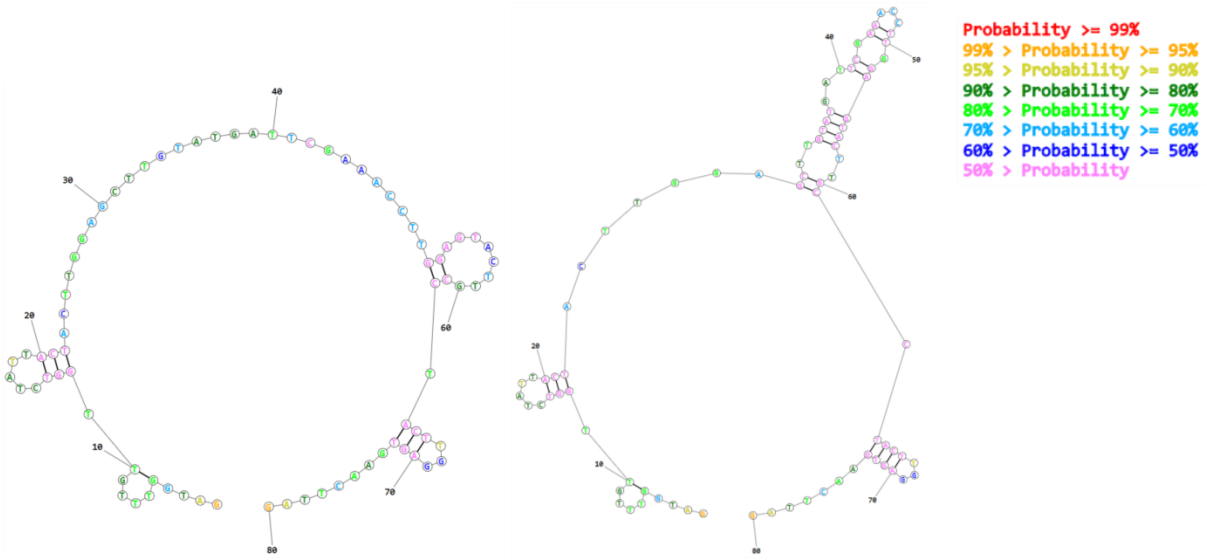

ΔG = -2.8 kcal/mole ΔG = -2.8 kcal/mole

557 secondary structure prediction

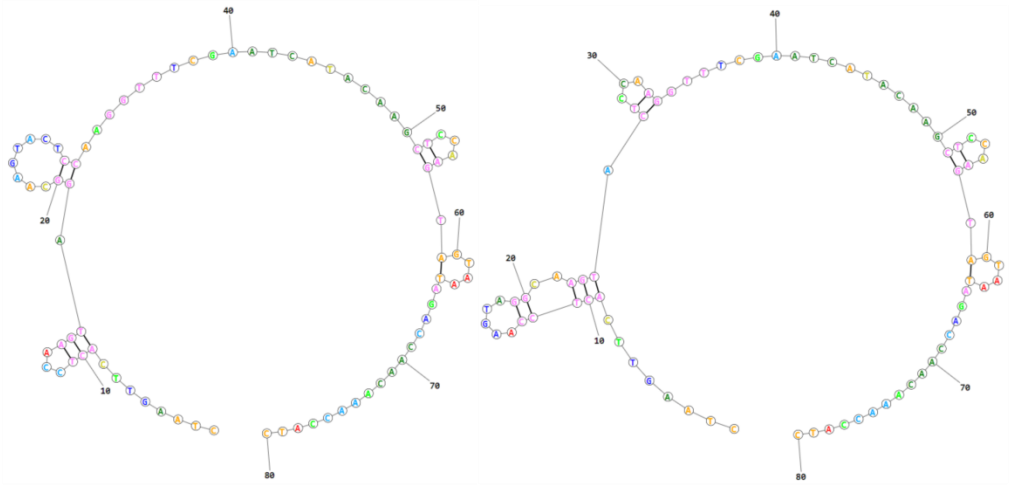

ΔG = -3.5 kcal/mole ΔG = -3.5 kcal/mole

Figure 5 | Improved ΔG values for the edited low-fluorescence substrate

Enhanced substrate v1 was composed of two oligonucleotides, 556 and 557. The predicted ΔG values of their secondary structures are -2.8 kcal/mole for 556 and -3.5 kcal/mole for 557.

As suspected, lower ΔG values cause a reduction in the likelihood of secondary structure formation. In turn, this enables a higher proportion of successful annealing between the two complementary oligonucleotides with an accompanying increase in fluorescence (Fig. 6). Although enhanced substrate v1 (556 and 557) does have the most positive ΔG compared to substrate v2 (396 and 400), there is no greater increase in fluorescence. This may be because the difference between their ΔG values is minor in comparison to enhanced substrate v1 and substrate v1 (381 and 468).

FIGURE 6

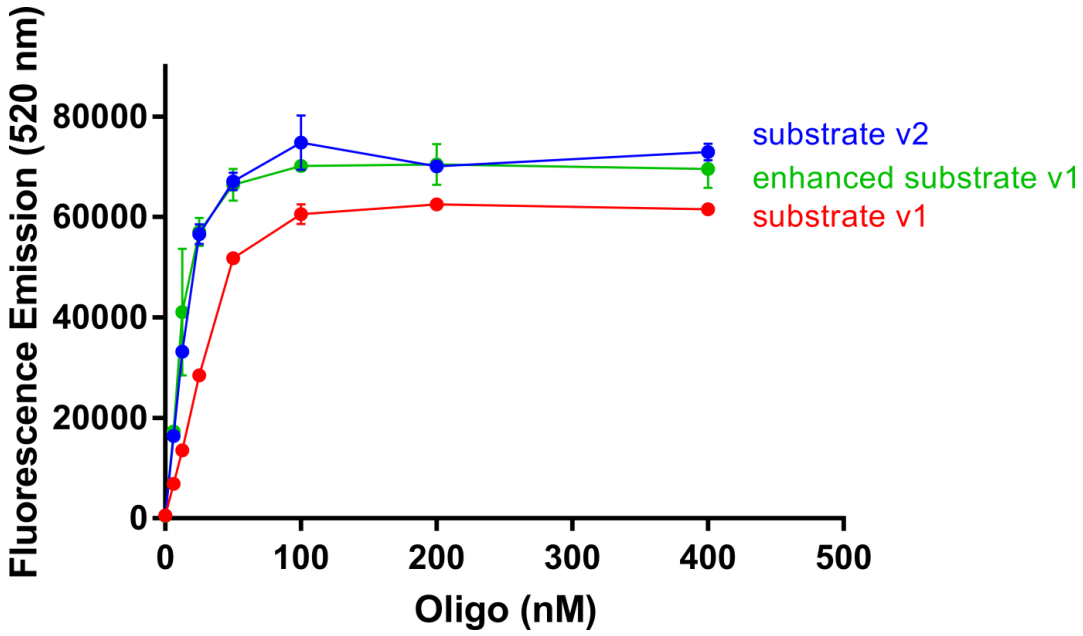

Figure 6 | Calibration curve of the two original 80-bp substrates and the enhanced substrate. A calibration curve of substrate v1 and substrate v2, including enhanced substrate v1, which was edited to reduce the formation of secondary structures at 37°C.

PG fluorescence is affected by buffer components

Evidence suggests that certain compounds exert either a positive or negative influence on the PicoGreen fluorescence signal, some of which are present in enzyme storage and reaction buffers. 2% (v/v) BSA reduces the signal by 16%, and 200 mM NaCl reduces the signal by 30%. This list of compounds is not exhaustive, however, and so the differential effects of the DNase I storage and reaction buffers were explored (Fig. 7). The storage buffer augments the fluorescent signal, whilst the reaction buffer has the opposite effect and reduces fluorescence. Altering the recommended concentrations of each buffer to 50% or 100% failed to make a significant difference to further improve the signal (Fig. 7 a-b).

FIGURE 7

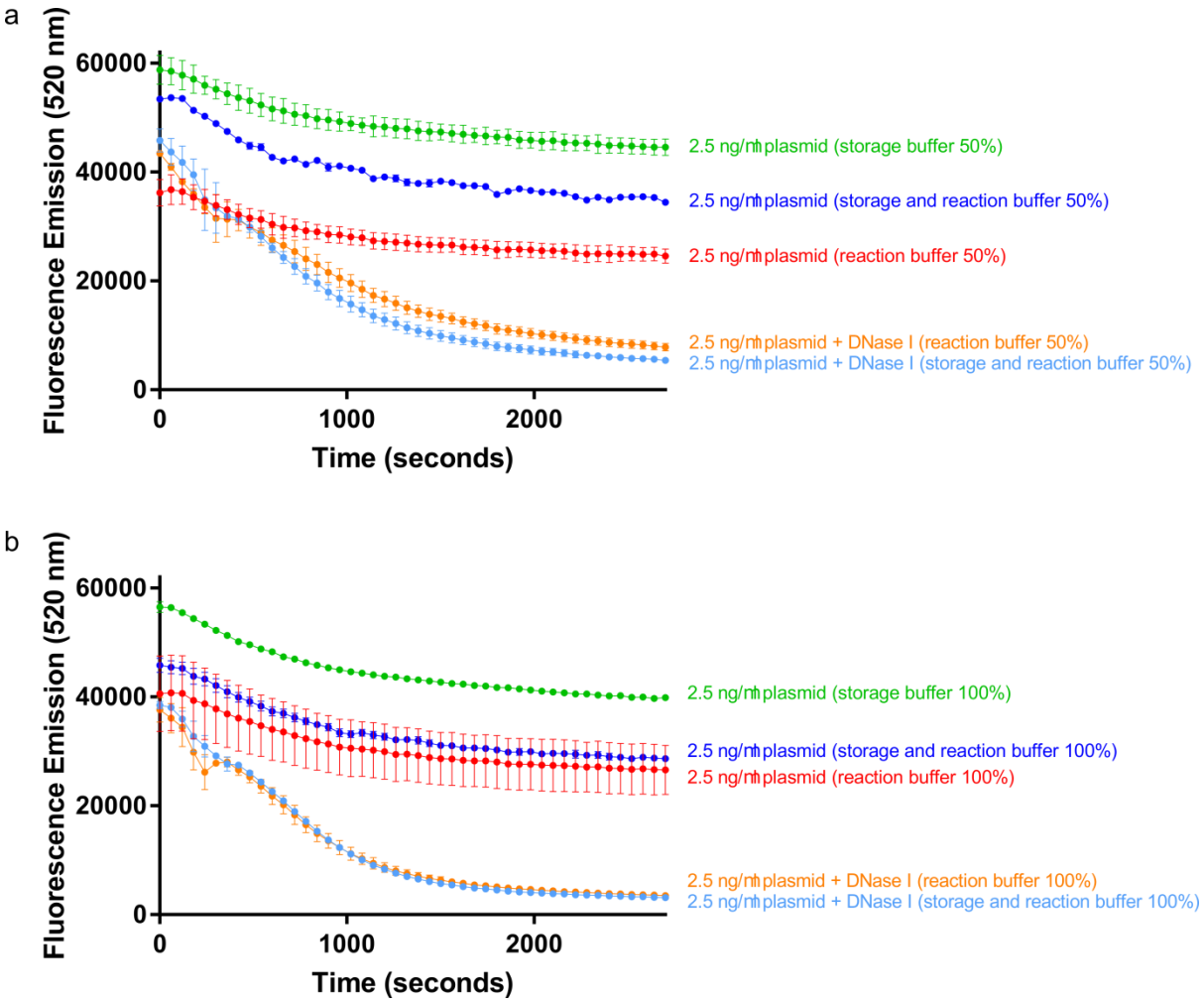

Figure 7 | Effect of DNase I reaction and storage buffers on PicoGreen fluorescence

a, and **b,** Comparisons of the fluorescent signal according to the DNase I storage and reaction buffers at both 50% and 100% of their recommended concentrations. The storage buffer augments fluorescence whilst the reaction buffer reduces the signal. Error bars represent SD; n=2 in all cases.

3.9 Optimisation of the assay using the non-specific DNase I

FIGURE 8

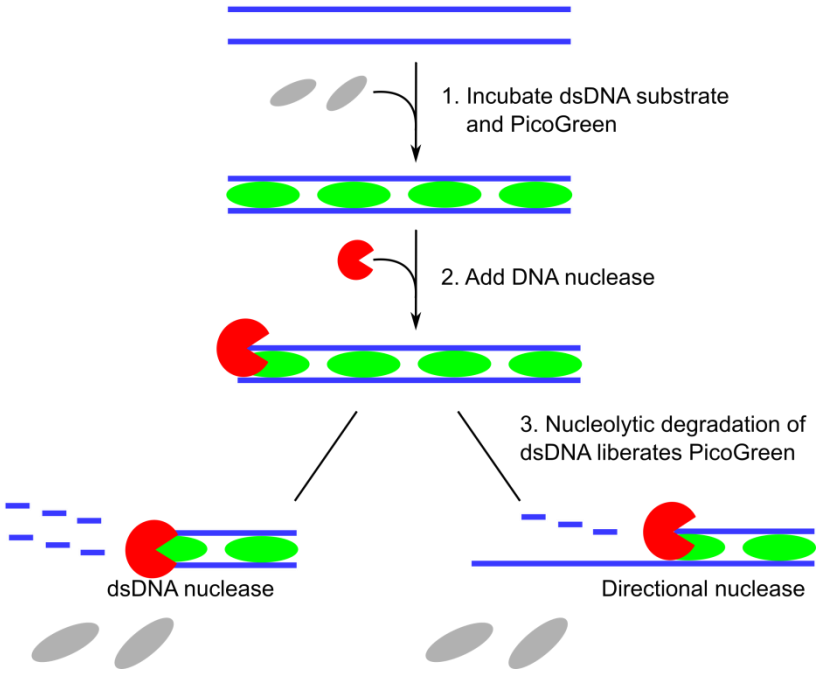

Figure 8 | Illustration depicting the concept of the continuous assay

PG intercalates with dsDNA to produce a measurable fluorescent signal. Addition of a dsDNA nuclease or resection nuclease disrupts the PG:dsDNA complex, liberating the PG and triggering a nuclease-dependent loss of fluorescence.

To confirm whether PG could be used to study nucleases in real-time (as illustrated in Fig. 8), its applicability and robustness was first validated with a non-specific nuclease. DNase I digests ssDNA, both strands of dsDNA, and does not show absolute sequence specificity (although it has shown a general preference for AT base pairs as opposed to GC base pairs (171)).

A calibration curve was established to determine the linear range in which the concentration of DNA is directly proportional to the fluorescent signal (Fig. 9a). Both plasmid DNA (13.1 kb) and oligonucleotide DNA (80 bp) were compared, and it was determined that the maximum concentration of DNA that could be used in the assay was 2.5 ng/µL, regardless of the length and structure of the DNA. Above 2.5 ng/µL, the fluorescent signal plateaued irrespective of the increase in DNA concentration (Fig. 9a).

As an alternative to converting fluorescence to molar concentrations, which vary according to the length of the DNA substrate, a standard curve was generated based on the signal produced from 80-, 60-, 40- and 20-bp substrates, as well as a 0-bp single-stranded 80-mer oligomer to represent the final resection product of other resection nucleases (Fig. 9b). PG binds ssDNA with a lower affinity than dsDNA, as indicated by the standard curve. For resection nucleases, rather than DNase, this is a more appropriate end-point of the reaction rather than the comparatively minor fluorescent signal produced in the absence of substrate. This standard curve shows a linear increase in fluorescence with the length of duplex DNA ($R^2 = 0.99$).

The purpose of the standard curve is to enable the conversion of fluorescence units to DNA base pairs to calculate the length of substrate remaining following nucleolytic attack. To convert the data from fluorescence units, the data is first normalised to their relevant control (absence of enzyme). This has the additional benefit of accounting for the inevitable photobleaching effect. As such, any decrease in fluorescence recorded is a result of nuclease activity and not photobleaching of the PG dye. The standard curve is then converted to base pairs by finding the gradient (m) and intercept (c) of the curve at each time point, and from this it is possible to determine the length of dsDNA (x-axis) from the fluorescent signal (y-axis) at each time point and experimental condition. A worked example is available in the Appendix.

FIGURE 9

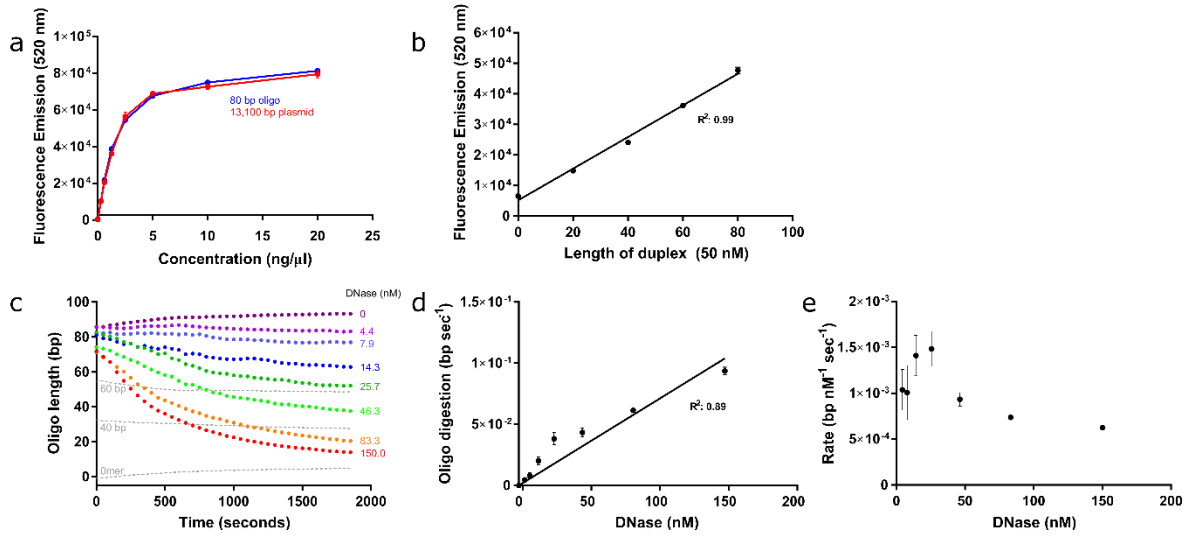

Figure 9 | Optimisation of assay parameters using the non-specific nuclease DNase I

a, Calibration curve indicating the fluorescent signal emitted by increasing concentrations of 80 bp dsDNA and 13.1 kb plasmid DNA. **b,** Standard curve composed of 80, 60, 40 and 20 bp sequences. The point shown at 0 on the x-axis is an 80-nt ssDNA oligomer to represent the end product of complete resection. **c,** DNase I titration on an 80 bp dsDNA substrate. Dotted grey lines represent controls containing standard duplexes of intermediate sizes. **d,** Extracted maximum gradient from (d) to determine the reaction rate at increasing concentrations of DNase I. **e,** Maximum rate analysis of resection per nM DNase I per second. Error bars represent SEM; n=3 in all cases.

A DNase I titration was run with the addition of the standard curve, allowing the conversion of the y-axis from fluorescence units to a measurement of the length of dsDNA (Fig. 9c). From this it was determined that the rate increases with the concentration of DNase I, therefore indicating that the reaction is first order with respect to the enzyme (Fig. 9d). Subsequently, the rate of DNase I-mediated digestion was calculated to be approximately 0.001 bp nM^{-1} sec^{-1} on a 2.5 ng/µL (50 nM) 80-bp dsDNA substrate at 37°C (Fig. 9e).

FIGURE 10

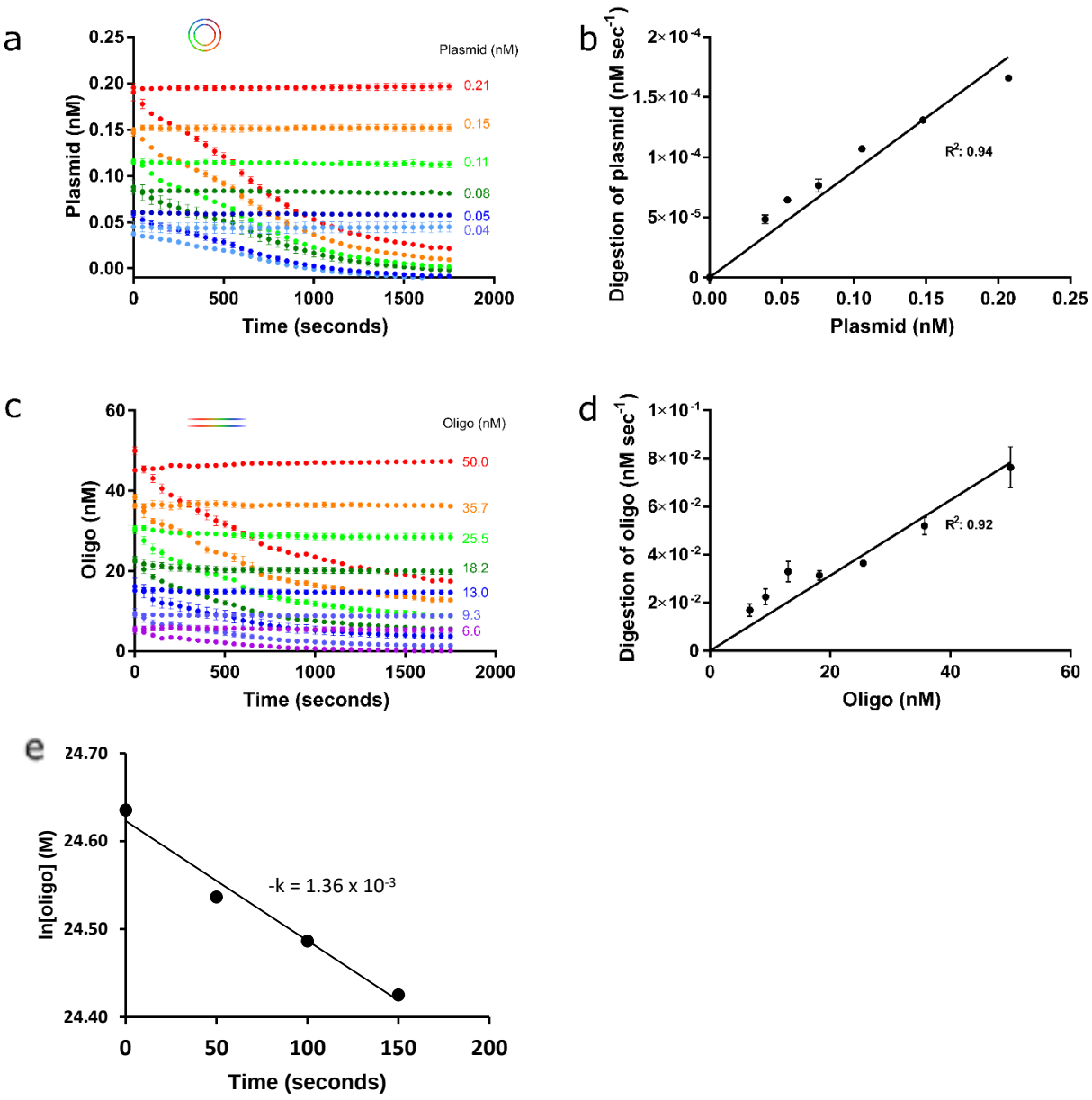

Figure 10 | Fluorescence units can be converted to nM concentrations of DNA substrate

a, Plasmid titration in the presence of 50 nM DNase I. **b,** Calculated the maximum rate of resection of increasing concentrations of plasmid based on the maximum gradients in (a). **c,** Oligonucleotide titration in the presence of 50 nM DNase I. **d,** Calculated the maximum rate of increasing concentrations of an 80-mer dsDNA substrate based on the maximum gradients in (c). **e,** Calculated the value of the rate constant for the reaction in (c) 50 nM oligo.

Alternatively, fluorescence units can be converted to nanomolar concentrations of substrate as opposed to base pairs of DNA. Utilising the fluorescence units used in the samples without DNase I, these figures were used as a calibration curve, allowing

us to convert fluorescence units into concentration of substrate. The calibration curve was used as a reference point at each time point, which could then be used to convert the Y-axis change in fluorescence (ΔF) into a measurement of the number of nucleotides cleaved, which was then converted into a value for rate. This method of normalising the data circumvents the effect of photobleaching as it subtracts the decrease in fluorescence from the controls and the substrates in the presence of DNase I, which ensures that the loss of fluorescence observed after normalisation is results only from nuclease activity.

The plasmid was titrated in the presence of 50 nM DNase I (Fig. 10a) and the rate of DNase I-dependent digestion was obtained at each concentration (Fig. 10b). The linear relationship between increasing substrate concentration and DNase I-dependent digestion indicates that the rate is dependent on the quantity of available plasmid. This also suggests that this is a first order reaction with respect to the plasmid at this concentration of DNase I.

This titration was replicated on 80 bp DNA substrates (Fig. 10c), and the control samples not treated with DNase I were used to generate a calibration curve at each time point. This, again, allows for the conversion of the raw fluorescence data to DNA concentration. From this the maximum rate in the reaction was obtained and, as with the plasmid, there is a linear relationship between the substrate concentration and the rate, indicating that this is a first order reaction with respect to the substrate (Fig. 10d). To confirm the order of the reaction, the following integrated rate equations was used:

$$1.\ \ln[\text{oligo}]_{t150} = -kt + \ln[\text{oligo}]_{t0}$$

Equation 1 follows the graph of a straight line (y=mx+c). The reaction was confirmed as first order by plotting time on the x-axis, and the natural log of the concentration of oligo at each time point from 0 to 150 seconds on the y-axis. These data points fall in a straight line, and therefore the reaction is first order. The reaction rate (-k) is calculated from the gradient of the line, and this is 1.36×10^{-3} (Fig. 10e).

These results show that this assay is versatile and can capture a range of kinetic information depending on what is required from the experiment. The only difficulty with using this method is that nanomolar concentrations of DNA substrate is dependent on the length of the oligomer and, as such, creates a situation where the activity of two substrates of different lengths cannot be easily compared. Therefore, converting to base pairs is a far more straightforward process.

3.10 Modifying DNA substrates to study structure-specific enzymes

Since the assay has proven to be proficient in garnering detailed kinetic analysis of a nonspecific nuclease, the assay then progressed to analysing less tolerant nucleases that exhibit structural specificities and directionality. To validate the assay for these resection nucleases, the 3'-5' bacterial Exonuclease III (ExoIII) and the T7 bacteriophage 5'-3' T7 exonuclease (T7 Exo) were employed (Fig. 11).

To cater for studying resection nucleases, it was necessary to design substrates that directed enzymatic activity to only one end of the substrate. This is due to limitations in the maximum length of oligonucleotide that can be synthesised. Therefore, generating substrates that are blocked at one end circumvents these limitations. An additional benefit of chemically blocking one end of the substrate is that it doesn't require any prior knowledge of inhibitory structures specific to each enzyme, which is a technique that has been used to great effect (13).

To account for having enough dsDNA region as well as structurally appropriate terminal ends to study nuclease structural preferences, substrates were designed that were blocked at one end to direct the enzyme to resect one single strand only, leaving a full-length, blocked, single-stranded 80-mer substrate as the end product (Fig. 11a). The substrates were blocked with biotin-triethyleneglycol (BITEG) at the necessary terminal ends (3' end for ExoIII and 5' end for T7 Exo). BITEG alone is insufficient to inhibit resection on substrates blocked at both terminal ends (Fig. 11b-c). However, inclusion of streptavidin in the reaction mix successfully protects the modified ends from resection (Fig. 11b-c). It was noticed that the presence of streptavidin, but not BITEG alone, is responsible for preventing total resection, prohibiting ExoIII from resecting the final 20 nucleotides (Fig. 11d). This combination of biotin and streptavidin has previously been shown to be effective (182).

FIGURE 11

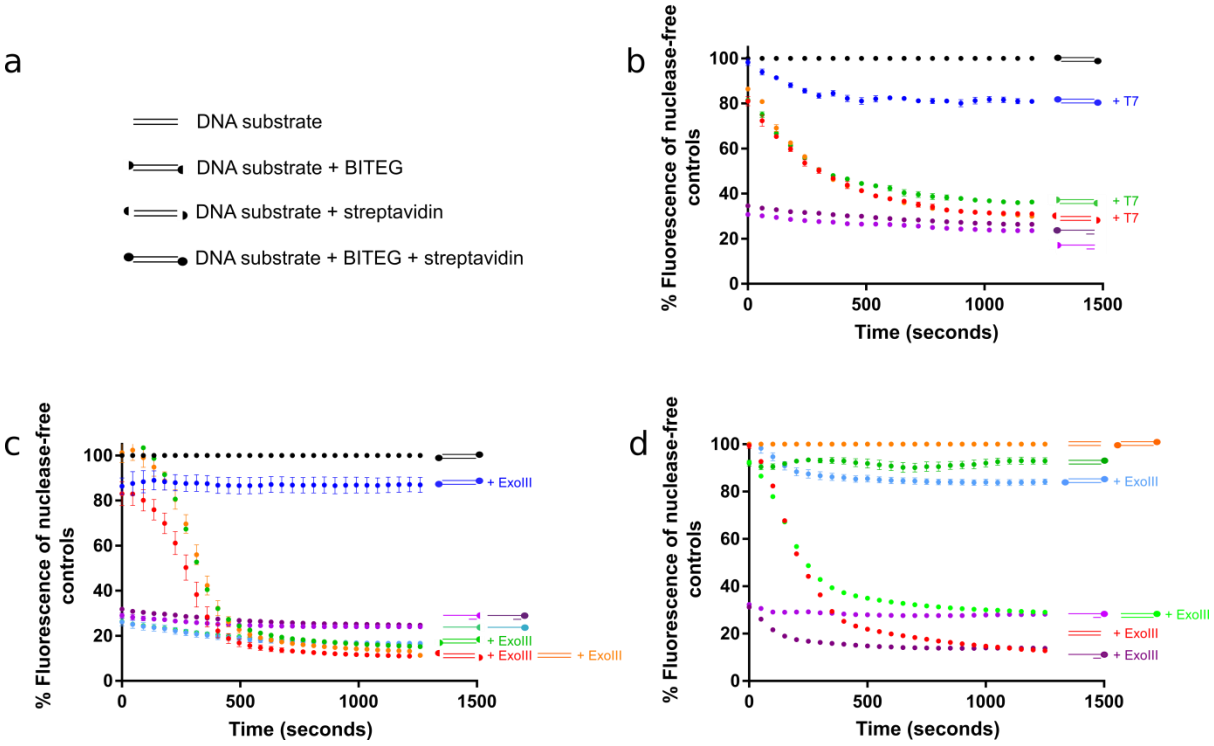

Figure 11 | BITEG alone is insufficient for preventing nuclease resection

a, Stick and ball figures illustrate the substrates and the distinguishing features of the BITEG and streptavidin modifications. **b,** Treated a range of substrates with and without the BITEG and streptavidin modifications in the presence of 12 nM T7 Exo. **c,** Treated a range of substrates with and without BITEG and streptavidin modifications in the presence of 10 nM ExoIII. **d,** Presence of streptavidin prevents total resection of the substrate. Error bars represent SEM; n=3 in all cases.

A streptavidin dilution was set up to determine the optimum concentration that would suitably prohibit enzymatic resection (Fig. 12). Ultimately, 0.02 ng/µL streptavidin was an appropriate concentration, as it appeared that within the range of 0.02 – 1 ng/µL the inhibitory effect was negligible. It is suspected that the low level of resection observed (10-20%) is attributable to a small proportion of oligonucleotide substrates that are shorter in length, or non-biotinylated, and are therefore prone to T7 Exo-mediated resection.

FIGURE 12

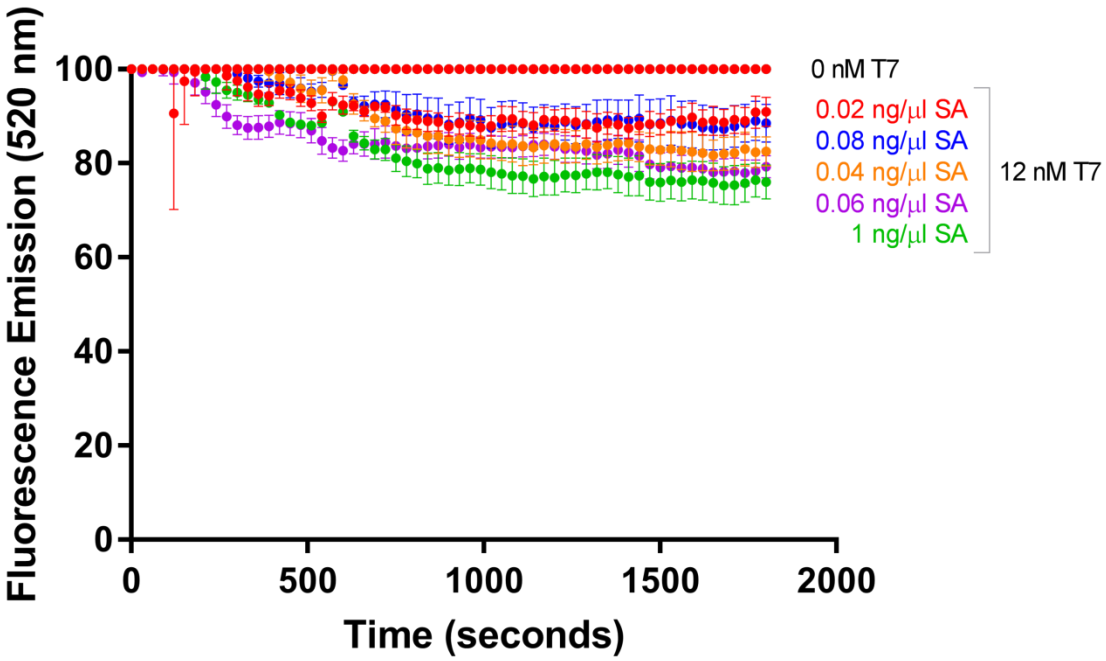

Figure 12 | 0.02 ng/µL streptavidin (SA) is sufficient to inhibit resection by 12 nM T7 Exo
Increasing concentrations of streptavidin (0.02 – 1 ng/µL) were added to substrates biotinylated at both 5' ends to inhibit T7 Exo-mediated resection.

To reduce the background levels of resection and ensure high levels of oligonucleotide purity, HPLC purification was deemed the most appropriate. PAGE purification was considered as it is the Integrated DNA Technologies-recommended technique for oligonucleotides >80 bases in length. However, 3'-BITEG substrates cannot be purified using this process. Therefore, as HPLC is capable of purifying oligonucleotides with both 5'- and 3'-BITEG modification, and routinely achieves a reasonable 85% purity, this was deemed the most suitable technique.

Other methods to block the DNA were considered. Several options are listed on the Integrated DNA Technologies website (https://eu.idtdna.com/pages/education/decoded/article/modification-highlight-modifications-that-block-nuclease-degradation), including 2'-O-methyl, 2' fluoro, 3'-phosphorylated, and inverted dT and ddT, phosphorothioate bonds. 2'-O-methyl is typically used to stabilise RNA duplexes and is not a commercially available modification for DNA. Furthermore, 2'-O-methyl only prevents attack by ssDNA

endonucleases, but not exonucleases. As a result, this modification is unsuitable for this application (398). 2'fluoro is also an RNA modification, and therefore is also inappropriate for this assay (399). 3'-phosphorylations are only inhibitory to some 3' exonucleases, Exonuclease III, for example, has intrinsic phosphatase activity, and therefore is not inhibited by this modification (400). Inverted dT (3'-3') or ddT (5'-5') terminal nucleotides were strongly considered, however very few articles have been published on their efficacy, and only in terms of stability against RNA nucleases (401). As such, inverted nucleotides were not incorporated into the design of this assay. Finally, phosphorothioate linkages were initially selected, and have been shown to be effective against RNA and DNA nucleases (402–404). However, the yield after purification is lower than for BITEG-modified oligonucleotides, and ultimately would have been more costly.

3.11 Discussion

PG has previously been used to visualise picogram concentrations of DNA in tissue samples (405), gel electrophoresis (383), flow cytometry (384), and discontinuous nuclease (387) and polymerase assays (389,390). While it has been used for several different applications, its value to continuous assays hasn't fully been recognised (394).

Various aspects of the assay have had to be optimised for this to become a possibility. PG had to be stabilised using glycerol to protect it from rapid photobleaching (395). In addition, the DNA substrates had to be edited so as to reduce the likelihood of secondary structure formation. This ensures the most efficient binding between the two complementary strands, and allows for more PG binding, which correlates to a much stronger fluorescent signal. This is important to capture enzymatic activity in the most detail.

Further to this, the DNA substrates were modified to cater for resection nucleases. To direct nuclease activity to one end of the substrate, BITEG was added to the terminal ends of the oligonucleotides. While BITEG alone proved to be insufficient to inhibit nuclease activity, the addition of streptavidin provided enough steric hindrance to prevent both 3' and 5' nucleases from resecting the DNA substrate.

To study the kinetics of nuclease activity, a calibration curve can be included in every assay to either convert the fluorescence units to base pairs or to nanomolar concentrations of DNA. This has the advantage of eliminating the effect of photobleaching and indicates the detail in which nucleases can be analysed. It is hoped that this assay will prove to be incredibly powerful when it is used to study more structure-specific nucleases, as explored in Chapter 4.

4 Validation of a fluorescence-based toolkit for measuring structure-specific nuclease activity and their substrates

4.1 Summary

DNA nucleases play a critical role in diverse DNA repair processes. Nevertheless, many nucleases have unknown or poorly characterized activities. Elucidating nuclease activity specificities and regulatory components can support a more definitive understanding of the DNA damage response in physiology and disease. Using fluorescence-based methods, a quick, safe, reproducible, cost-effective and continuous nuclease assay toolkit that could be used for small- and large- scale experimental assays was developed. Additionally, these data can be analysed to determine each reaction's unique enzyme kinetics. A library of DNA substrates has been designed that can be used to study resecting nucleases and nickases, conferring the ability to ascertain substrate preference and enzyme directionality. The assay is sensitive enough to detect kinetics of repair enzymes when confronted with DNA mismatches or DNA methylation sites. This assay has also been extended to consider analysing the kinetics of human single-strand DNA nuclease TREX2, and DNA polymerases, which are also involved in DNA repair, and have been associated with various disease conditions.

4.2 The combination of PicoGreen and a DNA substrate library enables the study of nucleic acid-active enzymes

Following the detailed introduction about nucleases and the novel assay developed in Chapter 3, potential applications of this novel fluorescence-based nuclease resection assay will hereby be elaborated on. The aim is to replace the classical radiolabelling-based assays (406,407). This toolkit has been optimised for a range of important representative nucleases, including: DNase I (a non-specific ss- and dsDNA nuclease), T7 exonuclease (a 5'–3' dsDNA bacteriophage nuclease) (13), Exonuclease III (a 3'–5' dsDNA *E. coli* nuclease) (408), human Trex2 (a 3'–5' ssDNA nuclease) (409), and a viral nickase, Nt.CviPII (410). These representative nucleases were chosen because of their 1) availability, stability, purity, and specificity (DNase I, T7, ExoIII, Klenow, and Nt.CviPII) and for their 2) importance for mammalian cell function (TREX2). TREX2 is a mammalian keratinocyte-specific nuclease that has

been shown to work in a 3'–5' non-processive manner to promote DNA repair or apoptosis in chemically- or UVB-induced carcinomas. Consistent with a role in keratinocyte carcinogenesis, polymorphisms in the Trex2 gene, and its aberrant expression, have been shown in human squamous cell carcinomas (179,411–414).

Furthermore, a library of DNA substrates was designed to account for these enzymes' differential activities. Due to oligomer length limitations, it was necessary to design substrates with biotin-TEG-modified 3' or 5' termini to control enzyme directionality. The addition of streptavidin to the biotinylated ends protects the substrate from resection at the modified end, as was demonstrated in a previous resection assay (182). This oligonucleotide library can be used to study a multitude of uncharacterised nucleases, and their substrate preferences, to elucidate their roles in DNA repair and genomic maintenance. To extend the power of this approach, physiologically relevant substrates have been designed that contain mismatches and methyl-cytosines. It has been posited that repair nucleases resect along a methylated sequence of DNA, thus permanently removing epigenetic markers. Human 5'–3' exonuclease, Exo1, resects through mismatches during mismatch repair (415,416). As such, it would be interesting to determine whether this mismatch is permissive to nucleases in general. As the assay relies on the loss or gain of the DNA duplex structure, other enzymes that reconstitute or compromise the DNA-pairing structure could also be validated in this assay. Furthermore, monitoring of polymerase activity has been demonstrated on the complementary strand. Picogreen (PG) has previously been used to visualise polymerase activity, but to the best of found knowledge, this is the first time it has been described in a continuous assay (389).

This work provides a robust and versatile toolkit to characterise DNA nucleases and determine their substrate preferences with high resolution and sensitivity. This assay can be adapted and modified to suit a wide range of DNA repair applications.

4.3 Materials and Methods

4.3.1 Plasmid and oligonucleotide substrates

DNA substrates were prepared by diluting a 7000 kb plasmid in HyClone water™ (GE healthcare), and unmodified HPLC-purified oligonucleotide substrates (Eurofins) in 1X annealing buffer (Sigma-Aldrich). Oligonucleotides were designed and optimised against secondary structure formation using the 'Predict a Secondary Structure Web Server' (https://rna.urmc.rochester.edu/RNAstructureWeb/Servers/Predict1/Predict1.html) (114) and annealed at a 1:1 molar ratio. Table 1 shows all the oligonucleotides and their respective illustrations, while Table 2 lists the oligonucleotide sequences and modifications.

Table 1

Oligomers	Illustration	Codes
S		RCOL556 / RCOL557
$_{*}S^{*}$		RCOL621/ RCOL626
S^{*}		RCOL621/ RCOL557
$_{+2}S^{*}$		RCOL621 / RCOL622
$_{+4}S^{*}$		RCOL621 / RCOL624
$^{*}S_{*}$		RCOL616 / RCOL620
$^{*}S$		RCOL616 / RCOL557
$^{*}S_{+2}$		RCOL616 / RCOL617
$^{*}S_{+10}$		RCOL616 / RCOL618
$^{*}S_{+20}$		RCOL616 / RCOL619
$_{G>A}S^{*}$		RCOL621 / RCOL715
$_{*}S$		RCOL556 / RCOL626
$_{*}S^{C>T}$		RCOL714 / RCOL626
$^{*}S_{G>A}$		RCOL616 / RCOL715
S_{*}		RCOL556 / RCOL620
$^{C>T}S_{*}$		RCOL714 / RCOL620
$_{*}S^{4M}$		RCOL710 / RCOL626
$_{*}S^{1M}$		RCOL711 / RCOL626
$^{4M}S_{*}$		RCOL710 / RCOL620
$^{1M}S_{*}$		RCOL711 / RCOL620
$_{*}S^{N*}$		RCOL648 / RCOL649 / RCOL626
$_{*}S^{G*}$		RCOL648 / RCOL650 / RCOL626
$^{*N}S_{*}$		RCOL645 / RCOL646 / RCOL620
$^{*G}S_{*}$		RCOL645 / RCOL647 / RCOL620
60nt for ladder		RCOL611
40nt for ladder		RCOL610
20nt for ladder		RCOL609
60nt overhang (^{20}S)		RCOL562 / RCOL557
40nt overhang (^{40}S)		RCOL560 / RCOL557
20nt overhang (^{60}S)		RCOL558 / RCOL557

Table 2

Oligo code	Sequence (5'–3')
RCOL556	GATGGTTTGTTGGTCTATTACTACTTGGAGCTTGTATGATTCGAAACCTTGGAGTACTTGCCTACTTGGAGTGAACTTAG
RCOL557	CTAAGTTCACTCCAAGTAGGCAAGTACTCCAAGGTTTCGAATCATACAAGCTCCAAGTAGTAATAGACCAACAAACCATC
RCOL621	GATGGTTTGTTGGTCTATTACTACTTGGAGCTTGTATGATTCGAAACCTTGGAGTACTTGCCTACTTGGAGTGAACTTAG-BITEG*
RCOL626	CTAAGTTCACTCCAAGTAGGCAAGTACTCCAAGGTTTCGAATCATACAAGCTCCAAGTAGTAATAGACCAACAAACCATC-BITEG*
RCOL622	CTAAGTTCACTCCAAGTAGGCAAGTACTCCAAGGTTTCGAATCATACAAGCTCCAAGTAGTAATAGACCAACAAACCATCTT
RCOL624	CTAAGTTCACTCCAAGTAGGCAAGTACTCCAAGGTTTCGAATCATACAAGCTCCAAGTAGTAATAGACCAACAAACCATCTTTT
RCOL616	BITEG-GATGGTTTGTTGGTCTATTACTACTTGGAGCTTGTATGATTCGAAACCTTGGAGTACTTGCCTACTTGGAGTGAACTTAG*
RCOL620	BITEG-CTAAGTTCACTCCAAGTAGGCAAGTACTCCAAGGTTTCGAATCATACAAGCTCCAAGTAGTAATAGACCAACAAACCATC*
RCOL617	TTCTAAGTTCACTCCAAGTAGGCAAGTACTCCAAGGTTTCGAATCATACAAGCTCCAAGTAGTAATAGACCAACAAACCATC
RCOL618	TTTTTTTTTTCTAAGTTCACTCCAAGTAGGCAAGTACTCCAAGGTTTCGAATCATACAAGCTCCAAGTAGTAATAGACCAACAAACCATC
RCOL619	TTTTTTTTTTTTTTTTTTTTCTAAGTTCACTCCAAGTAGGCAAGTACTCCAAGGTTTCGAATCATACAAGCTCCAAGTAGTAATAGACCAACAAACCATC
RCOL714	GATGGTTTGTTGGTTTATTACTACTTGGAGTTTGTATGATTTGAAACCTTGGAGTACTTGTCTACTTGGAGTGAACTTAG**
RCOL715	CTAAGTTCACTCCAAGTAGACAAGTACTCCAAGGTTTCAAATCATACAAACTCCAAGTAGTAATAAACCAACAAACCATC***
RCOL710	GATGGTTTGTTGGTCTATTACTACTTGGAGCTTGTATGATTCGAAACCTTGGAGTACTTGCCTACTTGGAGTGAACTTAG****
RCOL711	GATGGTTTGTTGGTCTATTACTACTTGGAGCTTGTATGATTCGAAACCTTGGAGTACTTGCCTACTTGGAGTGAACTTAG****
RCOL648	GTGAACTTAG-BITEG*
RCOL649	GATGGTTTGTTGGTCTATTACTACTTGGAGCTTGTATGATTCGAAACCTTGGAGTACTTGCCTACTTGGA
RCOL650	GATGGTTTGTTGGTCTATTACTACTTGGAGCTTGTATGATTCGAAACCTTGGAGTACTTGCCTACTTGG
RCOL645	BITEG-GATGGTTTGT*
RCOL646	TGGTCTATTACTACTTGGAGCTTGTATGATTCGAAACCTTGGAGTACTTGCCTACTTGGAGTGAACTTAG
RCOL647	GGTCTATTACTACTTGGAGCTTGTATGATTCGAAACCTTGGAGTACTTGCCTACTTGGAGTGAACTTAG
RCOL611	CTAAGTTCACTCCAAGTAGGCAAGTACTCCAAGGTTTCGAATCATACAAGCTCCAAGTAG
RCOL610	CTAAGTTCACTCCAAGTAGGCAAGTACTCCAAGGTTTCGA
RCOL609	CTAAGTTCACTCCAAGTAGG
RCOL562	GATGGTTTGTTGGTCTATTA
RCOL560	GATGGTTTGTTGGTCTATTACTACTTGGAGCTTGTATGAT
RCOL558	GATGGTTTGTTGGTCTATTACTACTTGGAGCTTGTATGATTCGAAACCTTGGAGTACTTG
RCOL739	TCGAAACCTTGGAGTACTTGCCTACTTGGAGTGAACTTAG
RCOL738	CCTACTTGGAGTGAACTTAG

*BITEG represents the biotin-TEG modification

**T bases in bold indicate sites of C>T base changes to generate a mismatched substrate

***A bases in bold indicate sites of G>A base changes to generate a mismatched substrate

****C bases in bold indicate methylcytosines

4.3.2 Nucleases and buffers

The nucleases used were RQ1 RNase-Free DNase I (Promega), T7 exonuclease (New England Biolabs), Exonuclease III (New England Biolabs), Trex2 (Stratech), Klenow Fragment (3' → 5' exo-; New England Biolabs). In preparation for each assay, nucleases used were diluted on ice in their appropriate storage buffers, omitting glycerol. All storage buffers and reaction buffers were made according to the recipes available on their respective NEB and Thermo Fisher web pages. DNase I storage buffer (10mM HEPES (pH 7.5), 10mM $CaCl_2$ and 10mM $MgCl_2$) and reaction

buffer (400mM Tris-HCl (pH 8.0), 100mM $MgSO_4$ and 10mM $CaCl_2$), T7 exonuclease storage buffer (10 mM Tris-HCl, 5 mM DTT, 0.1 mM EDTA, (Ph 8 at 25ºC)) and reaction buffer (50 mM potassium acetate, 20 mM Tris-Acetate, 10 mM magnesium acetate, 1 mM DTT), and Exonuclease III storage buffer (5 mM KPO_4, 200 mM KCl, 5 mM β-ME, 0.05 mM EDTA, 200 µg/mL BSA, (pH 6.5 at 25ºC)) and reaction buffer (10 mM Bis-Tris-Propane-HCl, 10 mM $MgCl_2$, 1 mM DTT (pH 7 at 25ºC)), Trex2 storage buffer (20 mM Tris-HCl (pH 8), 200 mM NaCl, 5 mM DTT) and reaction buffer (50 mM potassium acetate, 20 mM Tris-acetate, 10 mM magnesium acetate, 100 µg/mL BSA, (pH 7.9 at 25ºC)) and Klenow Fragment storage buffer (25 mM Tris-HCl, 1 mM DTT, 0.1 mM EDTA, (pH 7.4 at 25ºC)) and reaction buffer (50 mM NaCl, 10 mM Tris-HCl, 10 mM MgCl2, 1 mM DTT, (pH 7.9 at 25ºC)) were all filtered prior to use, and autoclaved where possible.

Trex2 (Stratech), Klenow Fragment (3' → 5' exo-; New England Biolabs). In preparation for each assay, nucleases used were diluted on ice in their appropriate storage buffers, omitting glycerol. DNase I, T7 exonuclease, Exonuclease III, Trex2 and Klenow fragment storage buffers and reaction buffers were all filtered prior to use, and autoclaved where possible.

4.3.3 Preparation of PicoGreen

The PG reagent from the Quant-iT™ PicoGreen™ dsDNA Assay Kit (Invitrogen) was prepared immediately before use by making a 1:200 dilution of the PG in TE buffer (10 mM Tris-HCl, 1 mM EDTA, pH 7.5) and 40% (v/v) glycerol.

4.3.4 Continuous assay experimental procedure

Each DNA substrate reaction mixture contained 50 nM DNA substrate, 1X reaction buffer (specific for each enzyme), 50 µL PG solution, 0.02 mg/mL streptavidin (cat. 21125, Thermo Fisher Scientific) if required, 0.25 mM dNTPs if required, 5 µL enzyme or relevant storage buffer. For the DNA nucleases, Milli-Q water was added to bring the total reaction volume to 100 µL. Reaction mixtures were prepared on ice and samples were tested in a 96-well, black flat bottom plate (cat. M9685, Sigma-Aldrich). The final components added were the storage buffers, then the enzyme mixtures to start the reaction.

A CLARIOstar microplate reader (BMG labtech) was pre-heated to 37°C. Samples were read every 40-50 s for 30-60 mins. Excitation and emission wavelengths used were 483-15 nm and 530-30 nm, with a focal height of 10.2, 20 flashes per well, with a shake before each read.

4.3.5 Data analysis

For statistical analysis of the data, one-way ANOVA with the Tukey's post-hoc tests were used. This was implemented using GraphPad Prism v7.03. An example of the workflow is available in the appendix.

4.6 Results

Having optimised PG and the DNA substrates in the previous chapter, this fluorescence-based toolkit was subsequently used to study a selection of nucleases with different activities and structural preferences. In addition, the substrates were further modified to study the processivity of nucleases on physiologically-appropriate substrates containing either DNA mismatches, reminiscent of substrates of mismatch repair, or methyl-cytosines, to mimic the decorated structures of genomic DNA.

4.7 Validating the assay for 3'–5' exonuclease: ExoIII

ExoIII is a well-characterised 3'–5' exonuclease that resects from blunt end substrates, and short 3'-overhangs, but is inhibited by 4-nt 3'-overhangs. These activities were replicated in this fluorescence-based assay. For ease, each assay is shown with a stick and ball diagram of the substrates used. The table (Fig. 1a) shows the substrates that have been used and their respective modifications.

A calibration curve was prepared in order to determine the linear range within which the fluorescent signal is directly proportional to the DNA substrate concentration with the addition of BITEG and streptavidin (Fig. 1b). The linear range is the same as with the unmodified DNA substrate (observed in Chapter 3, Fig. 9).

A range of ExoIII titrations were performed on three different substrates: blunt, 2-nt and 4-nt 3'overhangs (Fig. 1c-e). The preference of ExoIII for blunt and 2-nt overhangs is known, as is the inhibitory effect of 4-nt 3'-extensions, as these activities are often exploited for various sequencing and DNA detection techniques (417–420) (Fig. 1f). After determining the rate of resection on each substrate (Fig. 1g), the results suggest that the assay can detect previously reported activities and is suitably sensitive to determine substrate preference. Indeed, ExoIII is completely inhibited by 4-nt overhangs, and is resected at an equally low rate as the negative control, which has both 3'-ends blocked with BITEG and streptavidin. Unexpectedly, it appears that the reaction rate decreases on the blunt substrate and the 2-nt overhang substrate as enzyme concentration increases. It is possible that this inhibition is observed because, at higher rates, a larger pool of reaction products will be created, and ExoIII may bind to these reaction products instead of the full-length oligonucleotide. These reaction

products may function as ‘decoy’ molecules that slow ExoIII-mediated DNA degradation.

FIGURE 1

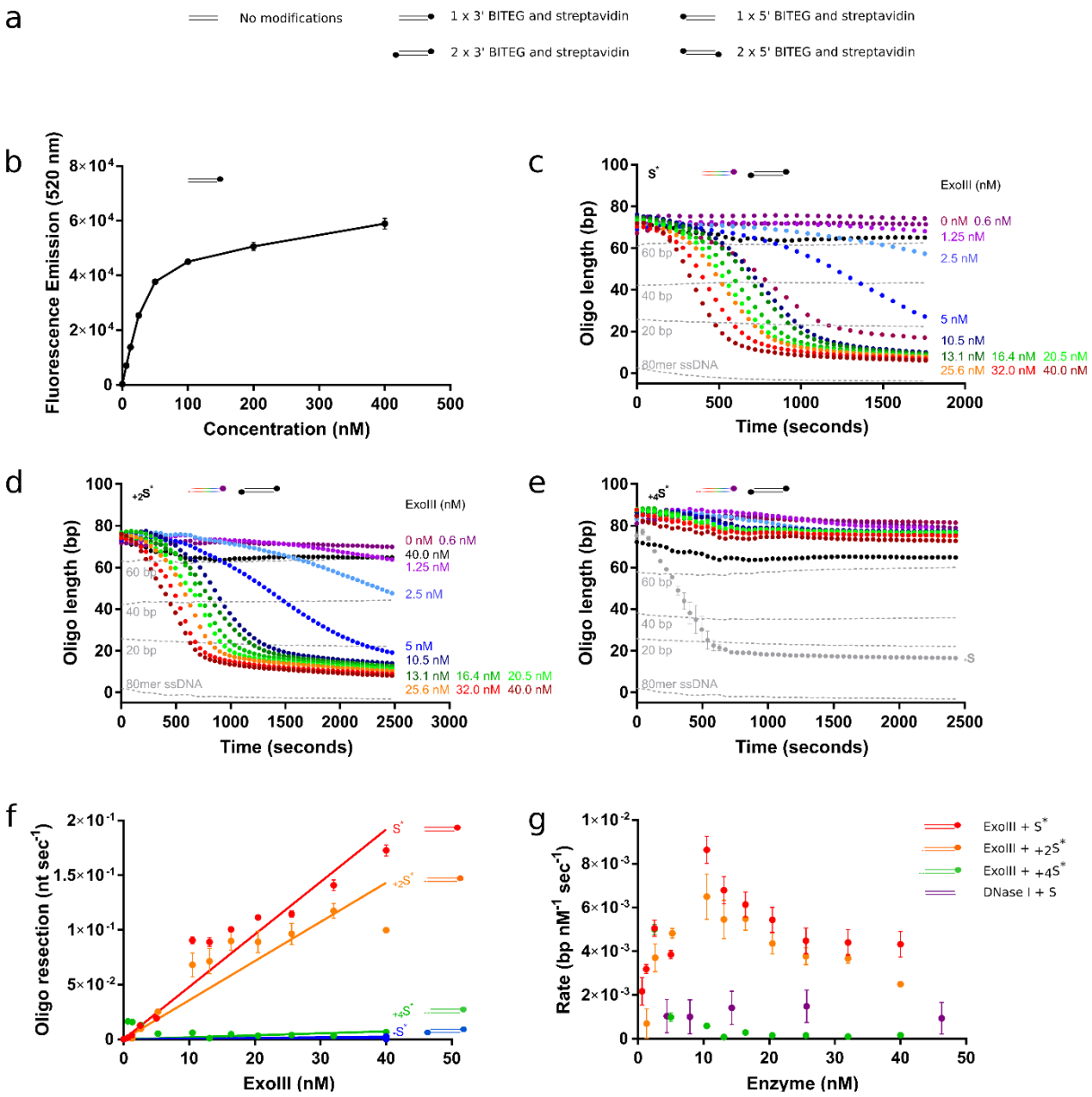

Figure 1 | Validation of the continuous assay for 3' – 5' nucleases

a, Key to stick and ball illustrations of the substrates. The parallel horizontal lines (=) represent the dsDNA substrate, and the coloured-in circle represents the combination of both biotin and streptavidin (●). **b,** Calibration curve depicting the fluorescent signal according to increasing concentrations of 80-bp oligomer substrate with one terminal BITEG modification and in the presence of 0.02 mg/ml streptavidin. **c-e,** ExoIII titrations as depicted in the figures on 50 nM substrates presenting a blunt terminus (c), 2-nt (d) or 4-nt (e) 3' overhang (multi-coloured cartoons), and negative controls (black cartoons) containing BITEG-modified 3'-ends. Results were normalised against their respective negative controls (absence of ExoIII) and converted to bp. The grey curve in (e) shows the equivalent reaction without an overhang, highlighting the loss of activity with a 4 bp 3' overhang. **f,** Rate of resection by ExoIII on the blunt (red), 2-nt (orange) and 4-nt (green) 3' overhangs and the negative control with BITEG-treated 3'-ends. Minimal loss of activity is observed with a 2-nt overhang, in contrast to almost

complete loss of activity with a 4-nt overhang. **g,** Comparison of ExoIII and DNase I activity on their respective substrates. Error bars represent SEM; n=3 in all cases.

4.8 Validating the assay for 5'–3' exonuclease: T7 exonuclease

Having demonstrated that this assay is suitable for 3'–5' nucleases, it was then confirmed that this assay could also be used to study 5'–3' nucleases. T7 Exo activity was investigated on a selection of substrates, including blunt, 2-, 10- and 20-nt 5'-overhangs (Fig. 2a). T7 Exo shows no significant difference between the affinity for blunt and 2'-nt 5'-overhangs. As had previously been observed, the rate of T7 Exo-mediated resection with a 20-nt overhang was approximately 50% of a short overhang(13) (Fig. 2b). Unexpectedly, as the length of the overhang increased, resection was slightly delayed. However, after resection commenced, it appeared to take place at a faster rate on the intermediate overhangs, seeing as the reaction culminates at approximately the same time point on all substrates ($p<0.002$ between $^{*}S$ and $^{*}S_{+10}$, and $p<0.0001$ between $^{*}S$ and $^{*}S_{+20}$) (Fig. 2b). Regardless, difference in rate is rather minimal. In contrast to ExoIII, T7 Exo is able to resect longer overhangs, and is restricted, but not inhibited, by the 20-nt overhang.

FIGURE 2

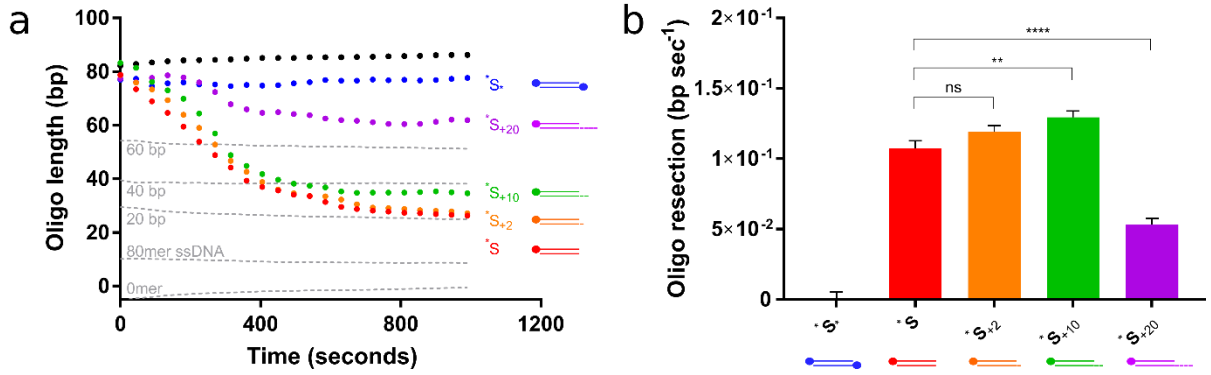

Figure 2 | T7 Exo is inhibited by 20-nt 5' overhangs

a, 12 nM T7 Exo-mediated resection on 50 nM substrates presenting a blunt (red), 2- (orange), 10- (green) and 20-nt (purple) 5' overhang with. The negative control was synthesised with two 5'-BITEG modifications (blue). Results were normalised against their respective negative controls and converted to bp. **b,** Analysis of the rate of resection on the substrates in (a). Error bars represent SEM; n=3 in all cases; **p<0.01, ****p<0.0001.

4.9 Studying enzyme resection through single-nucleotide mismatches

During mismatch repair, DNA nucleases resect through the mismatch to generate a single-stranded tract of DNA along which DNA polymerases can replicate (75,421–425). It has been suggested that these resection events may even remove epigenetic signatures on the DNA, such as 5-methyl-cytosine (426), which may then be permanently lost when repaired with an unmodified cytosine, and not targeted by *de novo* methyltransferases, Dnmt3a or Dnmt3b (427,428). It was therefore tested if this assay can detect differences in resection rates through mismatched and methylated substrates.

ExoIII activity was investigated on mismatched substrates compared to matching substrates and identified some unexpected activities (Fig. 3a–b). First, ExoIII was observed to resect the two perfectly matching substrates at substantially different rates, resecting $_{*}$S at a 1.7–2.0-fold faster rate than S* (Fig. 3c). $_{*}$S$^{C>T}$ contains a selection of C>T substitutions, whilst $_{G>A}$S* contains G>A substitutions, generating T:G and A:C mismatches, respectively. The presence of the T:G mismatches slows the rate of resection 0.09 – 0.16X compared to its perfectly matching counterpart ($p<0.001$ for 5 nM ExoIII; $p<0.05$ for 10 nM ExoIII; Fig. 3d). Conversely, incorporating A:C mismatches increases the rate of resection by 1.5–1.8X ($p<0.0001$ with both 5 and 10 nM ExoIII). There is some evidence for a nucleotide preference for ExoIII, although this does not appear to have been repeated (170). The rate of resection on both the perfectly matching substrate appears to have a delayed start, particularly for S*. Interestingly, *S is then resected at an accelerated rate compared to both mismatched substrates. The mismatches resect at a slower rate but, as their resection begins at the offset, the reaction on the mismatched substrates and *S finish at the same time point for both 5 and 10 nM ExoIII.

T7 exonuclease is considered to be sequence-independent as it lacks a defined DNA binding-motif, similar to other FEN family nucleases that bind DNA in a nonspecific manner (13,429). Nevertheless, it has previously been suggested that it might resect different nucleotides with variable efficiency (430). Indeed, T7 Exo was observed to resect the perfectly complementary *S with more difficulty than S$_{*}$ (Fig. 3e–g), which was noticeable at higher concentrations of T7 Exo (Fig. 3h). Similarly with T7 Exo, this assay detected a substrate strand preference (Fig. 3c and 3h).

The addition of four T:G mismatches did not slow or accelerate T7 Exo activity. However, incorporating A:C mismatches into the more resistant substrate did appear to slow resection, and this general trend was observed across all concentrations of T7 Exo. The effect of the mismatches was more evident at lower T7 Exo concentrations ($p<0.05$ for 7.5 nM and $p<0.01$ for 2 nM T7 Exo). These data suggest that mismatches may only be inhibitory to T7 Exo in certain sequence contexts. Indeed, T7 Exo has been shown to recognise single-nucleotide mismatches in an SNP-detection system (431).

FIGURE 3

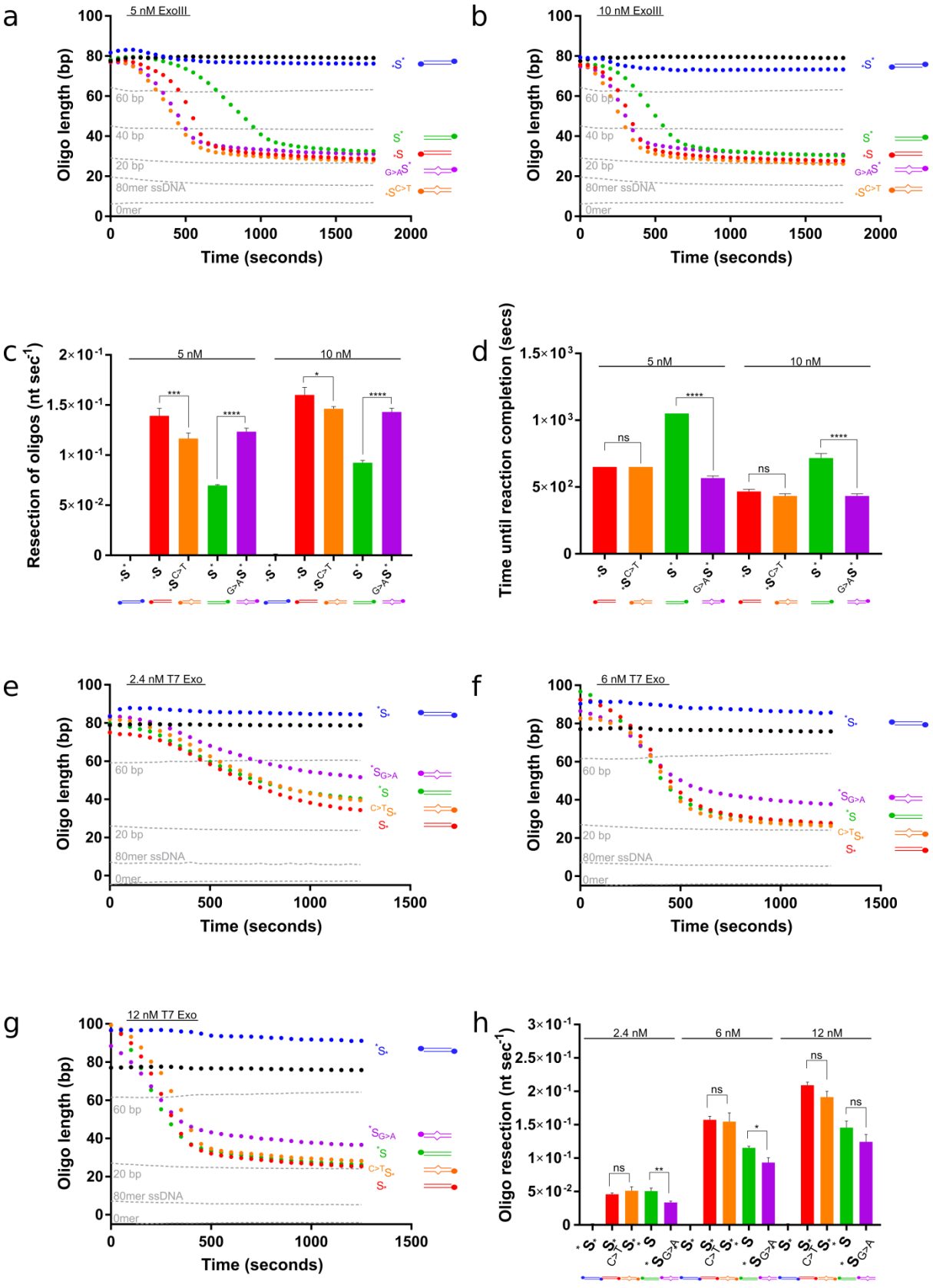
a
5 nM ExoIII
Oligo length (bp)
Time (seconds)
60 bp
40 bp
20 bp
80mer ssDNA
0mer
b
10 nM ExoIII
c
Resection of oligos (nt sec-1)
5 nM
10 nM
d
Time until reaction completion (secs)
ns
e
2.4 nM T7 Exo
f
6 nM T7 Exo
g
12 nM T7 Exo
h
Oligo resection (nt sec-1)
2.4 nM
6 nM
12 nM

Figure 3 | ExoIII and T7 Exo resect through single-nucleotide mismatches

a, 5 nM and **b,** 10 nM ExoIII was added to perfectly matched substrates ($_{*}$S and S*) and substrates containing four T:G or A:C mismatches, ($_{*}$S$^{C>T}$ and $_{G>A}$S*, respectively), and the resection reaction followed. Standard curve is represented by the grey dotted lines. **c**, Calculated resection rate of ExoIII on the complementary and mismatched substrates based on maximum gradients in (a) and (b). **d,** Time (seconds) until the ExoIII reaction reaches completion based on the point at which the reaction plateaus. **e,** 2 nM, **f,** 7.5 nM and **g,** 10 nM T7 Exo was added to complementary substrates (S$_{*}$ and *S) and substrates containing four T:G or A:C mismatches ($^{C>T}$S$_{*}$ and *S$_{G>A}$, respectively). Standard curve is represented by the grey dotted lines. **h,** Calculated resection rate of T7 Exo on the complementary and mismatched substrates. Error bars represent SEM; n=3 in all cases; *p<0.05, **p<0.01, ***p<0.001, ****p<0.0001.

4.10 Studying enzyme resection through methylated cytosines

FIGURE 4

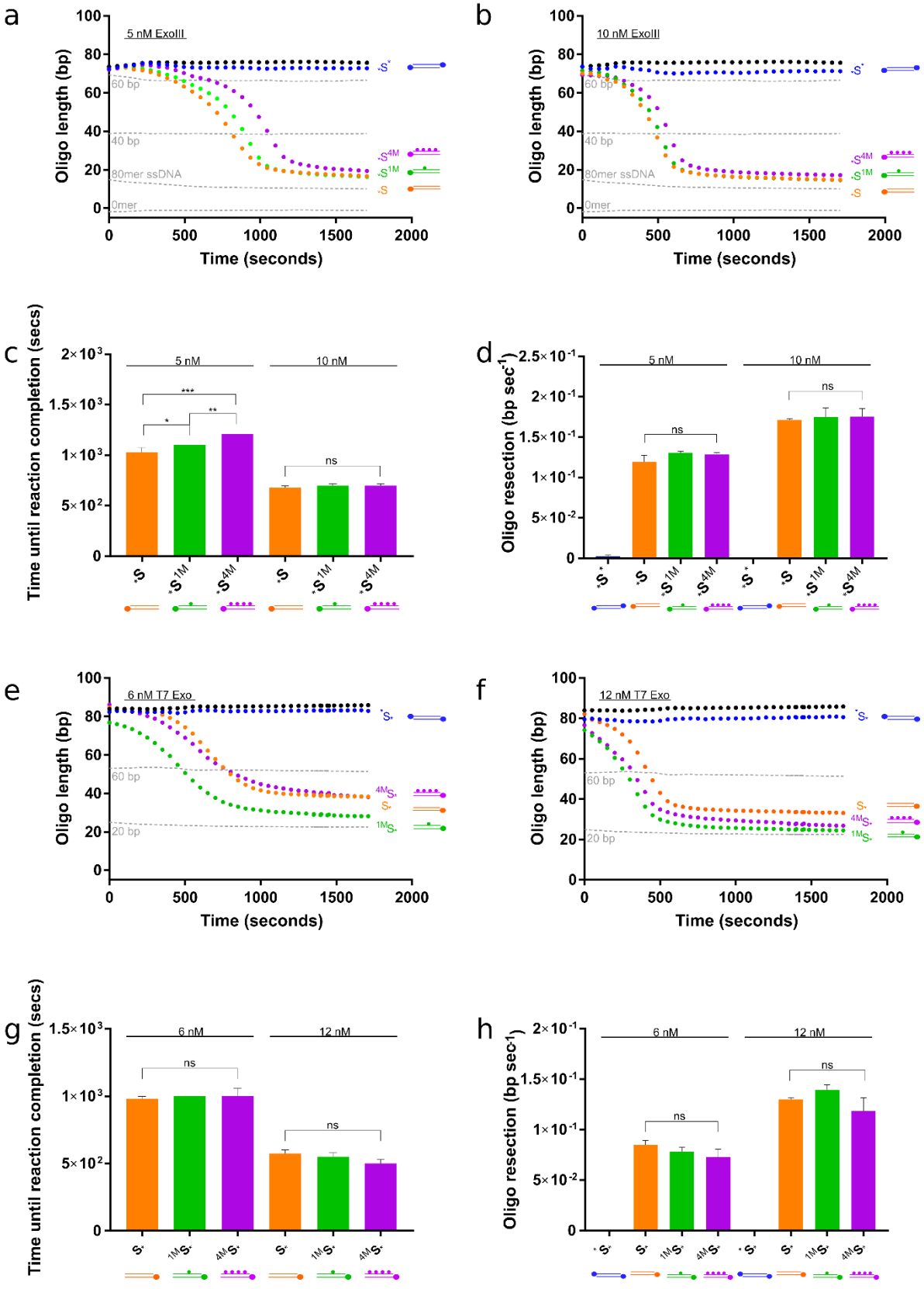

Figure 4 | Increased methylcytosine content delays ExoIII-mediated resection; but does not affect the rate of resection of either ExoIII or T7 Exo

a, 5 nM and **b,** 10 nM ExoIII was added to a non-methylated substrate, a substrate containing one methylated cytosine, and a substrate containing four methylated cytosines (*S, $_{*}S^{1M}$ and $_{*}S^{4M}$, respectively). Standard curve is represented by the grey dotted lines. **c,** Time (seconds) until the ExoIII reaction reaches completion on the methylated and unmethylated substrates based on the point at which the graphs plateau in (a) and (b). **d,** Calculated resection rate of ExoIII based on maximum gradients in (a) and (b). **e,** 6 nM and **f,** 12 nM T7 Exo on non-methylated and differentially methylated substrates. Standard curve is represented by the grey dotted lines. **g,** Time (seconds) until the T7 Exo reaction reaches completion on the methylated and unmethylated substrates based on point at which the graphs plateau in (e) and (f). **h,** Calculated resection rate of ExoIII. Error bars represent SEM; n=3 in all cases; *p<0.05, **p<0.01, ***p<0.001.

Neither ExoIII nor T7 Exo is substantially inhibited by methylated DNA in this experimental system. A non-methylated substrate, a substrate containing one methylated cytosine, and a substrate containing four methylated cytosines were each treated with either 5 nM or 10 nM ExoIII (Fig. 4a and 4b, respectively). ExoIII shows a small but significant trend towards taking longer to fully resect substrates with increasing numbers of methylated cytosines ($p<0.002$ for four methylated cytosines, Fig. 4c). This is most apparent at lower concentrations of ExoIII. The maximum reaction rate at which ExoIII resects through the methylated sites is not significantly different from the non-methylated substrate (Fig. 4d). This indicates that while there may be some hindrance in reaction initiation, once ExoIII begins to resect, the methyl groups are inconsequential. ExoIII may be indifferent to methylated substrates because bacterial DNA is methylated as part of the bacterial immune response against incoming DNA, including phages, and also influences bacterial gene expression and DNA repair. It therefore would not be farfetched to postulate that ExoIII is required for cleaving methylated DNA as well as non-methylated DNA (432). Furthermore, there is no significant difference in the time it takes for the reaction to reach completion. T7 Exo showed no significant effect on either maximum rate or time taken to resect in the presence of methylated cytosines (Fig. 4g–h). Currently, there is no data on the effect of methyl-cytosine on either ExoIII or T7 Exo resection with which to compare.

4.11 Validation of nuclease activity on DNA nicks and gaps, and its use in studying DNA nickases in combination with processive nucleases

FIGURE 5

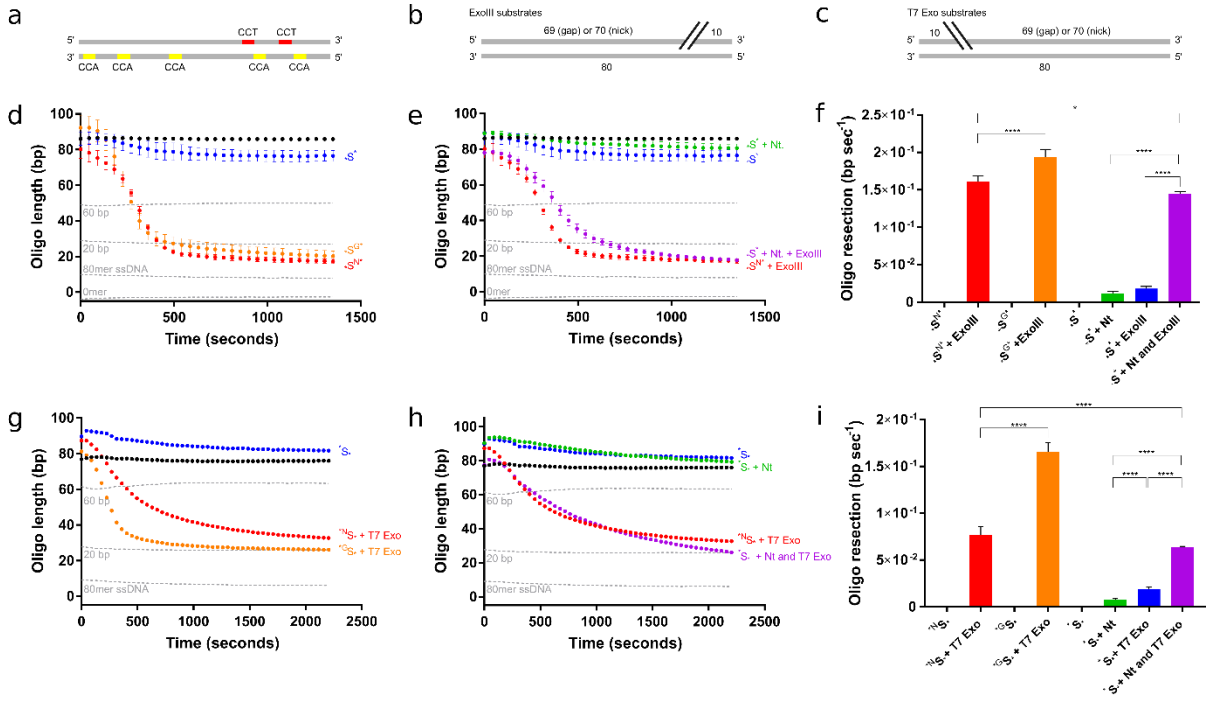

Figure 5 | ExoIII and T7 Exo preferentially resect from a nick than a gap

a, Schematic of the dsDNA substrate indicating the preferred nicking sites (yellow) and the least favourable nicking sites (red) of Nt.CviPII. **b–c,** Schematic of the dsDNA substrates presenting a nick or gap at either the 3'-end for ExoIII, or the 5'-end for T7 Exo. **d,** ExoIII is active against simulated nicked substrates. 40 nM ExoIII was added to a blocked substrate (blue) and related substrates designed with either a nick (red) or a gap (orange) towards the 3' end of one strand, showing similar activity against both modified substrates. Standard curve is represented by the grey dotted lines. **e,** Quantification of the Nt.CviPII nickase enzyme activity coupled to ExoIII. Nt.CviPII was added to the blocked substrate, either with (purple) or without (green) 40 nM ExoIII. Controls from b) are shown for comparison. **f,** Calculated resection rate of nicked and gapped substrates by ExoIII, extracted from the maximum gradient. Addition of the nickase significantly increases the resection rate, highlighting that the nickase activity is detected. **g,** T7 Exo is active against simulated nicked substrates. 12 nM T7 Exo was added to substrates with a nick (red) or a gap (orange) towards the 5' end of one strand. Negative control is in blue. Standard curve is represented by the grey dotted lines. **h,** Quantification of the Nt.CviPII enzyme activity coupled to T7 Exo. Nt.CviPII was added to the blocked substrate, either with (purple) or without (green) 12 nM T7. Negative control is in blue. **i,** Calculated resection rate of nicked and gapped substrates by T7 Exo, extracted from the maximum gradients in (g) and (h). Addition of the nickase significantly increases the resection rate, highlighting that the nickase activity is detected. Error bars represent SEM; n=3 in all cases; *p<0.05, ****p<0.0001.

Nicks and gaps are introduced as intermediates in DNA repair mechanisms, yet they need to be rapidly processed to prevent the accretion of double-strand breaks at replication forks, possibly leading to cell death (182,433). Due to the physiological relevance of nicks and gaps, the nucleolytic activity of ExoIII and T7 Exo on these structures was explored. In order to test this, a combination of substrates was used that had been designed to contain a nick or gap, in conjunction with blocking at both ends (both 5' or 3', respectively) to prevent resection from the terminal ends. A recently-purified nickase, Nt.CviPII (410) which is known to possess inherent exonuclease activity, was also included. Nickases cleave just one strand of duplex DNA, breaking the phosphodiester backbone. Nt.CviPII preferentially cuts CCA and CCG, but cuts less efficiently at CCT (410). One strand of the dsDNA substrate contains five evenly distributed CCA motifs, while the opposite strand only contains two CCT motifs, and therefore most of ExoIII's activity should be directed on the first strand (Fig. 5a). To minimise the exonuclease activity of Nt.CviPII, a low dilution of the nickase was used.

These results found that ExoIII functions marginally better on gaps rather than nicks ($p<0.0001$) (Fig. 5d and 5f), and this may reflect its role in base excision repair where it resects from an abasic site (408). ExoIII is nevertheless able to resect from a nick, and the rate is comparable to its activity on blunt ends, as previously observed (434). ExoIII also resected from the nickase-induced nicks at an almost equal rate to the substrates designed to contain a single nick (Fig. 5e–f). These data demonstrate that Nt.CviPII is a very fast acting nickase against its preferred substrate sequences as there is no delay in the start of ExoIII-mediated resection.

As with ExoIII, T7 Exo also resects from both nicks and gaps. It has a more defined preference for gaps, showing a rate approximately 2.5-fold greater than for nicks ($p<0.0001$; Fig. 20g and 20i). T7 Exo also resects from nicks generated by a nickase almost as efficiently as from a substrate already presenting a single nick (Fig. 5h–i). Typically, T7 endonuclease cleaves at nicked sites during infection to generate DNA double-stranded breaks that are susceptible to T7 Exo. As such, it is perhaps a redundant property of T7 Exo to resect from a nick (435).

4.12 Additional DNA enzymes that degrade or synthesise dsDNA can also be studied using this assay.

FIGURE 6

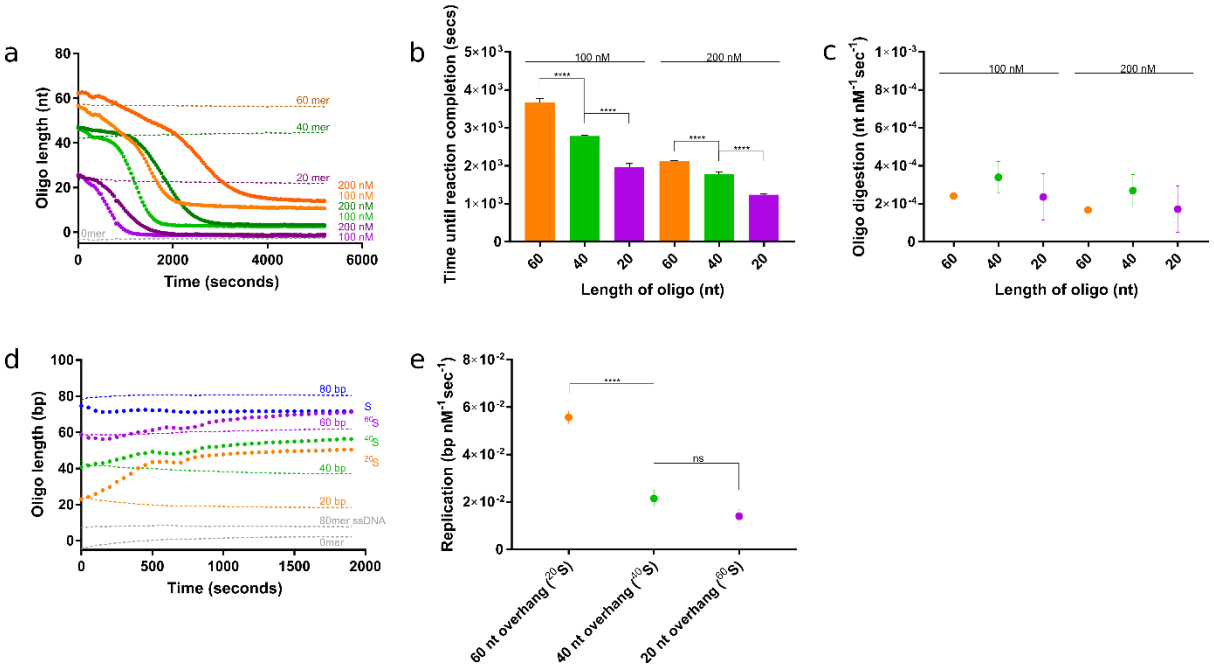

Figure 6 | Validation of the assay for alternative enzymes that digest ssDNA and generate dsDNA **a,** Mammalian Trex2 digestion of single stranded DNA quantified using the PG assay. Single-stranded 60-mer (orange), 40-mer (green) and 20-mer (purple) DNA substrates were treated with 100 and 200 nM Trex2. Robust digestion was observed in each case. **b,** Time (seconds) until reaction completion based on the point at which the graphs plateau in (a). **c,** Rate of digestion per nM Trex2. Trex2 degrades DNA at a similar rate irrespective of the length of the DNA substrate. **d,** The polymerase activity of the Klenow fragment polymerase determined using the PG assay. Three substrates with a 20-, 40- and 60- and overhang with a total 80 bases were incubated with 1 nM Klenow fragment. **e,** Calculated polymerisation rate of the Klenow fragment. A clear preference is shown for longer overhangs. Error bars represent SEM; n=3 in all cases; ****p<0.0001.

PG has been demonstrated to be an effective dye that can be used to study dsDNA nucleases from viruses and bacteria. Given the low, but not insignificant, fluorescent signal observed for the single-stranded 80-mer control in the standard curves, it was reasoned that this assay may have the sensitivity to address ssDNA nucleases, such as human Trex2 (436). This was confirmed by showing that the assay is sensitive enough to detect a Trex2 concentration-dependent decrease in fluorescence from ssDNA substrates ranging in size from 60 to 20 nts (Fig. 6a). This indicates that this assay has considerable potential for an even wider range of DNA nucleases, and very

high levels of sensitivity in order to capture such activity in detail. As expected, it takes longer for Trex2 to digest longer substrates (Fig. 6b). In terms of reaction kinetics, rate of resection is generally consistent, ranging between $1.7 \times 10^{-4} – 3.4 \times 10^{-4}$ nt sec^{-1} (Fig. 6c), which is comparable to previously published rates (437).

Since this assay has been shown to be powerful tool for observing nuclease activity, an attempt was made to study whether this assay could capture the reverse activity and visualise an increase in fluorescence upon addition of polymerase. To investigate this, the use of the well-characterised Klenow fragment polymerase (KF) was employed. KF requires a short DNA primer fragment hybridised to a ssDNA fragment along which it can replicate. A selection of 80-mer oligomers hybridised to a 20-, 40-, 60- and 80-mer oligomer were used (Fig. 6d). The data clearly indicate that KF-dependent blunting of the 20mer 5'-overhang is possible to visualise in the context of this real-time assay. KF appears to be unable to extend the 20- and 40-mer primers to produce the full-length 80 bp dsDNA product. KF-elongation of both substrates are inhibited once the primers have been extended to 50- or 55-mer lengths (Fig. 6d). It is understood that KF is sensitive to secondary structures in the ssDNA template, and the presence of a small hairpin adjacent to this region may be responsible for inhibiting polymerisation past this point. Previously, a terminal hairpin was not observed to inhibit KF processivity, although an internal hairpin, such as in this case, may have a different impact on KF (438). Analysis of the rate of replication suggests a preference for a longer ssDNA template, as KF polymerises at a much faster rate on the 60mer 5'-overhang, while the 40- and 20-mer 5'-overhangs are processed at a three-fold lower rate (Fig. 6e).

4.13 Discussion

A highly-sensitive, fluorescence-based nuclease assay was further developed to study nuclease activity in a continuous manner. In addition, a library of substrates was validated to investigate a wide number of single- and double-stranded DNA nucleases and polymerases. This assay can be used to calculate reaction kinetics and reaction completion times, providing a powerful quantitative tool for characterising enzymes active on nucleic acids. This technique has been successfully validated using well-studied enzymes and, in the process, identified previously unreported details of their mechanisms.

The continuous nuclease assay developed herein has important applications in comparing the relative activities of enzymes; both known nucleases and – more importantly – yet uncharacterised DNA metabolizing proteins. In our assay, ExoIII was validated to hydrolyse the DNA substrate at a faster rate than DNase I. DNase I exhibits a relatively low affinity for DNA, and higher affinity strains have been engineered for treatment of cystic fibrosis (439,440). DNase I may have evolved to be less efficient as it can digest all structures of DNA, irrespective of whether it is single- or double-stranded, and deregulation of this activity could be disastrous for the cell. This limitation in its binding may exert some control to prevent inappropriate activity from causing cellular damage. ExoIII shows a greater rate of resection per enzyme protomer, yet this is counteracted by its very limited structural specificity. The product of ExoIII resection during *E. coli* base excision repair is a single-stranded tract of DNA that can be much more easily repaired than the damage caused by DNase I (441,442).

Substrate specificities were also compared, as indicated by the preference of ExoIII for 3’-overhangs shorter than 4-nt and T7 Exo’s predilection for 5’-overhangs of 10-nt or fewer. As T7 Exo typically resects DNA from short 5’-overhangs introduced by T7 endonuclease during the infection process in *E. coli*, the results are consistent with its behaviour *in vitro* and *in vivo* (13,435).

In addition to substrate structures, other physiologically relevant substrates containing single-nucleotide mismatches and methylcytosines were considered. Unexpectedly, we found that ExoIII and T7 Exo exhibited a preference for one strand of the DNA substrate. There is evidence of a nucleotide preference for ExoIII; C>A~T>G, although

it seems that it depends on the sequence context (170). Nevertheless, the results of their mismatched counterparts do coincide with published ExoIII preferences (170). As such, this confirms previously reported preferences in both a qualitative and quantitative way. Work is continuing in the Chahwan lab to understand the mechanisms of ExoIII, and so it is hoped that its nucleotide preferences will be thoroughly elucidated.

As for the methylated substrates, lower concentrations of ExoIII were observed to be slightly inhibited by the presence of multiple methyl-cytosines in that resection is delayed. The rate of resection, however, remains consistent on all substrates. At higher concentrations, ExoIII does not appear to distinguish the methyl-cytosines. T7 Exo also shows no alteration in activity from the methyl groups. Its host, *E. coli*, contains a small percentage of methylated adenines and cytosines, and it appears that T7 Exo does not discriminate against them. This is in spite of a smaller percentage of methylated DNA ending up in the bacteriophage's progeny DNA than is present in the *E. coli* genome (443).

While this assay is predominantly useful for studying processive enzymes, it is possible to combine a nickase with an enzyme that resects from nicks, as indicated with nickase Nt.CviPII in conjunction with either ExoIII or T7 Exo. This is a powerful method to identify nicking or endonuclease activities, and study their efficiency based on when resection commences.

The superior sensitivity of PG in this assay also expanded the repertoire of enzymes to include ssDNA nucleases, such as Trex2. Trex2 is one of at least eight autonomous exonucleases in human cells, and is likely recruited to 3'-termini to alleviate blocks during replication arrest (179). It binds DNA very tightly, and this affinity for its substrate has been captured here due to its very high processivity. In addition to the study of enzymes that digest DNA, the study was extended to enzymes that polymerise DNA, such as the nuclease-deficient Klenow fragment polymerase. Its polymerase activity is ten-fold more rapid, for example, than ExoIII is at resecting DNA in their respective buffers. Therefore, the assay was used successfully to measure and differentiate between these vastly different protein kinetics.

Characterisation of DNA nucleases is integral for demystifying their roles in maintenance of genomic integrity. Loss of nucleases, or mutations in their structural or functional domains, can have disastrous effects on the health of an organism. For example, CTIP nuclease has been associated with Jawad and Seckel Syndromes (444), Exo1 is involved in mutated in some cancer patients (445–447) and loss of TREX1 mediates an auto-immune disease known as Aicardi-Goutières Syndrome (448,449). The impact of these mutations could affect resection rates or binding affinity to the DNA or interacting partners, and it is posited that this assay may be sensitive enough to capture and compare these characteristics. Interacting proteins may also influence nuclease activity, as has been observed in the MRN complex (15), or indeed by the addition of auxiliary RPA for optimal activity of the RecQ helicase (396,450). Nucleases may also represent anticancer targets, and this assay could offer an alternative method for studying the effect of future anticancer drugs on the activity of their target nuclease (451). In a similar instance, a discontinuous assay using PG was successfully performed to study the inhibitory role of actin on DNase I (406).

Many nucleases have been well-characterised, including those used in the optimisation of this assay, while many more have yet to be characterised at all, let alone identified. As such, this assay represents a safe, easy, rapid, robust, continuous study of dsDNA and ssDNA nucleases and polymerases. It is believed that it has the potential to revolutionise quantitative assessment of nucleic acid-active enzymes in a vast range of applications. Moreover, it is postulated that this assay would be even more applicable in studying RNA nucleases, which are historically less known than DNA nucleases even though they are more abundant throughout various genomes (452–456).

5 Chemical inhibition of Kat5 impacts efficiency of class switch recombination

5.1 Summary

Class switch recombination (CSR) is a process of secondary antibody diversification whereby the preliminary antibody isotype IgM is exchanged for an alternative isotype. This grants B cells different effector functions and is therefore vital for immunity. CSR is dependent on both transcription and DNA repair and is orchestrated by key histone modifications that recruit appropriate factors to specific sites along the antibody locus. Kat5 acetylates histone H4 at numerous sites in its N-terminal tail to unwind the local chromatin and make it accessible to transcription factors. Kat5 is also involved in canonical DNA repair through activation of DDR signalling (18,26,200). Taken together, this evidence suggests that Kat5 may have a role in CSR. An *in vitro* system was used to test this hypothesis. Chemical inhibitors differentially targeting Kat5 binding and catalytic activities were tested in the context of DNA repair and were subsequently used to inhibit Kat5 in cells stimulated to undergo CSR. Results indicate that inhibition of Kat5 using the inhibitors iChromo and TH1834, respectively, do affect class switching efficiencies, providing evidence for a role for Kat5 in B cell maturation.

5.2 Kat5 is involved in transcription, canonical DNA repair, and antibody diversification

Kat5 is responsible for the acetylation of histones, particularly H2A, H3 and H4 (200,457). The association of histone acetylation with transcriptionally active regions has been well documented. In particular, Histone H4 N-terminal acetylation (H4ac) increases sharply at active yeast promoters (202), and early reports found yeast cells unable to acetylate their target lysine (K) residues on the H4 tails exhibited altered patterns of transcription. Kat5 has been mapped to promoter regions of active genes in mouse embryonic stem cells (203), and treatment of mammalian cells with histone deacetylase inhibitors enhances gene expression (204).

During canonical DNA repair, Kat5 is involved in de-compaction of chromatin during canonical homologous recombination (HR). It is thought to play a substantial role influencing DNA repair through HR (26), yet mutations in the *S. cerevisiae* NuA4 complex, the homologue of mammalian Kat5 complex, renders cells hypersensitive to DNA-damage reagents and impairs DSB repair by NHEJ (201). Kat5 has also been associated with DSB repair in mammalian cells through nucleosome binding and activation of ATM kinase (40,42).

Kat5 may be implicit for CSR through its roles in transcription and DNA repair. Indeed, active transcription provides the single strand DNA substrate for AID-induced mutation (458–460). Acetylating histones in this vicinity of antibody promoters allows transcription machinery clear access to antibody loci; thereby enhancing the mutagenic process of AID (246,461).

Equally, CSR is dependent on DSB repair though NHEJ (98,462). Through ATM, Kat5 mediates phosphorylation of H2AX (γH2AX), which represents a typical marker for DNA repair both at DSBs to initiate DDR signalling, and during CSR to stimulate class switching (200,224). Furthermore, a histone target of Kat5, H3K9ac, is known to associate with S regions that undergo recombination. It precedes AID-dependent mutations, and therefore Kat5 may even support AID recruitment (463). One curious observation links loss of AID expression with a concomitant depletion of H4ac in B cells stimulated for CSR, providing some suggestion of an intimate relationship between Kat5 acetylation and AID (464). Additionally, Kat5 is specifically upregulated in the GC B cell environment. While, comparatively, the increased expression of AID in B cells is far more extreme, the upregulation of Kat5 is potentially biologically significant in the context of CSR (319) (Fig. 1). Finally, an unpublished genome-wide co-immunoprecipitation CSR screen (Edelmann, Scharff, and Chahwan; unpublished) has identified many of the Kat5 complex components to be crucial for antibody diversification.

FIGURE 1

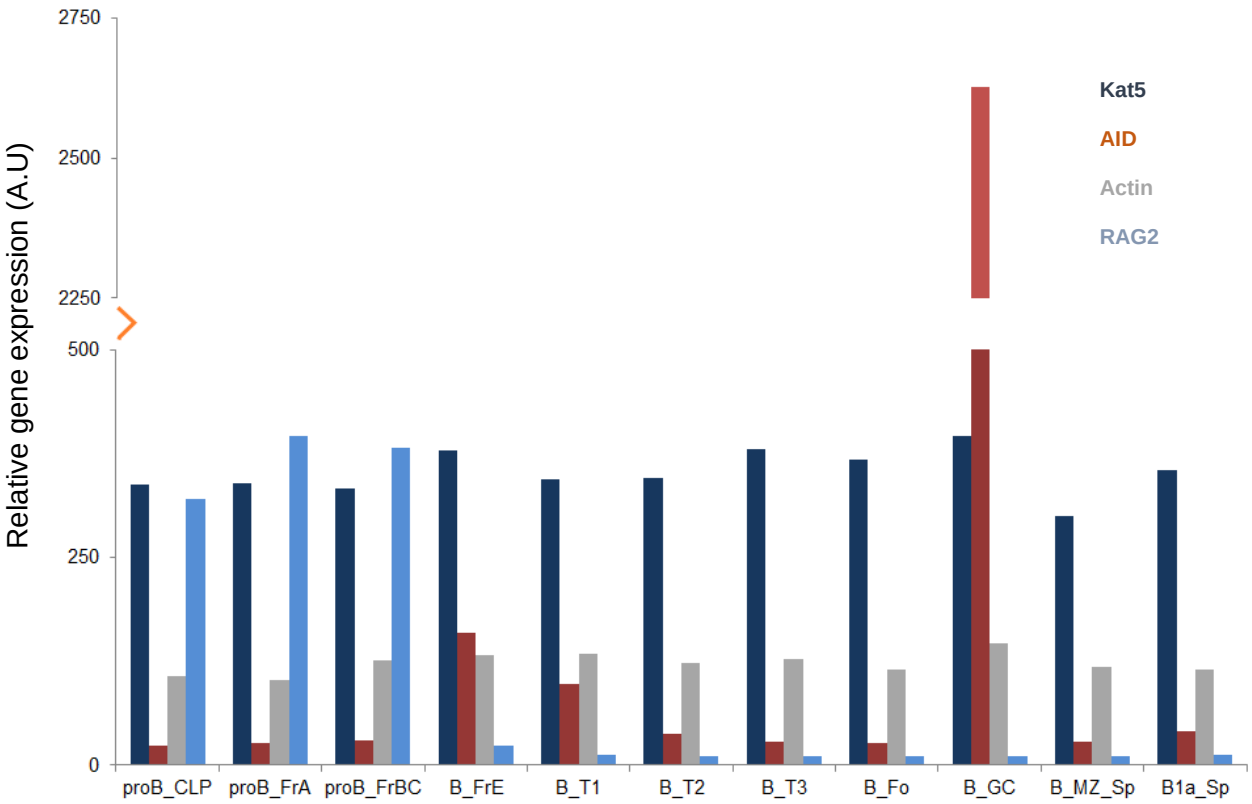

Figure 1 | Kat5 is marginally upregulated in B cell germinal centres

Histogram illustrates the relative expression of Kat5 and AID in B cell populations denoted from left to right according to their developmental maturity. ProB populations represent cells undergoing primary diversification processes of V(D)J recombination, as shown by the increased expression of RAG2. AID is specifically upregulated in germinal centre (GC) B cells to drive secondary antibody diversification processes, and slightly upregulated post-V(D)J recombination. Kat5 expression fluctuates between different B cell populations but is slightly upregulated at later stages of V(D)J recombination and in the GC (319).

5.3 Kat5 signalling cascade during DSB repair and implications for cancer

Immediately following the generation of a DSB, the repressive chromatin complex, Suv39h1/kap-1/HP1, is recruited to limit the mobility of the broken ends and hold them in close proximity (24,465,466). Kat5 is recruited to the break site by Ago2 and a DSB-induced RNA guide (467). Kat5 is acetylated by acetyl-CoA, permitting its subsequent acetylation of various lysine residues along the H4 tail (H4ac) (468). Alternatively, Kat5 can be phosphorylated at Tyr44 within its chromodomain by the global, hyperactive c-Abl kinase (469). The chromodomain is a specialised binding motif that recognises methyl groups on lysine residues, particularly on histone proteins (25). This

modification permits Kat5 binding to H3K9me3 (469) (Fig. 3). Concordantly, treatment with Kat5 preparations from IR-treated cells with λ-phosphatase reduces binding affinity of Kat5 to this motif (469). Phosphorylation of the Kat5 chromodomain in turn enables Kat5-dependent acetylation of ATM kinase, triggering its monomerisation to its active form. Interestingly, the phosphorylation status of Kat5 bears no effect on its acetylation of H4, yet interaction between Kat5 and H3K9me3 is necessary to stimulate Kat5-mediated acetylation of ATM at Lys-3016 (469). Therefore, H3K9me3 binding functions as an allosteric regulator by increasing Kat5 catalytic activity (28,43). Mutations within the chromodomain that prohibit this interaction also attenuate Kat5 acetylation of ATM. Correspondingly, mutation of the ATM acetylation site inhibits activation of ATM's kinase activity, indicating Kat5 is required for its activation (43). Monomeric ATM phosphorylates a number of targets, including H2AX, which is a common marker for DSB repair and also functions as a binding site for repair proteins (44,470–472). ATM also phosphorylates the kap-1 chromodomain, removing it from H3K9me3, and thus generating more binding sites for Kat5 (24,28).

Dysregulation of Kat5 has been implicated in various cancers. This relationship with tumorigenesis is likely due to its interactions with signalling proteins involved in maintaining genome integrity (21,28) as well as transcription factors known to participate in oncogenic pathways (21,473). Reduced expression of Kat5 has been observed in prostate cancer (474) and in 65% of metastatic prostate cancer biopsies (475). Similarly, low levels of Kat5 or its aberrant cellular localisation has been linked to breast cancer (476,477).

FIGURE 2

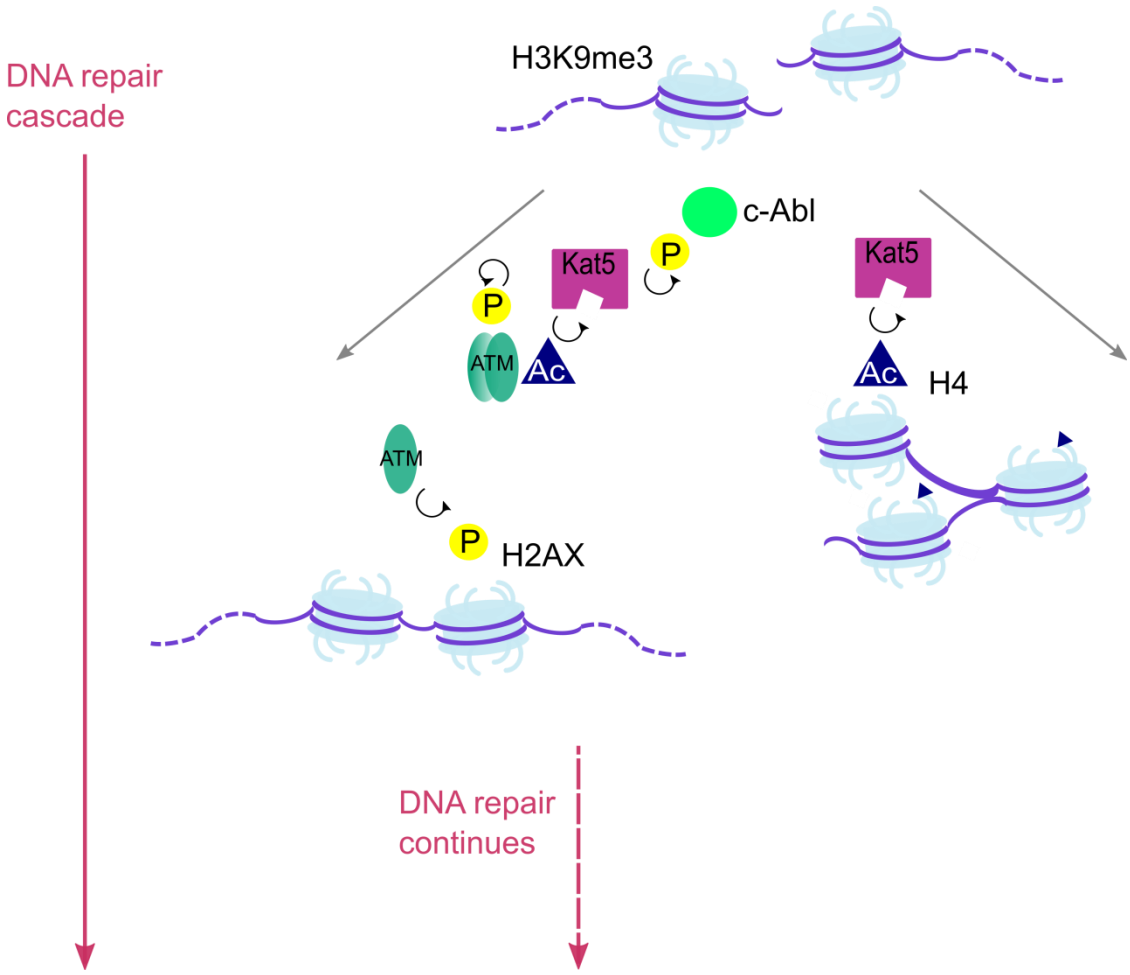

Figure 2 | Kat5 DNA damage repair signalling cascade to mediate effective DSB repair
Following a DSB, Kat5 is recruited to break sites. Phosphorylation by c-Abl kinase permits Kat5 binding to H3K9me3 via its chromodomain. This exerts an allosteric effect on Kat5 to acetylate ATM, triggering ATM autophosphorylation and monomerization into its active form. ATM then phosphorylates H2AX, which recruits downstream DNA repair factors. Independently of c-Abl, Kat5 acetylates H4 induce local chromatin unwinding and to ensure the underlying DNA is accessible to transcription and DNA repair proteins.

No known role for Kat5 in CSR has yet been described. Due to compounding evidence whereby histone acetylation is associated with active transcription and canonical DNA repair (Fig. 3), in addition to the specific upregulation of Kat5 in GC B cells (Fig. 1), a role for Kat5 in antibody diversification is proposed (18). A role for Kat5 will be tested using a well-characterised *in vitro* mouse model of CSR and chemical inhibitors. This

chapter describes the chemical separation of function of Kat5 activities by, 1) inhibiting its binding to methylated histone residues via the chromodomain by using inhibitors Imatinib (42,478) and iChromo (Kaidi A, unpublished), and 2) inhibiting its catalytic site which mediates protein acetylation by using the inhibitor TH1834 (207). In the associated Chapter 6, the development of a related genetic model to study the role of Kat5 in both mouse and human cells will be discussed.

FIGURE 3

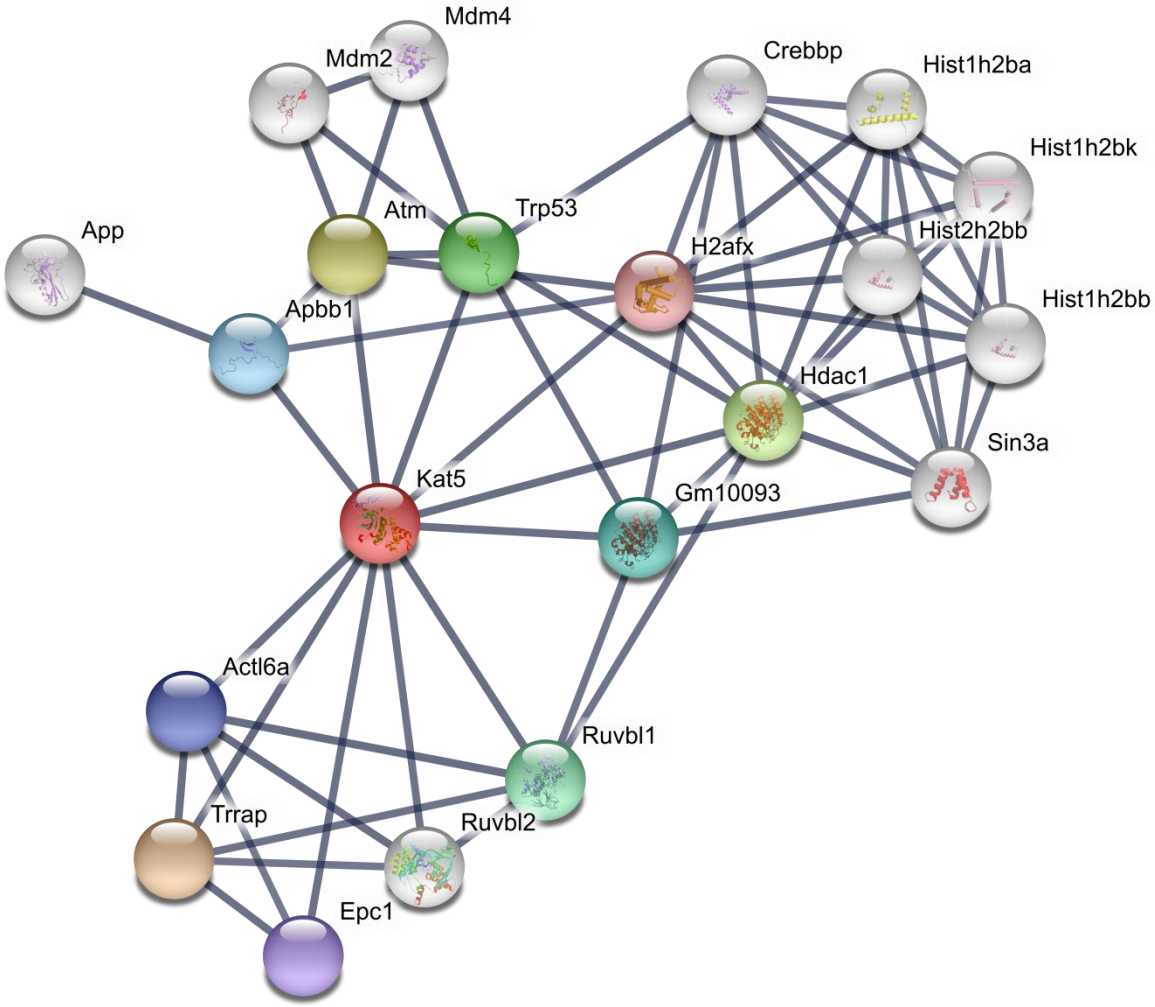

Figure 3 | Kat5 STRING network depicting the protein interaction of Kat5 in mouse cells

The STRING network for mouse Kat5 identifies a number of interacting proteins that are themselves involved in DNA repair (ATM, H2afx), transcription (Crebbp), and chromatin remodelling (RuvBL1, RuvBL2). The thickness of the connecting lines represents the level of confidence in the 10 Kat5 protein interactions. The interactions appear to have been clustered into histones and histone modifiers/chromatin remodelling proteins.

5.4 Materials and Methods

5.4.1 CH12F3 cell culture

CH12F3 B Cells were cultured in RPMI medium (cat. 11875, Gibco,), supplemented with 10% FBS (lot. 08F9038K, cat. 10500064, Hyclone), 5% NCTC 109 (cat. N1140, Sigma), 5% L-glutamine (cat. 25030024, Gibco), 5% pen/strep (cat. P4333, Sigma) and 1% β-mercaptoethanol. (cat. 21985023, Gibco).

5.4.2 DNA damage assays

For the DNA damage assays, cells were transferred to a 24-well plate (cat. 662160, Greiner Bio-One) and pre-treated with either imatinib (cat. ALX-270-492-M025, Enzo Life Sciences) for 1 hour, iChromo for 16 hours, or TH1834 (cat. 2339, Axon Med Chem) for 1 hour. Stock imatinib was prepared according to manufacturer's instructions; iChromo was reconstituted in DMSO to a final molar concentration of 30 mM; stock TH1834 was reconstituted in DMSO to a final molar concentration 50 mM. Cells were incubated at 37ºC and 5% CO_2. Following pre-treatments of inhibitors, 0.25 or 1 µM CPT (cat. C9911, Sigma) was subsequently added to the cells for 30 minutes prior to fixation.

5.4.3 CSR assays

To activate CH12F3 B cells for the CSR assays, anti-CD40 (1:200, cat.15258437, Fisher Scientific), IL-4 (1:1000, cat. 404-ML-050, R&D Systems) and TGF-β (1:1000, cat. 240-B-010, R&D Systems) were added to relevant wells alongside appropriate concentrations of iChromo or TH1834. IL-4 and TGF-β were prepared according to manufacturer's instructions. iChromo was replenished every 24 hours. TH1834 was replenished every 12 hours. Anti-CD40, IL-4 and TGF-β were replenished alongside the inhibitors as necessary over the first 48 hours.

5.4.4 Cell fixation and immunofluorescence staining

Antibodies used were FITC-conjugated anti-γH2AX (1:200 dilution, cat. ab26350, Abcam), APC-conjugated anti-IgM (1:200, cat. 17-5790-82, Fisher Scientific) and FITC-conjugation anti-IgA (1:200, cat. 559354, BD Biosciences). For DNA damage assays, cells were fixed and stained using Fixation/Permeabilization Solution Kit (BD Biosciences, 554714); aliquots were extracted (4 µL) and mounted on a slide with

DAPI mounting medium (4 µL, cat. ab104139, Abcam). Cells were analysed on ZEISS LSM 880 with Airyscan confocal microscope. Excitation wavelength was set at 488 nm for GFP-tagged anti-γH2AX antibody and 405 nm for DAPI. All images were recorded using Plan-Apochromat 100x/1.4 Oil DIC M27 and processed using ImageJ. For class switching assays, cells were stained in 0.01 M PBS and centrifuged 300 x g, 5 mins.

After staining, cells for the flow cytometer were washed in 0.01 M PBS and resuspended in 400 µL 0.01 M PBS. Fluorescence was measured using the BD Accuri C6 plus according to the manufacture's specifications (BD Biosciences). Live cells were gated for analysis.

5.4.5 Data analysis

Sequence alignments and building the phylogenetic tree were run on Jalview bioinformatics software (479). Flow cytometry results were analysed and presented using FlowJo 10.5.0 software. For presentation and statistical analysis of the data, one-way ANOVA with Dunnett's multiple comparisons tests were used. This was implemented using GraphPad Prism v7.03. Confocal images were processed on ImageJ software (480).

5.5 Results

Kat5 has been highly conserved throughout evolution, as highlighted in the sequence alignment (Fig. 4a). *Mus musculus* (mouse) and *Homo sapiens* (human) Kat5 protein sequences are highly similar, reaching 99.81% sequence identity, and this sequence identity perseveres throughout evolution; in *Gallus gallus* (chicken; 84.27%), *Danio rerio* (Zebrafish; 76.84%), *D. melanogaster* (57.92%), *C. elegans* (46.12%), *S. cerevisiae* (41.47%), *S. pombe* (39.57%) and *U. maydis* (38.92%) (479).

The sequence alignment of Kat5 from yeast to humans idetifies key domains. As a founding member of the MYST (MOZ, Ybf2/Sas3, SAS2, Tip60/Kat5) family of histone acetyltransferases, this region is highly conserved (Fig. 4a, pink) (481). MYST family members share functional and structural similarities, and all participate in a diverse range of cellular processes, including transcription regulation, DNA damage repair and apoptosis (481).

The acetyl-CoA binding groups and active site have also been highlighted (Fig. 4a, yellow and burgundy), and these sites are all very well conserved, indicating the crucial function of this activity. The acetyltransferase reaction requires deprotonation of Cys304 by Glu338, generation of a acetyl-Cys304 intermediate, deprotonation of the histone lysine residue by Glu338, and transfer of the acetyl moiety to the lysine substrate (482). In support of this model, individual mutations in Cys304 and Glu338 eliminated acetyltransferase activity of Esa1 *in vitro*, and co-crystals of Esa1 and Acetyl-CoA revealed the transfer of the acetyl group from Acetyl-CoA to Csy304. Failure of this transfer was observed in co-crystals of Esa1-E338Q and Acetyl-CoA (482,483). Critically, both Cys304 and Glu338 remains conserved throughout evolution (Fig. 4a, yellow and burgundy).

The zinc finger domain is a curious feature shared between Kat5 in all organisms, except for *S. cerevisiae*. Each protein contains the common $CxxxCX_{12}HxxxC$ motif (482). This particular zinc finger motif is associated with forging DNA-protein, RNA-protein and protein-protein interactions, which all coincide with Kat5's role in transcription, and the observation that Kat5 is often a member of large multiprotein complexes (26,203). Deletion studies of Sas3 revealed that this region is required for histone acetyltransferase activity (484). Interestingly, structural analysis of the yeast

protein indicates that the zinc finger region instead forms a classical TFIIA-type zinc finger hold, and zinc fingers of this subtype are also able to mediate DNA-protein and protein-interactions (485).

Chromodomains are well-studied functional domains that bind to methylated histones (486–488). Nevertheless, some reports have claimed an additional RNA or DNA interaction capabilities (489–491). Previously, the yeast Kat5 was presumed to encode a chromodomain, and structural analysis identified a well-folded structure that exhibited 3–10-fold greater binding affinity for RNA than DNA (492). Loss of this region sensitises yeast to DNA damage reagents, alters transcriptional activities and, crucially, the RNA-binding activity was found to be essential for viability (492). Whether this is the case for mammalian Kat5 is unknown. Critically, the Tyr44 residue is present in each organism (Fig. 4a, orange). This site requires phopshorylation for chromodomain binding (42).

One interesting feature that appeared in the search for protein domains was the identification of DNA polymerase III subunits gamma and tau. Gamma and tau are ATPases involved in loading and unloading the DNA polymerase replisome in bacteria (493). Based on the diverse range of motifs associated with this domain and the functions of gamma and tau, this find is quite dubious. Kat5 does not exhibit ATPase activity (494), however it may share some of the DNA-binding properties of these subunits.

Each phylogenetic tree of the individual domains within Kat5 shows the evolutionary relationships between selected species (Fig. 4b–g). Generally, the outcomes of each branch are to be expected; *S. pombe* and *S. cerevisiae* appear to share a more similar evolutionary history, as does mouse, human, dog and chicken. However, the phylogenetic tree formed on DNA polymerase III subunits gamma and tau domain shows an unexpected evolutionary history, particularly whereby *D. melanogaster* and *S. pombe,* and *C. elegans* and *S. cerevisiae,* share more common ancestors respectively.

Crucially, based on the sequence similarity specifically between mouse and human Kat5, it is highly probable that the Kat5 inhibitors will recognise both with equal affinity,

and any results captured in the mouse CSR model CH12F3 B cell line should be replicable in human B cells.

FIGURE 4

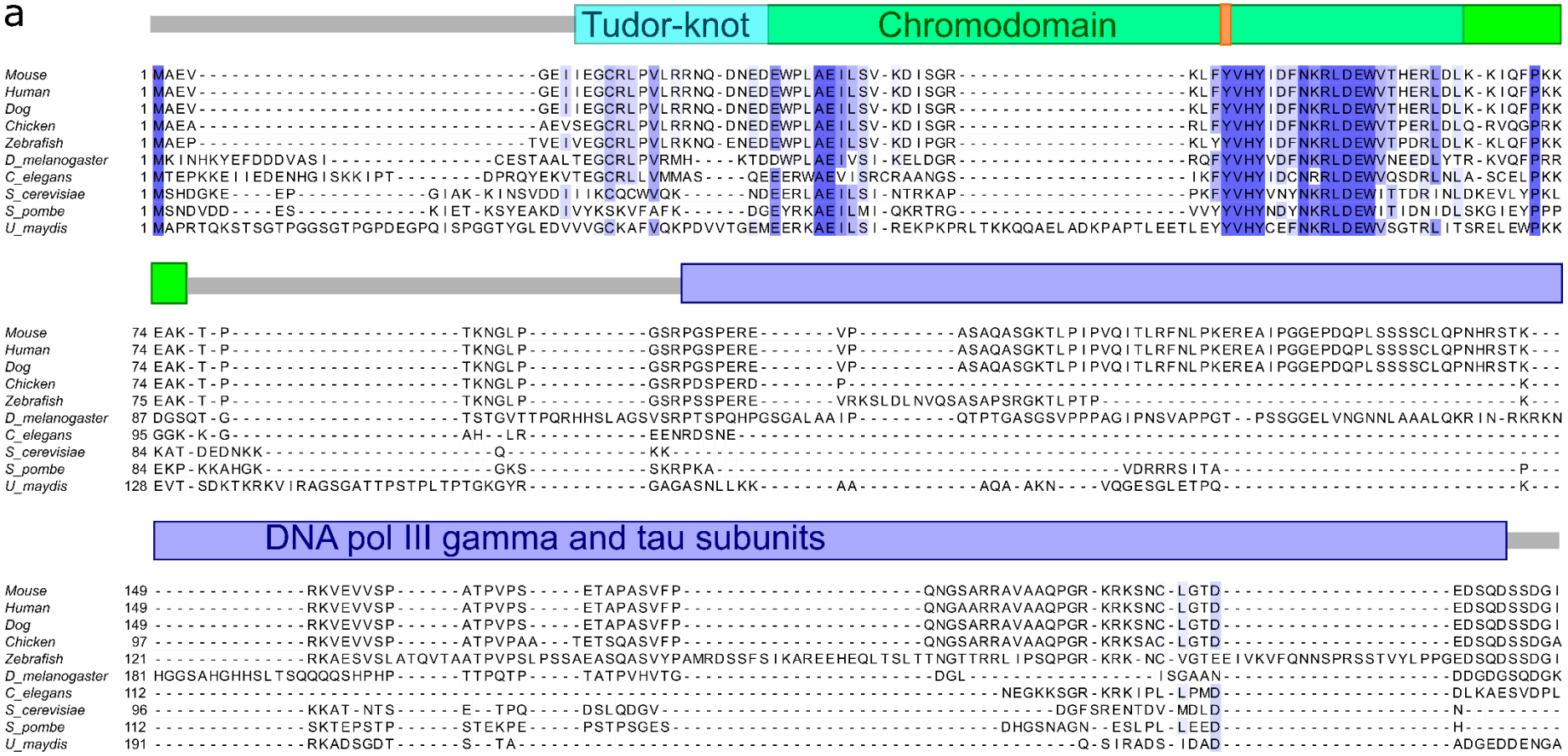
a
Tudor-knot
Chromodomain
DNA pol III gamma and tau subunits
Mouse
Human
Dog
Chicken
Zebrafish
D_melanogaster
C_elegans
S_cerevisiae
S_pombe
U_maydis

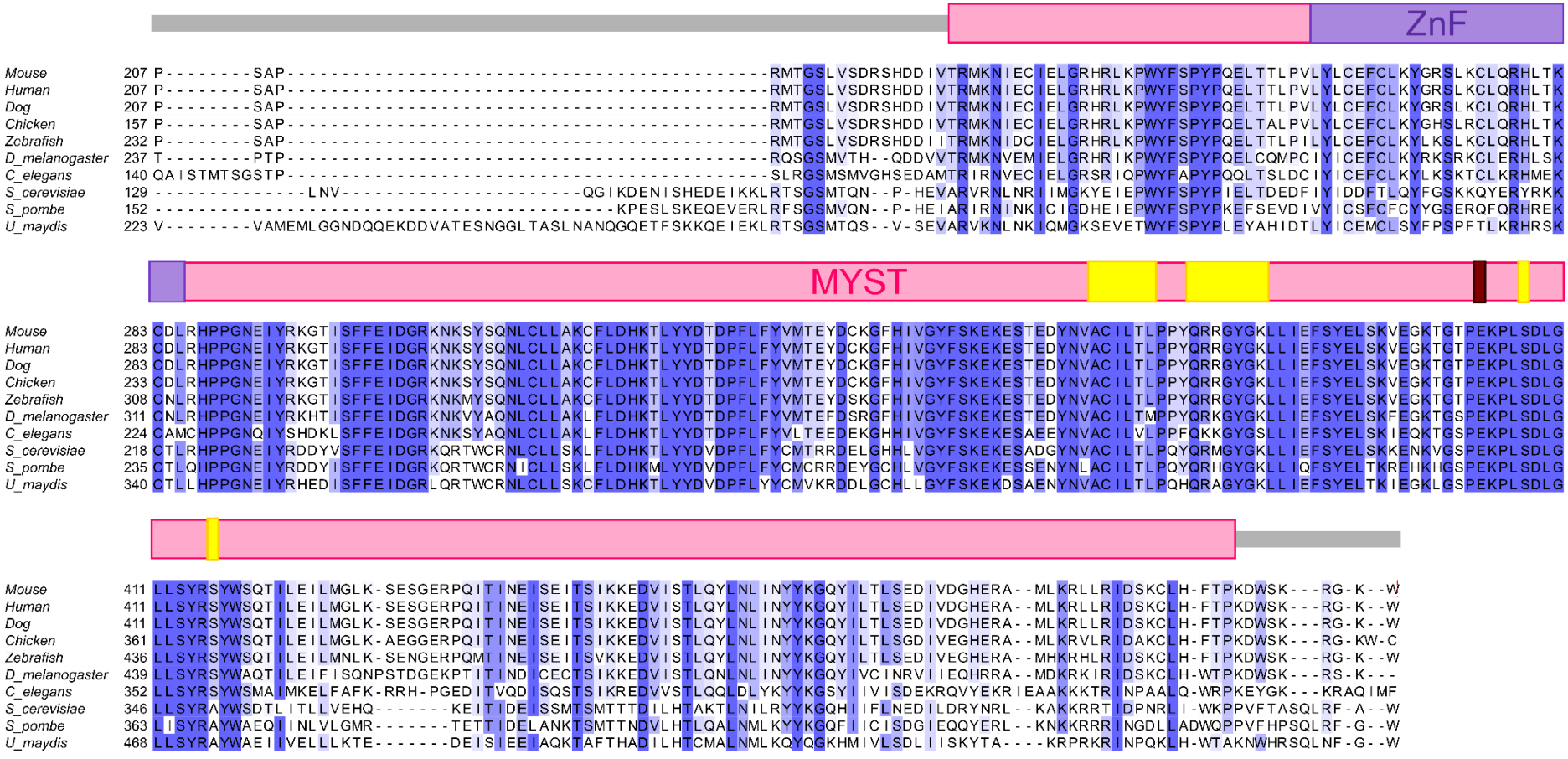
ZnF
MYST
Mouse 207 P--------SAP----------RMTGSLVSDRSHDDIVTRMKNIECIELGRHRLKPWYFSPYPQELTTLPVLYLCEFCLKYGRSLKCLQRHLTK
Human 207 P--------SAP----------RMTGSLVSDRSHDDIVTRMKNIECIELGRHRLKPWYFSPYPQELTTLPVLYLCEFCLKYGRSLKCLQRHLTK
Dog 207 P--------SAP----------RMTGSLVSDRSHDDIVTRMKNIECIELGRHRLKPWYFSPYPQELTTLPVLYLCEFCLKYGRSLKCLQRHLTK
Chicken 157 P--------SAP----------RMTGSLVSDRSHDDIVTRMKNIECIELGRHRLKPWYFSPYPQELTALPVLYLCEFCLKYGHSLRCLQRHLTK
Zebrafish 232 P--------SAP----------RMTGSLVSDRSHDDIITRMKNIDCIELGRHRLKPWYFSPYPQELTTLPILYLCEFCLKYLKSLKCLQRHLTK
D_melanogaster 237 T--------PTP----------RQSGSMVTH--QDDVVTRMKNVEMIELGRHRIKPWYFSPYPQELCQMPCIYICEFCLKYRKSRKCLERHLSK
C_elegans 140 QAISTMTSGSTP----------SLRGSMSMVGHSEDAMTRIRNVECIELGRSRIQPWYFAPYPQQLTSLDCIYICEFCLKYLKSKTCLKRHMEK
S_cerevisiae 129 ----------LNV----------QGIKDENISHEDEIKKLRTSGSMTQN--P-HEVARVRNLNRIIMGKYEIEPWYFSPYPIELTDEDFIYIDDFTLQYFGSKKQYERYRKK
S_pombe 152 ----------KPESLSKEQEVERLRFSGSMVQN--P-HEIARIRNINKICIGDHEIEPWYFSPYPKEFSEVDIVYICSFCFCYYGSERQFQRHREK
U_maydis 223 V--------VAMEMLGGNDQQEKDDVATESNGGLTASLNANQGQETFSKKQEIEKLRTSGSMTQS--V-SEVARVKNLNKIQMGKSEVETWYFSPYPLEYAHIDTLYICEMCLSYFPSPFTLKRHRSK
Mouse 283 CDLRHPPGNEIYRKGTISFFEIDGRKNKSYSQNLCLLAKCFLDHKTLYYDTDPFLFYVMTEYDCKGFHIVGYFSKEKESTEDYNVACILTLPPYQRRGYGKLLIEFSYELSKVEGKTGTPEKPLSDLG
Human 283 CDLRHPPGNEIYRKGTISFFEIDGRKNKSYSQNLCLLAKCFLDHKTLYYDTDPFLFYVMTEYDCKGFHIVGYFSKEKESTEDYNVACILTLPPYQRRGYGKLLIEFSYELSKVEGKTGTPEKPLSDLG
Dog 283 CDLRHPPGNEIYRKGTISFFEIDGRKNKSYSQNLCLLAKCFLDHKTLYYDTDPFLFYVMTEYDCKGFHIVGYFSKEKESTEDYNVACILTLPPYQRRGYGKLLIEFSYELSKVEGKTGTPEKPLSDLG
Chicken 233 CDLRHPPGNEIYRKGTISFFEIDGRKNKSYSQNLCLLAKCFLDHKTLYYDTDPFLFYVMTEYDCKGFHIVGYFSKEKESTEDYNVACILTLPPYQRRGYGKLLIEFSYELSKVEGKTGTPEKPLSDLG
Zebrafish 308 CNLRHPPGNEIYRKGTISFFEIDGRKNKMYSQNLCLLAKCFLDHKTLYYDTDPFLFYVMTEYDSKGFHIVGYFSKEKESTEDYNVACILTLPPYQRRGYGKLLIEFSYELSKVEGKTGTPEKPLSDLG
D_melanogaster 311 CNLRHPPGNEIYRKHTISFFEIDGRKNKVYAQNLCLLAKLFLDHKTLYYDTDPFLFYVMTEFDSRGFHIVGYFSKEKESTEDYNVACILTMPPYQRKGYGKLLIEFSYELSKFEGKTGSPEKPLSDLG
C_elegans 224 CAMCHPPGNQIYSHDKLSFFEIDGRKNKSYAQNLCLLAKLFLDHKTLYYDTDPFLFYVLTEEDEKGHHIVGYFSKEKESAEEYNVACILVLPPFQKKGYGSLLIEFSYELSKIEQKTGSPEKPLSDLG
S_cerevisiae 218 CTLRHPPGNEIYRDDYVSFFEIDGRKQRTWCRNLCLLSKLFLDHKTLYYDVDPFLFYCMTRRDELGHHLVGYFSKEKESADGYNVACILTLPQYQRMGYGKLLIEFSYELSKKENKVGSPEKPLSDLG
S_pombe 235 CTLQHPPGNEIYRDDYISFFEIDGRKQRTWCRNICLLSKLFLDHKMLYYDVDPFLFYCMCRRDEYGCHLVGYFSKEKESSENYNLACILTLPQYQRHGYGKLLIQFSYELTKREHKHGSPEKPLSDLG
U_maydis 340 CTLLHPPGNEIYRHEDISFFEIDGRLQRTWCRNLCLLSKCFLDHKTLYYDVDPFLYYCMVKRDDLGCHLLGYFSKEKDSAENYNVACILTLPQHQRAGYGKLLIEFSYELTKIEGKLGSPEKPLSDLG
Mouse 411 LLSYRSYWSQTILEILMGLK-SESGERPQITINEISEITSIKKEDVISTLQYLNLINYYKGQYILTLSEDIVDGHERA--MLKRLLRIDSKCLH-FTPKDWSK---RG-K--W
Human 411 LLSYRSYWSQTILEILMGLK-SESGERPQITINEISEITSIKKEDVISTLQYLNLINYYKGQYILTLSEDIVDGHERA--MLKRLLRIDSKCLH-FTPKDWSK---RG-K--W
Dog 411 LLSYRSYWSQTILEILMGLK-SESGERPQITINEISEITSIKKEDVISTLQYLNLINYYKGQYILTLSEDIVDGHERA--MLKRLLRIDSKCLH-FTPKDWSK---RG-K--W
Chicken 361 LLSYRSYWSQTILEILMGLK-AEGGERPQITINEISEITSIKKEDVISTLQYLNLINYYKGQYILTLSGDIVEGHERA--MLKRVLRIDAKCLH-FTPKDWSK---RG-KW-C
Zebrafish 436 LLSYRSYWSQTILEILMNLK-SENGERPQMTINEISEITSVKKEDVISTLQYLNLINYYKGQYILTLSEDIVEGHERA--MHKRHLRIDSKCLH-FTPKDWSK---RG-K--W
D_melanogaster 439 LLSYRSYWAQTILEIFISQNPSTDGEKPTITINDICECTSIKKEDVISTLQNLNLINYYKGQYIVCINRVIIEQHRRA--MDKRKIRIDSKCLH-WTPKDWSK---RS-K---
C_elegans 352 LLSYRSYWSMAIMKELFAFK-RRH-PGEDITVQDISQSTSIKREDVVSTLQQLDLYKYYKGSYIIVISDEKRQVYEKRIEAAKKKTRINPAALQ-WRPKEYGK---KRAQIMF
S_cerevisiae 346 LLSYRAYWSDTLITLLVEHQ-------KEITIDEISSMTSMTTTDILHTAKTLNILRYYKGQHIIFLNEDILDRYNRL--KAKKRRTIDPNRLI-WKPPVFTASQLRF-A--W
S_pombe 363 LISYRAYWAEQTINLVLGMR-------TETTIDELANKTSMTTNDVLHTLQALNMLKYYKGQFIICISDGIEQQYERL--KNKKRRRINGDLLADWQPPVFHPSQLRF-G--W
U_maydis 468 LLSYRAYWAEIIVELLLKTE-------DEISIEEIAQKTAFTHADILHTCMALNMLKQYQGKHMIVLSDLIISKYTA----KRPRKRINPQKLH-WTAKNWHRSQLNF-G--W

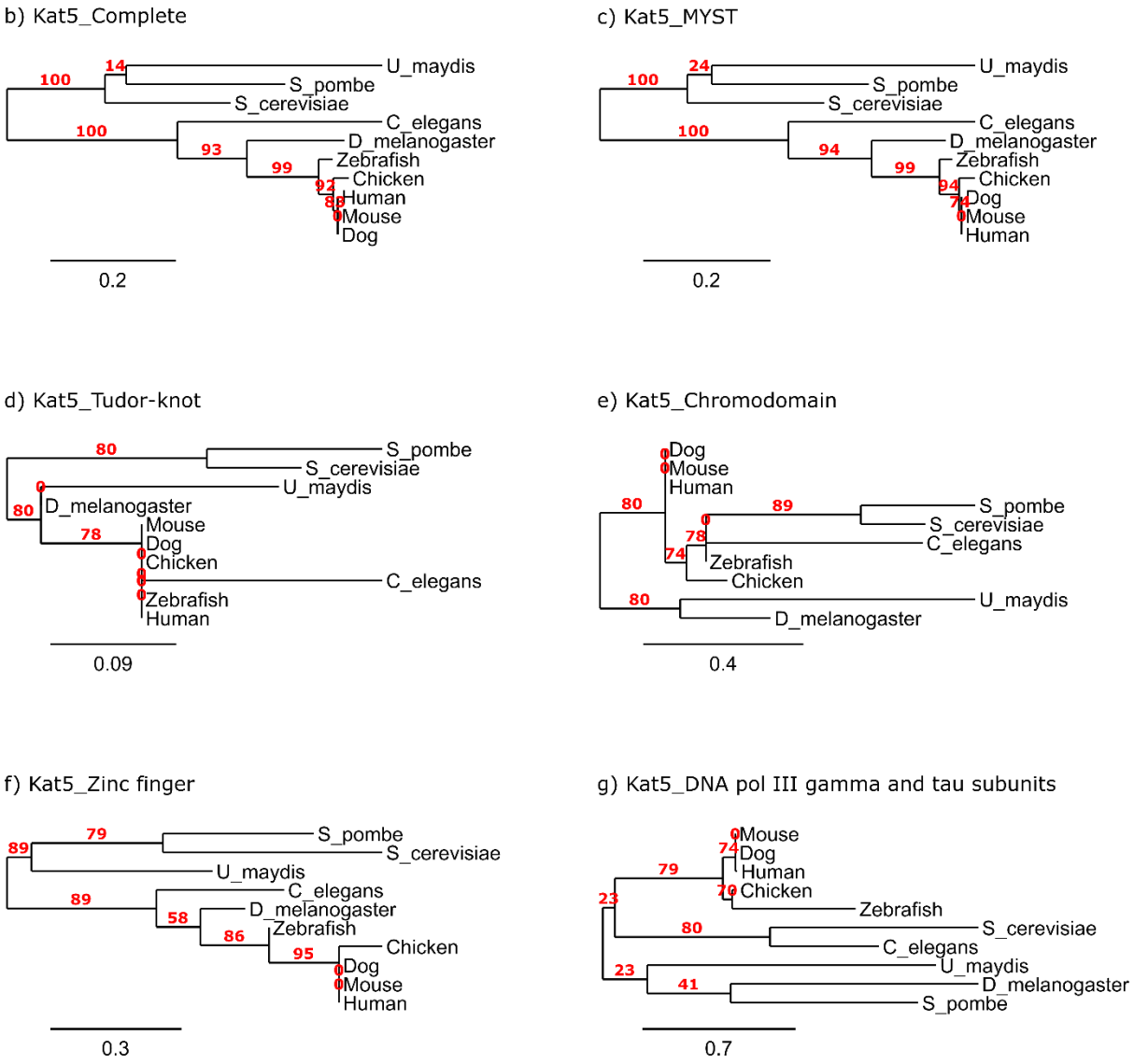

Figure 4 | Kat5 protein sequence is highly conserved throughout evolution

a, Sequence alignment of Kat5 lysine acetyltransferase across evolution. Analysed using the Pairwise Alignment tool on the Jalview Java alignment editor – version 2 (479) and presented with Percentage Identity multiple sequence alignment colour scheme based on 30% minimum conservation. Conserved domains are labelled: RNA-binding Tudor-knot of the chromodomain (turquoise), chromodomain (green), site of tyrosine phosphorylation (orange), query DNA polymerase III subunits gamma and tau (blue), conserved MYST domain present in MYST histone acetyltransferases (pink), Zinc finger domain (purple), Acetyl-CoA binding domains (yellow) and the active site (burgundy). These regions generally exhibit higher conservation than other regions. **b–g)** Phylogenetic trees on the full-length protein sequence of Kat5 (b), the MYST domain (c), the Tudor-knot (d), chromodomain (e), zinc finger (ZnF), f) and a possible hit for DNA polymerase III subunits gamma and tau. Each tree was rendered using MUSCLE multiple sequence alignment, PhyML for phylogenetic reconstruction and TreeDyn for image generation. All sequences used the Gblocks programme to eliminate poorly aligned positions and divergent regions, except (f) (495).

5.6 Imatinib inhibition of c-Abl kinase triggers spontaneous damage and eventual cell death

CH12F3 B cells were treated with small molecule inhibitors; either imatinib, iChromo, or TH1834. Each inhibitor mechanistically interacts with Kat5 differently, allowing for sensitive analysis of Kat5's activity during DNA repair and, ultimately, in CSR. The mode of action of each inhibitor is further elaborated below. First, these inhibitors were tested in the context of DNA repair to study the effect of Kat5 inhibition on DNA damage response signalling and, following a clear phenotype, the inhibitors were then employed in a class switching assay using the CH12F3 mouse B cell line. CH12F3 cells express IgM antibodies prior to activation by anti-CD40 and IL-4 and TGF-β cytokines, at which point they switch specifically to IgA-presenting cells. B cells were treated with the topoisomerase I inhibitor, camptothecin (CPT), to introduce DSBs during S-phase.

Phosphorylation by c-Abl kinase permits Kat5 binding to H3K9me3, eventually triggering H2AX phosphorylation (469). Treating CH12F3 B cells with imatinib prevents this phosphorylation event, permitting the investigation of this modification on DNA repair signalling. Initial treatment with imatinib was based on experiments involving fibroblasts whereby the cells had been treated with 0.1, 1 and 10 μM concentrations of imatinib (496,497). Following imatinib treatment, it was expected that there would be a reduction in gH2AX signalling, preventing the recruitment of downstream repair proteins. It should not impact Kat5-dependent chromatin remodelling, thereby permitting separation of function analyses of Kat5. Other mechanisms are in place to drive H2AX phosphorylation, such as by ATR (ataxia-telangiectasia and Rad3 related) and DKA-PK (498), so a total loss of γH2AX was not expected.

In an attempt to replicate these conditions, cells were pre-treated with 0 or 1 μM imatinib. In these conditions, irrespective of CPT treatment, this concentration of imatinib was toxic as observed by the dead cell distribution (100% and 99.98% dead cells) in the flow cytometry analysis (Figure 5a; left). Following successive rounds of optimisation, a narrow range of imatinib pre-treatments proved to have limited effect on Kat5 inhibition and downstream H2AX phosphorylation (Fig. 5b–d). This is not entirely unexpected as imatinib is used in treatments against B cell lymphomas (499–

501), and therefore very effective against B cell malignancies which our cell line CH12F3 is a model of (96). However, within a tight range of very low concentrations, a trend is observed whereby imatinib shows limited inhibition of DNA repair signalling before itself causing spontaneous cell damage and increasing H2AX phosphorylation independently from genotoxic treatments (Fig. 5b–d). An approximate 20% reduction in γH2AX is observed following treatment with 0.006 μM imatinib ($p<0.01$) compared to the mock treatment, yet with 0.01 μM imatinib, damage signalling is reduced by only 10%, although this reduction is not significant. Following treatment with 0.05 μM imatinib, 70% spontaneous DNA damage is observed independently of CPT treatment (Fig. 5b–d). As such, imatinib is clearly not suitable for this assay. Furthermore, c-Abl is a hyperactive kinase that phosphorylates a broad range of target proteins (502). Without Kat5 specificity, it is impossible to attribute any effect observed in these results being solely due to Kat5 inhibition. That is why it was decided to use alternative inhibitors which could give a more specific response and a better separation of function analysis**.**

Imatinib was briefly considered as an additional DNA damaging reagent alongside CPT. However, this was dismissed because imatinib targets a multitude of proteins that are involved in cell growth and survival, oxidative stress and DNA-damage responses, and actin-dynamics and cell migration (502). Potentially altering the behaviour of many cellular pathways could mask the activity of Kat5, which would impede any attempt to isolate its role in DNA repair.

FIGURE 5

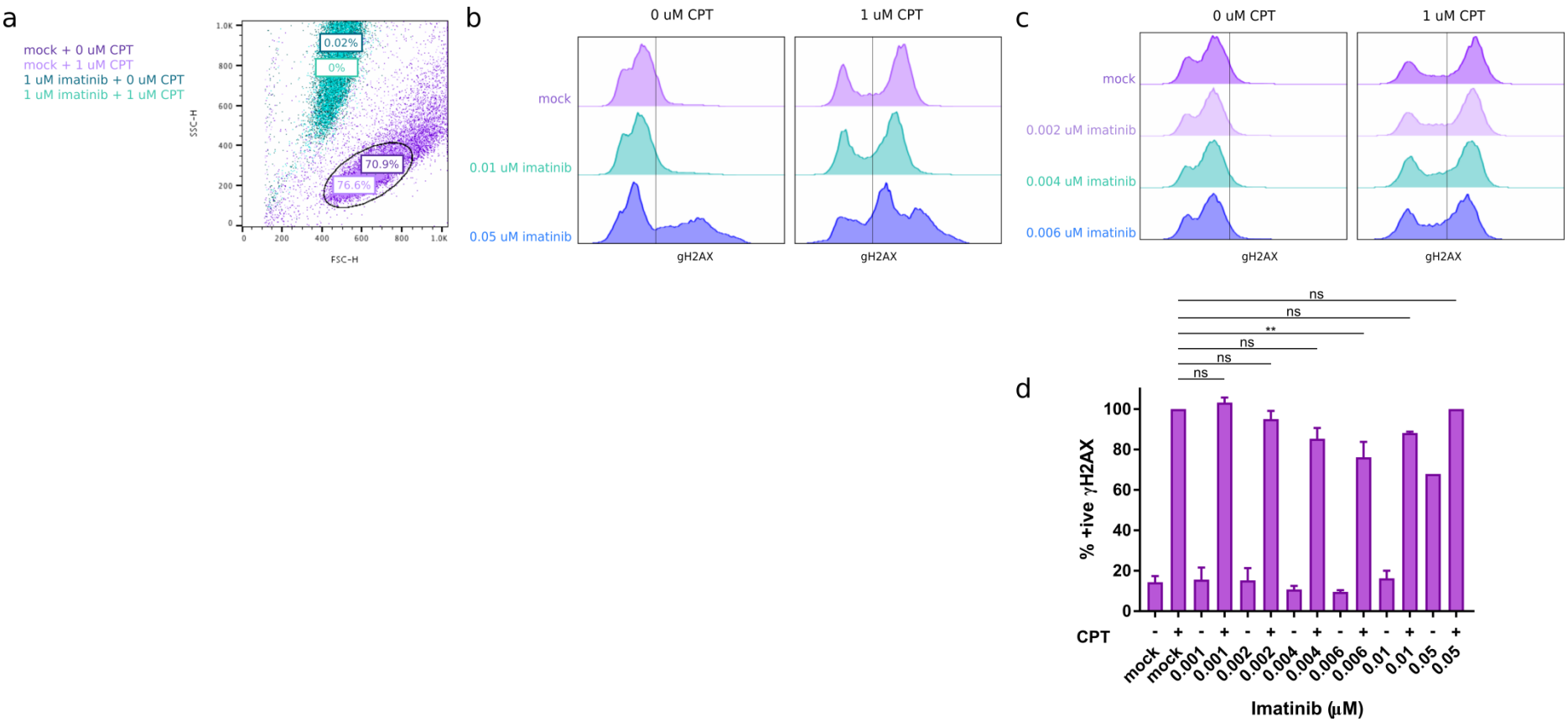

Figure 5 | Imatinib treatment causes extensive cell death

a, CH12F3 B cells were treated with 0 or 1 μM imatinib for 1 hour prior to incubation with 1 μM CPT for 1 hour. Cells were fixed and stained with GFP-tagged anti-γH2AX antibody. The light and dark purple populations on the scatter plot represent live cells and the light and dark teal populations represent dead cells that have ben treatmed with 1 μM imatinib. Values indicate the percentage of live cells in each population. **b** and **c,** Performed flow cytometry on cells treated with a range of concentrations of imatinib (0.001 – 0.05 μM). **d,** Histogram representing γH2AX positive populations across all samples tested and quantified as a percentage of the total damage inflicted on mock cells treated with CPT. Error bars represent SEM, n=3 in all cases; **p<0.01.

5.7 iChromo treatment inhibits DNA damage signalling

iChromo is a competitive inhibitor of c-Abl kinase, and effectively protects the Kat5 chromodomain against phosphorylation by preventing the docking of c-Abl (A. Kaidi, personal communications). In doing so, Kat5 fails to be recruited to sites of DNA damage – *via* the recognition of its chromodomain to H3K9me3 histone mark – thereby failing to activate ATM kinase which triggers the DDR signalling cascade. The iChromo-Kat5 complex however, is still able to acetylate H4 N-terminal tails (42) thereby allowing us to study the separation of function between Kat5 recruitment and acetylation activity. iChromo is a far more effective inhibitor than imatinib, successfully reducing γH2AX signalling by >20% between 20-50 μM iChromo, and nearly a further 70% at 75 and 100 μM iChromo, without inducing spontaneous damage (Fig. 6a–b). However, it appears that at the higher concentrations of inhibitor, cellular viability is significantly reduced ($p<0.0001$) to approximately 20% live cells, compared to a consistent 60–80% live at lower concentrations of iChromo (Fig. 6c).

CH12F3 B cells were subsequently visualised using immunofluorescence microscopy (Fig. 6d). It appears that CPT treatment induces DNA damage, and also causes the B cells to shrink in size to <10 um in the mock treatment. As iChromo concentration increases from 10–50 μM, the diameter of the cells visibly increases to >10 um. At 75 and 100 μM iChromo, the cells again appear very condensed (Fig. 6d). In addition, as iChromo concentration increases, the B cell nuclei appear fragmented in a phenomenon described as ‘blebbing,’ and this becomes much more prevalent at higher concentrations ($p<0.0001$; Fig. 6f).

FIGURE 6

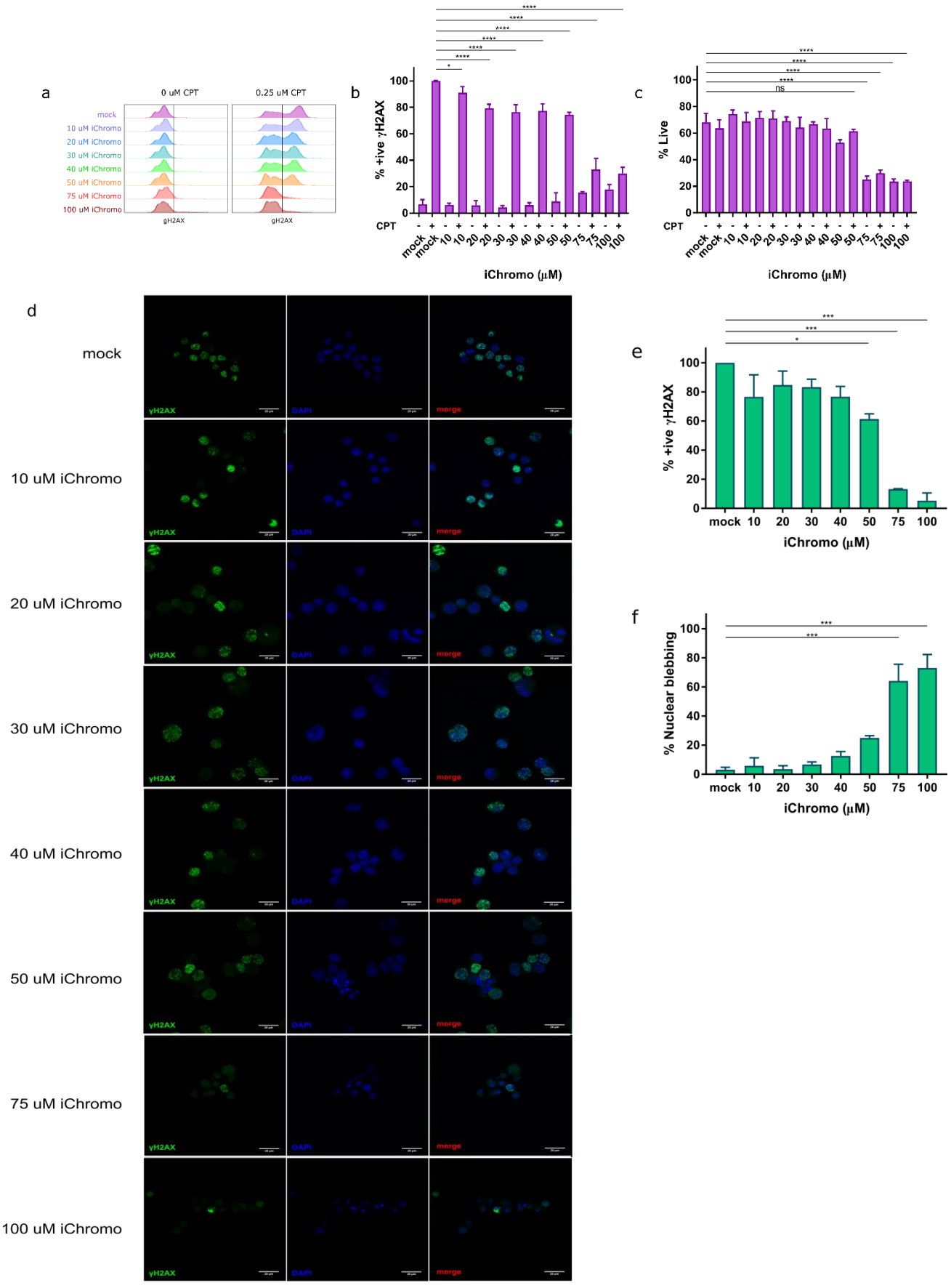
a
0 uM CPT
0.25 uM CPT
mock
10 uM iChromo
20 uM iChromo
30 uM iChromo
40 uM iChromo
50 uM iChromo
75 uM iChromo
100 uM iChromo
gH2AX
gH2AX
b
% +ive γH2AX
CPT
iChromo (μM)
c
% Live
ns
CPT
iChromo (μM)
d
mock
10 uM iChromo
20 uM iChromo
30 uM iChromo
40 uM iChromo
50 uM iChromo
75 uM iChromo
100 uM iChromo
γH2AX
DAPI
merge
e
% +ive γH2AX
iChromo (μM)
f
% Nuclear blebbing
iChromo (μM)

Figure 6 | Increasing concentrations of iChromo reduces DNA damage signalling

a, CH12F3 B cells were pre-treated for 16 hours with 0–100 μM iChromo prior to 30 minutes incubation with 0 or 0.25 μM CPT. Cells were stained with GFP-tagged anti-γH2AX antibody and analysed on the flow cytometer. **b,** Histogram quantifies the results in (a) from replicate experiments; results are normalised against total damage accrued in the mock treatment. **c,** Histogram indicates the % of live cells remaining following incubation with iChromo and CPT treatment; results are normalised against total damage accrued in the mock treatment. **d,** CPT-treated aliquots from (a) were visualised under a cofocal microscope with th addition of DAPI mounting dye for nuclear staining. **e,** Histogram represents the quantification of the observations in (d), normalised as a percentage of total damage accumulated in the mock treatment. **f,** Histogram indicates the % of cells presenting nuclear blebbing in each treatment. Error bars represent SEM, n=4 for each condition; *p<0.05, **p<0.01, ***p<0.001 and ****p<0.0001.

5.8 TH1834 treatment inhibits DNA damage signalling by blocking Kat5 acetylation function

TH1834 is a Kat5-specific histone acetyltransferase (HAT) inhibitor. Its *in silico* design was based on the structures of acetyl-CoA and the non-specific HAT inhibitor, pentamidine (207). An *in vivo* HAT assay indicates that TH1834 inhibition reduces γH2AX formation to a greater extent than pentamindine in DT40 cells (207). As TH1834 mimics its natural ligand acetyl-CoA it prevents Kat5-dependent acetylation of both H4 tails and ATM, thereby impacting on both the DNA repair and chromatin decompaction activities of Kat5.

To test the efficacy of the inhibitor, B cells were treated with 0–100 μM TH1834. Incubation with 25 and 50 μM TH1834 significantly reduces H2AX phosphorylation ($p<0.0001$; Fig. 7a–b). In addition, cellular survival during this period remains unchanged across the different treatments (Fig. 7c).

Following subsequent confocal microscopy (Fig. 7d), the quantification of damaged cells were not as significant as the data extracted from the flow cytometer. Nevertheless, there is a general trend whereby TH1834 does reduce DNA damage signalling (Fig. 7e). Another complementary explanation here could be the technical readout between fluorescence imaging and flow cytomerty. Whilst the former technique scores individual cell for their average positive or negative value for the green γH2AX fluorescence signal, flow cytomery looks at the average γH2AX fluorescence signal throughout the cell population. In that vein, it is possible that

TH1834 decreases γH2AX fluorescence signal overall per cell but without being able to deplete it completely. While iChromo could be more effective in specific cells, perhaps during a certain phase of the cell cycle, thereby causing a complete depletion of γH2AX signal in those particular cells. This aspect will be elaborated upoin in more detail in the discussion below. Unlike the iChromo-treated cells, very few occurences of nuclear blebbing were observed, suggesting that TH1834 does not contribute towards any morphological changes in B cells for the duration of this assay (Fig. 7f).

FIGURE 7

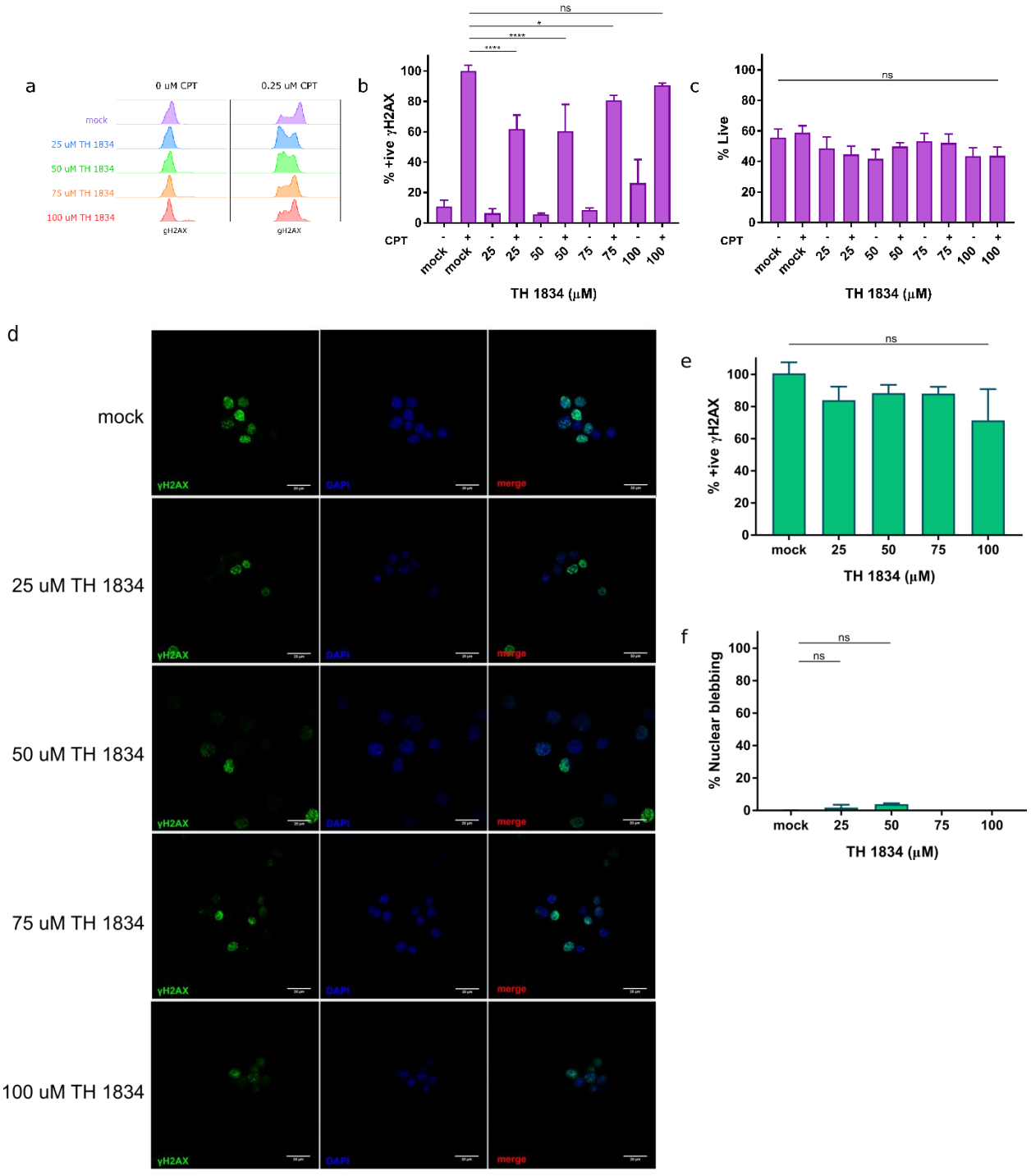
a
0 uM CPT
0.25 uM CPT
mock
25 uM TH 1834
50 uM TH 1834
75 uM TH 1834
100 uM TH 1834
γH2AX
γH2AX
b
% +ive γH2AX
CPT
TH 1834 (μM)
ns
*
****
****
c
% Live
CPT
TH 1834 (μM)
ns
d
mock
25 uM TH 1834
50 uM TH 1834
75 uM TH 1834
100 uM TH 1834
γH2AX
DAPI
merge
e
% +ive γH2AX
TH 1834 (μM)
ns
f
% Nuclear blebbing
TH 1834 (μM)
ns
ns

Figure 7 | Treatment with TH1834 reduces DNA damage signalling

a, CH12F3 B cells were pre-treated for 1 hour with 0–100 μM TH1834 prior to 30 minutes incubation with 0 or 0.25 μM CPT. Cells were stained with GFP-tagged anti-γH2AX antibody and analysed on the flow cytometer. **b,** Histogram quantifies the results in (a) from replicate experiments; results are normalised against total damage accrued in the mock treatment. **c,** Histogram indicates the % of live cells remaining following incubation with TH1834 and CPT treatment; results are normalised against total damage accrued in the mock treatment. **d,** CPT-treated aliquots from (a) were visualised under a cofocal microscope with th addition of DAPI mounting dye for nuclear staining. **e,** Histogram represents the quantification of the observations in (d), normalised as a percentage of total damage accumulated in the mock treatment. **f,** Histogram indicates the % of cells presenting nuclear blebbing in each treatment. Error bars represent SEM, n=4 for each condition; *p<0.05, **p<0.01, ***p<0.001 and ****p<0.0001.

5.9 Kat5 DNA damage recruitment ability contributes to CSR efficiency

Having determined the appropriate concentrations of iChromo that exert a phenotypic response to the inhibitor, the B cells were induced to class switch in the presence of 0–30 μM iChromo.

By 72 hours, it was clear that 20 and 30 μM iChromo reduces class switching efficiency by approximately 25 and 50% on gated live cells, respectively ($p<0.0001$). 10 μM iChromo enhanced class switching efficiency by nearly 20% compared to activated B cells in the absence of inhibitor (Fig. 8a). To gain further insight into this inconsistency, the survival rate was calculated over the course of the 72 hours (Fig. 8b). The extent of cell death substantially increased with iChromo concentration, and the flow cytometer counted a maximum of 400 cells in 30 μM iChromo at 48 and 72 hours, casting doubt on the validity of the results at this concentration.

FIGURE 8

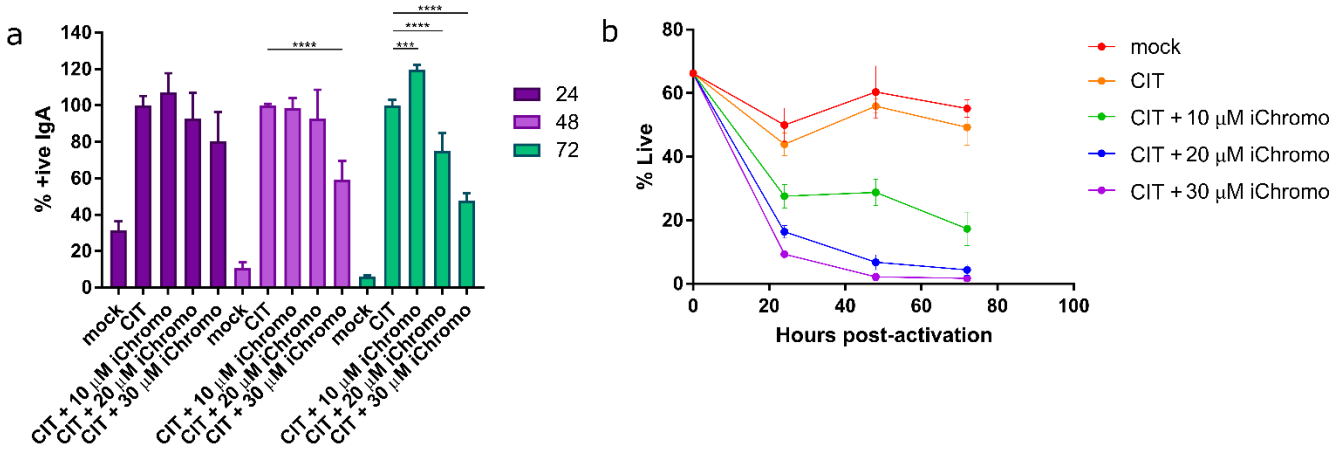

Figure 8 | Inhibition of Kat5 chromodomain with iChromo affects CSR efficiency

a, CH12F3 B cells were activated and treated with 0, 10, 20 and 30 μM iChromo. At 25, 48 and 72 hours post-activation, cells were stained with APC-tagged anti-IgM and FITC-tagged anti-IgA antibodies. Cells were analysed on the flow cytometer. The histogram quantifies the IgA in each condition from replicate experiments as a % of the activated control at each time point. **b,** Graph represents the % live population of cells at 24, 48 and 72 hours post-activation. Error bars represent SEM; n=4 in all cases; *p<0.05, **p<0.01, ***p<0.001 and ****p<0.0001.

5.10 Kat5 acetylation activity independently contributes to CSR efficiency

Cells were treated with TH1834 at a range of concentrations; 0, 10, 25 and 50 μM. As observed with iChromo, 10 μM TH1834 appears to stimulate CSR by a further 20–25% compared to the activated controls at each time point, while 25 and 50 μM TH1834 reduces CSR efficiency (Fig. 9a).

This assay was first performed in 2016 with very dissimilar results. Indeed, 10 μM TH1834 had a minor 15% reduction in class switching at each time point, and both 20 and 30 μM TH1834 exerted a 30–40% reduction in CSR (Fig. 9c). There is a clear dosing effect between 10 μM and 20 μM TH1834, yet it appears that increasing the concentration further to 30 μM does not further impede CSR, suggesting that Kat5 supports CSR to a certain extent, but perhaps other redundant pathways are also active to ensure that CSR is not completely abolished upon loss of Kat5-dependent acetylation.

To tease out the cause of these stark differences between the experiments in 2018 and 2016, survival rates were compared over the course of each assay. The survival rates for the assay carried out in 2018 mimic those of the iChromo, in which extensive cell death occurs swiftly over the course of 72 hours (Fig. 9c). The cell counts however counted <50 cells at 48 and 72 hours, casting doubt on the reliability of those results, and hence have been omitted from the histogram. However, in 2016, the live population remained stable throughout the 96 hours post-activation (Fig. 9d), indicating the either the cells are responding differently to the inhibitor, or the media is impacting cellular behaviour due to a different batch of FCS.

FIGURE 9

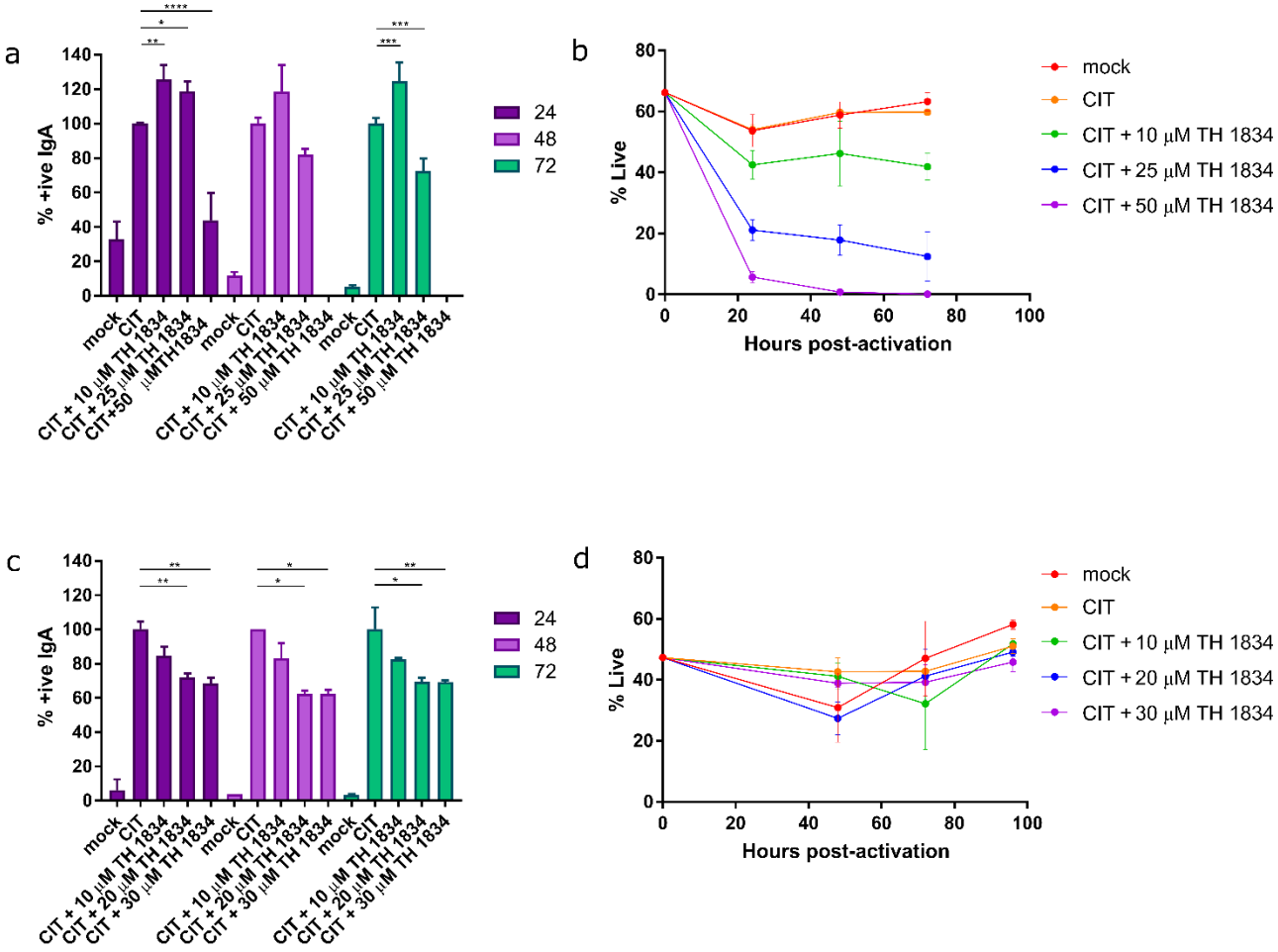

Figure 9 | Inhibition of Kat5 acetyltransferase activity affects CSR efficiency

a, CH12F3 B cells from 2018 were activated and treated with 0, 10, 25 and 50 µM TH1834. At 25, 48 and 72 hours post-activation, cells were stained with APC-tagged anti-IgM and FITC-tagged anti-IgA antibodies. Cells were analysed on the flow cytometer. The histogram quantifies the IgA in each condition from replicate experiments as a % of the activated control at each time point. b, CH12F3 B cells from 2016 were activated and treated with 0, 10, 20 and 30 µM TH1834. At 48, 72 and 96 hours post-activation, cells were stained with APC-tagged anti-IgM and FITC-tagged anti-IgA antibodies. Cells were analysed on the flow cytometer. The histogram quantifies the IgA in each condition from replicate experiments as a % of the activated control at each time point. c, Graph represents the % live population of cells at 24, 48 and 72 hours post-activation from the 2018 assay. d, Graph represents the % live population of cells at 48, 72 and 96 hours post-activation from the 2016 assay. Error bars represent SEM; n=4 in all cases; *p<0.05, **p<0.01, ***p<0.001 and ****p<0.0001.

5.11 Discussion

These results are the first evidence for Kat5 having a fundamentally critical role in CSR and immune diversification. Using a range of chemical inhibitors, Kat5 inhibition

reduced DNA repair signalling by prohibiting H2AX phosphorylation and affected CSR efficiency.

The small molecule inhibitor imatinib targets c-Abl kinase. By preventing c-Abl kinase mediated phosphorylation of Kat5 at Tyr44, Kat5 is rendered incapable of binding H3K9me3, and is therefore unable to activate ATM kinase and propagate DNA repair signalling (469). Whilst imatinib was capable of reducing H2AX phosphorylation, this took place within a very narrow range of concentrations and did not have a particularly strong effect. Increasing the concentration further then induced spontaneous damage, restricting any dose-ranging studiess. CH12F3 B cells are particularly susceptible to imatinib as it is used in treatments against B cell lymphomas (499–501). Furthermore, c-Abl kinase has many downstream targets including Kat5 and, as such, any observations made could not be attributed to only Kat5 inhibition (502). While imatinib could have been used as a DNA damage reagent in the same way that cells were treated with camptothecin, camptothecin has only one downstream target and produces DSBs as a result. Targeting c-Abl kinase would confuse the results as it has several protein targets that may impact DNA repair and Kat5 unpredictably and may produce a range of DNA damage structures that are not accounted for in the design of the assay. Based on these factors, imatinib was rejected as a potential inhibitor of Kat5 in subsequent class switching inhibition assays. It could be interesting to incorporate imatinib in the fluorescence assay to determine if it interacts with other nucleases or helicases to alter their activities, or indeed to determine whether imatinib causes DNA damage directly.

iChromo and TH1834 are other inhibitors of Kat5. As their mechanisms of targeting Kat5 differ, it was expected that the extent to which its acetylation activities in DNA repair or chromatin decompaction is most vital for efficient CSR. iChromo, similarly to imatinib, prevents Kat5 binding to H3K9me3. iChromo is a competitive inhibitor of the trimethyl group recognised by the Kat5 chromodomain (personal communications). iChromo had a much greater impact on DNA damage signalling, reducing the indicidence of H2AX phosphorylation, without inducing any spontaneous damage. It did, however, cause nuclear blebbing at higher concentrations, which is indicative of apoptosis.

TH1834 was designed *in silico* to bind to the Kat5 HAT domain (207), impeding acetylation of both ATM and H4 lysines (207,468), and thus having the combined effect of hindering DNA damage signalling and chromatin relaxation. This inhibitor successfully reduced the occurrence of γH2AX and, unlike iChromo, did not disrupt the integrity of the cell and the nucleus.

For both iChromo- and TH1834-mediated inhibition of Kat5, it would be expected that TH1834 treatment would produce a stronger phenotype as it influences both ATM and H4ac repair mechanisms, in contrast with iChromo which only affects the pathway through ATM. This is indeed the case for the DNA damage assay as TH1834 reduced γH2AX signalling by 40% compared to 20% by inhibiting chromodomain binding alone. Whether this is to be replicated in regards to class switching will wait to be seen. Furthermore, an additional chemical inhibitor which alters the tertiary structure of Kat5, while maintaining its catalytic functions, will help to expand our understanding of Kat5's catalytic and structural functions.

Both iChromo and TH1834 affect the Kat5 signalling pathway upstream of H2AX phosphorylation as the number of cells exhibiting DNA damage signalling was reduced, but the size of γH2AX foci in all conditions appeared very similar to controls. This suggests that DNA repair is not inhibited downstream of γH2AX as otherwise the γH2AX foci would have continued to expand, trapped in a positive feedback loop, as the break is left unrepaired (503).

In the presence of TH1834, there is adose-dependent decrease in class switching, with approximately 80% CSR taking place in 10 μM TH1834 and 60–70% in 20–30 μM TH1834. The rates of CSR are very similar between 20 and 30 μM TH1834, indicating that inhibition of Kat5 may only reduce CSR by a certain extent, and that the cells are not solely reliant on Kat5 for antibody diversification as other pathways must be in place to ensure a certain level of class switching takes place. A dose-dependent decrease in CSR is also observed with iChromo over the 72 hours, with 30 μM iChromo causing a 50% reduction CSR at 72 hours post-activation. Once the experimental conditions are optimised to ensure the high level of cell death is avoided, it would be interesting to repeat these CSR assays to determine whether TH1834 has

a greater impact on CSR than iChromo as observed in the earlier DNA damage assays.

It is worth noting that the incomplete DNA damage and CSR phenotype we observe in Kat5 inhibition could be attributed to various interpretations. 1) The chemical inhibitors used do not offer complete functional inhibition of Kat5 in B cells. There is some evidence in the literature that this could be the case. Although the TH1834 publication (207) suggests that this may not be case for this specific drug, it has not been tested specifically in B cells to confirm whether that is the case or not. 2) There is potential redundancy in Kat5 recuitment to DDR sites by factors other than H3K9me3. The putative RNA binding activity of Kat5 may support this possibility. Excitingly, a recent publication offered an interesting link between RNA and chromatin remodelling (467). DSB-induced RNAs (diRNAs) are ~21 nt small RNAs generated by Dicer and Drosha proteins. They are complementary to the sequences surrounding the break site in both plant and human cells (504,505). Ago2 (of the RNA-induced silencing complex) interacts with short RNAs, and was proposed to interact with Kat5 (467). Interestingly, these diRNAs are dispensible for Ago2 binding to Kat5, however, knockdown of Ago2 reduced Kat5 binding to the DSB, and the diRNAs were required for recuitment of Kat5 to the DSB (467). Ago2 has a much higher affinity for RNA than Kat5 (492,506), and it is possible that Kat5's RNA binding capabilities serve either to reinforce or the interaction, or as a contingency. 3) there is potential redundancy in ATM acetylation via other non-Kat5 HAT proteins. Some evidence to support this hypothesis stems from the role of another HAT protein called INO80 in DDR signaling (507) and in CSR (508). In the future it might be interesting to check the inhibition of both INO80 and Kat5 to address this question.

Once the conditions for studying class switching have been optimised, it will be possible to determine whether it is the role of Kat5 in DNA repair or transcription that is integral for CSR. This can be further determined by first looking into the proportion of the activated B cell population that is IgM- and IgA-negative. Accumulation of double-negative B cells would suggest transcriptional flaws. If this population of double-negative cells does not change significantly, then it is more likely that Kat5 functions predominately in DNA repair. To confirm this observation, RT-qPCR would need to be performed on B cell samples to confirm the transcriptional levels of Kat5,

AID, IgM and IgA S regions. Due to time limitations, the results for this experiment were never obtained.

As it stands, it is clear that inhibition of Kat5 activity has an effect on class switching. The extent to which it supports or hinders CSR remains unclear, including its mechanism. Nevertheles, these preliminary results are very promising and indicate that Kat5 does play an essential role in the development of highly versatile antibodies. And we thereby have contributed yet another piece of the histone code that regulates antibody diversification; starting with our protein/histone acetylation by Kat5, followed by histone phosphorylation by ATM/ATR/DNA-PKcs (102,328,509), ubiquitination by RNF8 (5,510), and poly-ubiquitination by RNF168 (511). Culminating in the recruitment of 53BP1 to bridge the 2 ends of DNA and mediating DNA repair (112).

6 Design of mouse and human Kat5 degron knockout constructs

6.1 Summary

Kat5 is essential for cellular viability. As such, generating Kat5 knockout cell lines is likely an impossible task. Confirming Kat5 knockdown is equally challenging as commercial antibodies raised against Kat5 bind with very low affinity. Generation of an inducible Kat5 knockout degron system overcomes both these concerns. As such, the stepwise design of an inducible Kat5 knockout degron system is described herein, including a discussion on the potential applications of this approach in terms of quickly and reversibly switching the protein expression of Kat5 on or off.

6.2 Kat5-depleted cells are inviable

As introduced in the previous chapter, Kat5 is an important and essential histone acetyltransferase protein. Kat5 is a challenging protein to manipulate intracellularly. Kat5 deletions have been found to be lethal in both mice and yeast (205,476,512). Indeed, $Kat5^{+/-}$ mice are viable and develop as normal, however double knockout $Kat5^{-/-}$ mice experience early embryonic lethality (205). As such, developing a Kat5 knockout CH12 B cell line was not feasible as any successful knockouts would have perished. In addition, commercial antibodies raised against Kat5 typically have poor affinity (personal communications). As a result, it is troublesome to visualise the success of an siRNA/shRNA knockdown via Western blot.

The aim is therefore to design an inducible and reversible system that allows for cell survival and Kat5 visualisation. In the system (described below), Kat5 is tagged with an intrinsically disordered protein, called a degron, that targets Kat5 for proteasomal degradation unless stabilised.

6.3 Tagging Kat5 with an inducible degron should prevent extensive cell death

To circumvent the issues of visualisation and viability, it was posited that generating a cell line with Kat5 tagged with an inducible, reversible degron could prevent extensive cell death. Degrons are specific, unstructured degradation systems that target proteins to the proteasome for degradation (513). The *E. coli* dihydrofolate reductase (eDHFR) is one example of a degron, and it allows for rapid manipulation of endogenous

mammalian proteins by altering their stability (208). As eDHFR is an intrinsically disordered protein, proteins tagged with eDHFR are constitutively degraded irrespective of their half-lives, unless they are stabilised by the addition of trimethoprim (TMP), which is innocuous in human cells (514,515). The aim is to tag the inducible eDHFR degron to the C-terminus of the Kat5 locus, integrating it into the genome using CRISPR/Cas9 genome-editing (208). While it is possible to generate an N-terminal degron, a large insertion at the initiation codon in one of the first exons is more likely to disrupt splicing than an insertion at the termination codon, and C-terminal tagging is amenable to degron insertion at an innocuous position downstream of the SV40 ply(A) site at the 3' end of the cassette (208). This inducible eDHFR degron is preferable to siRNAs or shRNAs due to the reversible nature of the system. This is especially useful for studying proteins such as Kat5 which are critical for cellular viability. This degron system is further advantageous due to the addition of an HA-tag inserted between the C-terminus of the protein of interest and the N-terminus of the eDHFR. HA is historically very immunogenic, and highly specific antibodies are available against this epitope, superseding the dependence on a suitable anti-Kat5 antibody. Indeed, FLAG-tagged/FLAG-HA-tagged Kat5 proteins are commonly used for protein tagging and visualisation (516–519).

6.4 Components of the degron cassette

The eDHFR degron cassette encodes for:

3xHA – eDHFR – P2A – puroR/blastR – SV40

This cassette will be integrated into the C-terminus of Kat5 in the mouse and human cell lines. The HA tags are a highly immunogenic protein that will allow for Kat5 staining by proxy (516–519). eDHFR is the intrinsically disordered dihydrofolate reductase that is responsible for targeting Kat5 to the proteasome for degradation and concomitant reduction in cellular protein levels (208). Both puromycin and blasticidin resistance (puroR/blastR) is essential for antibiotic selection. The antibiotic resistance genes will be carried in difference eDHFR cassettes to ensure that each eDHFR degron is successfully integrated into the two Kat5 alleles. P2A is a self-cleaving peptide that, once expressed, separates the degron from the antibiotics (520). P2A derives from

the porcine teschovirus-1, and cleaves the C-terminal proline (NPG | P) (521). Finally, SV40 functions as a terminator signal for RNA polymerase II (522).

The design of both the mouse and human Kat5 degron constructs was carried out by Emily Sheppard. The experimental data was produced under instruction by Laura Reffo and Erasmus student Miriam Lohr, and ligation protocols had previously been optimised by Erasmus student Angelina Bloch.

6.5 Materials and Methods

6.5.1 Celery juice assay

A modified version of the Surveyor assay, the celery juice assay, typically screens for Cas9 on-target activity. The CRISPR/Cas9 genome editing tool functions as RNA-guided molecular scissors to introduce a cut at the desired site on the genome. Error-prone DNA repair mechanisms target this damaged site for repair and may produce a frameshift mutation or stop codon to result in a truncated, inactive protein. DNA purified from wild type and Cas9-targeted Kat5 is extracted and mixed together to form heteroduplexes. Treatment with a mismatch-specific nuclease will cleave the DNA if mutation has been successful.

Analysis of the effects of Cas9 at the DNA level is based on a mismatch-specific nuclease. The assay consists of four steps; 1) PCR and PCR purification, 2) heteroduplex formation, 3) digest with mismatch-specific nuclease, and 4) visualisation of the reaction on a gel. The mismatch-specific nuclease was extracted from celery using the TILLING protocol (523).

6.5.2 Design of guide RNAs for the pX260 CRISPR/Cas9 and Kat5 knockout cell lines

Kat5 guide RNAs were designed based on scores generated by the
gRNA prediction software CRISPRdirect (524) and Zhang lab's Target Finder (http://crispr.mit.edu/). The designed gRNAs were synthesised according to the Church hCRISPR gRNA synthesis protocol (http://addgene.org/crispr/church/) and ligated into the gRNA_Cloning Vector (525) (Addgene, 41824).

mKat5 gRNA F: AAACTGAGTGGCGTGAGTGACGTCGT
mKat5 gRNA R: TAAAACGACGTCACTCACGCCACTCA

6.5.3 Transfection of 3T3 cells for Kat5 deletion

3T3 cells were cultured in DMEM media. Transfections for CRISPR/Cas9-mediated Kat5 deletion were performed using Lipofectamine 3000® (cat. L3000001, ThermoFisher,). Cells were extracted at 48- and 96-hours post-transfection, and

genomic DNA purified using GeneJET Genomic DNA Purification Kit (cat. K0721, Fermentas Stores).

6.5.4 Kat5 PCR primer design

PCR Primers were designed for the mouse Kat5 DNA sequence using Primer3 (526). Primers with suitable melting temperatures and location flanking the gRNA site in the sequence were chosen.

mKat5 F: GGAAGTGACGTCTCCCAGAG
mKat5 R: TAGAAAAGCTTTCGGCCACT

6.5.5 Design of guide RNAs for pX330 CRISPR/Cas9 for development of the inducible Kat5-degron knockdown cell lines

Kat5 sequences, primers and guide RNAs were designed using Benchling [Biology Software]. 2018. Retrieved from https://benchling.com. Benchling's CRISPR guides tool identified a Cas9 target site adjacent to the stop codon. The gRNAs were selected by virtue of distance from the stop codon, low off-target predictions and high on-target predictions. The forward gRNA sequence was prefixed with 'CACCg' and the reverse gRNA sequence was prefixed with 'CAAA' and suffixed with 'c'. The pX330 vector is digested by Bbs1 and the annealed gRNA oligos can cloned scarlessly into the vector.

mKat5 gRNA F: CACCgCACGAGAGCTGGCCGAACCA
mKat5 gRNA R: CAAATGGTTCGGCCAGCTCTCGTGc

hKat5 gRNA F: CACCgCCAAGACGGCAGCAGGACTG
hKat5 gRNA R: CAAACAGTCCTGCTGCCGTCTTGGc

6.5.6 Design of mouse and human Kat5 gBlocks® Gene Fragment homology region

Kat5 DNA sequence was downloaded onto Benchling. Retrieved a 1000 bp sequence spanning approximately 500 nucleotides either side of the Kat5 stop codon. Its

complexity is tested prior to order (https://www.idtdna.com/site/Order/gblockentry). Benchling's CRISPR guides tool identified a Cas9 target site adjacent to the stop codon. The PAM sequence in homology region was edited from NGG to NGA and the stop sequence was deleted. Either side of the homology region were short overhangs with complementarity to the pUC18 vector.

5' overhang: gattacgaattcgagctcggta
3' overhang: agttgcgcagcctgaatggcga

The total length of the homology arms was 1000 bp and was synthesised by IDT. The mutated PAM site in both homology regions are highlighted in red.

Table 1: Mouse and Human Kat5 homology region gBlocks® Gene Fragments

Target	Homology Region Sequence (5'–3')
mKat5	GATTACGAATTCGAGCTCGGTAAAGTGAGCCCAAATGCCCACCTGGGGGTTGTGGTTTGG TCTGTCTGTTCCTGGGGTTTCTGGGGACAGATGAATATCTTCAGGGGACTGAACTTTCCCC CACTTCCACCCCCACAGTGAGATCAGTGAAATCACTAGTATCAAGAAAGAAGATGTCATCT CCACACTGCAGTATCTCAACCTCATCAATTACTACAAGGTTAGGAGGCATGCTCAGGGGAT AGATGAGATATGGATGCAGGCTCTGAGCTGACATGAGCTGGCTCTATCTCTTGCTCAGGG CCAGTATATCCTAACTCTGTCAGAAGACATCGTGGATGGGCATGAGCGGGCTATGCTCAA GCGGCTCCTTCGGATTGACTCCAAGTGTCTGCACTTCACTCCCAAAGACTGGAGCAAGAG AGGAAAGTGGCACACACTACCCATTGCCATACCACGAGAGCTGGCCGAACCATG**T**CTAGCAC CCTGTCTTGTCCCATTTGAGCTTCGAAGAGGCACGCAAAGTGAGACAGGCCGAAGAACAG ACCCAAGAGGAGAAGAGGCCTAGGAGGGGCCCACTAGTGGCCAGTGCCAAGGCAAGCTC AGGTCTAGGCCAACTCCGAGGATAACTGGCTTACTGGCCCAGGTCCGCTCTGAACACGTG GACCAAAGGGATCCAGGCAGCTGTGTACATTAAGATGGGTGGGGAGCATTCTGTACAGGA CCGGTGATTGTAAAAATTTCTTTTATAAAGGAGGAGCTGGAGGGTGGGGTGGGCGCTGGTT GCAAAGTTCTGGCCCCTCTTGCCCCCAGAAATAAATTGTTTATATAGGCAGAGCTATCAGGA GTTCTTACCAAACTGGGTGCCATGTAATGGCAGCTTCAGGGTGCTAAGGTGCCCACAGACT CAGGCATTGTGAAGATCTCATTTATTGGGATAGAAACAGTCGCTCCAAGTGGTGAGAAGGG ATCTGTGACAGTTGCGCAGCCTGAATGGCGA
hKat5	GATTACGAATTCGAGCTCGGTACAGGGCTCCTGGGGACAGATAAAGGTCCTCAGGGAACCT GACCTGTGCTCTCCCACAGTGAGATTAGTGAAATCACCAGCATCAAGAAGGAGGATGTCATC TCCACTCTGCAGTACCTCAATCTCATCAACTACTACAAGGTAGGGAGGCAGGCAGGGGAGA CAGGTGTGTGGGATGCAGAGTGCAGTCCTCTGTGGGCTGACCACCTGCTGAACCCATCTCC TCTGCCCAGGGCCAGTACATCCTCACACTGTCAGAGGACATCGTGGATGGCCATGAGCGGG CCATGCTCAAGCGGCTCCTGCGGATCGACTCCAAGTGTCTGCACTTCACTCCCAAGGACTG GAGCAAGAGGGGGAAGTGGCCAGACACTGCCCACTGCAGTGCCAAGACGGCAGCAGGACT GGG**A**CTGATAGCCCACCCCGCCCCCACTGCAGCTCCCACAAAGCACTCTAAGGGAGATGG GGCTGAGGACAGCTCAAAAAGGAGAGGACAGGCCTGGCAGGGGCCCACTGGTGCCCAGC ACCAAGGCGAGCTCCGGGCTCAGACCAACTCCAAGGTCAGCTGGCCACAGGCCCAGGCCT CCTCTGAAGCAGGGACCAGAGGGAGCCAGGCAGCTGTGTACAGTGAGAAGGGATCCGGAT GGGGGAGCTCTGTACAGAGGGCTGGTGATTGTAAAAATTTCTTTTGTAAAGTAGAAGTTGGG GGTGGGGTGGGTGCTGGCTGCAAAAATTTCTGGCTTCTCTTACCCCTATTGCCCCCGGCAA TAAATTGTTTCTATATGCCAGAGCCATGCAAAGTTCTTGGTGGGGAGGGGGAAAGGGCCCAT GCTGGCTTAGGGGCTCTAAGGCGCCCAGACTCACAGGTGCTGTGAAGAGCTCCTTTATTGG GGTGATGGAATCGGTTCCAAAGAGCTGGTTTACTGCTGTGAAGGGATCGCAGCTTTGAATTT CAAGAGTTGCGCAGCCTGAATGGCGA

6.5.7 Primers used in the synthesis and validation of the degron constructs

Plasmid constructs and primers were designed using SnapGene software (from GSL Biotech; available at www.snapgene.com).

Table 2

Template	Primer	Sequence
pUC18	Linearise F	AGTTGCGCAGCCTGAATGGCGA
pUC18	Linearise R	TACCGAGCTCGAATTCGTAATC
pUC18-mKat5 HR	Linearise F	AAACTCATCAATGTATCTTACACACACTACCCATTGCCATACC
pUC18-mKat5 HR	Linearise R	TCGTATGGGTAACCGCCTCCGCCGCTGCCCCACTTTCCTCTCTTGCTCCAG
eDHFR (mKat5)	Amplification F	GGAGCAAGAGAGGAAAGTGGGGCAGCGGCGGAGGCGGTTACCCATAC
eDHFR (mKat5)	Amplification R	ATGGCAATGGGTAGTGTGTGTAAGATACATTGATGAGTTTGGAC
pUC18-hKat5 HR	Linearise F	AAACTCATCAATGTATCTTACCAGACACTGCCCACTG
pUC18-hKat5 HR	Linearise R	TCGTATGGGTAACCGCCTCCGCCGCTGCCCCACTTCCCCCTCTTGCT
eDHFR (hKat5)	Amplification F	GGAGCAAGAGGGGGAAGTGGGGCAGCGGCGGAGGCGGTTACCCATAC
eDHFR (hKat5)	Amplification R	CTGCAGTGGGCAGTGTCTGGTAAGATACATTGATGAGTTTGGAC
Screen for final Kat5-eDHFR product	F (inside puroR)	CCTGGTGCATGACCCGCAAG
Screen for final Kat5-eDHFR product	R (inside puroR)	GCTCGGTGACCCGCTCGATG
Screen for final Kat5-eDHFR product	F (inside blastR)	AGTGATGGACAGCCGACGGC
Screen for final Kat5-eDHFR product	R (inside blastR)	GCCCAGCACCACGAGTTCTGC

6.5.8 Overview of cloning Kat5-degron constructs

FIGURE 1

a

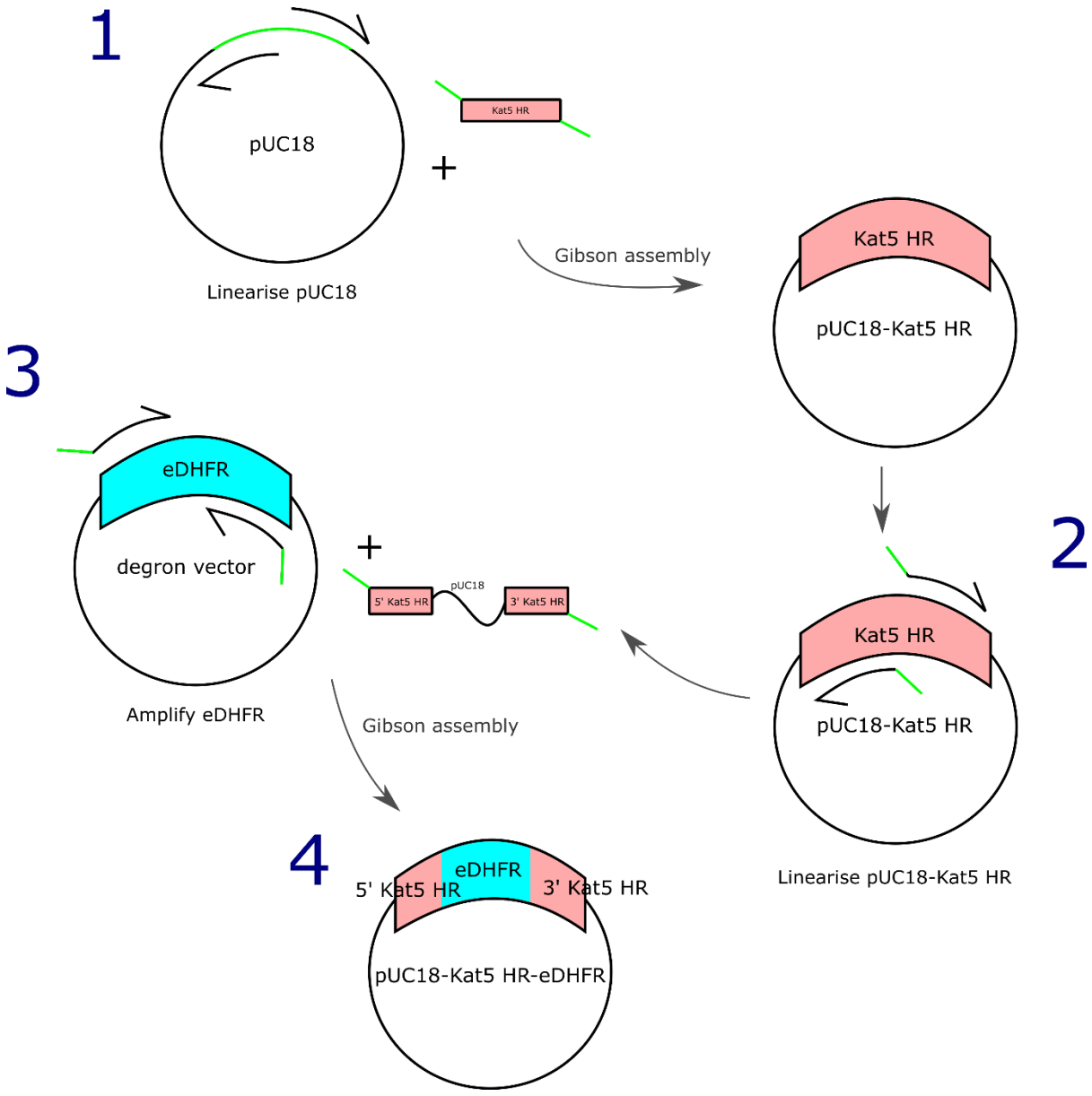

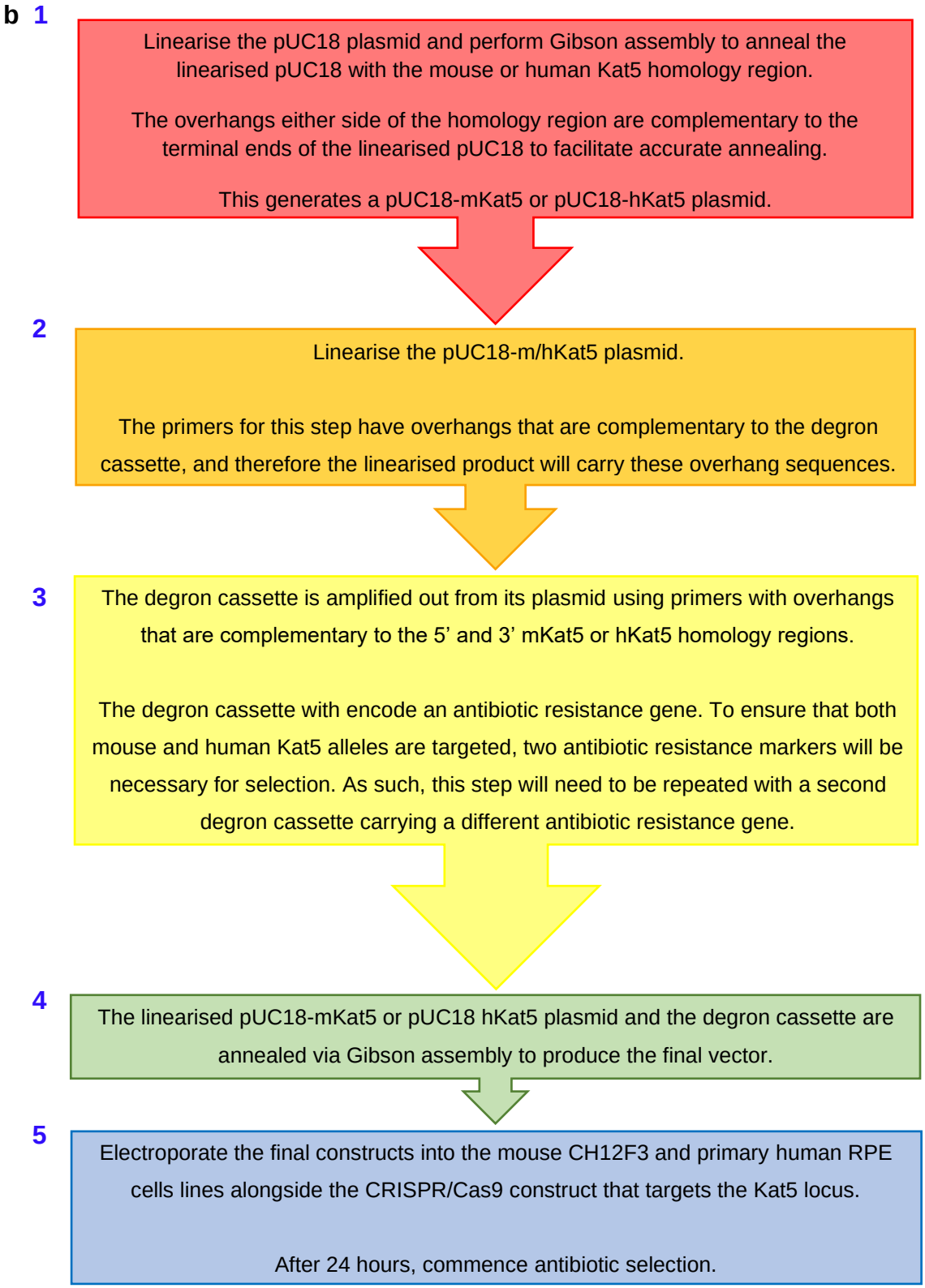

Figure 1 | Illustrations of the steps involved in cloning the pUC-18 m/hKat5 degron constructs
a, An overview of the steps required to synthesise the Kat5 degron plasmid. **b,** Flow chart depicting the sequential process that leads to the synthesis of the pUC18-m/hKat5-degron constructs. The numbered boxes match the numbered steps in (a).

6.6 Results

6.7 CRISPR/Cas9 Kat5-targeted knockout

In the gel below (Fig. 1) A and L are positive control sequences that are provided by the Surveyor assay. They are fully complementary except for a single nucleotide mismatch. Incubation of A alone with the celery juice enzyme does not form mismatches (Lane A). However, mixing A and L forms heteroduplexes that are recognised by the enzyme, resulting in 3 bands (Lane A/L), each a product of 1) homoduplex formation and 2) the two products that come from cleaving the mismatch following heteroduplex formation. It is clear from the single bands observed in Lanes 4–7 that either Kat5 has not been successfully targeted and cleaved by Cas9, or that those cells that have been targeted and cleaved by Cas9 are not viable. Irrespective, Kat5 is not a suitable target for Cas9.

FIGURE 2

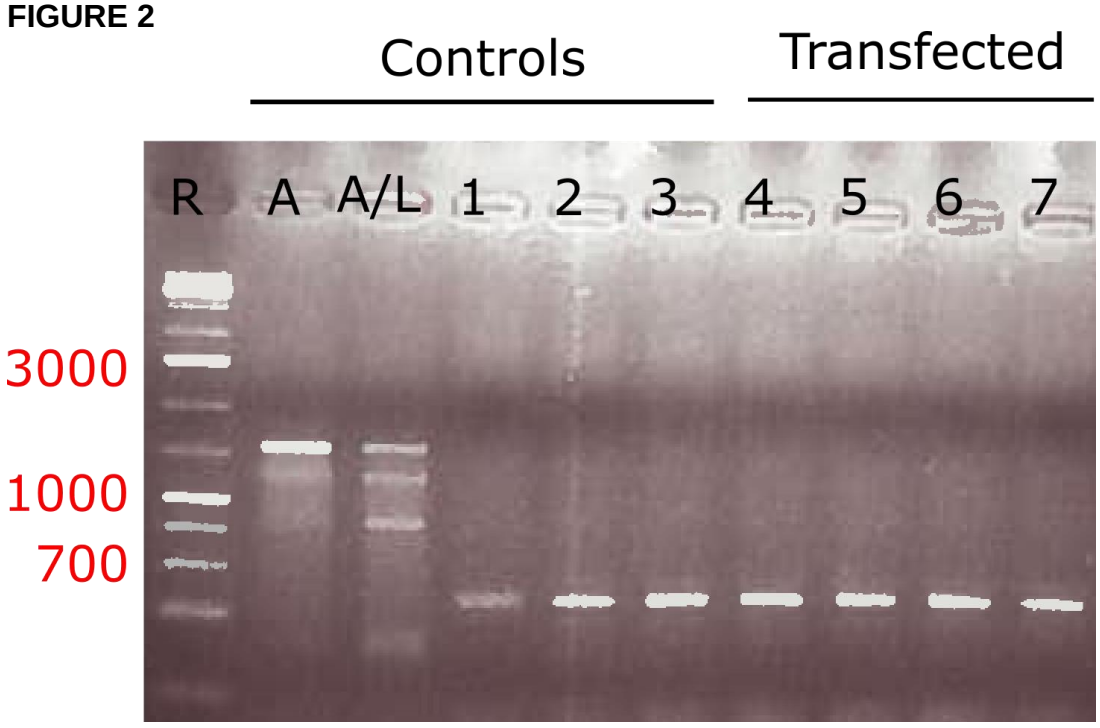

Figure 2 | Gel of the Kat5-gRNA targeted CRISPR/Cas9

R, is the GeneRuler, **A** and **A/L,** Negative and positive combinations of control sequences showing efficacy of the celery juice nuclease. **1, 2** and **3,** Genomic DNA extracted from untransfected 3T3 cells at 0, 48 and 92 hours. **4** and **5,** Genomic DNA extracted and mixed from untransfected and CRISPR/Cas9 transfected 3T3 cells at 48 and 96 hours. **6** and **7,** Genomic DNA extracted from CRISPR/Cas9 transfected 3T3 cells at 48 and 96 hours. Kat5 PCR amplification product is 600 bp. DNA stained with midori green.

6.8 Linearisation of the pUC18 plasmid

The first step in the design of the inducible degron system is to linearise the pUC18 plasmid. This will incorporate the Kat5 homology regions and the 3xHA-eDHFR-P2A-puroR/blastR-SV40 cassette in a sequential manner.

FIGURE 3

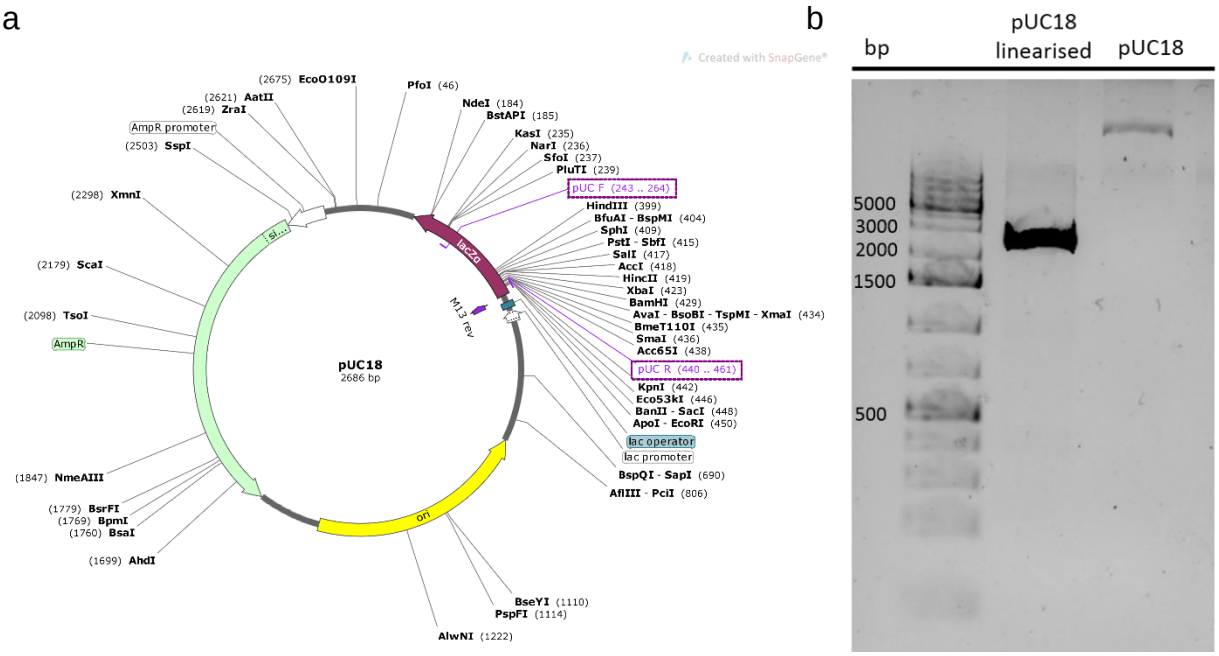

Figure 3 | Gel to show the successful linearisation of the pUC18 plasmid

a, Vector map of pUC18. The size of the plasmid is 2686 bp, and the linearization primers have been highlighted. **b,** The size of the band in the gel corresponds to the size of the pUC18 plasmid, showing successful linearization. DNA stained with midori green.

6.9 Isolation of pUC18-mKat5 HR and pUC18-hKat5 HR constructs

The linearised pUC18 and the mKat5 and hKat5 homology regions are cloned together using Gibson assembly. The products were transformed into DH5α *E. coli.* Colony PCR was performed on individual colonies, and the products were screened with linearising primers from within the mKat5 or hKat5 homology regions.

FIGURE 4

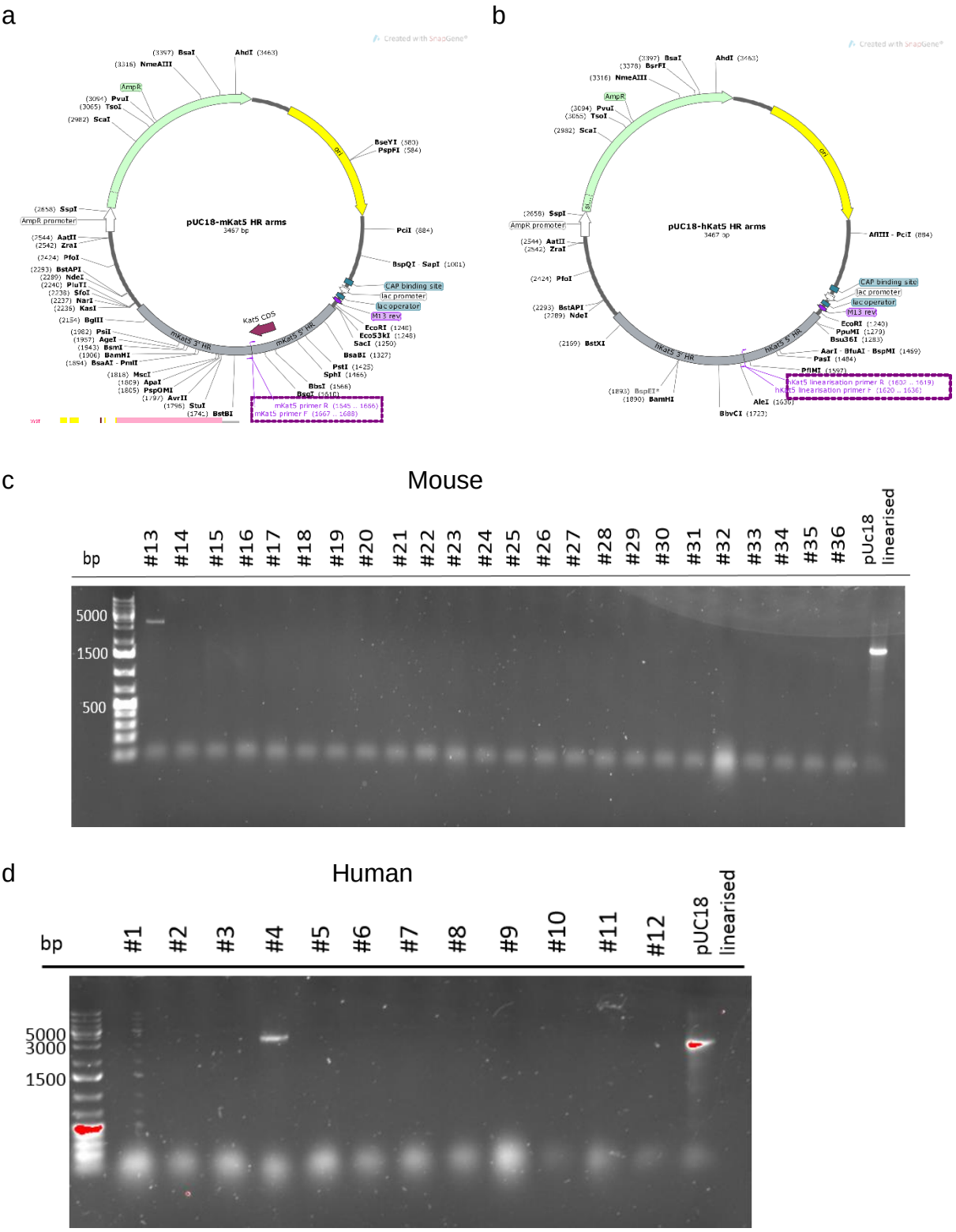

Figure 4 | Screening of the mouse and human pUC18-Kat5 HR

a and **b,** Plasmid vector maps denoting the pUC18-mKat5/hKat5 HR. The forward and reverse linearization screening primers have been highlighted. **c** and **d,** Gels show the successful incorporation of the mKat5 and hKat5 homology regions in Lanes 13 and 4, respectively. DNA stained with midori green.

6.10 Confirmation of the puC18-mKat5/hKat5 HR plasmids

To confirm the results on the gel (Fig. 4), the selected colonies were cultured and run again on a gel using the linearization primers as screening primers.

FIGURE 5

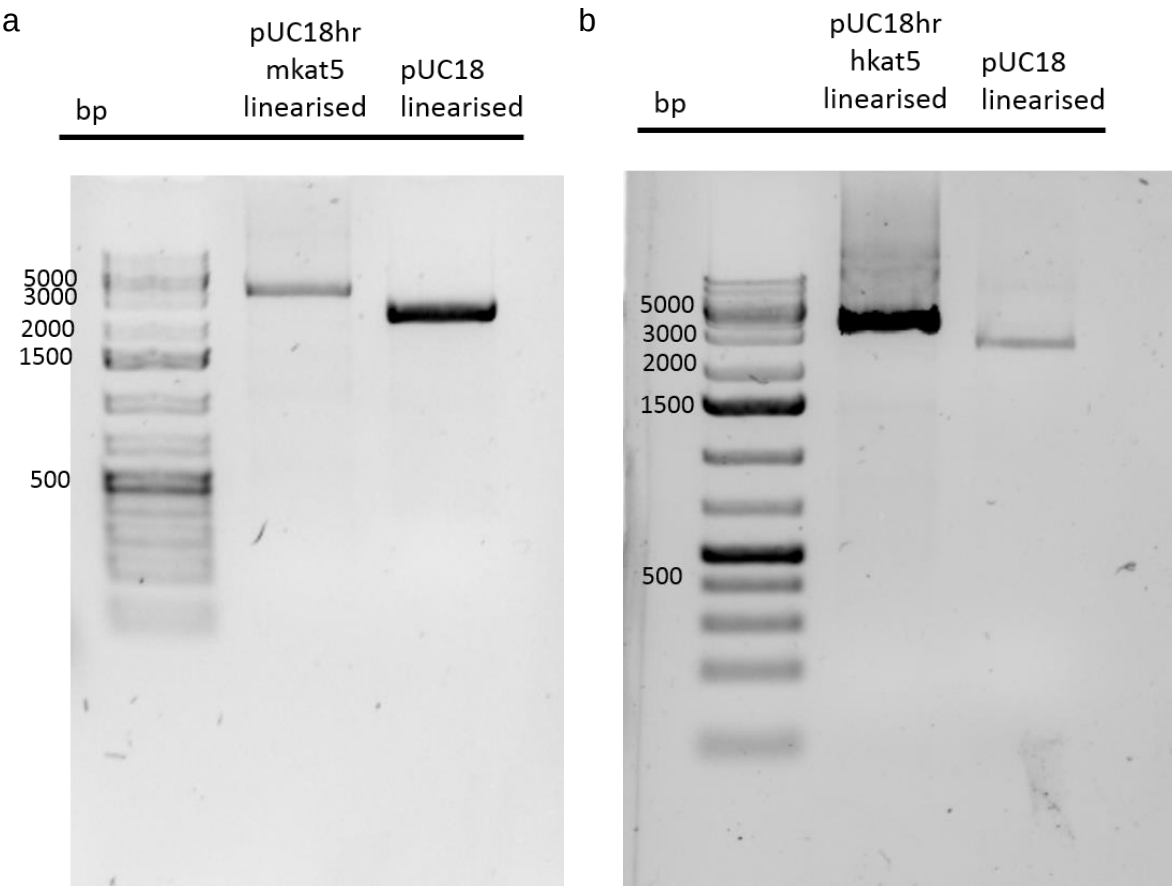

Figure 5 | Screening of the pUC18-mKat5/hKat5 HR plasmids

a and **b,** Clones 13 and 4 from Fig. 4 were cultured and re-run on the gel to confirm their integration into the pUC18 vector. DNA stained with midori green.

6.11 Amplification of the degron cassette

Next, the degron cassette, comprised of the 3xHA-eDHFR-P2A-puroR/blastR-SV40 sequences, was amplified using primers carrying overhangs that are complementary to the mouse or human Kat5 homology regions.

Figure 6

a

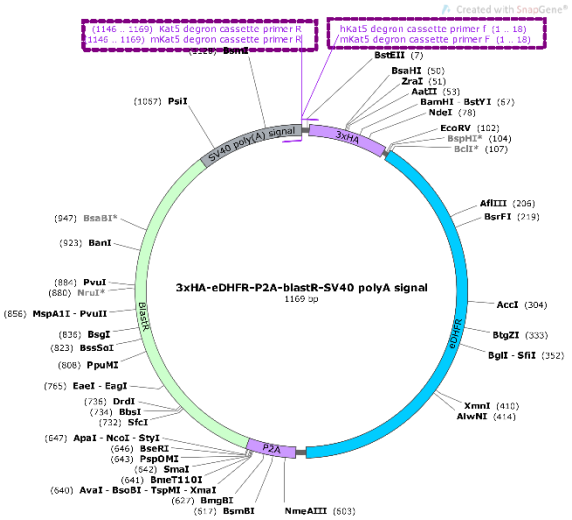

b

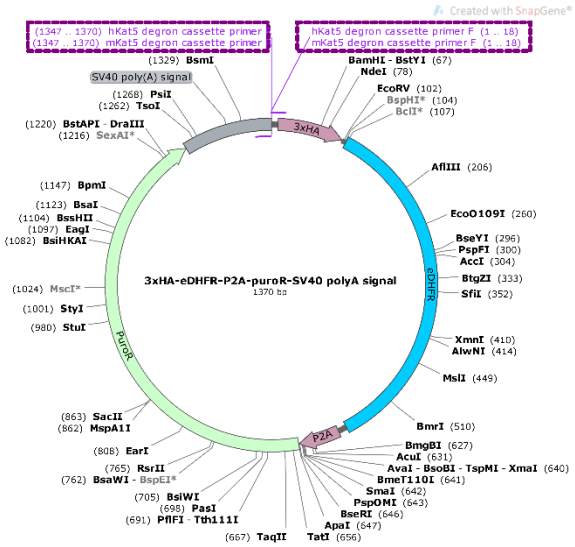

c

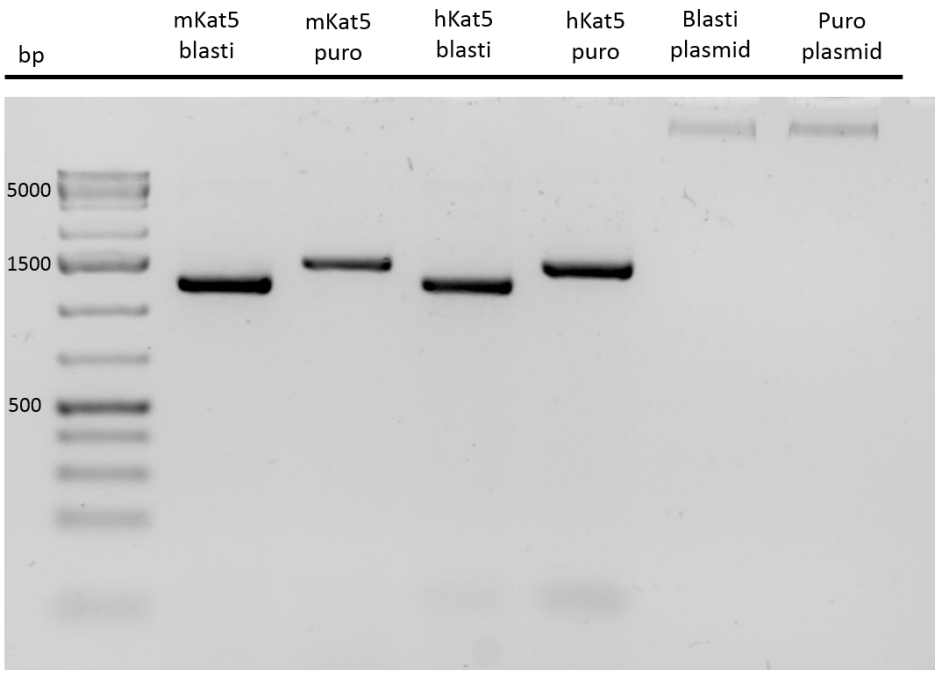

Figure 6 | Amplification of the degron cassette

a and **b,** Plasmid maps of the degron cassette carrying blasticidin (a) and puromycin (b) antibiotic resistance genes. **c,** Gel to show the successful amplification of the degron using amplification primers containing overhangs that are complementary to the mKat5/hKat5 homology regions within the pUC18-mKat5/hKat5 HR constructs. Gels stained with midori green.

6.12 Planned pUC18-mKat5/hKat5-3xHA-eDHFR-P2A-puroR/blastR-SV40 constructs

The next stage in this process will be to use Gibson assembly to anneal the degron cassette into the linearised pUC18-mKat5 HR and pUC18-hKat5 HR plasmids.

FIGURE 7

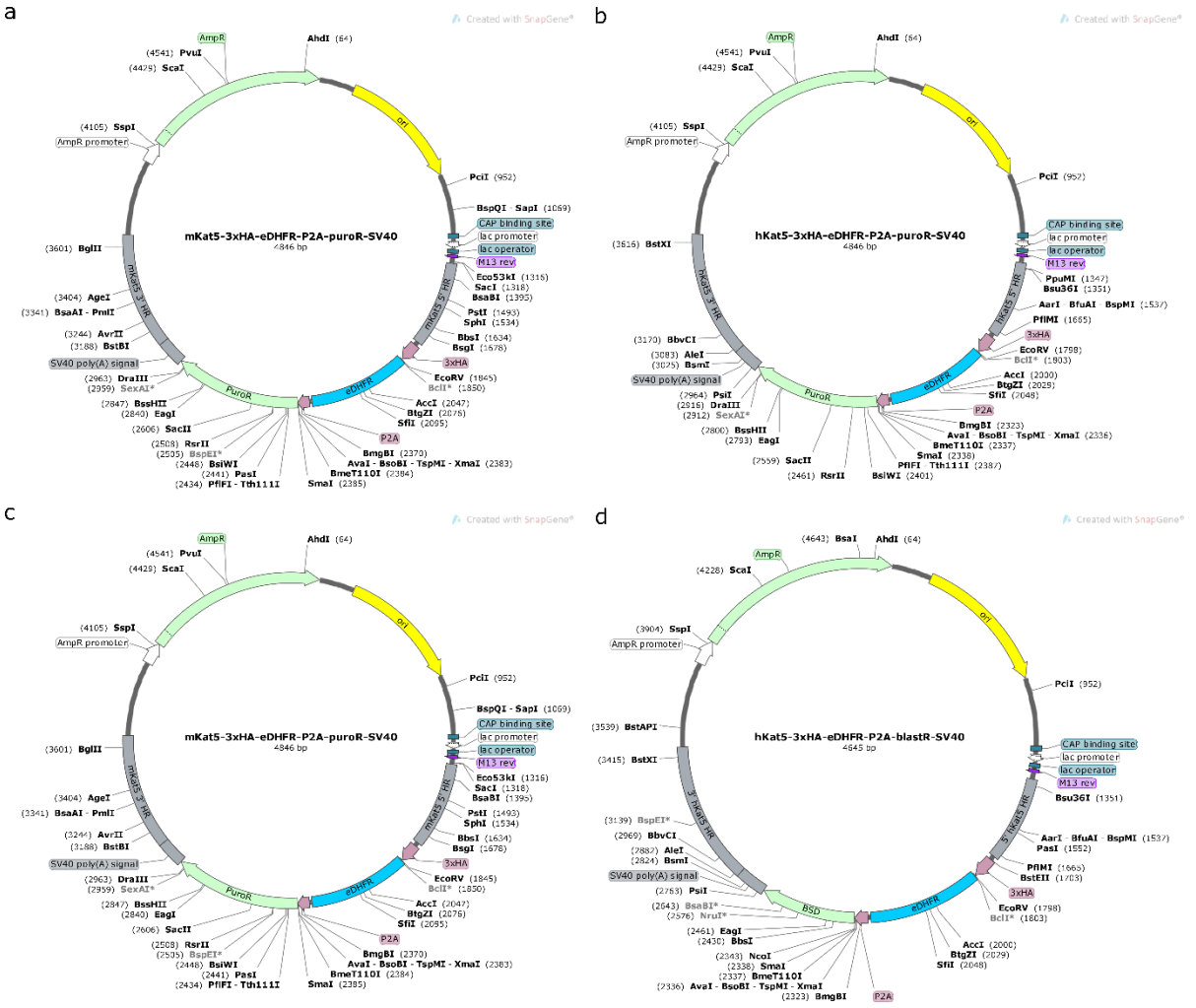

Figure 7 | Plasmid maps of the final mouse and human Kat5 degron constructs

a–d, Plasmid maps of the final Kat5 degron in both mouse and human, carrying either puroR or blastR.

6.13 Construction of mouse and human CRISPR-Cas9 targeting plasmid: pX330-mKat5/hKat5

The pX330 plasmids containing mKat5 and hKat5-targeted gRNAs will also need to be prepared. The purpose of the CRISPR/Cas9 system is to introduce a DSB break near the stop codon of genomic Kat5. The corresponding complementary Kat5 sequences in the pUC18 degron cassettes will provide a template for homologous recombination, and integration of the degron into the genome.

FIGURE 8

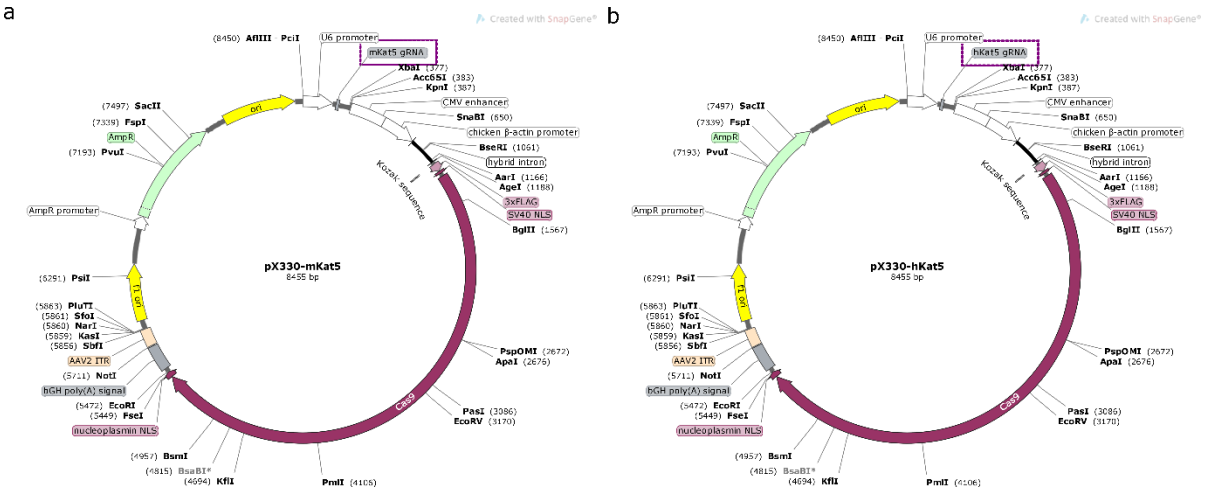

Figure 8 | Plasmid map of the pX330 vector encoding the mouse gRNA sequences

a and **b,** pX330 vector encoding the mouse (a) and human (b) gRNA sequences.

6.14 The final intracellular Kat5-degron product

Once the mouse CH12F3 B cells and primary human RPE cells have been successfully transfected and selected, the intention is for one Kat5 allele to integrate the degron cassette containing the puromycin resistance gene, and the other to integrate the blasticidin resistance gene, which ensures that both Kat5 proteins will be tagged with the degron.

FIGURE 9

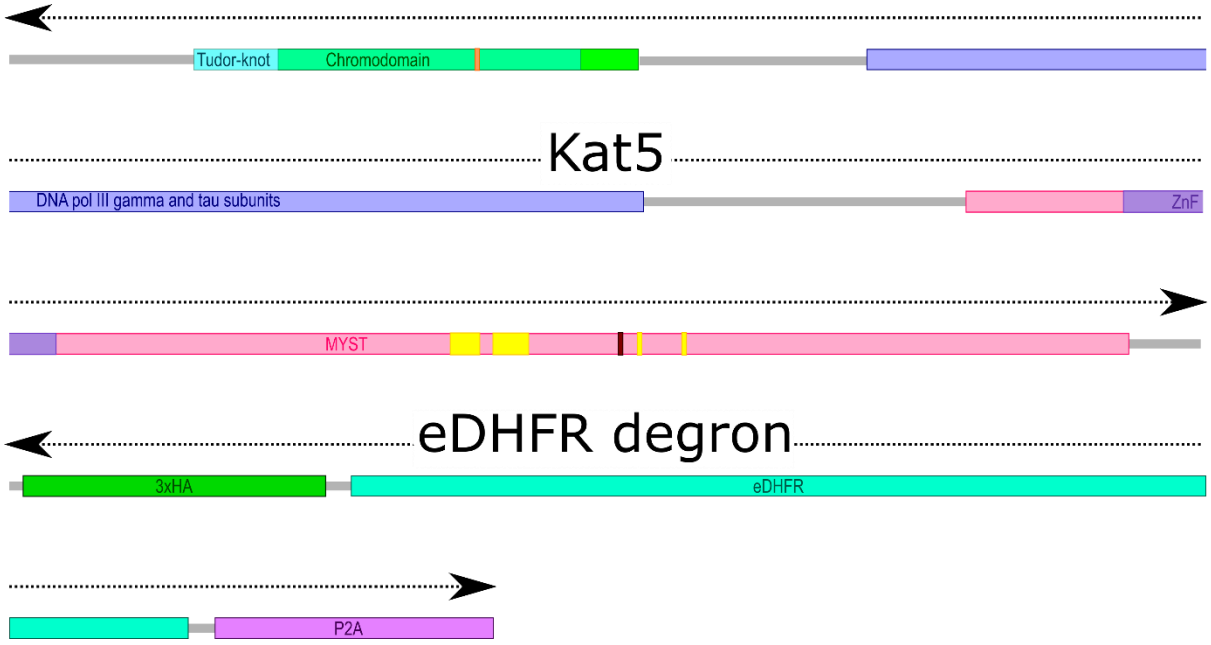

Figure 9 | Full length Kat5-degron protein construct

Once integrated into the genome, the translated protein construct composed of the Kat5, 3xHA, eDHFR degron and P2A self-cleaving peptide will total 731 amino acids, 513 belonging to Kat5, and 218 from the entire degron.

6.15 Discussion

Kat5 is essential for cellular viability, which has made it challenging to generate a Kat5 knockout cell line using CRISPR/Cas9 technology. Furthermore, it cannot be easily visualised as antibodies raised against it typically have very low affinity. As such, siRNA or shRNA-depletion of Kat5 would be difficult to study without being able to confirm the knockdown. As such, the degron system appears to offer an option that would save the cell line from perishing due to the reversible nature of the system (514,515), and the presence of an HA tag would make the Kat5 visible for Western blot, immunofluorescent staining for confocal, and possibly immunofluorescent staining for flow cytometry (516–519).

Good progress has been made so far in developing the pUC18 and pX330 constructs necessary for this degron system to be electroporated into the mouse CH12F3 and human RPE cell lines. However, there are a few concerns about this system as the degron is a bulky, not insignificant, addition to tag next to Kat5. Indeed, the degron itself is large protein made up of 218 amino acids, which is not much shorter than the 513 amino acid Kat5. Kat5 participates in DNA repair and transcription, and in doing so it has numerous interaction partners (16–18). Disrupting its ability to forge these interactions could have subtle and widespread implications on the cell (19–23,492), and therefore it is essential that the cell lines generated are validated such that any data obtained that suggests a role for Kat5 in CSR is reliable. Any successful transfections of CH12F3 and primary human RPE cell lines will need careful consolidation. A survival assay will be essential. As Kat5 is required for cellular survival, any disruption in its ability to function should have noticeable consequences, and its proliferation rate and survival rates would be expected to decrease. Additionally, Kat5 is involved in transcription activation, and therefore rt-qPCR to ascertain mRNA levels of its target proteins will help to validate the inducible degron technique (527). The effect of heterozygous incorporation of the eDHFR degron has been considered, and the presence of the degron on just one copy of Kat5 may offer a more subtle phenotype that could be studied without the risk of cell death, however heterozygous knockouts of Kat5 in mice have been reported to exhibit only minor defects in DDR signalling in a sensitised, pre-tumoural background (476). As such, it is possible that the activity of just one copy of Kat5 is enough to compensate for the loss of the other Kat5 protein. Yet again, the partial redundancy in that system could

be attributed to compensation of chronic haplo-insufficiency. We hope our DHFR system will provide an acute haplo-insufficiency which a cell may not have enough time to adapt to in the short span of time during our experiment; ideally between one and twelve hours.

In the event that this system is found to be suitable it is hoped that, in combination with the Kat5 inhibitors, it should provide an additional element to understand Kat5's role in both DNA repair and immune diversity. The iChromo and TH1834 inhibitors affect Kat5's catalytic activities but have no effect on the structure of the protein (207). As such, if Kat5 possesses a structural role in the support of CSR, as in the case for DNA uracil glycosylase, then the total loss of Kat5 offer a more holistic, all-encompassing view of its involvement in class switching. This would then also allow for the of compensation of the inducible deletion cells with point mutant Kat5 plasmids that could mimic and extrapolate further the data obtained from the chemical separation-of-function of Kat5 in genomic maintenance and immune diversity.

7 Discussion and future work

7.1 Overall conclusion

The research presented in this thesis has achieved the overall aim of the project by furthering our understanding of the mechanisms involved in the DNA damage response. Moreover, the specific research objectives have been completed by 1) developing a fluorescence-based assay that can study a wealth of proteins that affect the structural integrity of DNA, and 2) by investigating the Kat5 pathway in both canonical and non-canonical DNA repair using a combination of chemical inhibitors, and with genetic methods on the horizon. Much of the work within has contributed to published articles or is currently in submission.

7.2 Design and improvement of the PicoGreen-based nuclease toolkit

The development of a fluorescence-based toolkit has established itself as a safe, robust, rapid and highly sensitive technique for studying nucleases and polymerases. It has the capacity to capture reaction kinetics, and the flexibility to expand the DNA substrate library and physiologically relevant modifications to include more complex structures, including Y-structures, Holliday junctions, hydroxymethylated DNA, methylated DNA and hemimethylated dsDNA for characterisation of a wider variety enzymes.

PG had previously been used in discontinuous assays measuring the fluorescence read-out from dsDNA. Stabilising the dye with glycerol proved to maintain the fluorescent signal and slow the effect of photobleaching, allowing for it to be used for monitoring nuclease activity in real-time. This, in combination with sequence optimisation of the DNA substrates, produces a suitably strong fluorescent signal that accurately captures dsDNA nuclease activities, allowing for sensitive analysis of reaction kinetics and substrate preferences.

As evidenced, this fluorescence-based assay has much potential. The activities of dsDNA nucleases, ssDNA nucleases, nickases and polymerases can all be investigated using this system and, theoretically, should encompass all DNA denaturing enzymes, such as helicases or splicing proteins (253–255), as well as DNA

polymerising enzymes, including translesion polymerases. It is fortunate that, while hydrolysis of the phosphodiester bonds in DNA requires different divalent metal ions, none of the nuclease activity studied here was altered in the presence of PG (528). Indeed, any enzyme that impacts the structural integrity of DNA should be a suitable candidate for study using this method. In addition to the technological novelty of this new toolkit, it is expected to also offer new mechanistic and kinetic insights into DNA metabolizing enzymes in real time. This could generate a step change in the understanding of enzyme reaction speeds, transition states, subtle substrate preferences, and co-factor preferences and interferences.

7.3 Incorporating an RNA dye could further generate a universal nuclease assay

Several RNA dyes are available that could be used to characterise RNA nucleases (454,529–531). Confirming their utility with well-characterised enzymes, such as RNase A (532), would be essential but then have the potential to identify and study a wealth of RNA nucleases (452,453,455,456). RNA nucleases are particularly interesting as they are often associated with providing antimicrobial and antiviral immunity in viruses, bacteria and eukaryotes (452,533–540), in some cases, cancer (538,541–543). Ultimately, staining RNA delivers the opportunity to stain RNA/DNA hybrid structures and their degradation by RNA and DNA nucleases, such as RNase H and DNase I (452,544).

7.4 Nucleases in immunity and tumourigenesis

The ability to study both DNA and RNA nucleases is vital. Mutations in nucleases that impact either catalytic properties or interaction capabilities can have devastating effects on immune function and tumourigenesis. CTIP nuclease has been associated with Jawad and Seckel Syndromes (444), Exo1 is mutated in some cancer patients (445–447), a loss of function mutation in the human Trex1 gene causes the autoimmune disorder Aicardi-Goutières syndrome (545), and mutations in human WRN cause the autoimmune progeria disorder Werner Syndrome. Understanding the nature of the mutations affecting nuclease or helicase activities, protein interactions and/or protein stability will provide an accurate assessment of how these autoimmune syndromes have developed. Furthermore, meta-analyses have identified key polymorphisms in human RNase L that are associated with increased prostate cancer risk (546,547), and that RNase L antiviral activity targets Hepatitis C virus, West Nile

Virus and HIV (548). Its role in innate immunity can be modulated, and it therefore represents a possible target for therapeutic intervention (548).

With so many RNA and DNA nucleases as targets, the fluorescence-based assay can be utilised to study potential inhibitors or modulators of nuclease activity. Actin is a naturally occurring inhibitor of DNase I, and its inhibitory effects have been studied using a discontinuous fluorescence-based method (406).

7.5 Characterisation of nucleases and polymerases involved in SHM and CSR with the fluorescence-based nuclease toolkit

DNA repair is integral for the successful secondary antibody diversification processes of SHM and CSR. In canonical DDR, mechanisms are in place to ensure the delayed recruitment of error-prone translesion polymerases so as to promote error-free DNA replication at the break site (549). Due to a second mechanism dependent on the monoubiquitination of PCNA at Lys164, translesion polymerases, such as θ, η and ζ, are recruited to the V region during SHM to introduce a swathe of A and T mutations to enhance immune diversity (78,550). It would be worthwhile to compare the activities of all error-prone and error-free nucleases, and potential regulatory binding partners, to elucidate whether their kinetics of polymerisation represent another form of regulatory control.

As for CSR, although the DNA substrates used in the assay were optimised to reduce secondary structure formation and improve fluorescence, the assay is not restricted to relying on these sequences. Alternative substrates could be synthesised to mimic the G-rich S regions for analysis of nucleases involved in CSR. Moreover, R loops, G4-DNA and -RNA quadruplex structures are critical for efficient CSR (64,551,552). Processing G4 RNA structures, which target AID to transcribed S regions, presumably requires 5’ and 3’ RNA nucleases which have yet to be either isolated or characterised (144). The assay would be an excellent candidate for such genome wide high throughput screens. Possibly integrating it into microfluidics chips that combines protein expression droplets with fluorescent spectroscopy readouts in a high throughput manner.

7.6 Kat5 has a fundamental role in CSR

Histone “writers” play a crucial role in building the “histone code” which is essential in propagating adequate cell function. Evidence herein shows that Kat5, a histone acetylation “writer” has an important role in the DNA damage response in general and in immune diversification (CSR) in particular. Clearly, optimisation is required to quantify the extent to which Kat5 supports or downregulates CSR; nevertheless, inhibition of Kat5 distinctly alters CSR efficiency. Both inhibitors, iChromo (Kaidi A, unpublished) and TH1834 (207), target Kat5 and impede its activities in subtly different ways. iChromo prevents Kat5 propagating H2AX phosphorylation though the acetylation and activation of ATM (44,46,47,469,470). This prevents the subsequent phosphorylation of H2AX and recruitment of downstream repair proteins. TH1834 mimics Kat5’s natural ligand, Acetyl-CoA, functioning as a competitive inhibitor to prevent Kat5 acetylating either ATM or histone H4 (207), thereby reducing H2AX phosphorylation and histone H4 acetylation, and impacting both DNA repair and transcription. As such, the combination of these two inhibitors should help to determine the extent to which each function participates in CSR. Further studies using primary mouse B cells would consolidate the observed results.

It is exciting that another collaborator has developed another inhibitor of Kat5 that distorts Kat5’s tertiary structure but permits its catalytic activities. As Kat5 exists in a large protein complex, it would be intriguing to discover how much its function as a scaffold helps to drive CSR compared to its catalytic activities. This would offer a third separation-of-function element to develop a thorough understanding of the role Kat5 plays. Indeed, other proteins present in CSR are present as scaffolding proteins, rather than for their roles in catalysis, as is expected during canonical DNA repair. The uracil DNA glycosylase (UNG) typically contributes in base excision repair to remove misincorporated uracil in the DNA, which produces U:A mismatches (553), and UNG-deficient mice present with drastically reduced CSR. However, its primary purpose in CSR may instead be to function as a non-canonical scaffold that recruits essential repair proteins for S region recombination (554). The nuclease function of Exo1 is similarly dispensable for CSR, yet Exo1-null mice exhibit defective CSR, suggesting a non-canonical structural role (124).

On the basis that the Kat5 inducible degron constructs for mouse and human cell lines are a success, it will be possible to selectively knockdown Kat5 for studies of CSR efficiency (208). Combined with the chemical inhibitors, it will offer yet another level of detail that combines both the loss of Kat5 catalysis and its structural features. If this system works, following successful transfection and selection of a stable cell line, this could be a very powerful tool for studying Kat5 and other essential proteins. These human and mouse constructs could be introduced to any human or mouse cell line, and perhaps could be combined with degrons or inhibitors that target other proteins to build up a more complex system of protein depletion. If this system is deemed unreliable, and the presence of the degron impedes Kat5 binding to its partners, then a more straightforward method of HA- or FLAG-tagging Kat5 may be an option. This will enable visualisation of Kat5 during siRNA knockdown as antibodies recognise HA and FAG with very high affinity (516–519). While siRNA knockdown is a valuable and effective technique, there are a number of disadvantages including, but not limited to, the risk of off-target effects (555); furthermore, protein depletion *via* siRNA is indirect and depends on the stability of the target protein itself (556), and allows for upregulation of redundant pathways to counteract reduction in the levels of the target protein (555). In comparison, the eDHFR degron causes protein knockdown within a matter of a few hours as opposed to days. Neither system produces a total knockout, but a knockdown, which in the case of Kat5 may be more beneficial pending the low levels of Kat5 may be enough for cell survival (514).

7.7 The role of Kat5 in SHM

As in the case of CSR, a role for Kat5 in SHM has not yet been established. SHM can be monitored in Ramos human B cells which constitutively undergo SHM. Using FACS, it will be possible to measure the rate of loss of fluorescence released from an mCherry reporter protein inserted within the V region through the somatic mutation of its DNA sequence.

FIGURE 1

Figure 1 | Ramos cell line with mCherry reporter.

Diagram shows the structure of the Ig V region with the mCherry reporter inserted into the V region of the Ramos cell line.

Whilst a study into Kat5 and its involvement in SHM was not possible due to time constraints, treating Ramos cells with the inhibitors available should indicate whether Kat5 has a function in SHM, and whether this influence contributes to immune diversity. Interestingly, a role for Kat5 in inducing synthesis of free DNA nucleotides (dNTPs) necessary for DNA repair has been proposed (557). dNTP synthesis is increased in S phase to meet the demands of DNA replication. Occasionally, dNTP levels are insufficient for repair outside of S phase. The enzyme ribonucleotide reductase (RNR) controls the rate-limiting step in dNTP synthesis (558). Transcription of many RNR subunits is highly inducible in response to DNA damage and replication stress in eukaryotes (559). Mutations that reduce yeast RNR activity, or fail to induce it, exhibit increased sensitivity to DNA damage. In response to DNA damage, RNR is acetylated by Kat5, and is localised to damaged sites in a Kat5-dependent manner (560). It is suggested that this produces high local concentrations of dNTPs at the damage site, and therefore may provide high local concentrations of dNTPs required for optimal function of error-prone translesion polymerases (558). As translesion polymerases contribute towards the accumulation of mutations along the V region, Kat5 may therefore support SHM. DNA repair factors involved in immune diversification fall under four categories: the ones not affecting either SHM or CSR (not relevant in this discussion), the ones affecting both SHM and CSR, and the one that affect either SHM or CSR. It would be extremely interesting to see in which of the three categories Kat5 falls under.

7.8 Concluding statement

There were two main aims for this thesis; 1) to develop a fluorescence-based toolkit that has the potential to study dsDNA nucleases in real-time, and to deliver highly sensitive kinetic analyses, and 2) to establish a role for Kat5 in CSR.

Having validated the method for well-characterised nucleases, the nuclease assay also incorporated studies of ssDNA nucleases, nickases, and polymerases. It is hoped that this method will act as a valuable alternative to conventional methods. It should be capable of characterising all enzymes that affect the integrity of DNA, and it would be interesting to study point-mutants that have been linked to autoimmune disorders and cancer.

As for determining the role of Kat5 in CSR, the results suggest that Kat5 does have an important function for efficient CSR, yet the specific details remain elusive. Nevertheless, these studies have contributed another piece of the histone code that orchestrates secondary antibody diversification. Further study should determine whether Kat5's DNA repair, transcription, or scaffolding function is most influential for CSR.

Appendix

Analysis of nuclease rates

Part 1: Converting fluorescence units to length of duplex DNA

Raw data from a DNase I-mediated digestion of 80-bp dsDNA:

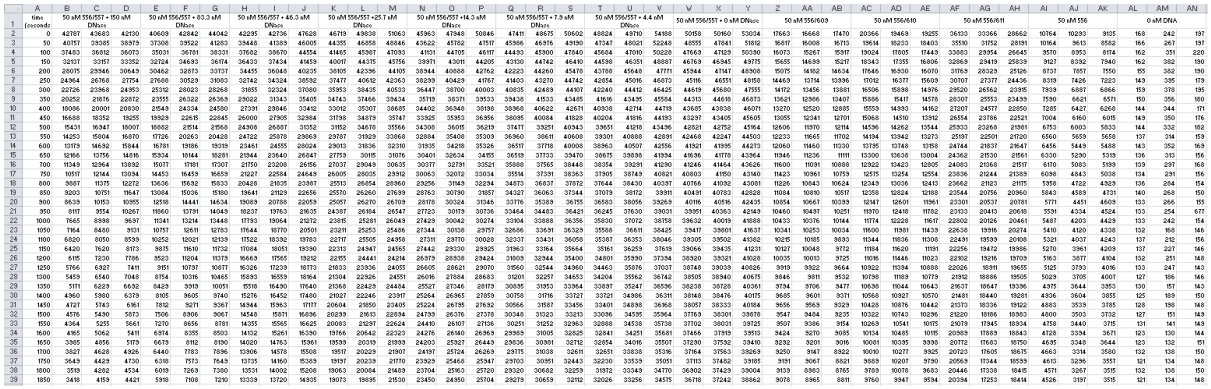

First the raw data was converted from the standard curve to a measurement of length of duplex DNA. To do this, the average fluorescence for each data set was calculated, and each column was labelled with the length of dsDNA they each represent. The standard curve was produced from the following oligonucleotides:

80 bp = S (556/557)

60 bp = S_{60} (556/611)

40 bp = S_{40} (556/610)

20 bp = S_{20} (556/609)

The latter assays which incorporated substrate variants were normalised as a percentage to their controls (no enzyme) before the standard curve was generated.

	A	B	C	D	E	F	G	H	I	J	K	L	M	N	O	P	Q	R	S	T	U	V	W
42	time (seconds)	50 nM 556/557 + 0 nM DNase			50 nM 556/609 + 0 nM DNase			50 nM 556/610 + 0 nM Dnase			50 nM 556/611 + 0 nM Dnase			0 nM DNA				time (seconds)	80	60	40	20	0
43	0	50158	50160	53034	17663	16668	17470	20366	19469	19255	36133	33366	28662	168	242	197		0	51117.3	32720.3	19696.7	17267	202.333
44	50	48555	47841	51812	16817	16008	16713	19614	18233	18403	35510	31752	28191	166	267	197		50	49402.7	31817.7	18750	16512.7	210
45	100	47669	47129	50390	16073	15267	15917	19024	17805	17449	33883	29954	26645	162	351	220		100	48396	30160.7	18092.7	15752.3	244.333
46	150	46769	46945	49775	15655	14699	15217	18343	17355	16806	32869	29419	25839	162	382	190		150	47829.7	29375.7	17501.3	15190.3	244.667
47	200	45944	47147	48908	15075	14182	14634	17646	16930	16070	31769	28329	25126	155	382	190		200	47333	28408	16882	14630.3	242.333
48	250	45116	46551	48158	14469	13714	13996	17012	16377	15609	30707	27377	24436	149	395	179		250	46608.3	27506.7	16332.7	14059.7	241
49	300	44619	45680	47555	14172	13456	13881	16506	15898	14976	29520	26562	23915	159	378	195		300	45951.3	26665.7	15793.3	13836.3	244
50	350	44313	44618	46873	13621	12986	13407	15886	15417	14578	28307	25553	23499	150	356	180		350	45268	25786.3	15293.7	13338	228.667
51	400	43685	43838	46071	13270	12520	12885	15559	14993	14162	27207	24577	22850	144	344	171		400	44531.3	24878	14904.7	12891.7	219.667
52	450	43297	43405	45605	13055	12341	12701	15068	14510	13912	26554	23786	22521	149	350	176		450	44102.3	24287	14496.7	12699	225
53	500	42821	42752	45164	12606	11970	12114	14596	14262	13544	25933	23268	21981	144	332	182		500	43579	23727.3	14134	12230	219.333
54	550	42468	42247	44503	12233	11665	11702	14194	13942	13273	25197	22501	21720	137	314	159		550	43072.7	23139.3	13803	11866.7	203.333
55	600	41921	41995	44273	12060	11460	11330	13795	13748	13158	24744	21837	21647	143	352	169		600	42729.7	22742.7	13567	11616.7	221.333
56	650	41696	41778	43964	11946	11236	11111	13300	13638	13004	24362	21530	21561	136	313	156		650	42479.3	22484.3	13314	11431	201.667
57	700	41246	41464	43626	11600	11091	10888	12922	13423	12805	24083	21368	21517	139	297	168		700	42112	22322.7	13050	11193	201.333
58	750	40803	41150	43140	11423	10961	10759	12575	13254	12554	23836	21244	21389	134	291	156		750	41697.7	22156.3	12794.3	11047.7	193.667
59	800	40766	41092	43081	11226	10843	10624	12349	13036	12413	23662	21123	21175	136	284	154		800	41646.3	21986.7	12599.3	10897.7	191.333
60	850	40491	40783	42828	11084	10810	10517	12358	12824	12188	23544	20756	20960	140	268	150		850	41367.3	21753.3	12456.7	10803.7	186
61	900	40116	40516	42435	10854	10667	10399	12147	12601	11961	23301	20537	20781	133	266	155		900	41022.3	21539.7	12236.3	10640	184.667
62	950	39951	40363	42149	10460	10497	10251	11970	12418	11782	23133	20413	20618	133	254	677		950	40821	21388	12056.7	10402.7	354.667
63	1000	39632	40019	41888	10433	10376	10144	11774	12228	11617	22802	20126	20461	133	242	154		1000	40513	21129.7	11873	10317.7	176.333
64	1050	39417	39801	41637	10341	10253	10034	11600	11981	11439	22638	19916	20274	132	168	146		1050	40285	20942.7	11673.3	10209.3	148.667
65	1100	39305	39502	41382	10215	10185	9893	11344	11836	11308	22491	19599	20108	137	212	156		1100	40063	20732.7	11496	10097.7	168.333
66	1150	39066	39435	41231	10127	10048	9772	11184	11620	11191	22256	19472	19986	137	227	146		1150	39910.7	20571.3	11351.7	9982.33	170
67	1200	38920	39321	41028	10035	10013	9725	11016	11446	11023	22102	19216	19709	132	251	148		1200	39756.3	20342.3	11161.7	9924.33	177

Next, we used these averaged values to determine the equation of the line, as indicated in Fig. 1c in the main text. We had to find the values for the gradient (m) and intercept (c) in the linear equation y = mx + c.

Equation to calculate the gradient (m): “=SLOPE(known_y’s, $known_x’s)”

E.g., the first equation at 0 seconds is: “=SLOPE(S43:W43,S$42:W$42)”

The “$” locks the known_x’s values, as these values remain constant in all iterations of this equation.

Equation to calculate the intercept (c): “=INTERCEPT(known_y’s, $known_x’s)”

E.g., the first equation at 0 seconds is: “=INTERCEPT(S43:W43,S$42:W$42)”

R	S	T	U	V	W	X	Y	Z
time (seconds)	80	60	40	20	0		slope (m)	intercept (c)
0	51117.3	32720.3	19696.7	17267	202.333		586.417	744.067
50	49402.7	31817.7	18750	16512.7	210		568.452	600.533
100	48396	30160.7	18092.7	15752.3	244.333		553.558	386.867
150	47829.7	29375.7	17501.3	15190.3	244.667		546.777	157.267
200	47333	28408	16882	14630.3	242.333		539.795	-92.6667
250	46608.3	27506.7	16332.7	14059.7	241		530.908	-286.667
300	45951.3	26665.7	15793.3	13836.3	244		521.22	-350.667
350	45268	25786.3	15293.7	13338	228.667		512.635	-522.467
400	44531.3	24878	14904.7	12891.7	219.667		503.048	-636.867
450	44102.3	24287	14496.7	12699	225		496.713	-706.533
500	43579	23727.3	14134	12230	219.333		491.083	-865.4
550	43072.7	23139.3	13803	11866.7	203.333		485.057	-985.267
600	42729.7	22742.7	13567	11616.7	221.333		480.713	-1053.07
650	42479.3	22484.3	13314	11431	201.667		478.043	-1139.67
700	42112	22322.7	13050	11193	201.333		474.755	-1214.4
750	41697.7	22156.3	12794.3	11047.7	193.667		470.583	-1245.4
800	41646.3	21986.7	12599.3	10897.7	191.333		469.995	-1335.53
850	41367.3	21753.3	12456.7	10803.7	186		466.562	-1349.07
900	41022.3	21539.7	12236.3	10640	184.667		462.875	-1390.4
950	40821	21388	12056.7	10402.7	354.667		459.59	-1379
1000	40513	21129.7	11873	10317.7	176.333		457.427	-1495.13
1050	40285	20942.7	11673.3	10209.3	148.667		455.03	-1549.4
1100	40063	20732.7	11496	10097.7	168.333		452.122	-1573.33
1150	39910.7	20571.3	11331.7	9982.33	170		450.352	-1620.87
1200	39756.3	20342.3	11161.7	9924.33	177		447.883	-1643

Using the calculated values for the slope and intercept, it was possible to convert the raw fluorescence values to length of dsDNA. In doing so, we had to solve for ‘x’ in the equation y = mx + c at each time point, where ‘y’ = a raw fluorescence value, ‘m’ = the gradient, calculated previously, and ‘c’ = the intercept.

SUM =(E3-$B3)/$A3

	A	B	C	D	E	F	G	H	I	J	K
1					Raw fluorescence values				Converted to length of dsDNA		
2	slope (m)	intercept (c)		time (seconds)	50 nM 556/557 + 150 nM DNase				50 nM 556/557 + 150 nM DNase		
3	586.4167	744.0667		0	42787	43683	42130		=(E3-$B3)/	73.22257	70.57428
4	568.4517	600.5333		50	40757	39385	38979		70.64183	68.22826	67.51404
5	553.5583	386.8667		100	37483	36812	36073		67.01396	65.8018	64.4668
6	546.7767	157.2667		150	32137	33157	33352		58.48774	60.35322	60.70986
7	539.795	-92.6667		200	28075	29946	30649		52.18216	55.64829	56.95063
8	530.9083	-286.667		250	24964	26768	27754		47.56126	50.95921	52.8164
9	521.22	-350.667		300	22726	23968	24953		44.27433	46.6572	48.547
10	512.635	-522.467		350	20252	21876	22872		40.52487	43.69282	45.63572
11	503.0483	-636.867		400	18086	20001	20830		37.21882	41.02561	42.67357
12	496.7133	-706.533		450	16688	18352	19255		35.01926	38.36928	40.18723
13	491.0833	-865.4		500	15431	16947	18007		33.18459	36.27164	38.43014
14	485.0567	-985.267		550	14253	15804	16870		31.41544	34.613	36.81068
15	480.7133	-1053.07		600	13179	14692	15844		29.60614	32.75355	35.14999
16	478.0433	-1139.67		650	12166	13756	14816		27.8336	31.15966	33.37703
17	474.755	-1214.4		700	11349	12964	13892		26.46291	29.86467	31.81936
18	470.5833	-1245.4		750	10517	12144	13094		24.99536	28.45277	30.47154
19	469.995	-1335.53		800	9887	11375	12272		23.87798	27.04398	28.95251
20	466.5617	-1349.07		850	9203	10751	11647		22.61666	25.93455	27.85498
21	462.875	-1390.4		900	8639	10153	10955		21.66762	24.93848	26.67113
22	459.59	-1379		950	8117	9554	10267		20.66189	23.78859	25.33998
23	457.4267	-1495.13		1000	7665	8998	9697		20.02536	22.93949	24.4676

This data can then be analysed to calculate maximal reaction rates using the equation ‘x = (y - c) / m) as shown in the above figure.

Part 2: Rate analysis

It is possible to calculate the rate of the reaction by calculating the gradient of the substrate vs DNase I concentration at its steepest. This is the maximal velocity at which the enzyme digests or resects the DNA substrate. Below, the rate at the highest concentration of DNase I (150 nM) and in the absence of DNase I (0 nM DNase I) is shown.

SUM =SLOPE(B5:B9,$A$5:$A$9)

	A	B	C	D	E	F	G
1	time (seconds)	50 nM 556/557 + 150 nM DNase			50 nM 556/557 + 0 nM DNase		
2	0	71.69464	73.22257	70.57428	84.2642	84.26761	89.16857
3	50	70.64183	68.22826	67.51404	84.3598	83.10375	90.08939
4	100	67.01396	65.8018	64.4668	85.41491	84.4394	90.33038
5	150	58.48774	60.35322	60.70986	85.24821	85.5701	90.74589
6	200	52.18216	55.64829	56.95063	85.28546	87.51409	90.77644
7	250	47.56126	50.95921	52.8164	85.51884	88.22176	91.24865
8	300	44.27433	46.6572	48.547	86.27771	88.31332	91.91065
9	350	40.52487	43.69282	45.63572	87.4608	88.05576	92.45461
10	1850	12.57635	14.32644	14.94523	91.22384	92.46141	96.28751
11							
12	Slope	=SLOPE(B5:B9	-0.08462	-0.0771	0.010835	0.011541	0.009103
13							
14							
15	Rate	150 nM Dnase	0 nM Dnase				
16		-0.08766714	0.010835		blank	0.010493	
17		-0.08462378	0.011541				
18		-0.07710382	0.009103				
19							
20	Rate minus average 0 nM Dnase	150 nM Dnase	0 nM DNase				
21		-0.09816023	0.000342				
22		-0.09511687	0.001048				
23		-0.08759691	-0.00139				

The rate for this reaction is calculated for each individual sample. An average of the rate when there is 0 nM DNase I is taken (0.010493) and this is subtracted from each calculation of the slope. This is termed ‘baseline interpolation’ and is a form of data normalisation.

The rate is then divided by the concentration of DNase I in nM. Each value is divided either by 150 (when treated with 150 nM DNase) or 0 (when treated with 0 nM DNase). When divided by 0, the result is ∞, however the result will be reported as 0 as there is no reaction when the enzyme is absent.

The rate is negative, as we are calculating the decrease in florescence over time. However, the rate can be presented in terms of positive integers, and so the negative values are multiplied by -1.

Error is represented by standard error of the mean. The equation for this is:

$$\sigma = \sqrt{\frac{\Sigma\ (x - \bar{x})^2}{n}}$$

σ = standard deviation

Σ = sum of

x = term

$\bar{x}$ = mean

n = total number of terms

In excel, this formula is entered as:

“=STDEV(range)/SQRT(COUNT(range))”.

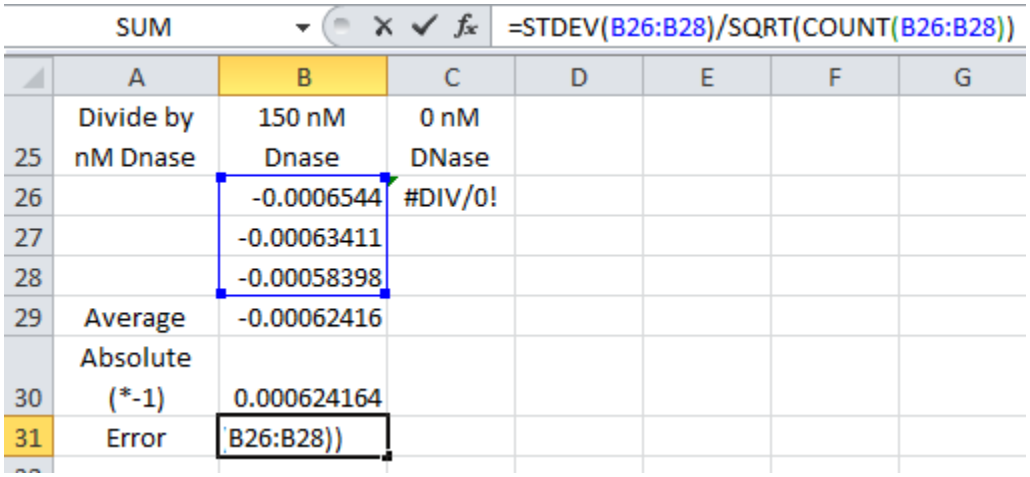

Kat5 FASTA sequences for protein alignment analyses

>Mouse_Kat5

MAEVGEIIEGCRLPVLRRNQDNEDEWPLAEILSVKDISGRKLFYVHYIDFNKRLDEWVTHER
LDLKKIQFPKKEAKTPTKNGLPGSRPGSPEREVPASAQASGKTLPIPVQITLRFNLPKEREA
IPGGEPDQPLSSSSCLQPNHRSTKRKVEVVSPATPVPSETAPASVFPQNGSARRAVAAQPGR
KRKSNCLGTDEDSQDSSDGIPSAPRMTGSLVSDRSHDDIVTRMKNIECIELGRHRLKPWYFS
PYPQELTTLPVLYLCEFCLKYGRSLKCLQRHLTKCDLRHPPGNEIYRKGTISFFEIDGRKNK
SYSQNLCLLAKCFLDHKTLYYDTDPFLFYVMTEYDCKGFHIVGYFSKEKESTEDYNVACILT
LPPYQRRGYGKLLIEFSYELSKVEGKTGTPEKPLSDLGLLSYRSYWSQTILEILMGLKSESG
ERPQITINEISEITSIKKEDVISTLQYLNLINYYKGQYILTLSEDIVDGHERAMLKRLLRID
SKCLHFTPKDWSKRGKW

>Human_Kat5

MAEVGEIIEGCRLPVLRRNQDNEDEWPLAEILSVKDISGRKLFYVHYIDFNKRLDEWVTHER
LDLKKIQFPKKEAKTPTKNGLPGSRPGSPEREVPASAQASGKTLPIPVQITLRFNLPKEREA
IPGGEPDQPLSSSSCLQPNHRSTKRKVEVVSPATPVPSETAPASVFPQNGAARRAVAAQPGR
KRKSNCLGTDEDSQDSSDGIPSAPRMTGSLVSDRSHDDIVTRMKNIECIELGRHRLKPWYFS
PYPQELTTLPVLYLCEFCLKYGRSLKCLQRHLTKCDLRHPPGNEIYRKGTISFFEIDGRKNK
SYSQNLCLLAKCFLDHKTLYYDTDPFLFYVMTEYDCKGFHIVGYFSKEKESTEDYNVACILT
LPPYQRRGYGKLLIEFSYELSKVEGKTGTPEKPLSDLGLLSYRSYWSQTILEILMGLKSESG
ERPQITINEISEITSIKKEDVISTLQYLNLINYYKGQYILTLSEDIVDGHERAMLKRLLRID
SKCLHFTPKDWSKRGKW

>Dog_Kat5

MAEVGEIIEGCRLPVLRRNQDNEDEWPLAEILSVKDISGRKLFYVHYIDFNKRLDEWVTHER
LDLKKIQFPKKEAKTPTKNGLPGSRPGSPEREVPASAQASGKTLPIPVQITLRFNLPKEREA
IPGGEPDQPLSSSSCLQPNHRSTKRKVEVVSPATPVPSETAPASVFPQNGSARRAVAAQPGR
KRKSNCLGTDEDSQDSSDGIPSAPRMTGSLVSDRSHDDIVTRMKNIECIELGRHRLKPWYFS
PYPQELTTLPVLYLCEFCLKYGRSLKCLQRHLTKCDLRHPPGNEIYRKGTISFFEIDGRKNK
SYSQNLCLLAKCFLDHKTLYYDTDPFLFYVMTEYDCKGFHIVGYFSKEKESTEDYNVACILT
LPPYQRRGYGKLLIEFSYELSKVEGKTGTPEKPLSDLGLLSYRSYWSQTILEILMGLKSESG
ERPQITINEISEITSIKKEDVISTLQYLNLINYYKGQYILTLSEDIVDGHERAMLKRLLRID
SKCLHFTPKDWSKRGKW

>Chicken_Kat5

MAEAAEVSEGCRLPVLRRNQDNEDEWPLAEILSVKDISGRRLFYVHYIDFNKRLDEWVTPER
LDLQRVQGPRKEAKTPTKNGLPGSRPDSPERDPKRKVEVVSPATPVPAATETSQASVFPQNG
SARRAVAAQPGRKRKSACLGTDEDSQDSSDGAPSAPRMTGSLVSDRSHDDIVTRMKNIECIE
LGRHRLKPWYFSPYPQELTALPVLYLCEFCLKYGHSLRCLQRHLTKCDLRHPPGNEIYRKGT
ISFFEIDGRKNKSYSQNLCLLAKCFLDHKTLYYDTDPFLFYVMTEYDCKGFHIVGYFSKEKE
STEDYNVACILTLPPYQRRGYGKLLIEFSYELSKVEGKTGTPEKPLSDLGLLSYRSYWSQTI
LEILMGLKAEGGERPQITINEISEITSIKKEDVISTLQYLNLINYYKGQYILTLSGDIVEGH
ERAMLKRVLRIDAKCLHFTPKDWSKRGKWC

>Western_Clawed_Frog_Kat5

MAEAEIVEGCRLPVLRKNQDNEVEWPLAEILSIKELTGKKLFYVHYIDFNKRLDEWVTHDRL
DLKKIQFPKKEAKTPTKNGLPGSRPSSPEREVRKIPELIPPPVVPPAAGGKSLPVPKRKVDI
VSPATPVPPPPETTQVTVFPQQAPCDVAGVSAHTVMLSQNGAVRRPSAPAVQPGRKRKSNCL
SADEDSQDSSDGIPSAPRMTGSLVSDRSHDDIITRMKNIECIELGRHRLKPWYFSPYPQELT
VLPVLYLCEFCLKYVKSLKCLQRHLTKCNLRHPPGNEIYRKGTISFFEIDGRKNKSYSQNLC
LLAKCFLDHKTLYYDTDPFLFYIMTEYDCKGFHIVGYFSKEKESTEDYNVACILTLPPYQRR
GYGKLLIEFSYELSKVEGKTGTPEKPLSDLGLLSYRSYWSQTILEILMELKTETGERPQITI
NEISEITSIKKEDVISTLQYLNLINYYKGQYILTLSEDIVEGHEKAMQKRVLRIDSKCLHFT
PKDWSKRGKW

>Zebrafish_Kat5

MAEPTVEIVEGCRLPVLRKNQENEDEWPLAEILSVKDIPGRKLYYVHYIDFNKRLDEWVTPD
RLDLKKLQFPKKEAKTPTKNGLPGSRPSSPEREVRKSLDLNVQSASAPSRGKTLPTPKRKAE
SVSLATQVTAATPVPSLPSSAEASQASVYPAMRDSSFSIKAREEHEQLTSLTTNGTTRRLIP
SQPGRKRKNCVGTEEIVKVFQNNSPRSSTVYLPPGEDSQDSSDGIPSAPRMTGSLVSDRSHD
DIITRMKNIDCIELGRHRLKPWYFSPYPQELTTLPILYLCEFCLKYLKSLKCLQRHLTKCNL
RHPPGNEIYRKGTISFFEIDGRKNKMYSQNLCLLAKCFLDHKTLYYDTDPFLFYVMTEYDSK
GFHIVGYFSKEKESTEDYNVACILTLPPYQRRGYGKLLIEFSYELSKVEGKTGTPEKPLSDL
GLLSYRSYWSQTILEILMNLKSENGERPQMTINEISEITSVKKEDVISTLQYLNLINYYKGQ
YILTLSEDIVEGHERAMHKRHLRIDSKCLHFTPKDWSKRGKW

>D_melangoster_Kat5

MKINHKYEFDDDVASICESTAALTEGCRLPVRMHKTDDWPLAEIVSIKELDGRRQFYVHYVD
FNKRLDEWVNEEDLYTRKVQFPRRDGSQTGTSTGVTTPQRHHSLAGSVSRPTSPQHPGSGAL
AAIPQTPTGASGSVPPPAGIPNSVAPPGTPSSGGELVNGNNLAAALQKRINRKRKNHGGSAH
GHHSLTSQQQQSHPHPTTPQTPTATPVHVTGDGLISGAANDDGDGSQDGKTPTPRQSGSMVT
HQDDVVTRMKNVEMIELGRHRIKPWYFSPYPQELCQMPCIYICEFCLKYRKSRKCLERHLSK
CNLRHPPGNEIYRKHTISFFEIDGRKNKVYAQNLCLLAKLFLDHKTLYYDTDPFLFYVMTEF
DSRGFHIVGYFSKEKESTEDYNVACILTMPPYQRKGYGKLLIEFSYELSKFEGKTGSPEKPL
SDLGLLSYRSYWAQTILEIFISQNPSTDGEKPTITINDICECTSIKKEDVISTLQNLNLINY
YKGQYIVCINRVIIEQHRRAMDKRKIRIDSKCLHWTPKDWSKRSK

>C_elegans_Kat5

MTEPKKEIIEDENHGISKKIPTDPRQYEKVTEGCRLLVMMASQEEERWAEVISRCRAANGSI
KFYVHYIDCNRRLDEWVQSDRLNLASCELPKKGGKKGAHLREENRDSNENEGKKSGRKRKIP
LLPMDDLKAESVDPLQAISTMTSGSTPSLRGSMSMVGHSEDAMTRIRNVECIELGRSRIQPW
YFAPYPQQLTSLDCIYICEFCLKYLKSKTCLKRHMEKCAMCHPPGNQIYSHDKLSFFEIDGR
KNKSYAQNLCLLAKLFLDHKTLYYDTDPFLFYVLTEEDEKGHHIVGYFSKEKESAEEYNVAC
ILVLPPFQKKGYGSLLIEFSYELSKIEQKTGSPEKPLSDLGLLSYRSYWSMAIMKELFAFKR
RHPGEDITVQDISQSTSIKREDVVSTLQQLDLYKYYKGSYIIVISDEKRQVYEKRIEAAKKK
TRINPAALQWRPKEYGKKRAQIMF

>S_cerevisiae_Kat5_(ESA1)

MSHDGKEEPGIAKKINSVDDIIIKCQCWVQKNDEERLAEILSINTRKAPPKFYVHYVNYNKR
LDEWITTDRINLDKEVLYPKLKATDEDNKKQKKKKATNTSETPQDSLQDGVDGFSRENTDVM
DLDNLNVQGIKDENISHEDEIKKLRTSGSMTQNPHEVARVRNLNRIIMGKYEIEPWYFSPYP
IELTDEDFIYIDDFTLQYFGSKKQYERYRKKCTLRHPPGNEIYRDDYVSFFEIDGRKQRTWC
RNLCLLSKLFLDHKTLYYDVDPFLFYCMTRRDELGHHLVGYFSKEKESADGYNVACILTLPQ
YQRMGYGKLLIEFSYELSKKENKVGSPEKPLSDLGLLSYRAYWSDTLITLLVEHQKEITIDE
ISSMTSMTTTDILHTAKTLNILRYYKGQHIIFLNEDILDRYNRLKAKKRRTIDPNRLIWKPP
VFTASQLRFAW

>S_pombe_Kat5

MSNDVDDESKIETKSYEAKDIVYKSKVFAFKDGEYRKAEILMIQKRTRGVVYYVHYNDYNKR
LDEWITIDNIDLSKGIEYPPPEKPKKAHGKGKSSKRPKAVDRRRSITAPSKTEPSTPSTEKP

EPSTPSGESDHGSNAGNESLPLLEEDHKPESLSKEQEVERLRFSGSMVQNPHEIARIRNINK
ICIGDHEIEPWYFSPYPKEFSEVDIVYICSFCFCYYGSERQFQRHREKCTLQHPPGNEIYRD
DYISFFEIDGRKQRTWCRNICLLSKLFLDHKMLYYDVDPFLFYCMCRRDEYGCHLVGYFSKE
KESSENYNLACILTLPQYQRHGYGKLLIQFSYELTKREHKHGSPEKPLSDLGLISYRAYWAE
QIINLVLGMRTETTIDELANKTSMTTNDVLHTLQALNMLKYYKGQFIICISDGIEQQYERLK
NKKRRRINGDLLADWQPPVFHPSQLRFGW

>U_maydis_Kat5

MAPRTQKSTSGTPGGSGTPGPDEGPQISPGGTYGLEDVVVGCKAFVQKPDVVTGEMEERKAE
ILSIREKPKPRLTKKQQAELADKPAPTLEETLEYYVHYCEFNKRLDEWVSGTRLITSRELEW
PKKEVTSDKTKRKVIRAGSGATTPSTPLTPTGKGYRGAGASNLLKKAAAQAAKNVQGESGLE
TPQKRKADSGDTSTAQSIRADSIDADADGEDDENGAVVAMEMLGGNDQQEKDDVATESNGGL
TASLNANQGQETFSKKQEIEKLRTSGSMTQSVSEVARVKNLNKIQMGKSEVETWYFSPYPLE
YAHIDTLYICEMCLSYFPSPFTLKRHRSKCTLLHPPGNEIYRHEDISFFEIDGRLQRTWCRN
LCLLSKCFLDHKTLYYDVDPFLYYCMVKRDDLGCHLLGYFSKEKDSAENYNVACILTLPQHQ
RAGYGKLLIEFSYELTKIEGKLGSPEKPLSDLGLLSYRAYWAEIIVELLLKTEDEISIEEIA
QKTAFTHADILHTCMALNMLKQYQGKHMIVLSDLIISKYTAKRPRKRINPQKLHWTAKNWHR
SQLNFGW

References

1. Parra D, Takizawa F, Sunyer JO. Evolution of B cell immunity. *Annu Rev Anim Biosci* (2013) **1**:65–97. doi:10.1146/annurev-animal-031412-103651
2. Bednarski JJ, Sleckman BP. At the intersection of DNA damage and immune responses. *Nat Rev Immunol* (2019)1. doi:10.1038/s41577-019-0135-6
3. Vuong BQ, Chaudhuri J. Combinatorial mechanisms regulating AID-dependent DNA deamination: interacting proteins and post-translational modifications. *Semin Immunol* (2012) **24**:264–72. doi:10.1016/j.smim.2012.05.006
4. Doktorgrades E, Lang S. Epigenetic Regulation of V (D) J Recombination in Early B Cell Development. *Naturwissenschaftlichen* (2008)
5. Kracker S, Durandy A. Insights into the B cell specific process of immunoglobulin class switch recombination. *Immunol Lett* (2011) **138**:97–103. doi:10.1016/j.imlet.2011.02.004
6. Maugeri-Sacca M, Bartucci M, De Maria R. DNA Damage Repair Pathways in Cancer Stem Cells. *Mol Cancer Ther* (2012) **11**:1627–1636. doi:10.1158/1535-7163.MCT-11-1040
7. Jackson SP, Bartek J. The DNA-damage response in human biology and disease. *Nature* (2009) **461**:1071–8. doi:10.1038/nature08467
8. Martinez-Fernandez L, Banyasz A, Esposito L, Markovitsi D, Improta R. UV-induced damage to DNA: effect of cytosine methylation on pyrimidine dimerization. *Signal Transduct Target Ther* (2017) **2**:17021. doi:10.1038/sigtrans.2017.21
9. Zhou BB, Elledge SJ. The DNA damage response: putting checkpoints in perspective. *Nature* (2000) **408**:433–9. doi:10.1038/35044005
10. Liu L, Kong M, Gassman NR, Freudenthal BD, Prasad R, Zhen S, Watkins SC, Wilson SH, Van Houten B. PARP1 changes from three-dimensional DNA damage searching to one-dimensional diffusion after auto-PARylation or in the presence of APE1. *Nucleic Acids Res* (2017) **45**:12834–12847. doi:10.1093/nar/gkx1047
11. Kato N, Kawasoe Y, Williams H, Coates E, Roy U, Shi Y, Beese LS, Schärer OD, Yan H, Gottesman ME, et al. Sensing and Processing of DNA Interstrand Crosslinks by the Mismatch Repair Pathway. *Cell Rep* (2017) **21**:1375–1385.

doi:10.1016/j.celrep.2017.10.032

12. Rotman G, Shiloh Y. Ataxia-telangiectasia: Is ATM a sensor of oxidative damage and stress? *BioEssays* (1997) **19**:911–917. doi:10.1002/bies.950191011
13. Mitsunobu H, Zhu B, Lee S-J, Tabor S, Richardson CC. Flap endonuclease activity of gene 6 exonuclease of bacteriophage T7. *J Biol Chem* (2014) **289**:5860–75. doi:10.1074/jbc.M113.538611
14. Myler LR, Gallardo IF, Zhou Y, Gong F, Yang S-H, Wold MS, Miller KM, Paull TT, Finkelstein IJ. Single-molecule imaging reveals the mechanism of Exo1 regulation by single-stranded DNA binding proteins. *Proc Natl Acad Sci* (2016) **113**:E1170–E1179. doi:10.1073/pnas.1516674113
15. Myler LR, Gallardo IF, Soniat MM, Deshpande RA, Gonzalez XB, Kim Y, Paull TT, Finkelstein IJ. Single-Molecule Imaging Reveals How Mre11-Rad50-Nbs1 Initiates DNA Break Repair. *Mol Cell* (2017) **67**:891–898.e4. doi:10.1016/j.molcel.2017.08.002
16. Kimura A, Horikoshi M. Tip60 acetylates six lysines of a specific class in core histones in vitro. *Genes Cells* (1998) **3**:789–800. Available at: http://www.ncbi.nlm.nih.gov/pubmed/10096020 [Accessed September 16, 2018]
17. Yamamoto T, Horikoshi M. Novel substrate specificity of the histone acetyltransferase activity of HIV-1-Tat interactive protein Tip60. *J Biol Chem* (1997) **272**:30595–8. doi:10.1074/JBC.272.49.30595
18. Sapountzi V, Logan IR, Robson CN. Cellular functions of TIP60. *Int J Biochem Cell Biol* (2006) **38**:1496–509. doi:10.1016/j.biocel.2006.03.003
19. Ikura T, Ogryzko V V, Grigoriev M, Groisman R, Wang J, Horikoshi M, Scully R, Qin J, Nakatani Y. Involvement of the TIP60 Histone Acetylase Complex in DNA Repair and Apoptosis. *Cell* (2000) **102**:463–473. doi:10.1016/S0092-8674(00)00051-9
20. Xu Y, Sun Y, Jiang X, Ayrapetov MK, Moskwa P, Yang S, Weinstock DM, Price BD. The p400 ATPase regulates nucleosome stability and chromatin ubiquitination during DNA repair. *J Cell Biol* (2010) **191**:31–43. doi:10.1083/jcb.201001160
21. Gorynia S, Bandeiras TM, Pinho FG, McVey CE, Vonrhein C, Round A, Svergun DI, Donner P, Matias PM, Carrondo MA. Structural and functional

insights into a dodecameric molecular machine - the RuvBL1/RuvBL2 complex. *J Struct Biol* (2011) **176**:279–91. doi:10.1016/j.jsb.2011.09.001

22. Josling G a., Selvarajah S a., Petter M, Duffy MF. The role of bromodomain proteins in regulating gene expression. *Genes (Basel)* (2012) **3**:320–343. doi:10.3390/genes3020320
23. Sanchez R, Zhou M-M. The role of human bromodomains in chromatin biology and gene transcription. *Curr Opin Drug Discov Devel* (2009) **12**:659–65. Available at: http://www.ncbi.nlm.nih.gov/pubmed/19736624 [Accessed September 16, 2018]
24. Ayrapetov MK, Gursoy-Yuzugullu O, Xu C, Xu Y, Price BD. DNA double-strand breaks promote methylation of histone H3 on lysine 9 and transient formation of repressive chromatin. *Proc Natl Acad Sci U S A* (2014) **111**:9169–74. doi:10.1073/pnas.1403565111
25. Eissenberg JC. Structural biology of the chromodomain: form and function. *Gene* (2012) **496**:69–78. doi:10.1016/j.gene.2012.01.003
26. Gursoy-Yuzugullu O, House N, Price BD. Patching broken DNA: Nucleosome dynamics and the repair of DNA breaks. *J Mol Biol* (2015) doi:10.1016/j.jmb.2015.11.021
27. Ikura T, Tashiro S, Kakino A, Shima H, Jacob N, Amunugama R, Yoder K, Izumi S, Kuraoka I, Tanaka K, et al. DNA Damage-Dependent Acetylation and Ubiquitination of H2AX Enhances Chromatin Dynamics. *Mol Cell Biol* (2007) **27**:7028–7040. doi:10.1128/MCB.00579-07
28. Sun Y, Jiang X, Xu Y, Ayrapetov MK, Moreau LA, Whetstine JR, Price BD. Histone H3 methylation links DNA damage detection to activation of the tumour suppressor Tip60. *Nat Cell Biol* (2009) **11**:1376–82. doi:10.1038/ncb1982
29. Xu Y, Ayrapetov MK, Xu C, Gursoy-Yuzugullu O, Hu Y, Price BD. Histone H2A.Z controls a critical chromatin remodeling step required for DNA double-strand break repair. *Mol Cell* (2012) **48**:723–33. doi:10.1016/j.molcel.2012.09.026
30. Kalashnikova AA, Porter-Goff ME, Muthurajan UM, Luger K, Hansen JC. The role of the nucleosome acidic patch in modulating higher order chromatin structure. *J R Soc Interface* (2013) **10**:20121022. doi:10.1098/rsif.2012.1022
31. Robinson PJJ, An W, Routh A, Martino F, Chapman L, Roeder RG, Rhodes D.

30 nm chromatin fibre decompaction requires both H4-K16 acetylation and linker histone eviction. *J Mol Biol* (2008) **381**:816–25. doi:10.1016/j.jmb.2008.04.050

32. Shogren-Knaak M, Ishii H, Sun J-M, Pazin MJ, Davie JR, Peterson CL. Histone H4-K16 acetylation controls chromatin structure and protein interactions. *Science* (2006) **311**:844–7. doi:10.1126/science.1124000
33. Tang J, Cho NW, Cui G, Manion EM, Shanbhag NM, Botuyan MV, Mer G, Greenberg RA. Acetylation limits 53BP1 association with damaged chromatin to promote homologous recombination. *Nat Struct Mol Biol* (2013) **20**:317–25. doi:10.1038/nsmb.2499
34. Chen L, Nievera CJ, Lee AY-L, Wu X. Cell cycle-dependent complex formation of BRCA1.CtIP.MRN is important for DNA double-strand break repair. *J Biol Chem* (2008) **283**:7713–20. doi:10.1074/jbc.M710245200
35. Callen E, Di Virgilio M, Kruhlak MJ, Nieto-Soler M, Wong N, Chen H-T, Faryabi RB, Polato F, Santos M, Starnes LM, et al. 53BP1 mediates productive and mutagenic DNA repair through distinct phosphoprotein interactions. *Cell* (2013) **153**:1266–80. doi:10.1016/j.cell.2013.05.023
36. Yu X, Wu LC, Bowcock AM, Aronheim A, Baer R. The C-terminal (BRCT) domains of BRCA1 interact in vivo with CtIP, a protein implicated in the CtBP pathway of transcriptional repression. *J Biol Chem* (1998) **273**:25388–92. Available at: http://www.ncbi.nlm.nih.gov/pubmed/9738006 [Accessed September 16, 2018]
37. Zhong Q, Chen CF, Li S, Chen Y, Wang CC, Xiao J, Chen PL, Sharp ZD, Lee WH. Association of BRCA1 with the hRad50-hMre11-p95 complex and the DNA damage response. *Science* (1999) **285**:747–50. Available at: http://www.ncbi.nlm.nih.gov/pubmed/10426999 [Accessed September 16, 2018]
38. Sartori AA, Lukas C, Coates J, Mistrik M, Fu S, Bartek J, Baer R, Lukas J, Jackson SP. Human CtIP promotes DNA end resection. *Nature* (2007) **450**:509–14. doi:10.1038/nature06337
39. Krejci L, Altmannova V, Spirek M, Zhao X. Homologous recombination and its regulation. *Nucleic Acids Res* (2012) **40**:5795–818. doi:10.1093/nar/gks270
40. Sun Y, Jiang X, Chen S, Fernandes N, Price BD. A role for the Tip60 histone acetyltransferase in the acetylation and activation of ATM. *Proc Natl Acad Sci*

U S A (2005) **102**:13182–7. doi:10.1073/pnas.0504211102

41. Sun Y, Xu Y, Roy K, Price BD. DNA damage-induced acetylation of lysine 3016 of ATM activates ATM kinase activity. *Mol Cell Biol* (2007) **27**:8502–9. doi:10.1128/MCB.01382-07
42. Kaidi A, Jackson SP. KAT5 tyrosine phosphorylation couples chromatin sensing to ATM signalling. *Nature* (2013) **498**:70–4. doi:10.1038/nature12201
43. Sun Y, Jiang X, Price BD. Tip60: connecting chromatin to DNA damage signaling. *Cell Cycle* (2010) **9**:930–6. doi:10.4161/cc.9.5.10931
44. Burma S, Chen BP, Murphy M, Kurimasa A, Chen DJ. ATM phosphorylates histone H2AX in response to DNA double-strand breaks. *J Biol Chem* (2001) **276**:42462–7. doi:10.1074/jbc.C100466200
45. Stucki M, Clapperton JA, Mohammad D, Yaffe MB, Smerdon SJ, Jackson SP. MDC1 directly binds phosphorylated histone H2AX to regulate cellular responses to DNA double-strand breaks. *Cell* (2005) **123**:1213–26. doi:10.1016/j.cell.2005.09.038
46. Mattiroli F, Vissers JHA, van Dijk WJ, Ikpa P, Citterio E, Vermeulen W, Marteijn JA, Sixma TK. RNF168 ubiquitinates K13-15 on H2A/H2AX to drive DNA damage signaling. *Cell* (2012) **150**:1182–95. doi:10.1016/j.cell.2012.08.005
47. Kleiner RE, Verma P, Molloy KR, Chait BT, Kapoor TM. Chemical proteomics reveals a γH2AX-53BP1 interaction in the DNA damage response. *Nat Chem Biol* (2015) **11**:807–814. doi:10.1038/nchembio.1908
48. Sivanand S, Rhoades S, Jiang Q, Lee J V, Benci J, Zhang J, Yuan S, Viney I, Zhao S, Carrer A, et al. Nuclear Acetyl-CoA Production by ACLY Promotes Homologous Recombination. *Mol Cell* (2017) **67**:252–265.e6. doi:10.1016/j.molcel.2017.06.008
49. Patel JH, Du Y, Ard PG, Phillips C, Carella B, Chen C-J, Rakowski C, Chatterjee C, Lieberman PM, Lane WS, et al. The c-MYC Oncoprotein Is a Substrate of the Acetyltransferases hGCN5/PCAF and TIP60. *Mol Cell Biol* (2004) **24**:10826–10834. doi:10.1128/MCB.24.24.10826-10834.2004
50. Frank SR, Parisi T, Taubert S, Fernandez P, Fuchs M, Chan H-M, Livingston DM, Amati B. MYC recruits the TIP60 histone acetyltransferase complex to chromatin. *EMBO Rep* (2003) **4**:575–80. doi:10.1038/sj.embor.embor861
51. Gavaravarapu S, Kamine J. Tip60 Inhibits Activation of CREB Protein by

Protein Kinase A. *Biochem Biophys Res Commun* (2000) **269**:758–766. doi:10.1006/bbrc.2000.2358

52. Subramanian V, Fields PA, Boyer LA. H2A.Z: a molecular rheostat for transcriptional control. *F1000Prime Rep* (2015) **7**:1. doi:10.12703/P7-01
53. Weber CM, Henikoff JG, Henikoff S. H2A.Z nucleosomes enriched over active genes are homotypic. *Nat Struct Mol Biol* (2010) **17**:1500–1507. doi:10.1038/nsmb.1926
54. Larijani M, Martin A. The biochemistry of activation-induced deaminase and its physiological functions. *Semin Immunol* (2012) **24**:255–63. doi:10.1016/j.smim.2012.05.003
55. Rada C, Di Noia JM, Neuberger MS. Mismatch recognition and uracil excision provide complementary paths to both Ig switching and the A/T-focused phase of somatic mutation. *Mol Cell* (2004) **16**:163–71. doi:10.1016/j.molcel.2004.10.011
56. Xue K, Rada C, Neuberger MS. The in vivo pattern of AID targeting to immunoglobulin switch regions deduced from mutation spectra in *msh2* $^{-/-}$ *ung* $^{-/-}$ mice. *J Exp Med* (2006) **203**:2085–2094. doi:10.1084/jem.20061067
57. Adelman K, Lis JT. Promoter-proximal pausing of RNA polymerase II: emerging roles in metazoans. *Nat Rev Genet* (2012) **13**:720–731. doi:10.1038/nrg3293
58. Stiernholm NB, Berinstein NL. A mutated promoter of a human Ig V lambda gene segment is associated with reduced germ-line transcription and a low frequency of rearrangement. *J Immunol* (1995) **154**:1748–61. Available at: http://www.ncbi.nlm.nih.gov/pubmed/7836759 [Accessed February 8, 2018]
59. Fukita Y, Jacobs H, Rajewsky K. Somatic Hypermutation in the Heavy Chain Locus Correlates with Transcription. *Immunity* (1998) **9**:105–114. doi:10.1016/S1074-7613(00)80592-0
60. Skourti-Stathaki K, Proudfoot NJ, Gromak N. Human Senataxin Resolves RNA/DNA Hybrids Formed at Transcriptional Pause Sites to Promote Xrn2-Dependent Termination. *Mol Cell* (2011) **42**:794–805. doi:10.1016/J.MOLCEL.2011.04.026
61. Skourti-Stathaki K, Proudfoot NJ. A double-edged sword: R loops as threats to genome integrity and powerful regulators of gene expression. *Genes Dev* (2014) **28**:1384–96. doi:10.1101/gad.242990.114

62. Aguilera A, García-Muse T. R loops: from transcription byproducts to threats to genome stability. *Mol Cell* (2012) **46**:115–24. doi:10.1016/j.molcel.2012.04.009
63. Salter JD, Bennett RP, Smith HC. The APOBEC Protein Family: United by Structure, Divergent in Function. *Trends Biochem Sci* (2016) **41**:578–594. doi:10.1016/j.tibs.2016.05.001
64. Qiao Q, Wang L, Meng F-L, Hwang JK, Alt FW, Wu H. AID Recognizes Structured DNA for Class Switch Recombination. *Mol Cell* (2017) **67**:361–373.e4. doi:10.1016/j.molcel.2017.06.034
65. Losey HC, Ruthenburg AJ, Verdine GL. Crystal structure of Staphylococcus aureus tRNA adenosine deaminase TadA in complex with RNA. *Nat Struct Mol Biol* (2006) **13**:153–159. doi:10.1038/nsmb1047
66. Stephens OM, Yi-Brunozzi HY, Beal PA. Analysis of the RNA-editing reaction of ADAR2 with structural and fluorescent analogues of the GluR-B R/G editing site. *Biochemistry* (2000) **39**:12243–51. Available at: http://www.ncbi.nlm.nih.gov/pubmed/11015203 [Accessed March 2, 2018]
67. Holz B. 2-Aminopurine as a fluorescent probe for DNA base flipping by methyltransferases. *Nucleic Acids Res* (1998) **26**:1076–1083. doi:10.1093/nar/26.4.1076
68. Slupphaug G, Mol CD, Kavli B, Arvai AS, Krokan HE, Tainer JA. A nucleotide-flipping mechanism from the structure of human uracil–DNA glycosylase bound to DNA. *Nature* (1996) **384**:87–92. doi:10.1038/384087a0
69. Jiang YL, Stivers JT, Song F. Base-flipping mutations of uracil DNA glycosylase: substrate rescue using a pyrene nucleotide wedge. *Biochemistry* (2002) **41**:11248–54. doi:10.1021/bi026227j
70. Deng L, Velikovsky CA, Xu G, Iyer LM, Tasumi S, Kerzic MC, Flajnik MF, Aravind L, Pancer Z, Mariuzza RA. A structural basis for antigen recognition by the T cell-like lymphocytes of sea lamprey. *Proc Natl Acad Sci* (2010) **107**:13408–13413. doi:10.1073/pnas.1005475107
71. Larijani M, Martin A. Single-Stranded DNA Structure and Positional Context of the Target Cytidine Determine the Enzymatic Efficiency of AID. *Mol Cell Biol* (2007) **27**:8038–8048. doi:10.1128/MCB.01046-07
72. Jiang YL, Kwon K, Stivers JT. Turning On Uracil-DNA Glycosylase Using a Pyrene Nucleotide Switch. *J Biol Chem* (2001) **276**:42347–42354. doi:10.1074/jbc.M106594200

73. Peled JU, Kuang FL, Iglesias-Ussel MD, Roa S, Kalis SL, Goodman MF, Scharff MD. The biochemistry of somatic hypermutation. *Annu Rev Immunol* (2008) **26**:481–511. doi:10.1146/annurev.immunol.26.021607.090236
74. Han L, Masani S, Yu K. Overlapping activation-induced cytidine deaminase hotspot motifs in Ig class-switch recombination. *Proc Natl Acad Sci* (2011) **108**:11584–11589. doi:10.1073/pnas.1018726108
75. Krokan HE, Bjørås M. Base excision repair. *Cold Spring Harb Perspect Biol* (2013) **5**:a012583. doi:10.1101/cshperspect.a012583
76. Chahwan R, Edelmann W, Scharff MD, Roa S. AIDing antibody diversity by error-prone mismatch repair. *Semin Immunol* (2012) **24**:293–300. doi:10.1016/j.smim.2012.05.005
77. Shao H, Baitinger C, Soderblom EJ, Burdett V, Modrich P. Hydrolytic function of Exo1 in mammalian mismatch repair. *Nucleic Acids Res* (2014) **42**:7104–12. doi:10.1093/nar/gku420
78. Casali P, Pal Z, Xu Z, Zan H. DNA repair in antibody somatic hypermutation. *Trends Immunol* (2006) **27**:313. doi:10.1016/J.IT.2006.05.001
79. Krijger PHL, Langerak P, van den Berk PCM, Jacobs H. Dependence of nucleotide substitutions on Ung2, Msh2, and PCNA-Ub during somatic hypermutation. *J Exp Med* (2009) **206**:2603–2611. doi:10.1084/jem.20091707
80. Langerak P, Nygren AOH, Krijger PHL, van den Berk PCM, Jacobs H. A/T mutagenesis in hypermutated immunoglobulin genes strongly depends on PCNAK164 modification. *J Exp Med* (2007) **204**:1989–98. doi:10.1084/jem.20070902
81. Stavnezer J, Guikema JEJ, Schrader CE. Mechanism and regulation of class switch recombination. *Annu Rev Immunol* (2008) **26**:261–92. doi:10.1146/annurev.immunol.26.021607.090248
82. Kracker S, Radbruch A. Immunoglobulin class switching: in vitro induction and analysis. *Methods Mol Biol* (2004) **271**:149–59. doi:10.1385/1-59259-796-3:149
83. Heyman B, Pilström L, Shulman MJ. Complement activation is required for IgM-mediated enhancement of the antibody response. *J Exp Med* (1988) **167**:1999–2004. doi:10.1084/jem.167.6.1999
84. Stone KD, Prussin C, Metcalfe DD. IgE, mast cells, basophils, and eosinophils. *J Allergy Clin Immunol* (2010) **125**:S73–S80. doi:10.1016/J.JACI.2009.11.017

85. Forthal DN. Functions of Antibodies. *Microbiol Spectr* (2014) **2**:1–17. doi:10.1128/microbiolspec.AID-0019-2014
86. Luby TM, Schrader CE, Stavnezer J, Selsing E. The μ switch region tandem repeats are important, but not required, for antibody class switch recombination. *J Exp Med* (2001) **193**:159–68. doi:10.1084/jem.193.2.159
87. Khamlichi AA, Glaudet F, Oruc Z, Denis V, Le Bert M, Cogné M. Immunoglobulin class-switch recombination in mice devoid of any S tandem repeat. *Blood* (2004) **103**:3828–3836. doi:10.1182/blood-2003-10-3470
88. Stavnezer J. Immunoglobulin class switching. *Curr Opin Immunol* (1996) **8**:199–205. doi:10.1016/S0952-7915(96)80058-6
89. Hein K, Lorenz MG, Siebenkotten G, Petry K, Christine R, Radbruch A. Processing of switch transcripts is required for targeting of antibody class switch recombination. *J Exp Med* (1998) **188**:2369–74. Available at: http://www.ncbi.nlm.nih.gov/pubmed/9858523 [Accessed February 18, 2018]
90. Shinkura R, Tian M, Smith M, Chua K, Fujiwara Y, Alt FW. The influence of transcriptional orientation on endogenous switch region function. *Nat Immunol* (2003) **4**:435–441. doi:10.1038/ni918
91. Stavnezer J, Radcliffe G, Lin YC, Nietupski J, Berggren L, Sitia R, Severinson E. Immunoglobulin heavy-chain switching may be directed by prior induction of transcripts from constant-region genes. *Proc Natl Acad Sci* (1988) **85**:
92. Rothman P, Lutzker S, Cook W, Coffman R, Alt FW. Mitogen plus interleukin 4 induction of C epsilon transcripts in B lymphoid cells. *J Exp Med* (1988) **168**:2385–9. doi:10.1084/JEM.168.6.2385
93. Lutzker S, Rothman P, Pollock R, Coffman R, Alt FW. Mitogen- and IL-4-regulated expression of germ-line Ig gamma 2b transcripts: evidence for directed heavy chain class switching. *Cell* (1988) **53**:177–84. Available at: http://www.ncbi.nlm.nih.gov/pubmed/2834063 [Accessed February 23, 2018]
94. Coffman RL, Lebman DA, Shrader B. Transforming growth factor beta specifically enhances IgA production by lipopolysaccharide-stimulated murine B lymphocytes. *J Exp Med* (1989) **170**:1039–44. doi:10.1084/JEM.170.3.1039
95. Sonoda E, Matsumoto R, Hitoshi Y, Ishii T, Sugimoto M, Araki S, Tominaga A, Yamaguchi N, Takatsu K. Transforming growth factor beta induces IgA production and acts additively with interleukin 5 for IgA production. *J Exp Med* (1989) **170**:1415–20. doi:10.1084/JEM.170.4.1415

96. Kinoshita K, Harigai M, Fagarasan S, Muramatsu M, Honjo T. A hallmark of active class switch recombination: Transcripts directed by I promoters on looped-out circular DNAs. *Proc Natl Acad Sci* (2001) **98**:12620–12623. doi:10.1073/pnas.221454398
97. Chun HH, Gatti RA. Ataxia–telangiectasia, an evolving phenotype. *DNA Repair (Amst)* (2004) **3**:1187–1196. doi:10.1016/j.dnarep.2004.04.010
98. Kotnis A, Du L, Liu C, Popov SW, Pan-Hammarstrom Q. Non-homologous end joining in class switch recombination: the beginning of the end. *Philos Trans R Soc B Biol Sci* (2009) **364**:653–665. doi:10.1098/rstb.2008.0196
99. Barlow C, Hirotsune S, Paylor R, Liyanage M, Eckhaus M, Collins F, Shiloh Y, Crawley JN, Ried T, Tagle D, et al. Atm-deficient mice: a paradigm of ataxia telangiectasia. *Cell* (1996) **86**:159–71. Available at: http://www.ncbi.nlm.nih.gov/pubmed/8689683 [Accessed September 16, 2018]
100. Elson A, Wang Y, Daugherty CJ, Morton CC, Zhou F, Campos-Torres J, Leder P. Pleiotropic defects in ataxia-telangiectasia protein-deficient mice. *Proc Natl Acad Sci U S A* (1996) **93**:13084–9. Available at: http://www.ncbi.nlm.nih.gov/pubmed/8917548 [Accessed September 16, 2018]
101. Xu Y, Ashley T, Brainerd EE, Bronson RT, Meyn MS, Baltimore D. Targeted disruption of ATM leads to growth retardation, chromosomal fragmentation during meiosis, immune defects, and thymic lymphoma. *Genes Dev* (1996) **10**:2411–22. Available at: http://www.ncbi.nlm.nih.gov/pubmed/8843194 [Accessed September 16, 2018]
102. Reina-San-Martin B, Chen HT, Nussenzweig A, Nussenzweig MC. ATM is required for efficient recombination between immunoglobulin switch regions. *J Exp Med* (2004) **200**:1103–10. doi:10.1084/jem.20041162
103. Lumsden JM, McCarty T, Petiniot LK, Shen R, Barlow C, Wynn TA, Morse HC, Gearhart PJ, Wynshaw-Boris A, Max EE, et al. Immunoglobulin class switch recombination is impaired in Atm-deficient mice. *J Exp Med* (2004) **200**:1111–21. doi:10.1084/jem.20041074
104. Celeste A, Petersen S, Romanienko PJ, Fernandez-Capetillo O, Chen HT, Sedelnikova OA, Reina-San-Martin B, Coppola V, Meffre E, Difilippantonio MJ, et al. Genomic instability in mice lacking histone H2AX. *Science* (2002) **296**:922–7. doi:10.1126/science.1069398
105. Petersen S, Casellas R, Reina-San-Martin B, Chen HT, Difilippantonio MJ,

Wilson PC, Hanitsch L, Celeste A, Muramatsuk M, Pilch DR, et al. AID is required to initiate Nbs1/gamma-H2AX focus formation and mutations at sites of class switching. *Nature* (2001) **414**:660–665. doi:10.1038/414660a

106. Reina-San-Martin B, Difilippantonio S, Hanitsch L, Masilamani RF, Nussenzweig A, Nussenzweig MC. H2AX Is Required for Recombination Between Immunoglobulin Switch Regions but Not for Intra-Switch Region Recombination or Somatic Hypermutation. *J Exp Med* (2003) **197**:1767–1778. doi:10.1084/jem.20030569
107. Franco S, Gostissa M, Zha S, Lombard DB, Murphy MM, Zarrin AA, Yan C, Tepsuporn S, Morales JC, Adams MM, et al. H2AX Prevents DNA Breaks from Progressing to Chromosome Breaks and Translocations. *Mol Cell* (2006) **21**:201–214. doi:10.1016/j.molcel.2006.01.005
108. Lou Z, Minter-Dykhouse K, Wu X, Chen J. MDC1 is coupled to activated CHK2 in mammalian DNA damage response pathways. *Nature* (2003) **421**:957–61. doi:10.1038/nature01447
109. Stewart GS, Wang B, Bignell CR, Taylor AMR, Elledge SJ. MDC1 is a mediator of the mammalian DNA damage checkpoint. *Nature* (2003) **421**:961–6. doi:10.1038/nature01446
110. Lou Z, Minter-Dykhouse K, Franco S, Gostissa M, Rivera MA, Celeste A, Manis JP, van Deursen J, Nussenzweig A, Paull TT, et al. MDC1 Maintains Genomic Stability by Participating in the Amplification of ATM-Dependent DNA Damage Signals. *Mol Cell* (2006) **21**:187–200. doi:10.1016/j.molcel.2005.11.025
111. Ward IM, Minn K, van Deursen J, Chen J. p53 Binding protein 53BP1 is required for DNA damage responses and tumor suppression in mice. *Mol Cell Biol* (2003) **23**:2556–63. doi:10.1128/MCB.23.7.2556-2563.2003
112. Manis JP, Morales JC, Xia Z, Kutok JL, Alt FW, Carpenter PB. 53BP1 links DNA damage-response pathways to immunoglobulin heavy chain class-switch recombination. *Nat Immunol* (2004) **5**:481–487. doi:10.1038/ni1067
113. Ward IM, Reina-San-Martin B, Olaru A, Minn K, Tamada K, Lau JS, Cascalho M, Chen L, Nussenzweig A, Livak F, et al. 53BP1 is required for class switch recombination. *J Cell Biol* (2004) **165**:459–64. doi:10.1083/jcb.200403021
114. Bellaousov S, Reuter JS, Seetin MG, Mathews DH. RNAstructure: web servers for RNA secondary structure prediction and analysis. *Nucleic Acids Res* (2013)

41:W471–W474. doi:10.1093/nar/gkt290

115. Rocha PP, Raviram R, Fu Y, Kim J, Luo VM, Aljoufi A, Swanzey E, Pasquarella A, Balestrini A, Miraldi ER, et al. A Damage-Independent Role for 53BP1 that Impacts Break Order and Igh Architecture during Class Switch Recombination. (2016). doi:10.1016/j.celrep.2016.05.073
116. Eccleston J, Yan C, Yuan K, Alt FW, Selsing E. Mismatch Repair Proteins MSH2, MLH1, and EXO1 Are Important for Class-Switch Recombination Events Occurring in B Cells That Lack Nonhomologous End Joining. *J Immunol* (2011) **186**:2336–2343. doi:10.4049/jimmunol.1003104
117. Schrader CE, Edelmann W, Kucherlapati R, Stavnezer J. Reduced isotype switching in splenic B cells from mice deficient in mismatch repair enzymes. *J Exp Med* (1999) **190**:323–30. Available at: http://www.ncbi.nlm.nih.gov/pubmed/10430621 [Accessed March 25, 2018]
118. Ehrenstein MR, Neuberger MS. Deficiency in Msh2 affects the efficiency and local sequence specificity of immunoglobulin class-switch recombination: parallels with somatic hypermutation. *EMBO J* (1999) **18**:3484–90. doi:10.1093/emboj/18.12.3484
119. Martomo SA, Yang WW, Gearhart PJ. A Role for Msh6 But Not Msh3 in Somatic Hypermutation and Class Switch Recombination. *J Exp Med* (2004) **200**:61–68. doi:10.1084/jem.20040691
120. Li Z, Scherer SJ, Ronai D, Iglesias-Ussel MD, Peled JU, Bardwell PD, Zhuang M, Lee K, Martin A, Edelmann W, et al. Examination of Msh6- and Msh3-deficient mice in class switching reveals overlapping and distinct roles of MutS homologues in antibody diversification. *J Exp Med* (2004) **200**:47–59. doi:10.1084/jem.20040355
121. Li Z, Zhao C, Iglesias-Ussel MD, Polonskaya Z, Zhuang M, Yang G, Luo Z, Edelmann W, Scharff MD. The Mismatch Repair Protein Msh6 Influences the In Vivo AID Targeting to the Ig Locus. *Immunity* (2006) **24**:393–403. doi:10.1016/J.IMMUNI.2006.02.011
122. Schrader CE, Vardo J, Stavnezer J. Mlh1 can function in antibody class switch recombination independently of Msh2. *J Exp Med* (2003) **197**:1377–83. doi:10.1084/jem.20022190
123. Ehrenstein MR, Rada C, Jones AM, Milstein C, Neuberger MS. Switch junction sequences in PMS2-deficient mice reveal a microhomology-mediated

mechanism of Ig class switch recombination. *Proc Natl Acad Sci U S A* (2001) **98**:14553–8. doi:10.1073/pnas.241525998

124. Schaetzlein S, Chahwan R, Avdievich E, Roa S, Wei K, Eoff RL, Sellers RS, Clark AB, Kunkel TA, Scharff MD, et al. Mammalian Exo1 encodes both structural and catalytic functions that play distinct roles in essential biological processes. *Proc Natl Acad Sci U S A* (2013) **110**:E2470-9. doi:10.1073/pnas.1308512110
125. Lähdesmäki A, Taylor AMR, Chrzanowska KH, Pan-Hammarström Q. Delineation of the role of the Mre11 complex in class switch recombination. *J Biol Chem* (2004) **279**:16479–87. doi:10.1074/jbc.M312796200
126. Digweed M, Sperling K. Nijmegen breakage syndrome: clinical manifestation of defective response to DNA double-strand breaks. *DNA Repair (Amst)* (2004) **3**:1207–1217. doi:10.1016/j.dnarep.2004.03.004
127. Gregorek H, Chrzanowska KH, Michałkiewicz J, Syczewska M, Madaliński K. Heterogeneity of humoral immune abnormalities in children with Nijmegen breakage syndrome: an 8-year follow-up study in a single centre. *Clin Exp Immunol* (2002) **130**:319–24. Available at: http://www.ncbi.nlm.nih.gov/pubmed/12390322 [Accessed September 16, 2018]
128. Pan Q, Petit-Frére C, Lähdesmäki A, Gregorek H, Chrzanowska KH, Hammarström L. Alternative end joining during switch recombination in patients with Ataxia-Telangiectasia. *Eur J Immunol* (2002) **32**:1300. doi:10.1002/1521-4141(200205)32:5<1300::AID-IMMU1300>3.0.CO;2-L
129. Kracker S, Bergmann Y, Demuth I, Frappart P-O, Hildebrand G, Christine R, Wang Z-Q, Sperling K, Digweed M, Radbruch A. Nibrin functions in Ig class-switch recombination. *Proc Natl Acad Sci* (2005) **102**:1584–1589. doi:10.1073/pnas.0409191102
130. Reina-San-Martin B, Nussenzweig MC, Nussenzweig A, Difilippantonio S. Genomic instability, endoreduplication, and diminished Ig class-switch recombination in B cells lacking Nbs1. *Proc Natl Acad Sci U S A* (2005) **102**:1590–5. doi:10.1073/pnas.0406289102
131. Dinkelmann M, Spehalski E, Stoneham T, Buis J, Wu Y, Sekiguchi JM, Ferguson DO. Multiple functions of MRN in end-joining pathways during isotype class switching. *Nat Struct Mol Biol* (2009) **16**:808–13.

doi:10.1038/nsmb.1639

132. Stewart GS, Maser RS, Stankovic T, Bressan DA, Kaplan MI, Jaspers NG, Raams A, Byrd PJ, Petrini JH, Taylor AM. The DNA double-strand break repair gene hMRE11 is mutated in individuals with an ataxia-telangiectasia-like disorder. *Cell* (1999) **99**:577–87. Available at: http://www.ncbi.nlm.nih.gov/pubmed/10612394 [Accessed September 16, 2018]
133. Nussenzweig A, Chen C, da Costa Soares V, Sanchez M, Sokol K, Nussenzweig MC, Li GC. Requirement for Ku80 in growth and immunoglobulin V(D)J recombination. *Nature* (1996) **382**:551–555. doi:10.1038/382551a0
134. Gu Y, Seidl KJ, Rathbun GA, Zhu C, Manis JP, van der Stoep N, Davidson L, Cheng HL, Sekiguchi JM, Frank K, et al. Growth retardation and leaky SCID phenotype of Ku70-deficient mice. *Immunity* (1997) **7**:653–65. Available at: http://www.ncbi.nlm.nih.gov/pubmed/9390689 [Accessed September 16, 2018]
135. Casellas R, Nussenzweig A, Wuerffel R, Pelanda R, Reichlin A, Suh H, Qin XF, Besmer E, Kenter A, Rajewsky K, et al. Ku80 is required for immunoglobulin isotype switching. *EMBO J* (1998) **17**:2404–11. doi:10.1093/emboj/17.8.2404
136. Manis JP, Gu Y, Lansford R, Sonoda E, Ferrini R, Davidson L, Rajewsky K, Alt FW. Ku70 is required for late B cell development and immunoglobulin heavy chain class switching. *J Exp Med* (1998) **187**:2081–9. Available at: http://www.ncbi.nlm.nih.gov/pubmed/9625768 [Accessed September 16, 2018]
137. Rolink A, Melchers F, Andersson J. The SCID but not the RAG-2 gene product is required for S mu-S epsilon heavy chain class switching. *Immunity* (1996) **5**:319–30. Available at: http://www.ncbi.nlm.nih.gov/pubmed/8885865 [Accessed September 16, 2018]
138. Blunt T, Gell D, Fox M, Taccioli GE, Lehmann AR, Jackson SP, Jeggo PA. Identification of a nonsense mutation in the carboxyl-terminal region of DNA-dependent protein kinase catalytic subunit in the scid mouse. *Proc Natl Acad Sci U S A* (1996) **93**:10285–90. Available at: http://www.ncbi.nlm.nih.gov/pubmed/8816792 [Accessed September 16, 2018]
139. Danska JS, Holland DP, Mariathasan S, Williams KM, Guidos CJ. Biochemical and genetic defects in the DNA-dependent protein kinase in murine scid lymphocytes. *Mol Cell Biol* (1996) **16**:5507–17. Available at:

http://www.ncbi.nlm.nih.gov/pubmed/8816463 [Accessed September 16, 2018]

140. Beamish HJ, Jessberger R, Riballo E, Priestley A, Blunt T, Kysela B, Jeggo PA. The C-terminal conserved domain of DNA-PKcs, missing in the SCID mouse, is required for kinase activity. *Nucleic Acids Res* (2000) **28**:1506–13. Available at: http://www.ncbi.nlm.nih.gov/pubmed/10710416 [Accessed September 16, 2018]
141. Manis JP, Dudley D, Kaylor L, Alt FW. IgH class switch recombination to IgG1 in DNA-PKcs-deficient B cells. *Immunity* (2002) **16**:607–17. Available at: http://www.ncbi.nlm.nih.gov/pubmed/11970883 [Accessed September 16, 2018]
142. Soulas-Sprauel P, Le Guyader G, Rivera-Munoz P, Abramowski V, Olivier-Martin C, Goujet-Zalc C, Charneau P, de Villartay J-P. Role for DNA repair factor XRCC4 in immunoglobulin class switch recombination. *J Exp Med* (2007) **204**:1717–27. doi:10.1084/jem.20070255
143. Yan CT, Boboila C, Souza EK, Franco S, Hickernell TR, Murphy M, Gumaste S, Geyer M, Zarrin AA, Manis JP, et al. IgH class switching and translocations use a robust non-classical end-joining pathway. *Nature* (2007) **449**:478–482. doi:10.1038/nature06020
144. Ribeiro de Almeida C, Dhir S, Dhir A, Moghaddam AE, Sattentau Q, Meinhart A, Proudfoot NJ. RNA Helicase DDX1 Converts RNA G-Quadruplex Structures into R-Loops to Promote IgH Class Switch Recombination. *Mol Cell* (2018) **70**:650–662.e8. doi:10.1016/j.molcel.2018.04.001
145. Robert I, Dantzer F, Reina-San-Martin B. Parp1 facilitates alternative NHEJ, whereas Parp2 suppresses IgH/c-myc translocations during immunoglobulin class switch recombination. *J Exp Med* (2009) **206**:1047–1056. doi:10.1084/jem.20082468
146. Kelley MR, Fishel ML. Overview of DNA repair pathways, current targets, and clinical trials bench to clinic. *DNA Repair Cancer Ther* (2016)1–54. doi:10.1016/B978-0-12-803582-5.00001-2
147. Nishino T, Morikawa K. Structure and function of nucleases in DNA repair: shape, grip and blade of the DNA scissors. *Oncogene* (2002) **21**:9022–9032. doi:10.1038/sj.onc.1206135
148. Nishino T, Ishino Y, Morikawa K. Structure-specific DNA nucleases: structural basis for 3D-scissors. *Curr Opin Struct Biol* (2006) **16**:60–67.

doi:10.1016/J.SBI.2006.01.009

149. Chen X, Kim I-K, Honaker Y, Paudyal SC, Koh WK, Sparks M, Li S, Piwnica-Worms H, Ellenberger T, You Z. 14-3-3 proteins restrain the Exo1 nuclease to prevent overresection. *J Biol Chem* (2015) **290**:12300–12. doi:10.1074/jbc.M115.644005
150. Hollis T. “Crystallization of Protein-DNA Complexes,” in (Humana Press), 225–237. doi:10.1007/978-1-59745-209-0_11
151. Orans J, McSweeney EA, Iyer RR, Hast MA, Hellinga HW, Modrich P, Beese LS. Structures of human exonuclease 1 DNA complexes suggest a unified mechanism for nuclease family. *Cell* (2011) **145**:212–23. doi:10.1016/j.cell.2011.03.005
152. Xu Y, Potapova O, Leschziner AE, Grindley ND, Joyce CM. Contacts between the 5’ nuclease of DNA polymerase I and its DNA substrate. *J Biol Chem* (2001) **276**:30167–77. doi:10.1074/jbc.M100985200
153. Davies OR, Forment J V, Sun M, Belotserkovskaya R, Coates J, Galanty Y, Demir M, Morton CR, Rzechorzek NJ, Jackson SP, et al. CtIP tetramer assembly is required for DNA-end resection and repair. *Nat Struct Mol Biol* (2015) **22**:150–157. doi:10.1038/nsmb.2937
154. Suck D, Lahm A, Oefner C. Structure refined to 2Å of a nicked DNA octanucleotide complex with DNase I. *Nature* (1988) **332**:464–468. doi:10.1038/332464a0
155. Mol CD, Kuo C-F, Thayer MM, Cunningham RP, Tainer JA. Structure and function of the multifunctional DNA-repair enzyme exonuclease III. *Nature* (1995) **374**:381–386. doi:10.1038/374381a0
156. Gorman MA, Morera S, Rothwell DG, de La Fortelle E, Mol CD, Tainer JA, Hickson ID, Freemont PS. The crystal structure of the human DNA repair endonuclease HAP1 suggests the recognition of extra-helical deoxyribose at DNA abasic sites. *EMBO J* (1997) **16**:6548–6558. doi:10.1093/emboj/16.21.6548
157. Beernink PT, Segelke BW, Hadi MZ, Erzberger JP, Wilson DM, Rupp B. Two divalent metal ions in the active site of a new crystal form of human apurinic/apyrimidinic endonuclease, ape1: implications for the catalytic mechanism 1 1Edited by I. A. Wilson. *J Mol Biol* (2001) **307**:1023–1034. doi:10.1006/jmbi.2001.4529

158. Liu Y, Kao H-I, Bambara RA. Flap Endonuclease 1: A Central Component of DNA Metabolism. *Annu Rev Biochem* (2004) **73**:589–615. doi:10.1146/annurev.biochem.73.012803.092453
159. Lee BI, Wilson DM. The RAD2 domain of human exonuclease 1 exhibits 5' to 3' exonuclease and flap structure-specific endonuclease activities. *J Biol Chem* (1999) **274**:37763–9. doi:10.1074/JBC.274.53.37763
160. West SC. The search for a human Holliday junction resolvase. *Biochem Soc Trans* (2009) **37**:519–26. doi:10.1042/BST0370519
161. Bębenek A, Ziuzia-Graczyk I. Fidelity of DNA replication—a matter of proofreading. *Curr Genet* (2018)1–12. doi:10.1007/s00294-018-0820-1
162. Kunkel TA, Bebenek K. DNA Replication Fidelity. *Annu Rev Biochem* (2000) **69**:497–529. doi:10.1146/annurev.biochem.69.1.497
163. McCulloch SD, Kunkel TA. The fidelity of DNA synthesis by eukaryotic replicative and translesion synthesis polymerases. *Cell Res* (2008) **18**:148–161. doi:10.1038/cr.2008.4
164. St Charles JA, Liberti SE, Williams JS, Lujan SA, Kunkel TA. Quantifying the contributions of base selectivity, proofreading and mismatch repair to nuclear DNA replication in Saccharomyces cerevisiae. *DNA Repair (Amst)* (2015) **31**:41–51. doi:10.1016/j.dnarep.2015.04.006
165. Goldsby RE, Hays LE, Chen X, Olmsted EA, Slayton WB, Spangrude GJ, Preston BD. High incidence of epithelial cancers in mice deficient for DNA polymerase delta proofreading. *Proc Natl Acad Sci U S A* (2002) **99**:15560–5. doi:10.1073/pnas.232340999
166. Uchimura A, Hidaka Y, Hirabayashi T, Hirabayashi M, Yagi T. DNA Polymerase δ Is Required for Early Mammalian Embryogenesis. *PLoS One* (2009) **4**:e4184. doi:10.1371/journal.pone.0004184
167. Albertson TM, Ogawa M, Bugni JM, Hays LE, Chen Y, Wang Y, Treuting PM, Heddle J a, Goldsby RE, Preston BD. DNA polymerase epsilon and delta proofreading suppress discrete mutator and cancer phenotypes in mice. *Proc Natl Acad Sci U S A* (2009) **106**:17101–4. doi:10.1073/pnas.0907147106
168. Flohr T, Dai JC, Büttner J, Popanda O, Hagmüller E, Thielmann HW. Detection of mutations in the DNA polymerase delta gene of human sporadic colorectal cancers and colon cancer cell lines. *Int J cancer* (1999) **80**:919–29. Available at: http://www.ncbi.nlm.nih.gov/pubmed/10074927 [Accessed September 12,

2018]

169. Daee DL, Mertz TM, Shcherbakova P V. A cancer-associated DNA polymerase delta variant modeled in yeast causes a catastrophic increase in genomic instability. *Proc Natl Acad Sci* (2010) **107**:157–162. doi:10.1073/pnas.0907526106
170. Linxweiler W, Hörz W. Sequence specificity of exonuclease III from E. coli. *Nucleic Acids Res* (1982) **10**:4845–4859. doi:10.1093/nar/10.16.4845
171. Herrera JE, Chaires JB. Characterization of Preferred Deoxyribonuclease I Cleavage Sites. *J Mol Biol* (1994) **236**:405–411. doi:10.1006/jmbi.1994.1152
172. Nimonkar A V, Genschel J, Kinoshita E, Polaczek P, Campbell JL, Wyman C, Modrich P, Kowalczykowski SC. BLM-DNA2-RPA-MRN and EXO1-BLM-RPA-MRN constitute two DNA end resection machineries for human DNA break repair. *Genes Dev* (2011) **25**:350–62. doi:10.1101/gad.2003811
173. Mansilla-Soto J, Cortes P. VDJ recombination: Artemis and its in vivo role in hairpin opening. *J Exp Med* (2003) **197**:543–7. doi:10.1084/JEM.20022210
174. Kirchgessner CU, Patil CK, Evans JW, Cuomo CA, Fried LM, Carter T, Oettinger MA, Brown JM. DNA-dependent kinase (p350) as a candidate gene for the murine SCID defect. *Science* (1995) **267**:1178–83. Available at: http://www.ncbi.nlm.nih.gov/pubmed/7855601 [Accessed September 12, 2018]
175. Moshous D, Callebaut I, de Chasseval R, Corneo B, Cavazzana-Calvo M, Le Deist F, Tezcan I, Sanal O, Bertrand Y, Philippe N, et al. Artemis, a novel DNA double-strand break repair/V(D)J recombination protein, is mutated in human severe combined immune deficiency. *Cell* (2001) **105**:177–86. Available at: http://www.ncbi.nlm.nih.gov/pubmed/11336668 [Accessed September 12, 2018]
176. Shevelev I V., Hübscher U. The 3′–5′ exonucleases. *Nat Rev Mol Cell Biol* (2002) **3**:364–376. doi:10.1038/nrm804
177. Marti TM, Fleck O. DNA repair nucleases. *Cell Mol Life Sci* (2004) **61**:336–354. doi:10.1007/s00018-003-3223-4
178. Burgers PM, Koonin E V, Bruford E, Blanco L, Burtis KC, Christman MF, Copeland WC, Friedberg EC, Hanaoka F, Hinkle DC, et al. Eukaryotic DNA polymerases: proposal for a revised nomenclature. *J Biol Chem* (2001) **276**:43487–90. doi:10.1074/jbc.R100056200
179. Perrino FW, Harvey S, McMillin S, Hollis T. The human TREX2 3’ → 5’-

exonuclease structure suggests a mechanism for efficient nonprocessive DNA catalysis. *J Biol Chem* (2005) **280**:15212–8. doi:10.1074/jbc.M500108200

180. Igor V. Shevelev1,2 KR, and Ulrich Hübscher1 *. The TREX2 3′→5′ Exonuclease Physically Interacts with DNA Polymerase δ and Increases Its Accuracy. *Sci World* (2002) **2**:275–281. Available at: file:///C:/Users/ecs210/Downloads/945346.pdf [Accessed March 27, 2018]
181. Claeys Bouuaert C, Keeney S. Distinct DNA-binding surfaces in the ATPase and linker domains of MutLγ determine its substrate specificities and exert separable functions in meiotic recombination and mismatch repair. *PLOS Genet* (2017) **13**:e1006722. doi:10.1371/journal.pgen.1006722
182. Anand R, Ranjha L, Cannavo E, Cejka P. Phosphorylated CtIP Functions as a Co-factor of the MRE11-RAD50-NBS1 Endonuclease in DNA End Resection. *Mol Cell* (2016) **64**:940–950. doi:10.1016/j.molcel.2016.10.017
183. Nowotny M, Gaidamakov SA, Crouch RJ, Yang W. Crystal structures of RNase H bound to an RNA/DNA hybrid: substrate specificity and metal-dependent catalysis. *Cell* (2005) **121**:1005–16. doi:10.1016/j.cell.2005.04.024
184. Wyatt HDM, Laister RC, Martin SR, Arrowsmith CH, West SC. The SMX DNA Repair Tri-nuclease. *Mol Cell* (2017) **65**:848–860.e11. doi:10.1016/j.molcel.2017.01.031
185. Abdullah UB, McGouran JF, Brolih S, Ptchelkine D, El-Sagheer AH, Brown T, McHugh PJ. RPA activates the XPF-ERCC1 endonuclease to initiate processing of DNA interstrand crosslinks. *EMBO J* (2017) **36**:2047–2060. doi:10.15252/embj.201796664
186. Buel E, Schwartz M. The use of DAPI as a replacement for ethidium bromide in forensic DNA analysis. *J Forensic Sci* (1995) **40**:275–8.
187. Schmidt F, Schmidt J, Riechers A, Haase S, Bosserhoff A-K, Heilmann J, König B. DNA Staining in Agarose Gels with ZN^{2+} -Cyclen-Pyrene. *Nucleosides, Nucleotides and Nucleic Acids* (2010) **29**:748–759. doi:10.1080/15257770.2010.515282
188. Gallagher SR. “Quantitation of DNA and RNA with Absorption and Fluorescence Spectroscopy,” in *Current Protocols in Immunology* (Hoboken, NJ, USA: John Wiley & Sons, Inc.), A.3L.1-A.3L.14. doi:10.1002/cpim.20
189. Bruijns B, Tiggelaar R, Gardeniers H. Dataset of the absorption, emission and excitation spectra and fluorescence intensity graphs of fluorescent cyanine

dyes for the quantification of low amounts of dsDNA. *Data Br* (2017) **10**:132–143. doi:10.1016/J.DIB.2016.11.090

190. Su X, Zhang C, Zhu X, Fang S, Weng R, Xiao X, Zhao M. Simultaneous Fluorescence Imaging of the Activities of DNases and 3′ Exonucleases in Living Cells with Chimeric Oligonucleotide Probes. *Anal Chem* (2013) **85**:9939–9946. doi:10.1021/ac402615c
191. Zhou Z, Zhu C, Ren J, Dong S. A graphene-based real-time fluorescent assay of deoxyribonuclease I activity and inhibition. *Anal Chim Acta* (2012) **740**:88–92. doi:10.1016/j.aca.2012.06.032
192. Sato S, Fujita K, Kanazawa M, Mukumoto K, Ohtsuka K, Waki M, Takenaka S. Electrochemical assay for deoxyribonuclease I activity. *Anal Biochem* (2008) **381**:233–239. doi:10.1016/j.ab.2008.07.014
193. Hillier SC, Frost CG, Jenkins ATA, Braven HT, Keay RW, Flower SE, Clarkson JM. An electrochemical study of enzymatic oligonucleotide digestion. *Bioelectrochemistry* (2004) **63**:307–310. doi:10.1016/j.bioelechem.2003.10.028
194. Sato S, Fujita K, Kanazawa M, Mukumoto K, Ohtsuka K, Takenaka S. Reliable ferrocenyloligonucleotide-immobilized electrodes and their application to electrochemical DNase I assay. *Anal Chim Acta* (2009) **645**:30–35. doi:10.1016/j.aca.2009.04.047
195. Ding J, Qin W. Potentiometric sensing of nuclease activities and oxidative damage of single-stranded DNA using a polycation-sensitive membrane electrode. *Biosens Bioelectron* (2013) **47**:559–565. doi:10.1016/j.bios.2013.03.066
196. Ye Y, Wen W, Xiang Y, Qi X, La Belle JT, Chen JJL, Wang J. Direct Electrochemical Monitoring of RNase Activity. *Electroanalysis* (2008) **20**:919–922. doi:10.1002/elan.200804172
197. Sato S, Takenaka S. Highly sensitive nuclease assays based on chemically modified DNA or RNA. *Sensors (Basel)* (2014) **14**:12437–50. doi:10.3390/s140712437
198. Aleksandrov R, Dotchev A, Poser I, Krastev D, Georgiev G, Panova G, Babukov Y, Danovski G, Dyankova T, Hubatsch L, et al. Protein Dynamics in Complex DNA Lesions. *Mol Cell* (2018) **69**:1046–1061.e5. doi:10.1016/j.molcel.2018.02.016

199. Helena J, Joubert A, Grobbelaar S, Nolte E, Nel M, Pepper M, Coetzee M, Mercier A. Deoxyribonucleic Acid Damage and Repair: Capitalizing on Our Understanding of the Mechanisms of Maintaining Genomic Integrity for Therapeutic Purposes. *Int J Mol Sci* (2018) **19**:1148. doi:10.3390/ijms19041148
200. Gospodinov A, Herceg Z. Chromatin structure in double strand break repair. *DNA Repair (Amst)* (2013) **12**:800–810. doi:10.1016/j.dnarep.2013.07.006
201. van Attikum H, Gasser SM. ATP-dependent chromatin remodeling and DNA double-strand break repair. *Cell Cycle* (2005) **4**:1011–4. Available at: http://www.ncbi.nlm.nih.gov/pubmed/16082209 [Accessed July 13, 2015]
202. Pokholok DK, Harbison CT, Levine S, Cole M, Hannett NM, Lee TI, Bell GW, Walker K, Rolfe PA, Herbolsheimer E, et al. Genome-wide map of nucleosome acetylation and methylation in yeast. *Cell* (2005) **122**:517–27. doi:10.1016/j.cell.2005.06.026
203. Ravens S, Yu C, Ye T, Stierle M, Tora L. Tip60 complex binds to active Pol II promoters and a subset of enhancers and co-regulates the c-Myc network in mouse embryonic stem cells. *Epigenetics Chromatin* (2015) **8**:45. doi:10.1186/s13072-015-0039-z
204. Struhl K. Histone acetylation and transcriptional regulatory mechanisms. *Genes Dev* (1998) **12**:599–606. doi:10.1101/gad.12.5.599
205. Hu Y, Fisher JB, Koprowski S, McAllister D, Kim M-S, Lough J. Homozygous disruption of the Tip60 gene causes early embryonic lethality. *Dev Dyn* (2009) **238**:2912–21. doi:10.1002/dvdy.22110
206. Nagar B. c-Abl Tyrosine Kinase and Inhibition by the Cancer Drug Imatinib (Gleevec/STI-571). *J Nutr* (2007) **137**:1518S–1523. Available at: http://jn.nutrition.org/content/137/6/1518S.full [Accessed August 18, 2015]
207. Gao C, Bourke E, Scobie M, Famme MA, Koolmeister T, Helleday T, Eriksson LA, Lowndes NF, Brown JAL. Rational design and validation of a Tip60 histone acetyltransferase inhibitor. *Sci Rep* (2014) **4**:5372. doi:10.1038/srep05372
208. Sheridan RM, Bentley DL. Selectable one-step PCR-mediated integration of a degron for rapid depletion of endogenous human proteins. *Biotechniques* (2016) **60**:69–74. doi:10.2144/000114378
209. Muramatsu M, Kinoshita K, Fagarasan S, Yamada S, Shinkai Y, Honjo T. Class switch recombination and hypermutation require activation-induced

cytidine deaminase (AID), a potential RNA editing enzyme. *Cell* (2000) **102**:553–63. doi:10.1016/S0092-8674(00)00078-7

210. Di Noia JM, Neuberger MS. Molecular mechanisms of antibody somatic hypermutation. *Annu Rev Biochem* (2007) **76**:1–22. doi:10.1146/annurev.biochem.76.061705.090740
211. Peled JU, Kuang FL, Iglesias-Ussel MD, Roa S, Kalis SL, Goodman MF, Scharff MD. The biochemistry of somatic hypermutation. *Annu Rev Immunol* (2008) **26**:481–511. doi:10.1146/annurev.immunol.26.021607.090236
212. Shaknovich R, Cerchietti L, Tsikitas L, Kormaksson M, De S, Figueroa ME, Ballon G, Yang SN, Weinhold N, Reimers M, et al. DNA methyltransferase 1 and DNA methylation patterning contribute to germinal center B-cell differentiation. *Blood* (2011) **118**:3559–69. doi:10.1182/blood-2011-06-357996
213. Chowdhury M, Forouhi O, Dayal S, McCloskey N, Gould HJ, Felsenfeld G, Fear DJ. Analysis of intergenic transcription and histone modification across the human immunoglobulin heavy-chain locus. *Proc Natl Acad Sci U S A* (2008) **105**:15872–7. doi:10.1073/pnas.0808462105
214. Jeevan-Raj BP, Robert I, Heyer V, Page A, Wang JH, Cammas F, Alt FW, Losson R, Reina-San-Martin B. Epigenetic tethering of AID to the donor switch region during immunoglobulin class switch recombination. *J Exp Med* (2011) **208**:1649–60. doi:10.1084/jem.20110118
215. Roa S, Kuang FL, Scharff MD. Does antisense make sense of AID targeting? *Proc Natl Acad Sci U S A* (2008) **105**:3661–2. doi:10.1073/pnas.0800935105
216. de Miranda NFCC, Peng R, Georgiou K, Wu C, Falk Sörqvist E, Berglund M, Chen L, Gao Z, Lagerstedt K, Lisboa S, et al. DNA repair genes are selectively mutated in diffuse large B cell lymphomas. *J Exp Med* (2013) **210**:1729–42. doi:10.1084/jem.20122842
217. Teive HAG, Moro A, Moscovich M, Arruda WO, Munhoz RP, Raskin S, Ashizawa T. Ataxia-telangiectasia — A historical review and a proposal for a new designation: ATM syndrome. *J Neurol Sci* (2015) **355**:3–6. doi:10.1016/j.jns.2015.05.022
218. Zan H, Casali P. Regulation of Aicda expression and AID activity. *Autoimmunity* (2013) **46**:83–101. doi:10.3109/08916934.2012.749244
219. Revy P, Muto T, Levy Y, Geissmann F, Plebani A, Sanal O, Catalan N, Forveille M, Dufourcq-Labelouse R, Gennery A, et al. Activation-induced

cytidine deaminase (AID) deficiency causes the autosomal recessive form of the Hyper-IgM syndrome (HIGM2). *Cell* (2000) **102**:565–75. doi:10.1016/S0092-8674(00)00079-9

220. Hwang JK, Alt FW, Yeap L-S. Related Mechanisms of Antibody Somatic Hypermutation and Class Switch Recombination. *Microbiol Spectr* (2015) **3**:MDNA3-0037-2014. doi:10.1128/microbiolspec.MDNA3-0037-2014
221. Duke JL, Liu M, Yaari G, Khalil AM, Tomayko MM, Shlomchik MJ, Schatz DG, Kleinstein SH. Multiple transcription factor binding sites predict AID targeting in non-Ig genes. *J Immunol* (2013) **190**:3878–88. doi:10.4049/jimmunol.1202547
222. Matthews AJ, Husain S, Chaudhuri J. Binding of AID to DNA Does Not Correlate with Mutator Activity. *J Immunol* (2014) **193**:252–257. doi:10.4049/jimmunol.1400433
223. Maeda K, Singh SK, Eda K, Kitabatake M, Pham P, Goodman MF, Sakaguchi N. GANP-mediated recruitment of activation-induced cytidine deaminase to cell nuclei and to immunoglobulin variable region DNA. *J Biol Chem* (2010) **285**:23945–53. doi:10.1074/jbc.M110.131441
224. Khair L, Guikema JEJ, Linehan EK, Ucher AJ, Leus NGJ, Ogilvie C, Lou Z, Schrader CE, Stavnezer J. ATM Increases Activation-Induced Cytidine Deaminase Activity at Downstream S Regions during Class-Switch Recombination. *J Immunol* (2014) **192**:4887–96. doi:10.4049/jimmunol.1303481
225. Perlot T, Li G, Alt FW. Antisense transcripts from immunoglobulin heavy-chain locus V(D)J and switch regions. *Proc Natl Acad Sci* (2008) **105**:3843–3848. doi:10.1073/pnas.0712291105
226. Muñoz IM, Rouse J. Control of histone methylation and genome stability by PTIP. *EMBO Rep* (2009) **10**:239–45. doi:10.1038/embor.2009.21
227. Stanlie A, Begum NA, Akiyama H, Honjo T. The DSIF subunits Spt4 and Spt5 have distinct roles at various phases of immunoglobulin class switch recombination. *PLoS Genet* (2012) **8**:e1002675. doi:10.1371/journal.pgen.1002675
228. Aida M, Hamad N, Stanlie A, Begum N a, Honjo T. Accumulation of the FACT complex, as well as histone H3.3, serves as a target marker for somatic hypermutation. *Proc Natl Acad Sci U S A* (2013) **110**:7784–9. doi:10.1073/pnas.1305859110

229. Husain A, Begum NA, Taniguchi T, Taniguchi H, Kobayashi M, Honjo T. Chromatin remodeller SMARCA4 recruits topoisomerase 1 and suppresses transcription-associated genomic instability. *Nat Commun* (2016) **7**:10549. doi:10.1038/ncomms10549
230. Kobayashi M, Sabouri Z, Sabouri S, Kitawaki Y, Pommier Y, Abe T, Kiyonari H, Honjo T. Decrease in topoisomerase I is responsible for activation-induced cytidine deaminase (AID)-dependent somatic hypermutation. *Proc Natl Acad Sci* (2011) **108**:19305–19310. doi:10.1073/pnas.1114522108
231. Romanello M, Schiavone D, Frey A, Sale JE. Histone H3.3 promotes IgV gene diversification by enhancing formation of AID-accessible single-stranded DNA. *EMBO J* (2016) **35**:1452–1464. doi:10.15252/embj.201693958
232. Kenter AL. AID targeting is dependent on RNA polymerase II pausing. *Semin Immunol* (2012) **24**:281–6. doi:10.1016/j.smim.2012.06.001
233. Kouzine F, Sanford S, Elisha-Feil Z, Levens D. The functional response of upstream DNA to dynamic supercoiling in vivo. *Nat Struct Mol Biol* (2008) **15**:146–154. doi:10.1038/nsmb.1372
234. Jeon J-H, Adamcik J, Dietler G, Metzler R. Supercoiling Induces Denaturation Bubbles in Circular DNA. *Phys Rev Lett* (2010) **105**:208101. doi:10.1103/PhysRevLett.105.208101
235. Stavnezer J, Linehan EK, Thompson MR, Habboub G, Ucher AJ, Kadungure T, Tsuchimoto D, Nakabeppu Y, Schrader CE. Differential expression of APE1 and APE2 in germinal centers promotes error-prone repair and A:T mutations during somatic hypermutation. *Proc Natl Acad Sci U S A* (2014)2–7. doi:10.1073/pnas.1405590111
236. Krijger PHL, van den Berk PCM, Wit N, Langerak P, Jansen JG, Reynaud C-A, de Wind N, Jacobs H. PCNA ubiquitination-independent activation of polymerase η during somatic hypermutation and DNA damage tolerance. *DNA Repair (Amst)* (2011) **10**:1051–9. doi:10.1016/j.dnarep.2011.08.005
237. Schöpf B, Bregenhorn S, Quivy J-P, Kadyrov FA, Almouzni G, Jiricny J. Interplay between mismatch repair and chromatin assembly. *Proc Natl Acad Sci U S A* (2012) **109**:1895–900. doi:10.1073/pnas.1106696109
238. Santos MA, Huen MSY, Jankovic M, Chen H-T, López-Contreras AJ, Klein IA, Wong N, Barbancho JLR, Fernandez-Capetillo O, Nussenzweig MC, et al. Class switching and meiotic defects in mice lacking the E3 ubiquitin ligase

RNF8. *J Exp Med* (2010) **207**:973–81. doi:10.1084/jem.20092308

239. Ramachandran S, Chahwan R, Nepal RM, Frieder D, Panier S, Roa S, Zaheen A, Durocher D, Scharff MD, Martin A. The RNF8/RNF168 ubiquitin ligase cascade facilitates class switch recombination. *Proc Natl Acad Sci U S A* (2010) **107**:809–814. doi:10.1073/pnas.0913790107
240. Zhang S, Chea J, Meng X, Zhou Y, Lee EYC, Lee MYWT. PCNA is ubiquitinated by RNF8. *Cell Cycle* (2008) **7**:3399–404. doi:10.4161/cc.7.21.6949
241. Schaetzlein S, Chahwan R, Avdievich E, Roa S, Wei K, Eoff RL, Sellers RS, Clark AB, Kunkel TA, Scharff MD, et al. Mammalian Exo1 encodes both structural and catalytic functions that play distinct roles in essential biological processes. *Proc Natl Acad Sci U S A* (2013) **110**:E2470-9. doi:10.1073/pnas.1308512110
242. van Nuland R, van Schaik FM, Simonis M, van Heesch S, Cuppen E, Boelens R, Timmers HM, van Ingen H. Nucleosomal DNA binding drives the recognition of H3K36-methylated nucleosomes by the PSIP1-PWWP domain. *Epigenetics Chromatin* (2013) **6**:12. doi:10.1186/1756-8935-6-12
243. Chahwan R, Edelmann W, Scharff MD, Roa S. AIDing antibody diversity by error-prone mismatch repair. *Semin Immunol* (2012) **24**:293–300. doi:10.1016/j.smim.2012.05.005
244. Kleczkowska HE, Marra G, Lettieri T, Jiricny J. hMSH3 and hMSH6 interact with PCNA and colocalize with it to replication foci. *Genes Dev* (2001) **15**:724–36. doi:10.1101/gad.191201
245. Ruthenburg AJ, Li H, Patel DJ, David Allis C. Multivalent engagement of chromatin modifications by linked binding modules. *Nat Rev Mol Cell Biol* (2007) **8**:983–994. doi:10.1038/nrm2298
246. Odegard VH, Kim ST, Anderson SM, Shlomchik MJ, Schatz DG. Histone modifications associated with somatic hypermutation. *Immunity* (2005) **23**:101–10. doi:10.1016/j.immuni.2005.05.007
247. Duquette ML, Huber MD, Maizels N. G-Rich Proto-Oncogenes Are Targeted for Genomic Instability in B-Cell Lymphomas. *Cancer Res* (2007) **67**:
248. Larijani M, Frieder D, Basit W, Martin A. The mutation spectrum of purified AID is similar to the mutability index in Ramos cells and in ung(-/-)msh2(-/-) mice. *Immunogenetics* (2005) **56**:840–845. doi:10.1007/s00251-004-0748-0

249. Pham P, Bransteitter R, Petruska J, Goodman MF. Processive AID-catalysed cytosine deamination on single-stranded DNA simulates somatic hypermutation. *Nature* (2003) **424**:103–107. doi:10.1038/nature01760
250. Küppers R, Dalla-Favera R. Mechanisms of chromosomal translocations in B cell lymphomas. *Oncogene* (2001) **20**:5580–5594. doi:10.1038/sj.onc.1204640
251. Akasaka T, Lossos IS, Levy R. BCL6 gene translocation in follicular lymphoma: a harbinger of eventual transformation to diffuse aggressive lymphoma. *Blood* (2003) **102**:1443–1448. doi:10.1182/blood-2002-08-2482
252. Rossi D, Berra E, Cerri M, Deambrogi C, Barbieri C, Franceschetti S, Lunghi M, Conconi A, Paulli M, Matolcsy A, et al. Aberrant somatic hypermutation in transformation of follicular lymphoma and chronic lymphocytic leukemia to diffuse large B-cell lymphoma. *Haematologica* (2006) **91**:1405–9.
253. Zheng S, Vuong BQ, Vaidyanathan B, Lin J-Y, Huang F-T, Chaudhuri J. Non-coding RNA Generated following Lariat Debranching Mediates Targeting of AID to DNA. *Cell* (2015) **161**:762–773. doi:10.1016/j.cell.2015.03.020
254. Nowak U, Matthews AJ, Zheng S, Chaudhuri J. The splicing regulator PTBP2 interacts with the cytidine deaminase AID and promotes binding of AID to switch-region DNA. *Nat Immunol* (2011) **12**:160–6. doi:10.1038/ni.1977
255. Conticello SG, Ganesh K, Xue K, Lu M, Rada C, Neuberger MS. Interaction between Antibody-Diversification Enzyme AID and Spliceosome-Associated Factor CTNNBL1. *Mol Cell* (2008) **31**:474–484. doi:10.1016/j.molcel.2008.07.009
256. Doi T, Kato L, Ito S, Shinkura R, Wei M, Nagaoka H, Wang J, Honjo T. The C-terminal region of activation-induced cytidine deaminase is responsible for a recombination function other than DNA cleavage in class switch recombination. *Proc Natl Acad Sci U S A* (2009) **106**:2758–2763. doi:10.1073/pnas.0813253106
257. Barreto V, Reina-San-Martin B, Ramiro AR, McBride KM, Nussenzweig MC. C-terminal deletion of AID uncouples class switch recombination from somatic hypermutation and gene conversion. *Mol Cell* (2003) **12**:501–508. doi:10.1016/S1097-2765(03)00309-5
258. Basu U, Meng F-L, Keim C, Grinstein V, Pefanis E, Eccleston J, Zhang T, Myers D, Wasserman CR, Wesemann DR, et al. The RNA exosome targets the AID cytidine deaminase to both strands of transcribed duplex DNA

substrates. *Cell* (2011) **144**:353–63. doi:10.1016/j.cell.2011.01.001

259. Pefanis E, Wang J, Rothschild G, Lim J, Chao J, Rabadan R, Economides AN, Basu U. Noncoding RNA transcription targets AID to divergently transcribed loci in B cells. *Nature* (2014) **514**:389–393. doi:10.1038/nature13580
260. Pefanis E, Wang J, Rothschild G, Lim J, Kazadi D, Sun J, Federation A, Chao J, Elliott O, Liu Z-P, et al. RNA Exosome-Regulated Long Non-Coding RNA Transcription Controls Super-Enhancer Activity. *Cell* (2015) **161**:774–789. doi:10.1016/j.cell.2015.04.034
261. Kluiver J, Haralambieva E, de Jong D, Blokzijl T, Jacobs S, Kroesen B-J, Poppema S, van den Berg A. Lack of BIC and microRNA miR-155 expression in primary cases of Burkitt lymphoma. *Genes Chromosomes Cancer* (2006) **45**:147–53. doi:10.1002/gcc.20273
262. Garrett FE, Emelyanov A V, Sepulveda MA, Flanagan P, Volpi S, Li F, Loukinov D, Eckhardt LA, Lobanenkov V V, Birshtein BK. Chromatin architecture near a potential 3’ end of the igh locus involves modular regulation of histone modifications during B-Cell development and in vivo occupancy at CTCF sites. *Mol Cell Biol* (2005) **25**:1511–25. doi:10.1128/MCB.25.4.1511-1525.2005
263. Giambra V, Volpi S, Emelyanov A V, Pflugh D, Bothwell ALM, Norio P, Fan Y, Ju Z, Skoultchi AI, Hardy RR, et al. Pax5 and linker histone H1 coordinate DNA methylation and histone modifications in the 3’ regulatory region of the immunoglobulin heavy chain locus. *Mol Cell Biol* (2008) **28**:6123–33. doi:10.1128/MCB.00233-08
264. Dorsett Y, McBride KM, Jankovic M, Gazumyan A, Thai T-H, Robbiani DF, Di Virgilio M, Reina San-Martin B, Heidkamp G, Schwickert TA, et al. MicroRNA-155 suppresses activation-induced cytidine deaminase-mediated Myc-Igh translocation. *Immunity* (2008) **28**:630–8. doi:10.1016/j.immuni.2008.04.002
265. Fairfax KA, Gantier MP, Mackay F, Williams BRG, McCoy CE. IL-10 regulates Aicda expression through miR-155. *J Leukoc Biol* (2015) **97**:71–78. doi:10.1189/jlb.2A0314-178R
266. de Yébenes VG, Belver L, Pisano DG, González S, Villasante A, Croce C, He L, Ramiro AR. miR-181b negatively regulates activation-induced cytidine deaminase in B cells. *J Exp Med* (2008) **205**:2199–206. doi:10.1084/jem.20080579

267. Borchert GM, Holton NW, Larson ED. Repression of human activation induced cytidine deaminase by miR-93 and miR-155. *BMC Cancer* (2011) **11**:347. doi:10.1186/1471-2407-11-347
268. Teng G, Hakimpour P, Landgraf P, Rice A, Tuschl T, Casellas R, Papavasiliou FN. MicroRNA-155 is a negative regulator of activation-induced cytidine deaminase. *Immunity* (2008) **28**:621–9. doi:10.1016/j.immuni.2008.03.015
269. Basso K, Schneider C, Shen Q, Holmes AB, Setty M, Leslie C, Dalla-Favera R. BCL6 positively regulates AID and germinal center gene expression via repression of miR-155. *J Exp Med* (2012) **209**:2455–65. doi:10.1084/jem.20121387
270. Wang X, Wang K, Han L, Zhang A, Shi Z, Zhang K, Zhang H, Yang S, Pu P, Shen C, et al. PRDM1 is directly targeted by miR-30a-5p and modulates the Wnt/β-catenin pathway in a Dkk1-dependent manner during glioma growth. *Cancer Lett* (2013) **331**:211–219. doi:10.1016/j.canlet.2013.01.005
271. Gururajan M, Haga CL, Das S, Leu C-M, Hodson D, Josson S, Turner M, Cooper MD. MicroRNA 125b inhibition of B cell differentiation in germinal centers. *Int Immunol* (2010) **22**:583–592. doi:10.1093/intimm/dxq042
272. Rossi RL, Rossetti G, Wenandy L, Curti S, Ripamonti A, Bonnal RJP, Birolo RS, Moro M, Crosti MC, Gruarin P, et al. Distinct microRNA signatures in human lymphocyte subsets and enforcement of the naive state in CD4+ T cells by the microRNA miR-125b. *Nat Immunol* (2011) **12**:796–803. doi:10.1038/ni.2057
273. White CA, Pone EJ, Lam T, Tat C, Hayama KL, Li G, Zan H, Casali P. Histone deacetylase inhibitors upregulate B cell microRNAs that silence AID and Blimp-1 expression for epigenetic modulation of antibody and autoantibody responses. *J Immunol* (2014) **193**:5933–50. doi:10.4049/jimmunol.1401702
274. Lu D, Nakagawa R, Lazzaro S, Staudacher P, Abreu-Goodger C, Henley T, Boiani S, Leyland R, Galloway A, Andrews S, et al. The miR-155-PU.1 axis acts on Pax5 to enable efficient terminal B cell differentiation. *J Exp Med* (2014) **211**:2183–98. doi:10.1084/jem.20140338
275. Nakagawa R, Leyland R, Meyer-Hermann M, Lu D, Turner M, Arbore G, Phan TG, Brink R, Vigorito E. MicroRNA-155 controls affinity-based selection by protecting c-MYC+ B cells from apoptosis. *J Clin Invest* (2016) **126**:377–88. doi:10.1172/JCI82914

276. Rodriguez A, Vigorito E, Clare S, Warren M V, Couttet P, Soond DR, van Dongen S, Grocock RJ, Das PP, Miska EA, et al. Requirement of bic/microRNA-155 for normal immune function. *Science* (2007) **316**:608–11. doi:10.1126/science.1139253
277. Vigorito E, Perks KL, Abreu-Goodger C, Bunting S, Xiang Z, Kohlhaas S, Das PP, Miska EA, Rodriguez A, Bradley A, et al. microRNA-155 regulates the generation of immunoglobulin class-switched plasma cells. *Immunity* (2007) **27**:847–59. doi:10.1016/j.immuni.2007.10.009
278. Thai T-H, Calado DP, Casola S, Ansel KM, Xiao C, Xue Y, Murphy A, Frendewey D, Valenzuela D, Kutok JL, et al. Regulation of the germinal center response by microRNA-155. *Science* (2007) **316**:604–608. doi:10.1126/science.1141229
279. Valadi H, Ekström K, Bossios A, Sjöstrand M, Lee JJ, Lötvall JO. Exosome-mediated transfer of mRNAs and microRNAs is a novel mechanism of genetic exchange between cells. *Nat Cell Biol* (2007) **9**:654–659. doi:10.1038/ncb1596
280. Squadrito ML, Baer C, Burdet F, Maderna C, Gilfillan GD, Lyle R, Ibberson M, De Palma M. Endogenous RNAs Modulate MicroRNA Sorting to Exosomes and Transfer to Acceptor Cells. *Cell Rep* (2014) **8**:1432–1446. doi:10.1016/j.celrep.2014.07.035
281. Turner M, Galloway A, Vigorito E. Noncoding RNA and its associated proteins as regulatory elements of the immune system. *Nat Immunol* (2014) **15**:484–91. doi:10.1038/ni.2887
282. Montecalvo A, Larregina AT, Shufesky WJ, Stolz DB, Sullivan MLG, Karlsson JM, Baty CJ, Gibson GA, Erdos G, Wang Z, et al. Mechanism of transfer of functional microRNAs between mouse dendritic cells via exosomes. *Blood* (2012) **119**:756–66. doi:10.1182/blood-2011-02-338004
283. Cerutti A. The regulation of IgA class switching. *Nat Rev Immunol* (2008) **8**:421–34. doi:10.1038/nri2322
284. Muntasell A, Berger AC, Roche PA. T cell-induced secretion of MHC class II–peptide complexes on B cell exosomes. *EMBO J* (2007) **26**:4263–4272. doi:10.1038/sj.emboj.7601842
285. Wang L, Whang N, Wuerffel R, Kenter AL. AID-dependent histone acetylation is detected in immunoglobulin S regions. *J Exp Med* (2006) **203**:215–26. doi:10.1084/jem.20051774

286. Wang L, Wuerffel R, Feldman S, Khamlichi AA, Kenter AL. S region sequence, RNA polymerase II, and histone modifications create chromatin accessibility during class switch recombination. *J Exp Med* (2009) **206**:1817–30. doi:10.1084/jem.20081678
287. Daniel JA, Santos MA, Wang Z, Zang C, Schwab KR, Jankovic M, Filsuf D, Chen H-T, Gazumyan A, Yamane A, et al. PTIP promotes chromatin changes critical for immunoglobulin class switch recombination. *Science* (2010) **329**:917–23. doi:10.1126/science.1187942
288. Nambu Y, Sugai M, Gonda H, Lee C-G, Katakai T, Agata Y, Yokota Y, Shimizu A. Transcription-coupled events associating with immunoglobulin switch region chromatin. *Science* (2003) **302**:2137–40. doi:10.1126/science.1092481
289. Kuang FL, Luo Z, Scharff MD. H3 trimethyl K9 and H3 acetyl K9 chromatin modifications are associated with class switch recombination. *Pnas* (2009) **106**:5288–5293.
290. Stanlie A, Aida M, Muramatsu M, Honjo T, Begum N a. Histone3 lysine4 trimethylation regulated by the facilitates chromatin transcription complex is critical for DNA cleavage in class switch recombination. *Proc Natl Acad Sci U S A* (2010) **107**:22190–22195. doi:10.1073/pnas.1016923108
291. Yamane A, Resch W, Kuo N, Kuchen S, Li Z, Sun H, Robbiani DF, McBride K, Nussenzweig MC, Casellas R. Deep-sequencing identification of the genomic targets of the cytidine deaminase AID and its cofactor RPA in B lymphocytes. *Nat Immunol* (2011) **12**:62–9. doi:10.1038/ni.1964
292. Starnes LM, Su D, Pikkupeura LM, Weinert BT, Santos MA, Mund A, Soria R, Cho Y-W, Pozdnyakova I, Kubec Højfeldt M, et al. A PTIP-PA1 subcomplex promotes transcription for IgH class switching independently from the associated MLL3/MLL4 methyltransferase complex. *Genes Dev* (2016) **30**:149–63. doi:10.1101/gad.268797.115
293. Ortega-Molina A, Boss IW, Canela A, Pan H, Jiang Y, Zhao C, Jiang M, Hu D, Agirre X, Niesvizky I, et al. The histone lysine methyltransferase KMT2D sustains a gene expression program that represses B cell lymphoma development. *Nat Med* (2015) **21**:1199–208. doi:10.1038/nm.3943
294. Lindsley AW, Saal HM, Burrow TA, Hopkin RJ, Shchelochkov O, Khandelwal P, Xie C, Bleesing J, Filipovich L, Risma K, et al. Defects of B-cell terminal differentiation in patients with type-1 Kabuki syndrome. *J Allergy Clin Immunol*

(2016) **137**:179–187.e10. doi:10.1016/j.jaci.2015.06.002

295. Aida M, Honjo T. FACT and H3.3: New markers for the somatic hypermutation. *Cell Cycle* (2013) **12**:2923–2924. doi:10.4161/cc.26178
296. Kobayashi M, Aida M, Nagaoka H, Begum NA, Kitawaki Y, Nakata M, Stanlie A, Doi T, Kato L, Okazaki I, et al. AID-induced decrease in topoisomerase 1 induces DNA structural alteration and DNA cleavage for class switch recombination. *Proc Natl Acad Sci U S A* (2009) **106**:22375–80. doi:10.1073/pnas.0911879106
297. Rodríguez-Cortez VC, Martínez-Redondo P, Català-Moll F, Rodríguez-Ubreva J, Garcia-Gomez A, Poorani-Subramani G, Ciudad L, Hernando H, Pérez-García A, Company C, et al. Activation-induced cytidine deaminase targets SUV4-20-mediated histone H4K20 trimethylation to class-switch recombination sites. *Sci Rep* (2017) **7**:7594. doi:10.1038/s41598-017-07380-9
298. Schotta G, Sengupta R, Kubicek S, Malin S, Kauer M, Callen E, Celeste A, Pagani M, Opravil S, De La Rosa-Velazquez IA, et al. A chromatin-wide transition to H4K20 monomethylation impairs genome integrity and programmed DNA rearrangements in the mouse. *Genes Dev* (2008) **22**:2048–2061. doi:10.1101/gad.476008
299. Kapoor-Vazirani P, Kagey JD, Vertino PM. SUV420H2-mediated H4K20 trimethylation enforces RNA polymerase II promoter-proximal pausing by blocking hMOF-dependent H4K16 acetylation. *Mol Cell Biol* (2011) **31**:1594–609. doi:10.1128/MCB.00524-10
300. Sun Y, Jiang X, Xu Y, Ayrapetov MK, Moreau L a, Whetstine JR, Price BD. Histone H3 methylation links DNA damage detection to activation of the tumour suppressor Tip60. *Nat Cell Biol* (2009) **11**:1376–1382. doi:10.1038/ncb1982
301. Gospodinov A, Herceg Z. Chromatin structure in double strand break repair. *DNA Repair (Amst)* (2013) **12**:800–810. doi:10.1016/j.dnarep.2013.07.006
302. Li G, White C a., Lam T, Pone EJ, Tran DC, Hayama KL, Zan H, Xu Z, Casali P. Combinatorial H3K9acS10ph histone modification in igh locus s regions targets 14-3-3 adaptors and aid to specify antibody class-switch DNA recombination. *Cell Rep* (2013) **5**:702–714. doi:10.1016/j.celrep.2013.09.031
303. Winter S, Fischle W, Seiser C. Modulation of 14-3-3 interaction with phosphorylated histone H3 by combinatorial modification patterns. *Cell Cycle*

(2008) **7**:1336–1342. doi:10.4161/cc.7.10.5946

304. Walter W, Clynes D, Tang Y, Marmorstein R, Mellor J, Berger SL. 14-3-3 interaction with histone H3 involves a dual modification pattern of phosphoacetylation. *Mol Cell Biol* (2008) **28**:2840–2849. doi:10.1128/MCB.01457-07
305. Xu Z, Fulop Z, Wu G, Pone EJ, Zhang J, Mai T, Thomas LM, Al-Qahtani A, White CA, Park S-R, et al. 14-3-3 adaptor proteins recruit AID to 5'-AGCT-3'-rich switch regions for class switch recombination. *Nat Struct Mol Biol* (2010) **17**:1124–35. doi:10.1038/nsmb.1884
306. Noon AT, Goodarzi A a. 53BP1-mediated DNA double strand break repair: Insert bad pun here. *DNA Repair (Amst)* (2011) **10**:1071–1076. doi:10.1016/j.dnarep.2011.07.012
307. Nakamura K, Sakai W, Kawamoto T, Bree RT, Lowndes NF, Takeda S, Taniguchi Y. Genetic dissection of vertebrate 53BP1: A major role in non-homologous end joining of DNA double strand breaks. *DNA Repair (Amst)* (2006) **5**:741–749. doi:10.1016/j.dnarep.2006.03.008
308. Dimitrova N, Chen Y-CM, Spector DL, de Lange T. 53BP1 promotes non-homologous end joining of telomeres by increasing chromatin mobility. *Nature* (2008) **456**:524–8. doi:10.1038/nature07433
309. Ward IM. 53BP1 is required for class switch recombination. *J Cell Biol* (2004) **165**:459–464. doi:10.1083/jcb.200403021
310. Manis JP, Morales JC, Xia Z, Kutok JL, Alt FW, Carpenter PB. 53BP1 links DNA damage-response pathways to immunoglobulin heavy chain class-switch recombination. *Nat Immunol* (2004) **5**:481–7. doi:10.1038/ni1067
311. Bothmer A, Robbiani DF, Feldhahn N, Gazumyan A, Nussenzweig A, Nussenzweig MC. 53BP1 regulates DNA resection and the choice between classical and alternative end joining during class switch recombination. *J Exp Med* (2010) **207**:855–65. doi:10.1084/jem.20100244
312. Zimmermann M, de Lange T. 53BP1: pro choice in DNA repair. *Trends Cell Biol* (2014) **24**:108–117. doi:10.1016/j.tcb.2013.09.003
313. Botuyan MV, Lee J, Ward IM, Kim JE, Thompson JR, Chen J, Mer G. Structural Basis for the Methylation State-Specific Recognition of Histone H4-K20 by 53BP1 and Crb2 in DNA Repair. *Cell* (2006) **127**:1361–1373. doi:10.1016/j.cell.2006.10.043

314. Fradet-Turcotte A, Canny MD, Escribano-Díaz C, Orthwein A, Leung CCY, Huang H, Landry M-C, Kitevski-LeBlanc J, Noordermeer SM, Sicheri F, et al. 53BP1 is a reader of the DNA-damage-induced H2A Lys 15 ubiquitin mark. *Nature* (2013) **499**:50–56. doi:10.1038/nature12318
315. Rocha PP, Raviram R, Fu Y, Kim J, Luo VM, Aljoufi A, Swanzey E, Pasquarella A, Balestrini A, Miraldi ER, et al. A Damage-Independent Role for 53BP1 that Impacts Break Order and Igh Architecture during Class Switch Recombination. (2016). doi:10.1016/j.celrep.2016.05.073
316. Pfeiffer A, Luijsterburg MS, Acs K, Wiegant WW, Helfricht A, Herzog LK, Minoia M, Böttcher C, Salomons FA, van Attikum H, et al. Ataxin-3 consolidates the MDC1-dependent DNA double-strand break response by counteracting the SUMO-targeted ubiquitin ligase RNF4. *EMBO J* (2017) **36**:1066–1083. doi:10.15252/embj.201695151
317. Pei H, Wu X, Liu T, Yu K, Jelinek DF, Lou Z. The histone methyltransferase MMSET regulates class switch recombination. *J Immunol* (2013) **190**:756–63. doi:10.4049/jimmunol.1201811
318. Pei H, Zhang L, Luo K, Qin Y, Chesi M, Fei F, Bergsagel PL, Wang L, You Z, Lou Z. MMSET regulates histone H4K20 methylation and 53BP1 accumulation at DNA damage sites. *Nature* (2011) **470**:124–128. doi:10.1038/nature09658
319. Heng TSP, Painter MW, Elpek K, Lukacs-Kornek V, Mauermann N, Turley SJ, Koller D, Kim FS, Wagers AJ, Asinovski N, et al. The Immunological Genome Project: networks of gene expression in immune cells. *Nat Immunol* (2008) **9**:1091–1094. doi:10.1038/ni1008-1091
320. Oda H, Hübner MR, Beck DB, Vermeulen M, Hurwitz J, Spector DL, Reinberg D, Abbas T, Sivaprasad U, Terai K, et al. Regulation of the histone H4 monomethylase PR-Set7 by CRL4(Cdt2)-mediated PCNA-dependent degradation during DNA damage. *Mol Cell* (2010) **40**:364–76. doi:10.1016/j.molcel.2010.10.011
321. Mattiroli F, Vissers JH a, Van Dijk WJ, Ikpa P, Citterio E, Vermeulen W, Marteijn J a., Sixma TK. RNF168 ubiquitinates K13-15 on H2A/H2AX to drive DNA damage signaling. *Cell* (2012) **150**:1182–1195. doi:10.1016/j.cell.2012.08.005
322. Gatti M, Pinato S, Maspero E, Soffientini P, Polo S, Penengo L. A novel

ubiquitin mark at the N-terminal tail of histone H2As targeted by RNF168 ubiquitin ligase. *Cell Cycle* (2012) **11**:2538–2544. doi:10.4161/cc.20919

323. Kocyłowski MK, Rey AJ, Stewart GS, Halazonetis TD. Ubiquitin-H2AX fusions render 53BP1 recruitment to DNA damage sites independent of RNF8 or RNF168. *Cell Cycle* (2015)37–41. doi:10.1080/15384101.2015.1010918
324. Acs K, Luijsterburg MS, Ackermann L, Salomons FA, Hoppe T, Dantuma NP. The AAA-ATPase VCP/p97 promotes 53BP1 recruitment by removing L3MBTL1 from DNA double-strand breaks. *Nat Struct Mol Biol* (2011) **18**:1345–50. doi:10.1038/nsmb.2188
325. Mallette FA, Mattiroli F, Cui G, Young LC, Hendzel MJ, Mer G, Sixma TK, Richard S. RNF8- and RNF168-dependent degradation of KDM4A/JMJD2A triggers 53BP1 recruitment to DNA damage sites. *EMBO J* (2012) **31**:1865–78. doi:10.1038/emboj.2012.47
326. Fierz B, Chatterjee C, McGinty RK, Bar-Dagan M, Raleigh DP, Muir TW. Histone H2B ubiquitylation disrupts local and higher-order chromatin compaction. *Nat Chem Biol* (2011) **7**:113–9. doi:10.1038/nchembio.501
327. Ramachandran S, Haddad D, Li C, Le MX, Ling AK, So CC, Nepal RM, Gommerman JL, Yu K, Ketela T, et al. The SAGA Deubiquitination Module Promotes DNA Repair and Class Switch Recombination through ATM and DNAPK-Mediated gH2AX Formation. *Cell Rep* (2016) **15**:1554–1565. doi:10.1016/j.celrep.2016.04.041
328. Callén E, Jankovic M, Wong N, Zha S, Chen H-T, Difilippantonio S, Di Virgilio M, Heidkamp G, Alt FW, Nussenzweig A, et al. Essential role for DNA-PKcs in DNA double-strand break repair and apoptosis in ATM-deficient lymphocytes. *Mol Cell* (2009) **34**:285–97. doi:10.1016/j.molcel.2009.04.025
329. Dey A, Chitsaz F, Abbasi A, Misteli T, Ozato K. The double bromodomain protein Brd4 binds to acetylated chromatin during interphase and mitosis. *Proc Natl Acad Sci U S A* (2003) **100**:8758–8763. doi:10.1073/pnas.1433065100
330. Stanlie A, Yousif AS, Akiyama H, Honjo T, Begum N a. Chromatin reader Brd4 functions in Ig class switching as a repair complex adaptor of nonhomologous end-joining. *Mol Cell* (2014) **55**:97–110. doi:10.1016/j.molcel.2014.05.018
331. Kracker S, Virgilio D, Schwartzentruber J, Cuenin C, Di Virgilio M, Schwartzentruber J, Cuenin C, Forveille M, Deau M-C, McBride KM, et al. An inherited immunoglobulin class-switch recombination deficiency associated

with a defect in the INO80 chromatin remodeling complex. *J Allergy Clin Immunol* (2014) doi:10.1016/j.jaci.2014.08.030

332. Gospodinov A, Vaissiere T, Krastev DB, Legube G, Anachkova B, Herceg Z. Mammalian Ino80 mediates double-strand break repair through its role in DNA end strand resection. *Mol Cell Biol* (2011) **31**:4735–45. doi:10.1128/MCB.06182-11
333. Min J-N, Tian Y, Xiao Y, Wu L, Li L, Chang S. The mINO80 chromatin remodeling complex is required for efficient telomere replication and maintenance of genome stability. *Cell Res* (2013) **23**:1396–413. doi:10.1038/cr.2013.113
334. Hodge CD, Ismail IH, Edwards RA, Hura GL, Xiao AT, Tainer JA, Hendzel MJ, Glover JNM. RNF8 E3 Ubiquitin Ligase Stimulates Ubc13 E2 Conjugating Activity That Is Essential for DNA Double Strand Break Signaling and BRCA1 Tumor Suppressor Recruitment. *J Biol Chem* (2016) **291**:9396–410. doi:10.1074/jbc.M116.715698
335. Zhao Y, Brickner JR, Majid MC, Mosammaparast N. Crosstalk between ubiquitin and other post-translational modifications on chromatin during double-strand break repair. *Trends Cell Biol* (2014) **24**:426–34. doi:10.1016/j.tcb.2014.01.005
336. Panier S, Boulton SJ. Double-strand break repair: 53BP1 comes into focus. *Nat Rev Mol Cell Biol* (2013) **15**:7–18. doi:10.1038/nrm3719
337. Morris JR, Boutell C, Keppler M, Densham R, Weekes D, Alamshah A, Butler L, Galanty Y, Pangon L, Kiuchi T, et al. The SUMO modification pathway is involved in the BRCA1 response to genotoxic stress. *Nature* (2009) **462**:886–90. doi:10.1038/nature08593
338. Galanty Y, Belotserkovskaya R, Coates J, Polo S, Miller KM, Jackson SP. Mammalian SUMO E3-ligases PIAS1 and PIAS4 promote responses to DNA double-strand breaks. *Nature* (2009) **462**:935–9. doi:10.1038/nature08657
339. Galanty Y, Belotserkovskaya R, Coates J, Jackson SP. RNF4, a SUMO-targeted ubiquitin E3 ligase, promotes DNA double-strand break repair. *Genes Dev* (2012) **26**:1179–95. doi:10.1101/gad.188284.112
340. Drané P, Brault M-E, Cui G, Meghani K, Chaubey S, Detappe A, Parnandi N, He Y, Zheng X-F, Botuyan MV, et al. TIRR regulates 53BP1 by masking its histone methyl-lysine binding function. *Nature* (2017) **543**:211–216.

doi:10.1038/nature21358

341. Chapman JR, Barral P, Vannier J-B, Borel V, Steger M, Tomas-Loba A, Sartori AA, Adams IR, Batista FD, Boulton SJ. RIF1 is essential for 53BP1-dependent nonhomologous end joining and suppression of DNA double-strand break resection. *Mol Cell* (2013) **49**:858–71. doi:10.1016/j.molcel.2013.01.002
342. Bunting SF, Callén E, Wong N, Chen H-T, Polato F, Gunn A, Bothmer A, Feldhahn N, Fernandez-Capetillo O, Cao L, et al. 53BP1 inhibits homologous recombination in Brca1-deficient cells by blocking resection of DNA breaks. *Cell* (2010) **141**:243–54. doi:10.1016/j.cell.2010.03.012
343. Jacquet K, Fradet-Turcotte A, Avvakumov N, Lambert JP, Roques C, Pandita RK, Paquet E, Herst P, Gingras AC, Pandita TK, et al. The TIP60 Complex Regulates Bivalent Chromatin Recognition by 53BP1 through Direct H4K20me Binding and H2AK15 Acetylation. *Mol Cell* (2016) **62**:409–421. doi:10.1016/j.molcel.2016.03.031
344. Rai K, Huggins IJ, James SR, Karpf AR, Jones DA, Cairns BR. DNA Demethylation in Zebrafish Involves the Coupling of a Deaminase, a Glycosylase, and Gadd45. *Cell* (2008) **135**:1201–1212. doi:10.1016/j.cell.2008.11.042
345. Kumar R, DiMenna L, Schrode N, Liu T-C, Franck P, Muñoz-Descalzo S, Hadjantonakis A-K, Zarrin AA, Chaudhuri J, Elemento O, et al. AID stabilizes stem-cell phenotype by removing epigenetic memory of pluripotency genes. *Nature* (2013) **500**:89–92. doi:10.1038/nature12299
346. Popp C, Dean W, Feng S, Cokus SJ, Andrews S, Pellegrini M, Jacobsen SE, Reik W. Genome-wide erasure of DNA methylation in mouse primordial germ cells is affected by AID deficiency. *Nature* (2010) **463**:1101–5. doi:10.1038/nature08829
347. Fritz EL, Rosenberg BR, Lay K, Mihailović A, Tuschl T, Papavasiliou FN. A comprehensive analysis of the effects of the deaminase AID on the transcriptome and methylome of activated B cells. *Nat Immunol* (2013) **14**:749–55. doi:10.1038/ni.2616
348. Fraenkel S, Mostoslavsky R, Novobrantseva TI, Pelanda R, Chaudhuri J, Esposito G, Jung S, Alt FW, Rajewsky K, Cedar H, et al. Allelic “choice” governs somatic hypermutation in vivo at the immunoglobulin kappa-chain locus. *Nat Immunol* (2007) **8**:715–22. doi:10.1038/ni1476

349. Nabel CS, Jia H, Ye Y, Shen L, Goldschmidt HL, Stivers JT, Zhang Y, Kohli RM. AID/APOBEC deaminases disfavor modified cytosines implicated in DNA demethylation. *Nat Chem Biol* (2012) **8**:751–758. doi:10.1038/nchembio.1042
350. Dominguez PM, Teater M, Chambwe N, Kormaksson M, Redmond D, Ishii J, Vuong B, Chaudhuri J, Melnick A, Vasanthakumar A, et al. DNA Methylation Dynamics of Germinal Center B Cells Are Mediated by AID. *Cell Rep* (2015) **12**:2086–2098. doi:10.1016/j.celrep.2015.08.036
351. Rogozin IB, Lada AG, Goncearenco A, Green MR, De S, Nudelman G, Panchenko AR, Koonin E V, Pavlov YI. Activation induced deaminase mutational signature overlaps with CpG methylation sites in follicular lymphoma and other cancers. *Sci Rep* (2016) **6**:38133. doi:10.1038/srep38133
352. Tsagaratou A, Lio C-WJ, Yue X, Rao A. TET Methylcytosine Oxidases in T Cell and B Cell Development and Function. *Front Immunol* (2017) **8**:220. doi:10.3389/fimmu.2017.00220
353. Ito S, Shen L, Dai Q, Wu SC, Collins LB, Swenberg JA, He C, Zhang Y. Tet proteins can convert 5-methylcytosine to 5-formylcytosine and 5-carboxylcytosine. *Science* (2011) **333**:1300–3. doi:10.1126/science.1210597
354. Tsagaratou A, Äijö T, Lio C-WJ, Yue X, Huang Y, Jacobsen SE, Lähdesmäki H, Rao A. Dissecting the dynamic changes of 5-hydroxymethylcytosine in T-cell development and differentiation. *Proc Natl Acad Sci U S A* (2014) **111**:E3306-15. doi:10.1073/pnas.1412327111
355. Ito S, Shen L, Dai Q, Wu SC, Collins LB, Swenberg JA, He C, Zhang Y. Tet proteins can convert 5-methylcytosine to 5-formylcytosine and 5-carboxylcytosine. *Science* (2011) **333**:1300–3. doi:10.1126/science.1210597
356. He Y-F, Li B-Z, Li Z, Liu P, Wang Y, Tang Q, Ding J, Jia Y, Chen Z, Li L, et al. Tet-mediated formation of 5-carboxylcytosine and its excision by TDG in mammalian DNA. *Science* (2011) **333**:1303–7. doi:10.1126/science.1210944
357. Wu SC, Zhang Y. Active DNA demethylation: many roads lead to Rome. *Nat Rev Mol Cell Biol* (2010) **11**:607–20. doi:10.1038/nrm2950
358. Liutkevičiūtė Z, Kriukienė E, Ličytė J, Rudytė M, Urbanavičiūtė G, Klimašauskas S. Direct Decarboxylation of 5-Carboxylcytosine by DNA C5-Methyltransferases. *J Am Chem Soc* (2014) **136**:5884–5887. doi:10.1021/ja5019223
359. Orlanski S, Labi V, Reizel Y, Spiro A, Lichtenstein M, Levin-Klein R, Koralov

SB, Skversky Y, Rajewsky K, Cedar H, et al. Tissue-specific DNA demethylation is required for proper B-cell differentiation and function. *Proc Natl Acad Sci U S A* (2016) **113**:5018–23. doi:10.1073/pnas.1604365113

360. Kulis M, Merkel A, Heath S, Queirós AC, Schuyler RP, Castellano G, Beekman R, Raineri E, Esteve A, Clot G, et al. Whole-genome fingerprint of the DNA methylome during human B cell differentiation. *Nat Genet* (2015) **47**:746–756. doi:10.1038/ng.3291
361. Quivoron C, Couronné L, Della Valle V, Lopez CK, Plo I, Wagner-Ballon O, Do Cruzeiro M, Delhommeau F, Arnulf B, Stern M-H, et al. TET2 inactivation results in pleiotropic hematopoietic abnormalities in mouse and is a recurrent event during human lymphomagenesis. *Cancer Cell* (2011) **20**:25–38. doi:10.1016/j.ccr.2011.06.003
362. Cimmino L, Dawlaty MM, Ndiaye-Lobry D, Yap YS, Bakogianni S, Yu Y, Bhattacharyya S, Shaknovich R, Geng H, Lobry C, et al. TET1 is a tumor suppressor of hematopoietic malignancy. *Nat Immunol* (2015) **16**:653–662. doi:10.1038/ni.3148
363. Lio C-W, Zhang J, González-Avalos E, Hogan PG, Chang X, Rao A. Tet2 and Tet3 cooperate with B-lineage transcription factors to regulate DNA modification and chromatin accessibility. *Elife* (2016) **5**: doi:10.7554/eLife.18290
364. Zhao Z, Chen L, Dawlaty MM, Pan F, Weeks O, Zhou Y, Cao Z, Shi H, Wang J, Lin L, et al. Combined Loss of Tet1 and Tet2 Promotes B Cell, but Not Myeloid Malignancies, in Mice. *Cell Rep* (2015) **13**:1692–1704. doi:10.1016/j.celrep.2015.10.037
365. Rangam G, Schmitz K-M, Cobb AJA, Petersen-Mahrt SK, MacDougall E. AID Enzymatic Activity Is Inversely Proportional to the Size of Cytosine C5 Orbital Cloud. *PLoS One* (2012) **7**:e43279. doi:10.1371/journal.pone.0043279
366. Guo JU, Su Y, Zhong C, Ming G, Song H. Hydroxylation of 5-Methylcytosine by TET1 Promotes Active DNA Demethylation in the Adult Brain. *Cell* (2011) **145**:423–434. doi:10.1016/j.cell.2011.03.022
367. Minegishi Y, Lavoie A, Cunningham-Rundles C, Bédard P-M, Hébert J, Côté L, Dan K, Sedlak D, Buckley RH, Fischer A, et al. Mutations in Activation-Induced Cytidine Deaminase in Patients with Hyper IgM Syndrome. *Clin Immunol* (2000) **97**:203–210. doi:10.1006/clim.2000.4956

368. De S, Shaknovich R, Riester M, Elemento O, Geng H, Kormaksson M, Jiang Y, Woolcock B, Johnson N, Polo JM, et al. Aberration in DNA Methylation in B-Cell Lymphomas Has a Complex Origin and Increases with Disease Severity. *PLoS Genet* (2013) **9**:e1003137. doi:10.1371/journal.pgen.1003137
369. Yamane A, Resch W, Kuo N, Kuchen S, Li Z, Sun H, Robbiani DF, McBride K, Nussenzweig MC, Casellas R. Deep-sequencing identification of the genomic targets of the cytidine deaminase AID and its cofactor RPA in B lymphocytes. *Nat Immunol* (2011) **12**:62–9. doi:10.1038/ni.1964
370. Matsumoto Y, Marusawa H, Kinoshita K, Niwa Y, Sakai Y, Chiba T. Up-regulation of Activation-Induced Cytidine Deaminase Causes Genetic Aberrations at the CDKN2b-CDKN2a in Gastric Cancer. *Gastroenterology* (2010) **139**:1984–1994. doi:10.1053/j.gastro.2010.07.010
371. Shinmura K, Igarashi H, Goto M, Tao H, Yamada H, Matsuura S, Tajima M, Matsuda T, Yamane A, Funai K, et al. Aberrant Expression and Mutation-Inducing Activity of AID in Human Lung Cancer. *Ann Surg Oncol* (2011) **18**:2084–2092. doi:10.1245/s10434-011-1568-8
372. Muñoz DP, Lee EL, Takayama S, Coppé J-P, Heo S-J, Boffelli D, Di Noia JM, Martin DIK. Activation-induced cytidine deaminase (AID) is necessary for the epithelial-mesenchymal transition in mammary epithelial cells. *Proc Natl Acad Sci U S A* (2013) **110**:E2977-86. doi:10.1073/pnas.1301021110
373. Endo Y, Marusawa H, Kinoshita K, Morisawa T, Sakurai T, Okazaki I-M, Watashi K, Shimotohno K, Honjo T, Chiba T. Expression of activation-induced cytidine deaminase in human hepatocytes via NF-κB signaling. *Oncogene* (2007) **26**:5587–5595. doi:10.1038/sj.onc.1210344
374. Stresemann C, Lyko F. Modes of action of the DNA methyltransferase inhibitors azacytidine and decitabine. *Int J Cancer* (2008) **123**:8–13. doi:10.1002/ijc.23607
375. Orthwein A, Patenaude A, Affar EB, Lamarre A, Young JC, Noia JM Di. Regulation of activation-induced deaminase stability and antibody gene diversification by Hsp90. (2010) **207**:2751–2765.
376. Goetz MP, Toft D, Reid J, Ames M, Stensgard B, Safgren S, Adjei AA, Sloan J, Atherton P, Vasile V, et al. Phase I Trial of 17-Allylamino-17-Demethoxygeldanamycin in Patients With Advanced Cancer. *J Clin Oncol* (2005) **23**:1078–1087. doi:10.1200/JCO.2005.09.119

377. Rebhandl S, Geisberger R. AIDing cancer treatment: Reducing AID activity via HSP90 inhibition. *Eur J Immunol* (2015)n/a-n/a. doi:10.1002/eji.201545832
378. Bartosova Z, Krejci L. Nucleases in homologous recombination as targets for cancer therapy. *FEBS Lett* (2014) **588**:2446–2456. doi:10.1016/J.FEBSLET.2014.06.010
379. Paull TT, Deshpande RA. The Mre11/Rad50/Nbs1 complex: recent insights into catalytic activities and ATP-driven conformational changes. *Exp Cell Res* (2014) **329**:139–47. doi:10.1016/j.yexcr.2014.07.007
380. Makharashvili N, Paull TT. CtIP: A DNA damage response protein at the intersection of DNA metabolism. *DNA Repair (Amst)* (2015) **32**:75–81. doi:10.1016/J.DNAREP.2015.04.016
381. Kosinski J, Feder M, Bujnicki JM. The PD-(D/E)XK superfamily revisited: identification of new members among proteins involved in DNA metabolism and functional predictions for domains of (hitherto) unknown function. *BMC Bioinformatics* (2005) **6**:172. doi:10.1186/1471-2105-6-172
382. Babbs C, Roberts NA, Sanchez-Pulido L, McGowan SJ, Ahmed MR, Brown JM, Sabry MA, Bentley DR, McVean GA, Donnelly P, et al. Homozygous mutations in a predicted endonuclease are a novel cause of congenital dyserythropoietic anemia type I. *Haematologica* (2013) **98**:1383–1387. doi:10.3324/haematol.2013.089490
383. Georgiou CD, Papapostolou I, Grintzalis K. Protocol for the quantitative assessment of DNA concentration and damage (fragmentation and nicks). *Nat Protoc* (2009) **4**:125–131.
384. Costa F, Barbisan F, Assmann CE, Araújo NKF, de Oliveira AR, Signori JP, Rogalski F, Bonadiman B, Fernandes MS, da Cruz IBM. Seminal cell-free DNA levels measured by PicoGreen fluorochrome are associated with sperm fertility criteria. *Zygote* (2017) **25**:111–119. doi:10.1017/S0967199416000307
385. Blotta I, Prestinaci F, Mirante S, Cantafora A. Quantitative assay of total dsDNA with PicoGreen reagent and real-time fluorescent detection. *Ann Ist Super Sanita* (2005) **41**:119–23.
386. Singer VL, Jones LJ, Yue ST, Haugland RP. Characterization of PicoGreen Reagent and Development of a Fluorescence-Based Solution Assay for Double-Stranded DNA Quantitation. *Anal Biochem* (1997) **249**:228–238. doi:10.1006/ABIO.1997.2177

387. Choi SJ, Szoka FC. Fluorometric determination of deoxyribonuclease I activity with PicoGreen. *Anal Biochem* (2000) **281**:95–97. doi:10.1006/abio.2000.4529
388. McKnight RE, Gleason AB, Keyes JA, Sahabi S. Binding mode and affinity studies of DNA-binding agents using topoisomerase I DNA unwinding assay. *Bioorg Med Chem Lett* (2007) **17**:1013–1017. doi:10.1016/J.BMCL.2006.11.038
389. Tveit H, Kristensen T. Fluorescence-based DNA polymerase assay. *Anal Biochem* (2001) **289**:96–98. doi:10.1006/abio.2000.4903
390. Driscoll MD, Rentergent J, Hay S. A quantitative fluorescence-based steady-state assay of DNA polymerase. *FEBS J* (2014) **281**:2042–50. doi:10.1111/FEBS.12760
391. Nasiri HR, Kiss L, Krämer J. A fluorescence polarization based assay for the identification and characterization of polymerase inhibitors. *Bioorg Med Chem Lett* (2016) **26**:4433–4435. doi:10.1016/J.BMCL.2016.08.003
392. Gelmini S, Caldini A, Becherini L, Capaccioli S, Pazzagli M, Orlando C. Rapid, quantitative nonisotopic assay for telomerase activity in human tumors. *Clin Chem* (1998) **44**:2133–8.
393. Koepsell SA, Hanson S, Hinrichs SH, Griep MA. Fluorometric assay for bacterial primases. *Anal Biochem* (2005) **339**:353–355. doi:10.1016/J.AB.2004.12.004
394. Rentergent J, Driscoll MD, Hay S. Time Course Analysis of Enzyme-Catalyzed DNA Polymerization. *Biochemistry* (2016) **55**:5622–5634. doi:10.1021/acs.biochem.6b00442
395. Dragan AI, Casas-Finet JR, Bishop ES, Strouse RJ, Schenerman MA, Geddes CD. Characterization of PicoGreen interaction with dsDNA and the origin of its fluorescence enhancement upon binding. *Biophys J* (2010) **99**:3010–9. doi:10.1016/j.bpj.2010.09.012
396. Harmon FG, Kowalczykowski SC. RecQ helicase, in concert with RecA and SSB proteins, initiates and disrupts DNA recombination. *Genes Dev* (1998) **12**:1134–44.
397. Bochman ML, Paeschke K, Zakian VA. DNA secondary structures: stability and function of G-quadruplex structures. *Nat Rev Genet* (2012) **13**:770–80. doi:10.1038/nrg3296
398. Sproat BS, Lamond AI, Beijer B, Neuner P, Ryder U. Highly efficient chemical

synthesis of 2’-O-methyloligoribonucleotides and tetrabiotinylated derivatives; novel probes that are resistant to degradation by RNA or DNA specific nucleases. *Nucleic Acids Res* (1989) **17**:3373–86. Available at: http://www.ncbi.nlm.nih.gov/pubmed/2726482 [Accessed June 3, 2018]

399. Patra A, Paolillo M, Charisse K, Manoharan M, Rozners E, Egli M. 2’-Fluoro RNA shows increased Watson-Crick H-bonding strength and stacking relative to RNA: evidence from NMR and thermodynamic data. *Angew Chem Int Ed Engl* (2012) **51**:11863–6. doi:10.1002/anie.201204946
400. Richardson CC, Kornberg A. A Deoxyribonucleic Acid Phosphatase-Exonuclease from Escherichia coli I. PURIFICATION OF THE ENZYME AND CHARACTERIZATION OF THE PHOSPHATASE ACTIVITY*. *J BIOLOQICAL Chem* (1964) **239**: Available at: http://www.jbc.org/content/239/1/242.full.pdf [Accessed June 3, 2018]
401. Ma MY, Jacob-Samuel B, Dignam JC, Pace U, Goldberg AR G ST. Nuclease-Resistant External Guide Sequence-Induced Cleavage of Target RNA by Human Ribonuclease P. *Antisense Nucleic Acid Drug Dev* (1998) **8**:415–426. doi:10.1089/oli.1.1998.8.415
402. Amarzguioui M, Holen T, Babaie E, Prydz H. Tolerance for mutations and chemical modifications in a siRNA. *Nucleic Acids Res* (2003) **31**:589–595. doi:10.1093/nar/gkg147
403. Braasch DA, Paroo Z, Constantinescu A, Ren G, Öz OK, Mason RP, Corey DR. Biodistribution of phosphodiester and phosphorothioate siRNA. *Bioorg Med Chem Lett* (2004) **14**:1139–1143. doi:10.1016/j.bmcl.2003.12.074
404. Geary RS, Yu RZ, Levin AA. Pharmacokinetics of phosphorothioate antisense oligodeoxynucleotides. *Curr Opin Investig Drugs* (2001) **2**:562–73. Available at: http://www.ncbi.nlm.nih.gov/pubmed/11566019 [Accessed June 3, 2018]
405. McGowan KB, Kurtis MS, Lottman LM, Watson D, Sah RL. Biochemical quantification of DNA in human articular and septal cartilage using PicoGreen and Hoechst 33258. *Osteoarthr Cartil* (2002) **10**:580–7. Available at: http://www.ncbi.nlm.nih.gov/pubmed/12127839 [Accessed June 3, 2018]
406. Choi S-J, Szoka FC. Fluorometric Determination of Deoxyribonuclease I Activity with PicoGreen. *Anal Biochem* (2000) **281**:95–97. doi:10.1006/abio.2000.4529
407. Tolun G, Myers RS. A real-time DNase assay (ReDA) based on PicoGreen

fluorescence. *Nucleic Acids Res* (2003) **31**:e111.

408. Lovett ST. The DNA Exonucleases of Escherichia coli. *EcoSal Plus* (2011) **4**: doi:10.1128/ecosalplus.4.4.7
409. Chen M-J, Ma S-M, Dumitrache LC, Hasty P. Biochemical and cellular characteristics of the 3’ -> 5’ exonuclease TREX2. *Nucleic Acids Res* (2007) **35**:2682–2694. doi:10.1093/nar/gkm151
410. Ponnaluri VKC, Zhang G, Estève P-O, Spracklin G, Sian S, Xu S, Benoukraf T, Pradhan S. NicE-seq: high resolution open chromatin profiling. *Genome Biol* (2017) **18**:122. doi:10.1186/s13059-017-1247-6
411. Udesh de Silva FWP and TH. DNA binding induces active site conformational change in the human TREX2 3’-exonuclease. *Nucleic Acids Res* (2009) **37**:2411–2417. doi:10.1093/nar/gkp025
412. Perrino FW, de Silva U, Harvey S, Pryor EE, Cole DW, Hollis T, Hollis T. Cooperative DNA binding and communication across the dimer interface in the TREX2 3’ → 5’-exonuclease. *J Biol Chem* (2008) **283**:21441–52. doi:10.1074/jbc.M803629200
413. Manils J, Gómez D, Salla-Martret M, Fischer H, Fye JM, Marzo E, Marruecos L, Serrano I, Salgado R, Rodrigo JP, et al. Multifaceted role of TREX2 in the skin defense against UV-induced skin carcinogenesis. *Oncotarget* (2015) **6**:22375–96. doi:10.18632/oncotarget.4296
414. Parra D, Manils J, Castellana B, Viña-Vilaseca A, Morán-Salvador E, Vázquez-Villoldo N, Tarancón G, Borràs M, Sancho S, Benito C, et al. Increased Susceptibility to Skin Carcinogenesis in TREX2 Knockout Mice. *Cancer Res* (2009) **69**:6676–84. doi:10.1158/0008-5472.CAN-09-1208
415. Genschel J, Bazemore LR, Modrich P. Human exonuclease I is required for 5’ and 3’ mismatch repair. *J Biol Chem* (2002) **277**:13302–11. doi:10.1074/jbc.M111854200
416. Tishkoff DX, Boerger AL, Bertrand P, Filosi N, Gaida GM, Kane MF, Kolodner RD. Identification and characterization of Saccharomyces cerevisiae EXO1, a gene encoding an exonuclease that interacts with MSH2. *Proc Natl Acad Sci U S A* (1997) **94**:7487–92. Available at: http://www.ncbi.nlm.nih.gov/pubmed/9207118 [Accessed June 3, 2018]
417. Henikoff S. Ordered deletions for DNA sequencing and in vitro mutagenesis by polymerase extension and exonuclease III gapping of circular templates.

Nucleic Acids Res **18**:

418. Henikoff S. Unidirectional digestion with exonuclease III creates targeted breakpoints for DNA sequencing. *Gene* (1984) **28**:351–9.
419. Ren B, Zhou J-M, Komiyama M. Straightforward detection of SNPs in double-stranded DNA by using exonuclease III/nuclease S1/PNA system. *Nucleic Acids Res* (2004) **32**:e42. doi:10.1093/nar/gnh039
420. Tao C, Yan Y, Xiang H, Zhu D, Cheng W, Ju H, Ding S. A new mode for highly sensitive and specific detection of DNA based on exonuclease III-assisted target recycling amplification and mismatched catalytic hairpin assembly. *Chem Commun (Camb)* (2015) **51**:4220–2. doi:10.1039/c5cc00385g
421. Tubbs A, Nussenzweig A. Endogenous DNA Damage as a Source of Genomic Instability in Cancer. (2017) doi:10.1016/j.cell.2017.01.002
422. Hsieh P, Zhang Y. The Devil is in the details for DNA mismatch repair. doi:10.1073/pnas.1702747114
423. Helleday T, Lo J, Vangent D, Engelward B. DNA double-strand break repair: From mechanistic understanding to cancer treatment. *DNA Repair (Amst)* (2007) **6**:923–935. doi:10.1016/j.dnarep.2007.02.006
424. Kim Y-J, M. Wilson III D. Overview of Base Excision Repair Biochemistry. *Curr Mol Pharmacol* (2012) **5**:3–13. Available at: http://www.ingentaconnect.com/content/ben/cmp/2012/00000005/00000001/art00002 [Accessed April 26, 2018]
425. Bessho T, Sancar A, Thompson LH, Thelen MP. Reconstitution of human excision nuclease with recombinant XPF-ERCC1 complex. *J Biol Chem* (1997) **272**:3833–7. doi:10.1074/JBC.272.6.3833
426. Franchini D-M, Chan C-F, Morgan H, Incorvaia E, Rangam G, Dean W, Santos F, Reik W, Petersen-Mahrt SK. Processive DNA Demethylation via DNA Deaminase-Induced Lesion Resolution. *PLoS One* (2014) **9**:e97754. doi:10.1371/journal.pone.0097754
427. Okano M, Xie S, Li E. Cloning and characterization of a family of novel mammalian DNA (cytosine-5) methyltransferases. *Nat Genet* (1998) **19**:219–220. doi:10.1038/890
428. Gowher H, Jeltsch A. Enzymatic properties of recombinant Dnmt3a DNA methyltransferase from mouse: the enzyme modifies DNA in a non-processive manner and also methylates non-CpA sites. *J Mol Biol* (2001) **309**:1201–1208.

doi:10.1006/jmbi.2001.4710
429. Grasby JA, Finger LD, Tsutakawa SE, Atack JM, Tainer JA. Unpairing and gating: sequence-independent substrate recognition by FEN superfamily nucleases. *Trends Biochem Sci* (2012) **37**:74–84. doi:10.1016/j.tibs.2011.10.003
430. Shinozaki K, Okazaki T. T7 gene 6 exonuclease has an RNase H activity. *Nucleic Acids Res* (1978) **5**:4245–61.
431. Wu Z-K, Zhou D-M, Wu Z, Chu X, Yu R-Q, Jiang J-H. Single-base mismatch discrimination by T7 exonuclease with target cyclic amplification detection. *Chem Commun Chem Commun* (2954) **51**:2954–2956. doi:10.1039/c4cc09984b
432. Kahramanoglou C, Prieto AI, Khedkar S, Haase B, Gupta A, Benes V, Fraser GM, Luscombe NM, Seshasayee ASN. Genomics of DNA cytosine methylation in Escherichia coli reveals its role in stationary phase transcription. *Nat Commun* (2012) **3**:886. doi:10.1038/ncomms1878
433. Uphoff S, Reyes-Lamothe R, Garza de Leon F, Sherratt DJ, Kapanidis AN. Single-molecule DNA repair in live bacteria. *Proc Natl Acad Sci U S A* (2013) **110**:8063–8. doi:10.1073/pnas.1301804110
434. Masamune Y, Fleischman RA, Richardson CC. Enzymatic Removal and Replacement of Nucleotides at Single Strand Breaks in Deoxyribonucleic Acid. *J Biol Chem* (1971) **246**:2680–2691.
435. Guan C, Kumar S. A single catalytic domain of the junction-resolving enzyme T7 endonuclease I is a non-specific nicking endonuclease. *Nucleic Acids Res* (2005) **33**:6225–34. doi:10.1093/nar/gki921
436. Mazur DJ, Perrino FW. Identification and expression of the TREX1 and TREX2 cDNA sequences encoding mammalian 3'-->5' exonucleases. *J Biol Chem* (1999) **274**:19655–60.
437. Mazur DJ, Perrino FW. Excision of 3' termini by the Trex1 and TREX2 3'-->5' exonucleases. Characterization of the recombinant proteins. *J Biol Chem* (2001) **276**:17022–9. doi:10.1074/jbc.M100623200
438. Takahashi S, Brazier JA, Sugimoto N. Topological impact of noncanonical DNA structures on Klenow fragment of DNA polymerase. doi:10.1073/pnas.1704258114
439. Pan CQ, Ulmer JS, Herzka A, Lazarus RA. Mutational analysis of human

DNase I at the DNA binding interface: Implications for DNA recognition, catalysis, and metal ion dependence. *Prorein Sci* (1998) **7**:628–636. doi:10.1002/pro.5560070312

440. Pan CQ, Lazarus RA. Hyperactivity of human DNase I variants. Dependence on the number of positively charged residues and concentration, length, and environment of DNA. *J Biol Chem* (1998) **273**:11701–8.
441. Taylor AF, Weiss B. Role of exonuclease III in the base excision repair of uracil-containing DNA. *J Bacteriol* (1982) **151**:351–7.
442. Samejima K, Earnshaw WC. Trashing the genome: the role of nucleases during apoptosis. *Nat Rev Mol Cell Biol* (2005) **6**:677–688. doi:10.1038/nrm1715
443. Britain G. Is the DNA of Virus T7 Methylated ? *J Gen Virol* (1979) **4**:609–613. doi:10.1099/0022-1317-44-3-609
444. Qvist P, Huertas P, Jimeno S, Nyegaard M, Hassan MJ, Jackson SP, Børglum AD. CtIP Mutations Cause Seckel and Jawad Syndromes. *PLoS Genet* (2011) **7**:e1002310. doi:10.1371/journal.pgen.1002310
445. Wu Y, Berends MJ, Post JG, Mensink RG, Verlind E, Van Der Sluis T, Kempinga C, Sijmons RH, van der Zee AG, Hollema H, et al. Germline mutations of EXO1 gene in patients with hereditary nonpolyposis colorectal cancer (HNPCC) and atypical HNPCC forms. *Gastroenterology* (2001) **120**:1580–7. Available at: http://www.ncbi.nlm.nih.gov/pubmed/11375940 [Accessed September 14, 2018]
446. Duan F, Song C, Dai L, Cui S, Zhang X, Zhao X, Siegel R, Naishadham D, Jemal A, Lichtenstein P, et al. The Significance of Exo1 K589E Polymorphism on Cancer Susceptibility: Evidence Based on a Meta-Analysis. *PLoS One* (2014) **9**:e96764. doi:10.1371/journal.pone.0096764
447. Liberti SE, Rasmussen LJ. Is hEXO1 a cancer predisposing gene? *Mol Cancer Res* (2004) **2**:427–32. Available at: http://www.ncbi.nlm.nih.gov/pubmed/15328369 [Accessed May 28, 2018]
448. Orebaugh CD, Fye JM, Harvey S, Hollis T, Perrino FW. The TREX1 Exonuclease R114H Mutation in Aicardi-Goutières Syndrome and Lupus Reveals Dimeric Structure Requirements for DNA Degradation Activity. *J Biol Chem* (2011) **286**:40246–40254. doi:10.1074/jbc.M111.297903
449. Li P, Du J, Goodier JL, Hou J, Kang J, Kazazian HH, Zhao K, Yu X-F. Aicardi–

Goutières syndrome protein TREX1 suppresses L1 and maintains genome integrity through exonuclease-independent ORF1p depletion. *Nucleic Acids Res* (2017) **45**:4619–4631. doi:10.1093/nar/gkx178

450. Harmon FG, Kowalczykowski SC. Biochemical Characterization of the DNA Helicase Activity of the Escherichia coli RecQ Helicase. *J Biol Chem* (2001) **276**:232–43. doi:10.1074/jbc.M006555200
451. Kumar S, Peng X, Daley J, Yang L, Shen J, Nguyen N, Bae G, Niu H, Peng Y, Hsieh H-J, et al. Inhibition of DNA2 nuclease as a therapeutic strategy targeting replication stress in cancer cells. *Oncogenesis* (2017) **6**:e319–e319. doi:10.1038/oncsis.2017.15
452. Moelling K, Broecker F, Russo G, Sunagawa S. RNase H As Gene Modifier, Driver of Evolution and Antiviral Defense. *Front Microbiol* (2017) **8**:1745. doi:10.3389/fmicb.2017.01745
453. Majorek KA, Dunin-Horkawicz S, Steczkiewicz K, Muszewska A, Nowotny M, Ginalski K, Bujnicki JM. The RNase H-like superfamily: new members, comparative structural analysis and evolutionary classification. *Nucleic Acids Res* (2014) **42**:4160–79. doi:10.1093/nar/gkt1414
454. Condon C, Putzer H. The phylogenetic distribution of bacterial ribonucleases. *Nucleic Acids Res* (2002) **30**:5339–5346. doi:10.1093/nar/gkf691
455. Altman S. Ribonuclease P. *Philos Trans R Soc Lond B Biol Sci* (2011) **366**:2936–41. doi:10.1098/rstb.2011.0142
456. Sun F-J, Caetano-Anollés G. The ancient history of the structure of ribonuclease P and the early origins of Archaea. *BMC Bioinformatics* (2010) **11**:153. doi:10.1186/1471-2105-11-153
457. Jacquet K, Fradet-Turcotte A, Avvakumov N, Lambert J-P, Roques C, Pandita RK, Paquet E, Herst P, Gingras A-C, Pandita TK, et al. The TIP60 Complex Regulates Bivalent Chromatin Recognition by 53BP1 through Direct H4K20me Binding and H2AK15 Acetylation. *Mol Cell* (2016) **62**:409–21. doi:10.1016/j.molcel.2016.03.031
458. Ronai D, Iglesias-Ussel MD, Fan M, Li Z, Martin A, Scharff MD. Detection of chromatin-associated single-stranded DNA in regions targeted for somatic hypermutation. *J Exp Med* (2007) **204**:181–90. doi:10.1084/jem.20062032
459. Kenter AL. AID targeting is dependent on RNA polymerase II pausing. *Semin Immunol* (2012) **24**:281–6. doi:10.1016/j.smim.2012.06.001

460. Lemay J-F, Larochelle M, Marguerat S, Atkinson S, Bähler J, Bachand F. The RNA exosome promotes transcription termination of backtracked RNA polymerase II. *Nat Struct Mol Biol* (2014) **21**:919–26. doi:10.1038/nsmb.2893
461. Choukrallah MA, Matthias P. The interplay between chromatin and transcription factor networks during B cell development: Who pulls the trigger first? *Front Immunol* (2014) **5**:
462. Jolly CJ, Cook AJL, Manis JP. Fixing DNA breaks during class switch recombination. *J Exp Med* (2008) **205**:509–13. doi:10.1084/jem.20080356
463. Kuang FL, Luo Z, Scharff MD. H3 trimethyl K9 and H3 acetyl K9 chromatin modifications are associated with class switch recombination. *Proc Natl Acad Sci U S A* (2009) **106**:5288–93. doi:10.1073/pnas.0901368106
464. Wang L, Whang N, Wuerffel R, Kenter AL. AID-dependent histone acetylation is detected in immunoglobulin S regions. *J Exp Med* (2006) **203**:215–26. doi:10.1084/jem.20051774
465. Pankotai T, Bonhomme C, Chen D, Soutoglou E. DNAPKcs-dependent arrest of RNA polymerase II transcription in the presence of DNA breaks. *Nat Struct Mol Biol* (2012) **19**:276–82. doi:10.1038/nsmb.2224
466. Pankotai T, Soutoglou E. Double strand breaks: hurdles for RNA polymerase II transcription? *Transcription* (2013) **4**:34–8. doi:10.4161/trns.22879
467. Wang Q, Goldstein M. *Small RNAs recruit chromatin modifying enzymes MMSET and Tip60 to reconfigure damaged DNA upon double-strain break and facilitate repair*. (2016). doi:10.1158/0008-5472.CAN-15-2334
468. Berndsen CE, Denu JM. Catalysis and substrate selection by histone/protein lysine acetyltransferases. *Curr Opin Struct Biol* (2008) **18**:682–9. doi:10.1016/j.sbi.2008.11.004
469. Kaidi A, Jackson SP. KAT5 tyrosine phosphorylation couples chromatin sensing to ATM signalling. *Nature* (2013) **498**:70–4. doi:10.1038/nature12201
470. Stucki M, Clapperton JA, Mohammad D, Yaffe MB, Smerdon SJ, Jackson SP. MDC1 directly binds phosphorylated histone H2AX to regulate cellular responses to DNA double-strand breaks. *Cell* (2005) **123**:1213–26. doi:10.1016/j.cell.2005.09.038
471. Mattiroli F, Vissers JH a, Van Dijk WJ, Ikpa P, Citterio E, Vermeulen W, Marteijn J a., Sixma TK. RNF168 ubiquitinates K13-15 on H2A/H2AX to drive DNA damage signaling. *Cell* (2012) **150**:1182–1195.

doi:10.1016/j.cell.2012.08.005

472. Kleiner RE, Verma P, Molloy KR, Chait BT, Kapoor TM. Chemical proteomics reveals a γH2AX-53BP1 interaction in the DNA damage response. *Nat Chem Biol* (2015) **11**:807–814. Available at: http://dx.doi.org/10.1038/nchembio.1908 [Accessed September 8, 2015]
473. Ogiwara H, Sasaki M, Mitachi T, Oike T, Higuchi S, Tominaga Y, Kohno T. Targeting p300 Addiction in CBP-Deficient Cancers Causes Synthetic Lethality by Apoptotic Cell Death due to Abrogation of MYC Expression. *Cancer Discov* (2016) **6**:430–45. doi:10.1158/2159-8290.CD-15-0754
474. Ramaswamy S, Ross KN, Lander ES, Golub TR. A molecular signature of metastasis in primary solid tumors. *Nat Genet* (2003) **33**:49–54. doi:10.1038/ng1060
475. Halkidou K, Gnanapragasam VJ, Mehta PB, Logan IR, Brady ME, Cook S, Leung HY, Neal DE, Robson CN. Expression of Tip60, an androgen receptor coactivator, and its role in prostate cancer development. *Oncogene* (2003) **22**:2466–77. doi:10.1038/sj.onc.1206342
476. Gorrini C, Squatrito M, Luise C, Syed N, Perna D, Wark L, Martinato F, Sardella D, Verrecchia A, Bennett S, et al. Tip60 is a haplo-insufficient tumour suppressor required for an oncogene-induced DNA damage response. *Nature* (2007) **448**:1063–7. doi:10.1038/nature06055
477. Kim JH, Kim B, Cai L, Choi HJ, Ohgi KA, Tran C, Chen C, Chung CH, Huber O, Rose DW, et al. Transcriptional regulation of a metastasis suppressor gene by Tip60 and β-catenin complexes. *Nature* (2005) **434**:921–926. doi:10.1038/nature03452
478. Buchdunger E, Zimmermann J, Mett H, Meyer T, Müller M, Druker BJ, Lydon NB. Inhibition of the Abl protein-tyrosine kinase in vitro and in vivo by a 2-phenylaminopyrimidine derivative. *Cancer Res* (1996) **56**:100–4. Available at: http://www.ncbi.nlm.nih.gov/pubmed/8548747 [Accessed June 15, 2015]
479. Waterhouse AM, Procter JB, Martin DMA, Clamp M, Barton GJ. Jalview Version 2: a multiple sequence alignment editor and analysis workbench. *Bioinformatics* (2009) **25**:1189–1191. doi:10.1093/bioinformatics/btp033
480. Schindelin J, Arganda-Carreras I, Frise E, Kaynig V, Longair M, Pietzsch T, Preibisch S, Rueden C, Saalfeld S, Schmid B, et al. Fiji: an open-source platform for biological-image analysis. *Nat Methods* (2012) **9**:676–682.

doi:10.1038/nmeth.2019

481. Utley RT, Côté J. The MYST family of histone acetyltransferases. *Curr Top Microbiol Immunol* (2003) **274**:203–36. Available at: http://www.ncbi.nlm.nih.gov/pubmed/12596909 [Accessed September 15, 2018]
482. Yan Y, Barlev NA, Haley RH, Berger SL, Marmorstein R. Crystal structure of yeast Esa1 suggests a unified mechanism for catalysis and substrate binding by histone acetyltransferases. *Mol Cell* (2000) **6**:1195–205. Available at: http://www.ncbi.nlm.nih.gov/pubmed/11106757 [Accessed September 15, 2018]
483. Yan Y, Harper S, Speicher DW, Marmorstein R. The catalytic mechanism of the ESA1 histone acetyltransferase involves a self-acetylated intermediate. *Nat Struct Biol* (2002) **9**:862–9. doi:10.1038/nsb849
484. Takechi S, Nakayama T. Sas3 Is a Histone Acetyltransferase and Requires a Zinc Finger Motif. *Biochem Biophys Res Commun* (1999) **266**:405–410. doi:10.1006/bbrc.1999.1836
485. Schwabe JWR, Klug A. Zinc mining for protein domains. *Nat Struct Mol Biol* (1994) **1**:345–349. doi:10.1038/nsb0694-345
486. Brehm A, Tufteland KR, Aasland R, Becker PB. The many colours of chromodomains. *BioEssays* (2004) **26**:133–140. doi:10.1002/bies.10392
487. Eissenberg JC. Molecular biology of the chromo domain: an ancient chromatin module comes of age. *Gene* (2001) **275**:19–29. Available at: http://www.ncbi.nlm.nih.gov/pubmed/11574148 [Accessed September 15, 2018]
488. Nielsen PR, Nietlispach D, Mott HR, Callaghan J, Bannister A, Kouzarides T, Murzin AG, Murzina N V., Laue ED. Structure of the HP1 chromodomain bound to histone H3 methylated at lysine 9. *Nature* (2002) **416**:103–107. doi:10.1038/nature722
489. Akhtar A, Zink D, Becker PB. Chromodomains are protein-RNA interaction modules. *Nature* (2000) **407**:405–9. doi:10.1038/35030169
490. Bernstein E, Duncan EM, Masui O, Gil J, Heard E, Allis CD. Mouse Polycomb Proteins Bind Differentially to Methylated Histone H3 and RNA and Are Enriched in Facultative Heterochromatin. *Mol Cell Biol* (2006) **26**:2560–2569. doi:10.1128/MCB.26.7.2560-2569.2006

491. Bouazoune K, Mitterweger A, Längst G, Imhof A, Akhtar A, Becker PB, Brehm A. The dMi-2 chromodomains are DNA binding modules important for ATP-dependent nucleosome mobilization. *EMBO J* (2002) **21**:2430–2440. doi:10.1093/emboj/21.10.2430
492. Shimojo H, Sano N, Moriwaki Y, Okuda M, Horikoshi M, Nishimura Y. Novel structural and functional mode of a knot essential for RNA binding activity of the Esa1 presumed chromodomain. *J Mol Biol* (2008) **378**:987–1001. doi:10.1016/j.jmb.2008.03.021
493. Walker JR, Hervas C, Ross JD, Blinkova A, Walbridge MJ, Pumarega EJ, Park MO, Neely HR. Escherichia coli DNA polymerase III tau- and gamma-subunit conserved residues required for activity in vivo and in vitro. *J Bacteriol* (2000) **182**:6106–13. Available at: http://www.ncbi.nlm.nih.gov/pubmed/11029431 [Accessed September 15, 2018]
494. Jha S, Gupta A, Dar A, Dutta A. RVBs are required for assembling a functional TIP60 complex. *Mol Cell Biol* (2013) **33**:1164–74. doi:10.1128/MCB.01567-12
495. Dereeper A, Guignon V, Blanc G, Audic S, Buffet S, Chevenet F, Dufayard J-F, Guindon S, Lefort V, Lescot M, et al. Phylogeny.fr: robust phylogenetic analysis for the non-specialist. *Nucleic Acids Res* (2008) **36**:W465–W469. doi:10.1093/nar/gkn180
496. Gioni V, Karampinas T, Voutsinas G, Roussidis AE, Papadopoulos S, Karamanos NK, Kletsas D. Imatinib mesylate inhibits proliferation and exerts an antifibrotic effect in human breast stroma fibroblasts. *Mol Cancer Res* (2008) **6**:706–14. doi:10.1158/1541-7786.MCR-07-0355
497. Nies AT, Schaeffeler E, van der Kuip H, Cascorbi I, Bruhn O, Kneba M, Pott C, Hofmann U, Volk C, Hu S, et al. Cellular uptake of imatinib into leukemic cells is independent of human organic cation transporter 1 (OCT1). *Clin Cancer Res* (2014) **20**:985–94. doi:10.1158/1078-0432.CCR-13-1999
498. Podhorecka M, Skladanowski A, Bozko P. H2AX Phosphorylation: Its Role in DNA Damage Response and Cancer Therapy. *J Nucleic Acids* (2010) **2010**: doi:10.4061/2010/920161
499. Ruan J, Luo M, Wang C, Fan L, Yang SN, Cardenas M, Geng H, Leonard JP, Melnick A, Cerchietti L, et al. Imatinib disrupts lymphoma angiogenesis by targeting vascular pericytes. *Blood* (2013) **121**:5192–5202. doi:10.1182/blood-2013-03-490763

500. Harrison C. Anticancer drugs: Imatinib hits anaplastic large cell lymphoma. *Nat Rev Drug Discov* (2012) **11**:908–908. doi:10.1038/nrd3902
501. Chute JP, Himburg HA. Imatinib tackles lymphoma via the PDGFRβ+ pericyte. *Blood* (2013) **121**:5107–8. doi:10.1182/blood-2013-05-501205
502. Hantschel O, Superti-Furga G. Regulation of the c-Abl and Bcr-Abl tyrosine kinases. *Nat Rev Mol Cell Biol* (2004) **51. Hantsc**:33–44. doi:10.1038/nrm1280
503. Martín M, Terradas M, Hernández L, Genescà A. γH2AX foci on apparently intact mitotic chromosomes: not signatures of misrejoining events but signals of unresolved DNA damage. *Cell Cycle* (2014) **13**:3026–36. doi:10.4161/15384101.2014.947786
504. Francia S, Michelini F, Saxena A, Tang D, de Hoon M, Anelli V, Mione M, Carninci P, d'Adda di Fagagna F. Site-specific DICER and DROSHA RNA products control the DNA-damage response. *Nature* (2012) **488**:231–235. doi:10.1038/nature11179
505. Wei W, Ba Z, Gao M, Wu Y, Ma Y, Amiard S, White CI, Rendtlew Danielsen JM, Yang Y-G, Qi Y. A Role for Small RNAs in DNA Double-Strand Break Repair. *Cell* (2012) **149**:101–112. doi:10.1016/j.cell.2012.03.002
506. Wee LM, Flores-Jasso CF, Salomon WE, Zamore PD. Argonaute divides its RNA guide into domains with distinct functions and RNA-binding properties. *Cell* (2012) **151**:1055–67. doi:10.1016/j.cell.2012.10.036
507. Kitayama K, Kamo M, Oma Y, Matsuda R, Uchida T, Ikura T, Tashiro S, Ohyama T, Winsor B, Harata M. The human actin-related protein hArp5: Nucleo-cytoplasmic shuttling and involvement in DNA repair. *Exp Cell Res* (2009) **315**:206–217. doi:10.1016/j.yexcr.2008.10.028
508. Kracker S, Di Virgilio M, Schwartzentruber J, Cuenin C, Forveille M, Deau M-C, McBride KM, Majewski J, Gazumyan A, Seneviratne S, et al. An inherited immunoglobulin class-switch recombination deficiency associated with a defect in the INO80 chromatin remodeling complex. *J Allergy Clin Immunol* (2015) **135**:998–1007.e6. doi:10.1016/j.jaci.2014.08.030
509. Khair L, Guikema JEJ, Linehan EK, Ucher AJ, Leus NGJ, Ogilvie C, Lou Z, Schrader CE, Stavnezer J. ATM increases activation-induced cytidine deaminase activity at downstream S regions during class-switch recombination. *J Immunol* (2014) **192**:4887–96. doi:10.4049/jimmunol.1303481

510. Li L, Halaby M-J, Hakem A, Cardoso R, El Ghamrasni S, Harding S, Chan N, Bristow R, Sanchez O, Durocher D, et al. Rnf8 deficiency impairs class switch recombination, spermatogenesis, and genomic integrity and predisposes for cancer. *J Exp Med* (2010) **207**:983–997. doi:10.1084/jem.20092437
511. Ramachandran S, Chahwan R, Nepal RM, Frieder D, Panier S, Roa S, Zaheen A, Durocher D, Scharff MD, Martin A. The RNF8/RNF168 ubiquitin ligase cascade facilitates class switch recombination. *Proc Natl Acad Sci U S A* (2010) **107**:809–14. doi:10.1073/pnas.0913790107
512. Torres-Machorro AL, Pillus L. Bypassing the requirement for an essential MYST acetyltransferase. *Genetics* (2014) **197**:851–63. doi:10.1534/genetics.114.165894
513. Schrader EK, Harstad KG, Matouschek A. Targeting proteins for degradation. *Nat Chem Biol* (2009) **5**:815–22. doi:10.1038/nchembio.250
514. Iwamoto M, Björklund T, Lundberg C, Kirik D, Wandless TJ. A General Chemical Method to Regulate Protein Stability in the Mammalian Central Nervous System. *Chem Biol* (2010) **17**:981–988. doi:10.1016/j.chembiol.2010.07.009
515. Matthews DA, Bolin JT, Burridge JM, Filman DJ, Volz KW, Kraut J. Dihydrofolate reductase. The stereochemistry of inhibitor selectivity. *J Biol Chem* (1985) **260**:392–9. Available at: http://www.ncbi.nlm.nih.gov/pubmed/3880743 [Accessed September 11, 2018]
516. Halkidou K, Logan IR, Cook S, Neal DE, Robson CN. Putative involvement of the histone acetyltransferase Tip60 in ribosomal gene transcription. *Nucleic Acids Res* (2004) **32**:1654–65. doi:10.1093/nar/gkh296
517. Jacquet K, Fradet-Turcotte A, Avvakumov N, Lambert JP, Roques C, Pandita RK, Paquet E, Herst P, Gingras AC, Pandita TK, et al. The TIP60 Complex Regulates Bivalent Chromatin Recognition by 53BP1 through Direct H4K20me Binding and H2AK15 Acetylation. *Mol Cell* (2016) **62**:409–421. doi:10.1016/j.molcel.2016.03.031
518. Peng L, Ling H, Yuan Z, Fang B, Bloom G, Fukasawa K, Koomen J, Chen J, Lane WS, Seto E. SIRT1 negatively regulates the activities, functions, and protein levels of hMOF and TIP60. *Mol Cell Biol* (2012) **32**:2823–36. doi:10.1128/MCB.00496-12
519. Dar A, Shibata E, Dutta A. Deubiquitination of Tip60 by USP7 determines the

activity of the p53-dependent apoptotic pathway. *Mol Cell Biol* (2013) **33**:3309–20. doi:10.1128/MCB.00358-13

520. Wang Y, Wang F, Wang R, Zhao P, Xia Q. 2A self-cleaving peptide-based multi-gene expression system in the silkworm Bombyx mori. *Sci Rep* (2015) **5**:16273. doi:10.1038/srep16273
521. Kim JH, Lee S-R, Li L-H, Park H-J, Park J-H, Lee KY, Kim M-K, Shin BA, Choi S-Y. High Cleavage Efficiency of a 2A Peptide Derived from Porcine Teschovirus-1 in Human Cell Lines, Zebrafish and Mice. *PLoS One* (2011) **6**:e18556. doi:10.1371/journal.pone.0018556
522. Kim SJ, Martinson HG. Poly(A)-dependent transcription termination: continued communication of the poly(A) signal with the polymerase is required long after extrusion in vivo. *J Biol Chem* (2003) **278**:41691–701. doi:10.1074/jbc.M306304200
523. Till BJ, Zerr T, Comai L, Henikoff S. A protocol for TILLING and Ecotilling in plants and animals. *Nat Protoc* (2006) **1**:2465–77. doi:10.1038/nprot.2006.329
524. Naito Y, Hino K, Bono H, Ui-Tei K. CRISPRdirect: software for designing CRISPR/Cas guide RNA with reduced off-target sites. *Bioinformatics* (2015) **31**:1120–3. doi:10.1093/bioinformatics/btu743
525. Mali P, Yang L, Esvelt KM, Aach J, Guell M, DiCarlo JE, Norville JE, Church GM. RNA-guided human genome engineering via Cas9. *Science* (2013) **339**:823–6. doi:10.1126/science.1232033
526. Untergasser A, Cutcutache I, Koressaar T, Ye J, Faircloth BC, Remm M, Rozen SG. Primer3--new capabilities and interfaces. *Nucleic Acids Res* (2012) **40**:e115. doi:10.1093/nar/gks596
527. Carleton KL. “Quantification of Transcript Levels with Quantitative RT-PCR,” in *Methods in molecular biology (Clifton, N.J.)*, 279–295. doi:10.1007/978-1-61779-228-1_17
528. Molina R, Stella S, Redondo P, Gomez H, Marcaida MJ, Orozco M, Prieto J, Montoya G. Visualizing phosphodiester-bond hydrolysis by an endonuclease. *Nat Struct Mol Biol* (2015) **22**:65–72. doi:10.1038/nsmb.2932
529. Proudnikov D, Mirzabekov A. Chemical methods of DNA and RNA fluorescent labeling. *Nucleic Acids Res* (1996) **24**:4535–42. Available at: http://www.ncbi.nlm.nih.gov/pubmed/8948646 [Accessed September 18, 2018]
530. Solomatin S, Herschlag D. “Methods of Site-Specific Labeling of RNA with

Fluorescent Dyes," in *Methods in enzymology*, 47–68. doi:10.1016/S0076-6879(09)69003-0

531. Lu Y-J, Deng Q, Hu D-P, Wang Z-Y, Huang B-H, Du Z-Y, Fang Y-X, Wong W-L, Zhang K, Chow C-F. A molecular fluorescent dye for specific staining and imaging of RNA in live cells: a novel ligand integration from classical thiazole orange and styryl compounds. *Chem Commun (Camb)* (2015) **51**:15241–4. doi:10.1039/c5cc05551b
532. Cuchillo CM, Nogués MV, Raines RT. Bovine pancreatic ribonuclease: fifty years of the first enzymatic reaction mechanism. *Biochemistry* (2011) **50**:7835–41. doi:10.1021/bi201075b
533. Koczera P, Martin L, Marx G, Schuerholz T. The Ribonuclease A Superfamily in Humans: Canonical RNases as the Buttress of Innate Immunity. *Int J Mol Sci* (2016) **17**: doi:10.3390/ijms17081278
534. Chakrabarti A, Jha BK, Silverman RH. New insights into the role of RNase L in innate immunity. *J Interferon Cytokine Res* (2011) **31**:49–57. doi:10.1089/jir.2010.0120
535. Ezelle HJ, Malathi K, Hassel BA. The Roles of RNase-L in Antimicrobial Immunity and the Cytoskeleton-Associated Innate Response. *Int J Mol Sci* (2016) **17**: doi:10.3390/ijms17010074
536. Harder J, Schroder J-M. RNase 7, a novel innate immune defense antimicrobial protein of healthy human skin. *J Biol Chem* (2002) **277**:46779–84. doi:10.1074/jbc.M207587200
537. Stavrou S, Ross SR. APOBEC3 Proteins in Viral Immunity. *J Immunol* (2015) **195**:4565–70. doi:10.4049/jimmunol.1501504
538. Rebhandl S, Huemer M, Greil R, Geisberger R. AID/APOBEC deaminases and cancer. *Oncoscience* (2015) **2**:320–33. Available at: http://www.ncbi.nlm.nih.gov/pubmed/26097867
539. Choudhary NL, Yadav OP, Lodha ML. Ribonuclease, deoxyribonuclease, and antiviral activity of Escherichia coli-expressed Bougainvillea xbuttiana antiviral protein 1. *Biochem* (2008) **73**:273–277. doi:10.1134/S000629790803005X
540. Cuthbert BJ, Burley KH, Goulding CW. Introducing the new bacterial branch of the RNase A superfamily. *RNA Biol* (2018) **15**:9–12. doi:10.1080/15476286.2017.1387710
541. Kim W-C, Lee CH. The role of mammalian ribonucleases (RNases) in cancer.

Biochim Biophys Acta - Rev Cancer (2009) **1796**:99–113. doi:10.1016/j.bbcan.2009.05.002

542. Leland PA, Raines RT. Cancer chemotherapy--ribonucleases to the rescue. *Chem Biol* (2001) **8**:405–13. Available at: http://www.ncbi.nlm.nih.gov/pubmed/11358688 [Accessed September 18, 2018]
543. Mironova N, Patutina O, Brenner E, Kurilshikov A, Vlassov V, Zenkova M. The systemic tumor response to RNase A treatment affects the expression of genes involved in maintaining cell malignancy. *Oncotarget* (2017) **8**:78796–78810. doi:10.18632/oncotarget.20228
544. Sutton DH, Conn GL, Brown T, Lane AN. The dependence of DNase I activity on the conformation of oligodeoxynucleotides. (1997). Available at: https://www.ncbi.nlm.nih.gov/pmc/articles/PMC1218094/pdf/9020884.pdf [Accessed September 18, 2018]
545. Crow YJ, Hayward BE, Parmar R, Robins P, Leitch A, Ali M, Black DN, Van Bokhoven H, Brunner HG, Hamel BC, et al. Mutations in the gene encoding the 3’-5’ DNA exonuclease TREX1 cause Aicardi-Goutières syndrome at the AGS1 locus. *Nat Genet* (2006) **38**:917–920. doi:10.1038/ng1845
546. Mi Y, Yu Q, Min Z, Xu B, Zhang L, Zhang W, Feng N, Hua L. Arg462Gln and Asp541Glu polymorphisms in ribonuclease L and prostate cancer risk: a meta-analysis. *J Biomed Res* (2010) **24**:365–373. doi:10.1016/S1674-8301(10)60049-8
547. Li H, Tai BC. RNASEL Gene Polymorphisms and the Risk of Prostate Cancer: a Meta-analysis. *Clin Cancer Res* (2006) **12**:5713–5719. doi:10.1158/1078-0432.CCR-05-2799
548. Ezelle HJ, Hassel BA. Pathologic effects of RNase-L dysregulation in immunity and proliferative control. *Front Biosci (Schol Ed)* (2012) **4**:767–86. Available at: http://www.ncbi.nlm.nih.gov/pubmed/22202089 [Accessed July 31, 2018]
549. Aleksandrov R, Dotchev A, Poser I, Krastev D, Georgiev G, Panova G, Babukov Y, Danovski G, Dyankova T, Hubatsch L, et al. Protein Dynamics in Complex DNA Lesions. *Mol Cell* (2018) **69**:1046–1061.e5. doi:10.1016/j.molcel.2018.02.016
550. Langerak P, Nygren AOH, Krijger PHL, Berk PCM van den, Jacobs H. A/T mutagenesis in hypermutated immunoglobulin genes strongly depends on

PCNAK164 modification. *J Exp Med* (2007) **204**:1989. doi:10.1084/JEM.20070902

551. Wang L, Whang N, Wuerffel R, Kenter AL. AID-dependent histone acetylation is detected in immunoglobulin S regions. *J Exp Med* (2006) **203**:215–26. doi:10.1084/jem.20051774
552. Zheng S, Vuong BQ, Vaidyanathan B, Lin J-Y, Huang F-T, Chaudhuri J. Non-coding RNA Generated following Lariat Debranching Mediates Targeting of AID to DNA. *Cell* (2015) **161**:762–773. doi:10.1016/j.cell.2015.03.020
553. Doseth B, Visnes T, Wallenius A, Ericsson I, Sarno A, Pettersen HS, Flatberg A, Catterall T, Slupphaug G, Krokan HE, et al. Uracil-DNA glycosylase in base excision repair and adaptive immunity: species differences between man and mouse. *J Biol Chem* (2011) **286**:16669–80. doi:10.1074/jbc.M111.230052
554. Yousif AS, Stanlie A, Begum NA, Honjo T. Opinion: uracil DNA glycosylase (UNG) plays distinct and non-canonical roles in somatic hypermutation and class switch recombination. *Int Immunol* (2014) **26**:575–8. doi:10.1093/intimm/dxu071
555. Campeau E, Gobeil S. RNA interference in mammals: behind the screen. *Brief Funct Genomics* (2011) **10**:215–226. doi:10.1093/bfgp/elr018
556. Nishimura K, Fukagawa T, Takisawa H, Kakimoto T, Kanemaki M. An auxin-based degron system for the rapid depletion of proteins in nonplant cells. *Nat Methods* (2009) **6**:917–922. doi:10.1038/nmeth.1401
557. Ciccia A, Elledge SJ. The DNA damage response: making it safe to play with knives. *Mol Cell* (2010) **40**:179–204. doi:10.1016/j.molcel.2010.09.019
558. Nordlund P, Reichard P. Ribonucleotide reductases. *Annu Rev Biochem* (2006) **75**:681–706. doi:10.1146/annurev.biochem.75.103004.142443
559. Elledge SJ, Davis RW. DNA damage induction of ribonucleotide reductase. *Mol Cell Biol* (1989) **9**:4932–40. Available at: http://www.ncbi.nlm.nih.gov/pubmed/2513480 [Accessed September 19, 2018]
560. Niida H, Katsuno Y, Sengoku M, Shimada M, Yukawa M, Ikura M, Ikura T, Kohno K, Shima H, Suzuki H, et al. Essential role of Tip60-dependent recruitment of ribonucleotide reductase at DNA damage sites in DNA repair during G1 phase. *Genes Dev* (2010) **24**:333–8. doi:10.1101/gad.1863810